Computational Analysis of a Slotted, Natural-Laminar-Flow Transonic Truss-Braced Wing Aircraft Configuration

by

Cody L. Perkins, B.S.M.E.

Master of Science Defense Presentation

Department of Mechanical Engineering

<u>Committee</u>
Dr. Dimitri Mavriplis – Chairperson
Dr. Bart Geerts – Outside Member
Dr. Michael Stoellinger – Department Member

Time: August 25th, 3:00-4:00 PM

COLLEGE OF
ENGINEERING &
APPLIED SCIENCE

UNIVERSITY OF WYOMING

Presentation Overview

1. Introduction
    1. Need for improvement
    2. Slotted, Natural-Laminar-Flow Technology
    3. The S207 SNLF Airfoil and Relevant Configuration
2. Methodology
3. 2D Analysis of the S207 SNLF Airfoil
4. 3D Analysis of an S207-Based Vehicle
5. Computational Results for the S207 Wind Tunnel Model
6. Conclusions

Presentation Overview

1. Introduction
2. Methodology
    1. Predicting Transition
    2. Solvers
    3. Validation Efforts
3. 2D Analysis of the S207 SNLF Airfoil
4. 3D Analysis of an S207-Based Vehicle
5. Computational Results for the S207-Based Wind Tunnel Model
6. Conclusions

Presentation Overview

1. Introduction
2. Methodology
3. 2D Analysis of the S207 SNLF Airfoil
    1. Computational Mesh for the S207 Airfoil Analysis
    2. Simulation at Cruise
    3. Sensitivity of Performance to Flap Positioning
4. 3D Analysis of an S207-Based Vehicle
5. Computational Results for the S207-Based Wind Tunnel Model
6. Conclusions

Presentation Overview

1. Introduction
2. Methodology
3. 2D Analysis of the S207 SNLF Airfoil
4. 3D Analysis of an S207-Based Vehicle
    1. The Geometry and Its Evolution
    2. Results for the Initial Configuration
    3. Shock Wave Elimination
    4. Initial Results for Configuration 3
    5. Polars for the Final Geometry
5. Computational Results for the S207-Based Wind Tunnel Model
6. Conclusions

Presentation Overview

1. Introduction
2. Methodology
3. 2D Analysis of the S207 SNLF Airfoil
4. 3D Analysis of an S207-Based Vehicle
5. Computational Results for the S207-Based Wind Tunnel Model
    1. The NASA Ames Wind Tunnel Tests
    2. Wind Tunnel Model Grid
    3. Computational Results for the Wind Tunnel Model Grid
6. Conclusions

Presentation Overview

1. Introduction
2. Methodology
3. 2D Analysis of the S207 SNLF Airfoil
4. 3D Analysis of an S207-Based Vehicle
5. Computational Results for the S207-Based Wind Tunnel Model
6. Conclusions

1. Introduction

1.1 Need for Improvement

- International Energy Agency reported a 104.6% increase in international aviation energy consumption between 1990 and 2015 [1]
    - United states attaining a growth of 80.1%

1.1 Need for Improvement

- International Energy Agency reported a 104.6% increase in international aviation energy consumption between 1990 and 2015 [1]
  - United states attaining a growth of 80.1%

- Private aircraft alone make contributions of 7500 tons of emitted CO_2 [2]
- 2.18 ppm increase in atmospheric concentrations of CO_2 due to the aviation industry [3]

1.1 Need for Improvement

- International Energy Agency reported a 104.6% increase in international aviation energy consumption between 1990 and 2015 [1]
    - United states attaining a growth of 80.1%

- Private aircraft alone make contributions of 7500 tons of emitted CO_2 [2]
- 2.18 ppm increase in atmospheric concentrations of CO_2 due to the aviation industry [3]

- Air travel is playing a progressively larger role in the global warming crisis
- Necessity to develop and implement preventative improvements to aircraft technology

1.1 Need for Improvement

- International Energy Agency reported a 104.6% increase in international aviation energy consumption between 1990 and 2015 [1]
  - United states attaining a growth of 80.1%

- Private aircraft alone make contributions of 7500 tons of emitted CO_2 [2]
- 2.18 ppm increase in atmospheric concentrations of CO_2 due to the aviation industry [3]

- Air travel is playing a progressively larger role in the global warming crisis
- Necessity to develop and implement preventative improvements to aircraft technology

NASA Aeronautics Research Mission Directorate

Six Thrusts [4]

1. Safe, Efficient Growth in Global Operations
2. Innovation in Commercial Supersonic Aircraft
3. Ultra-Efficient Subsonic Transports
4. Safe, Quiet, and Affordable Vertical Lift Air Vehicles
5. In-Time System-Wide Safety Assurance
6. Assured Autonomy for Aviation Transformation

Each thrust has near- (N+1), mid- (N+2), and far- (N+3) metrics

1.1 Need for Improvement

NASA Aeronautics Research Mission Directorate

Six Thrusts [4]

1. Safe, Efficient Growth in Global Operations
2. Innovation in Commercial Supersonic Aircraft
3. Ultra-Efficient Subsonic Transports
4. Safe, Quiet, and Affordable Vertical Lift Air Vehicles
5. In-Time System-Wide Safety Assurance
6. Assured Autonomy for Aviation Transformation

Each thrust has near- (N+1), mid- (N+2), and far- (N+3) metrics

1.1 Need for Improvement

NASA Aeronautics Research Mission Directorate

Six Thrusts [4]

1. Safe, Efficient Growth in Global Operations
2. Innovation in Commercial Supersonic Aircraft
3. Ultra-Efficient Subsonic Transports
4. Safe, Quiet, and Affordable Vertical Lift Air Vehicles
5. In-Time System-Wide Safety Assurance
6. Assured Autonomy for Aviation Transformation

Each thrust has near- (N+1), mid- (N+2), and far- (N+3) metrics

Technology associated with N+3 criteria will contribute to a fleet-level net reduction in emissions of 50% compared to a 2005 baseline

1.2 Slotted, Natural-Laminar-Flow Technology

- Slotted, Natural-Laminar-Flow (SNLF) technology first proposed by Dan Somers in 2005 [5]
- Targets laminar flow as its mechanism for reduced drag, more laminar flow means less skin friction drag [6]
- Seeks to improve upon the performance of NLF airfoils, which achieve 70% laminar flow [7]
    - Differs through the addition of an aft element

Example of a SNLF Airfoil as Illustrated in Reference [5]

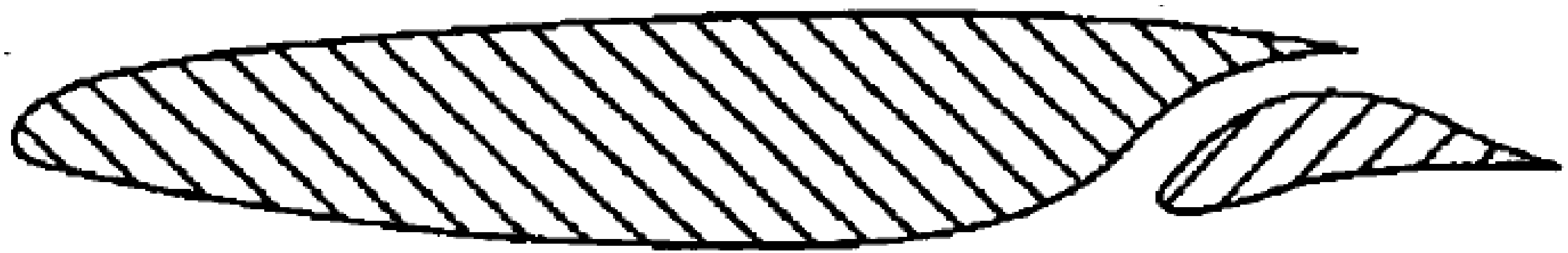

1.2 Slotted, Natural-Laminar-Flow Technology

- Slotted, Natural-Laminar-Flow (SNLF) technology first proposed by Dan Somers in 2005 [5]
- Targets laminar flow as its mechanism for reduced drag, more laminar flow means less skin friction drag [6]
- Seeks to improve upon the performance of NLF airfoils, which achieve 70% laminar flow [7]
    - Differs through the addition of an aft element

Example of a SNLF Airfoil as Illustrated in Reference [5]

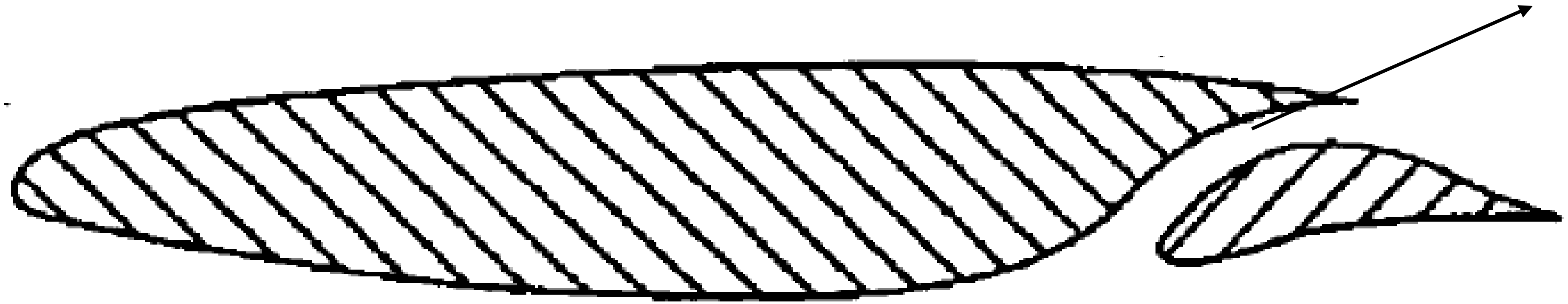

1.2 Slotted, Natural-Laminar-Flow Technology

- Slotted, Natural-Laminar-Flow (SNLF) technology first proposed by Dan Somers in 2005 [5]
- Targets laminar flow as its mechanism for reduced drag, more laminar flow means less skin friction drag [6]
- Seeks to improve upon the performance of NLF airfoils, which achieve 70% laminar flow [7]
  - Differs through the addition of an aft element

Example of a SNLF Airfoil as Illustrated in Reference [5]

The Slot: Region between fore and aft elements

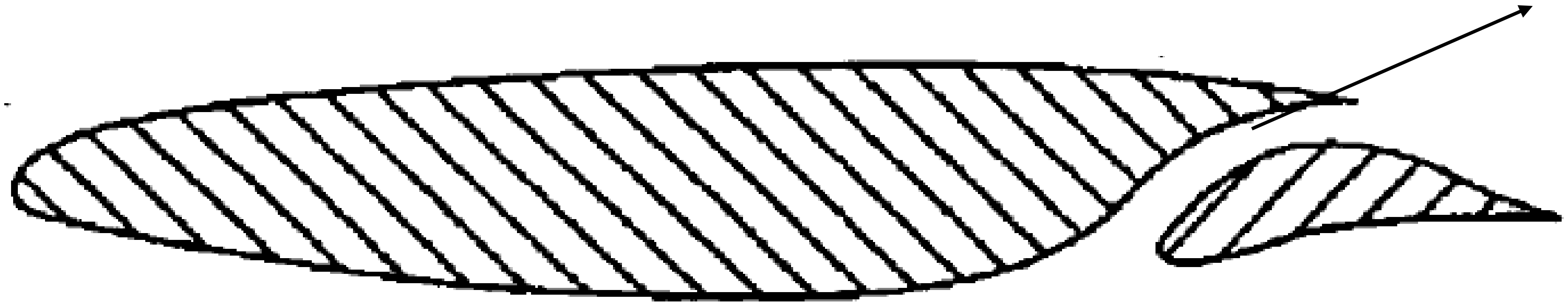

The slot….
- creates a pressure on the fore element upper surface that is lower than freestream pressure due to the velocity at the slot exit [8], also known as the dumping velocity [9]
- facilitates a favorable pressure gradient on the upper surface of the fore element near the trailing edge

1.2 Slotted, Natural-Laminar-Flow Technology

- Slotted, Natural-Laminar-Flow (SNLF) technology first proposed by Dan Somers in 2005 [5]
- Targets laminar flow as its mechanism for reduced drag, more laminar flow means less skin friction drag [6]
- Seeks to improve upon the performance of NLF airfoils, which achieve 70% laminar flow [7]
  - Differs through the addition of an aft element

Example of a SNLF Airfoil as Illustrated in Reference [5]

The Slot: Region between fore and aft elements

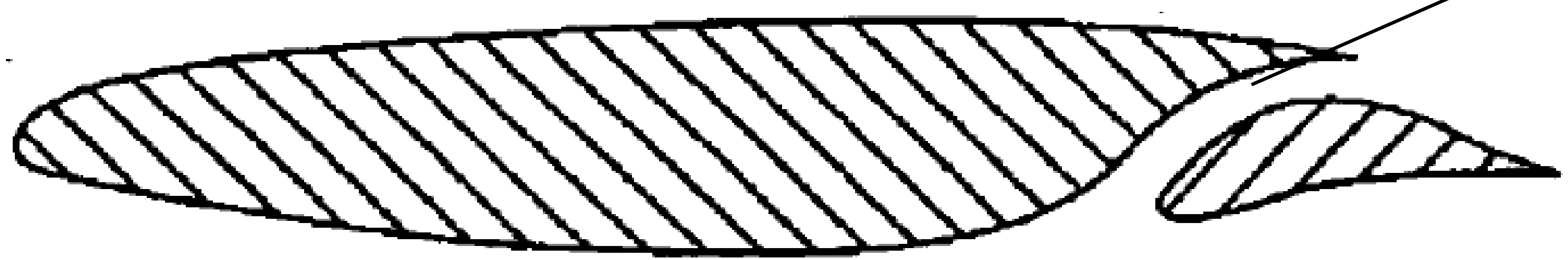

The slot….
- creates a pressure on the fore element upper surface that is lower than freestream pressure due to the velocity at the slot exit [8], also known as the dumping velocity [9]
- facilitates a favorable pressure gradient on the upper surface of the fore element near the trailing edge

Boundary layer is stabilized offering two distinct benefits…
1. Laminar flow is achieved for roughly entire chord length of the fore element, and notable portion of the aft
2. Prevents flow separation which in turn reduces profile drag, which accounts for 1/3 of transonic aircraft drag [6]

1.2 Slotted, Natural-Laminar-Flow Technology

- Low-drag bucket is an attribute unique to NLF, and by extension SNLF, type airfoils
  - Characterized by a minimum in drag across a wide range of lift coefficient (C_L) values

Example of a Low-Drag Bucket for SNLF Type Wing

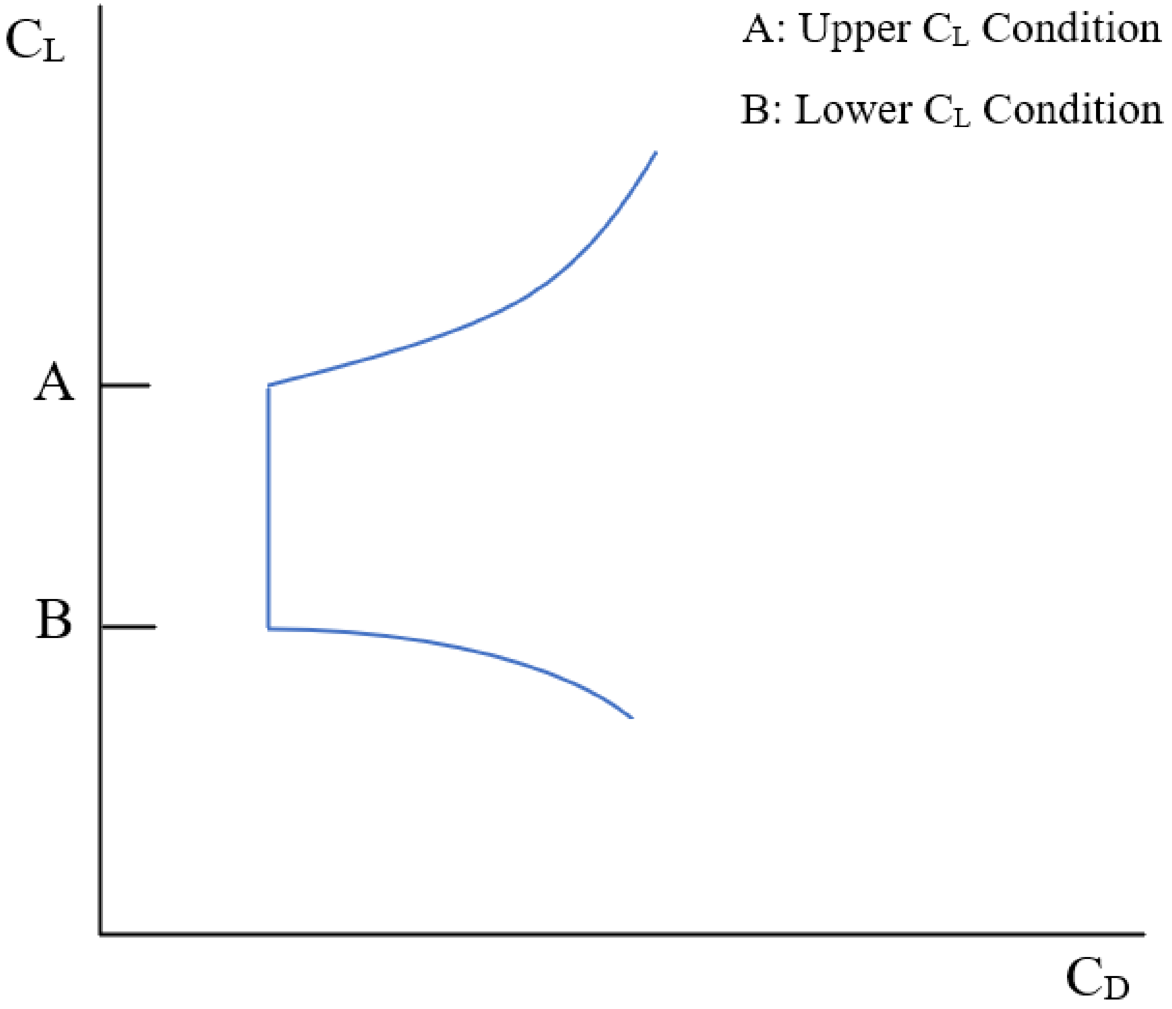

1.2 Slotted, Natural-Laminar-Flow Technology

- Low-drag bucket is an attribute unique to NLF, and by extension SNLF, type airfoils
  - Characterized by a minimum in drag across a wide range of lift coefficient (C_L) values

Example of a Low-Drag Bucket for SNLF Type Wing

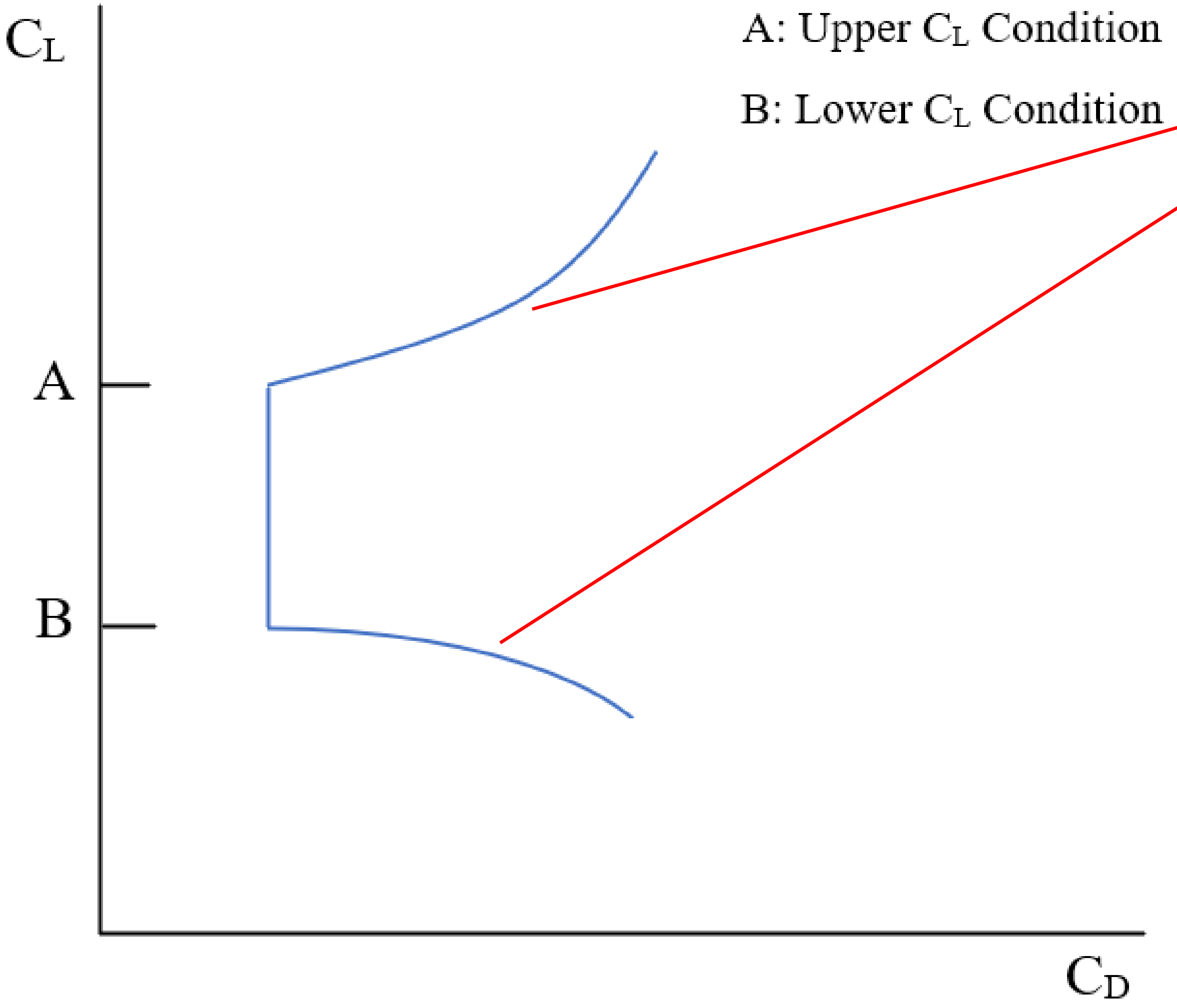

Beyond upper and lower C_L conditions, significant increase in drag is observed

1.2 Slotted, Natural-Laminar-Flow Technology

- Low-drag bucket is an attribute unique to NLF, and by extension SNLF, type airfoils
  - Characterized by a minimum in drag across a wide range of lift coefficient (C_L) values

Example of a Low-Drag Bucket for SNLF Type Wing

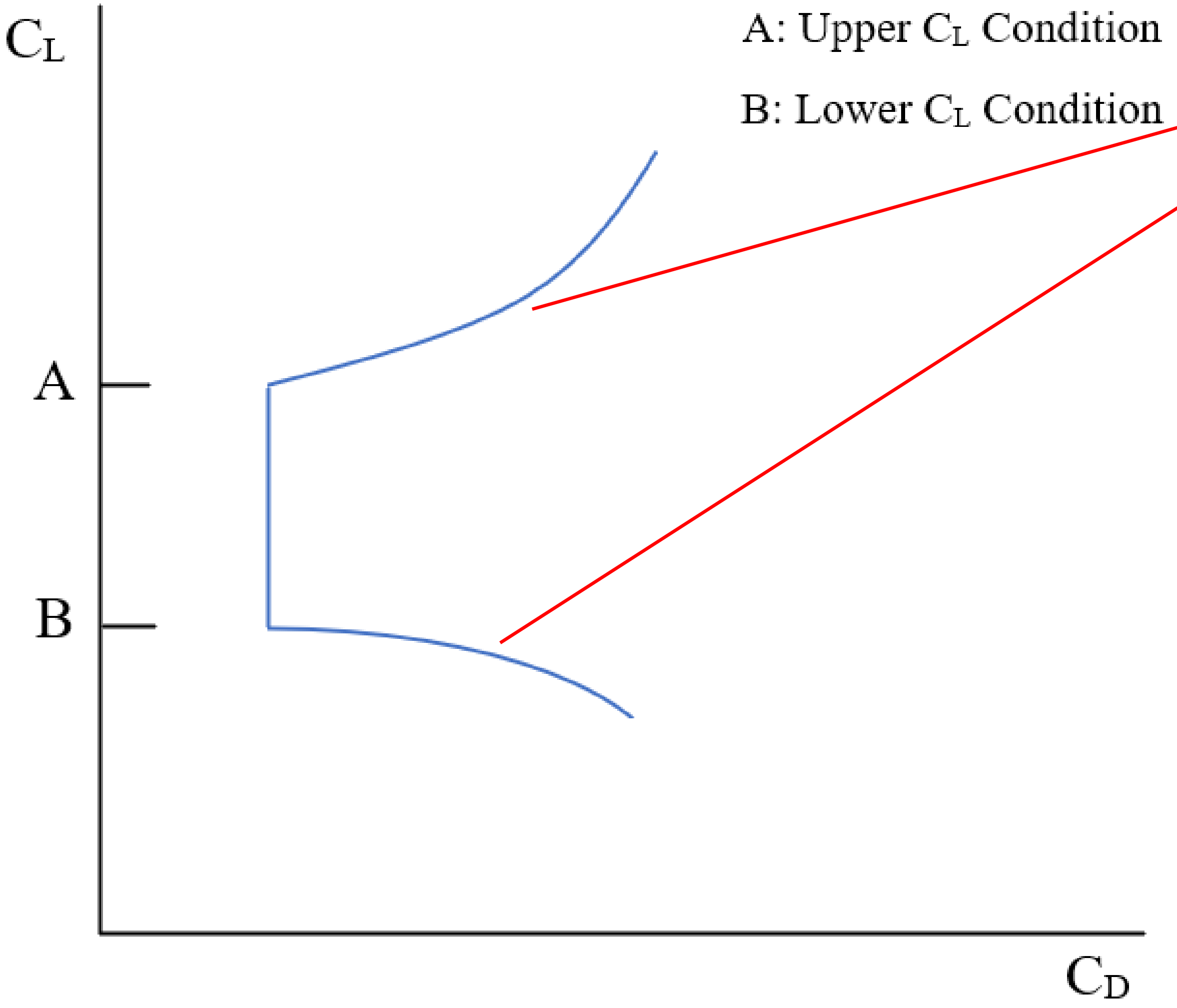

Beyond upper and lower C_L conditions, significant increase in drag is observed

Due to the movement of the boundary-layer transition line further upstream, resulting in increased turbulence

1.3 The S207 SNLF Airfoil and Relevant Configuration

- S207 is a 13.49%-thick SNLF airfoil designed for transonic transport applications [8,10]
  - Insensitive to roughness
  - Lower and upper C_L values predicted to be 0.37 and 0.74 for Cruise[10]

The S207 SNLF Airfoil

1.3 The S207 SNLF Airfoil and Relevant Configuration

- S207 is a 13.49%-thick SNLF airfoil designed for transonic transport applications [8,10]
  - Insensitive to roughness
  - Lower and upper C_L values predicted to be 0.37 and 0.74 for Cruise[10]

The S207 SNLF Airfoil

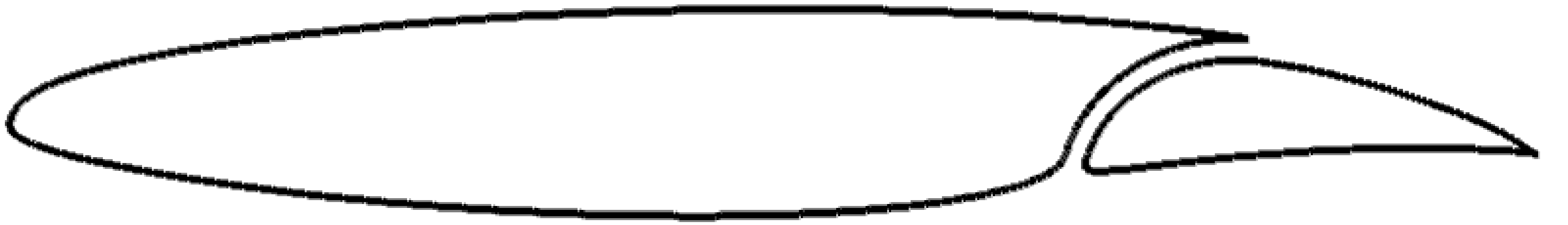

- Metrics derived from the Boeing Mach 0.745 Transonic Truss-Braced Wing (TTBW) aircraft [8]
  - Concept that utilizes a large aspect-ratio wing and was designed under the Subsonic Ultra Green Aircraft Research (SUGAR) initiative [11]
- Transition is expected to occur on the upper surface of the aft element near the trailing-edge [8]

1.3 The S207 SNLF Airfoil and Relevant Configuration

- Advanced Aerodynamic Design Center for Ultra-Efficient Commercial Vehicles
  - NASA funded University Leadership Initiative (ULI) led by University of Tennessee at Knoxville (UTK)
  - Focused on extensive analysis of a S207-based SNLF TTBW Vehicle with 70% reduction in fuel and energy burn compared to a 2005 baseline being the goal [12]
  - Already completed work demonstrates the superior performance of this vehicle in comparison to modern aircraft [13]

SNLF TTBW Aircraft Concept

2. Methodology

2.1 Predicting Transition

- Most modern-day transport aircraft today employ a high lift system
  - Main element, slat at the leading-edge, select number of trailing-edge flaps

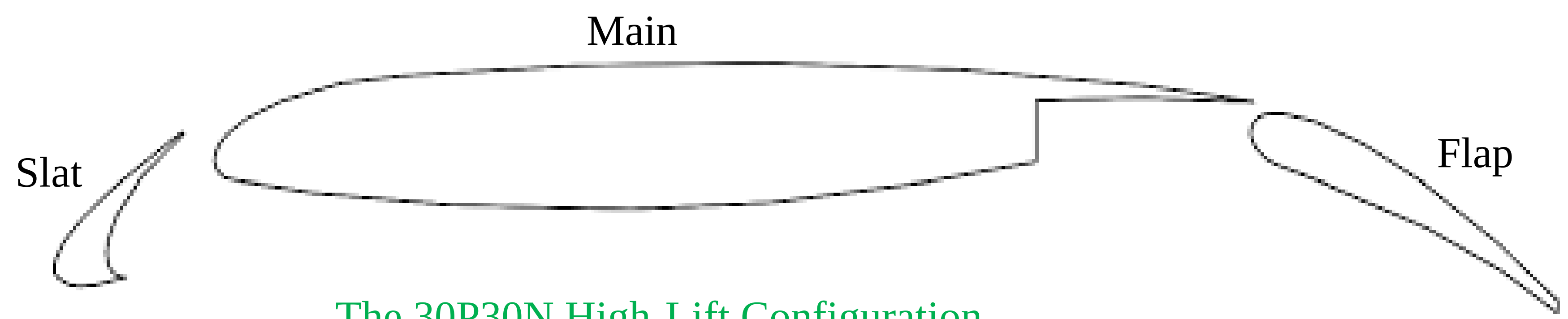

The 30P30N High-Lift Configuration

2.1 Predicting Transition

- Most modern-day transport aircraft today employ a high lift system
  - Main element, slat at the leading-edge, select number of trailing-edge flaps

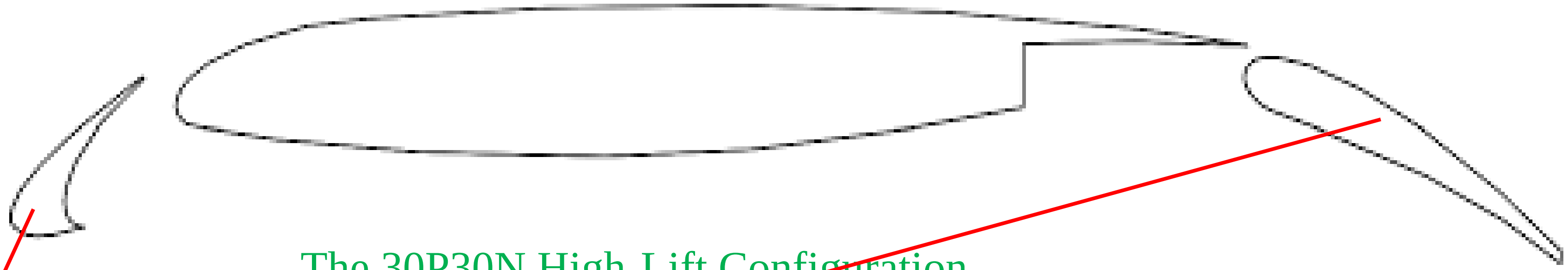

The 30P30N High-Lift Configuration

- Deployed during takeoff and landing to increase lift
- Stowed away during cruise to create a more streamlined airfoil shape

2.1 Predicting Transition

- Most modern-day transport aircraft today employ a high lift system
  - Main element, slat at the leading-edge, select number of trailing-edge flaps

The 30P30N High-Lift Configuration

- Deployed during takeoff and landing to increase lift
- Stowed away during cruise to create a more streamlined airfoil shape

- Retraction of slat produces a step geometry in the streamlined airfoil shape
- Transition is induced at the leading edge of the wing [7]
- Not compatible with laminar flow

2.1 Predicting Transition

- Most modern-day transport aircraft today employ a high lift system
  - Main element, slat at the leading-edge, select number of trailing-edge flaps

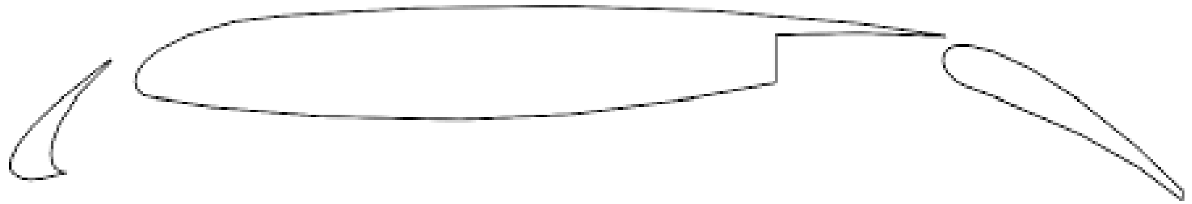

The 30P30N High-Lift Configuration

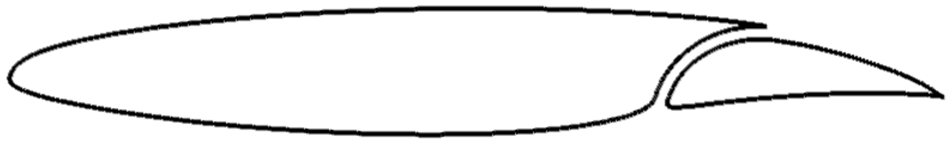

The S207 SNLF Airfoil

- Deployed during takeoff and landing to increase lift
- Stowed away during cruise to create a more streamlined airfoil shape

- Retraction of slat produces a step geometry in the streamlined airfoil shape
- Transition is induced at the leading edge of the wing [7]
- Not compatible with laminar flow

- Cannot use a slat with an SNLF airfoil
- Mostly laminar flow
- Turbulence is only expected on upper surface of aft element [8]

2.1 Predicting Transition

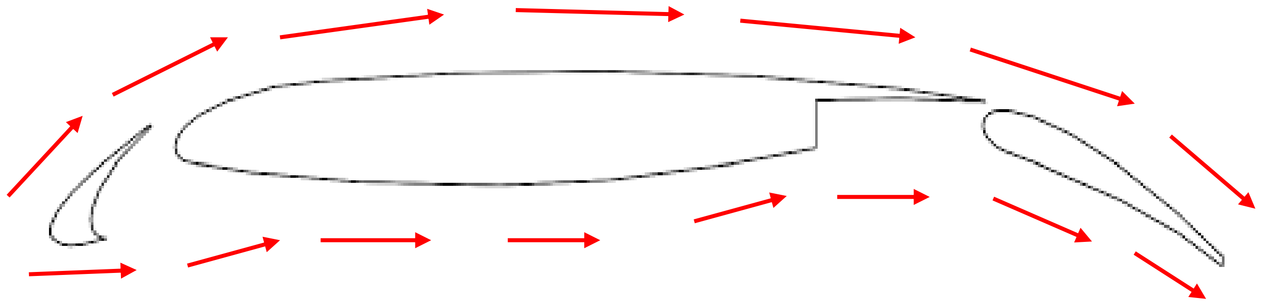

The 30P30N High-Lift Configuration

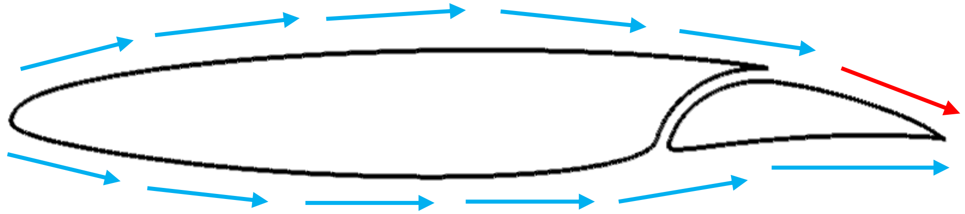

The S207 SNLF Airfoil

Flow is fully turbulent all around the shape of the airfoil

Laminar except for on upper surface of aft element (Theoretically)

2.1 Predicting Transition

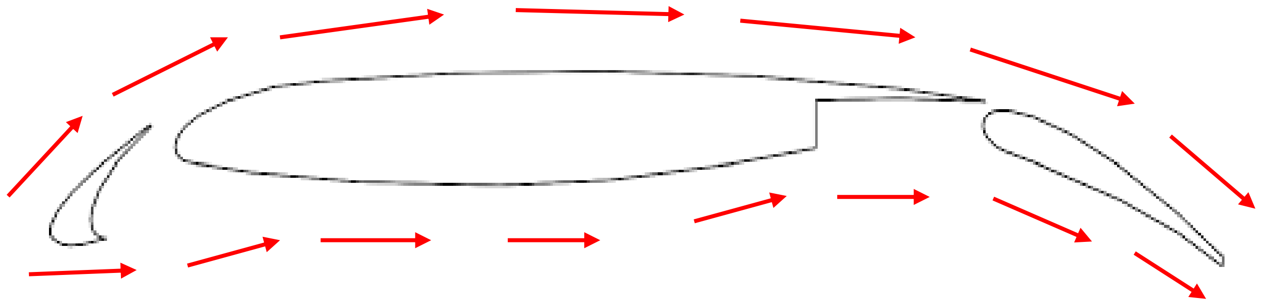

The 30P30N High-Lift Configuration

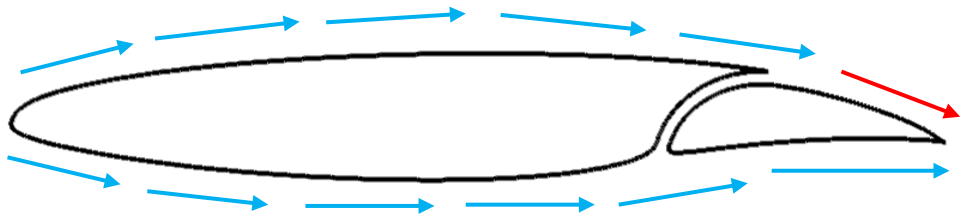

The S207 SNLF Airfoil

Flow is fully turbulent all around the shape of the airfoil

↓

Computationally analyzed with a turbulence model alone

Laminar except for on upper surface of aft element (Theoretically)

↓

Both a turbulence model and a transition prediction model is needed to analyze computationally (Free transition)

2.1 Predicting Transition

- This work concerns itself with two transition prediction models

Menter Single Equation Model [14]

2.1 Predicting Transition

- This work concerns itself with two transition prediction models

Menter Single Equation Model [14]

- Founded on the concept of Local-Correlation-based Transition Modeling (LCTM)
- Improvement on the γ-Re model [15,16]
  - Need for the Re equation is removed
- Exclusively dependent on the turbulence intermittency for triggering the transition from laminar to turbulent flow

2.1 Predicting Transition

- This work concerns itself with two transition prediction models

Menter Single Equation Model [14]

Two Equation Amplification Factor Transport Model (AFT2 or AFT2019) [17]

- Founded on the concept of Local-Correlation-based Transition Modeling (LCTM)
- Improvement on the γ-Re model [15,16]
  - Need for the Re equation is removed
- Exclusively dependent on the turbulence intermittency for triggering the transition from laminar to turbulent flow

2.1 Predicting Transition

- This work concerns itself with two transition prediction models

Menter Single Equation Model [14]	Two Equation Amplification Factor Transport Model (AFT2 or AFT2019) [17]
• Founded on the concept of Local-Correlation-based Transition Modeling (LCTM) • Improvement on the γ-Re model [15,16] • Need for the Re equation is removed • Exclusively dependent on the turbulence intermittency for triggering the transition from laminar to turbulent flow	• Founded on linear stability theory • Model computes progression of the amplification factor associated with streamwise instabilities • Coupled with an intermittency equation • Transition occurs once the maximum amplification ration of any instability in the boundary layer is reached, denoted as N_{crit} • N_{crit} can be computed from freestream turbulence intensity (Tu_{inf}) using Mack's relationship [17,18]

2.1 Predicting Transition

- This work concerns itself with two transition prediction models

Menter Single Equation Model [14]	Two Equation Amplification Factor Transport Model (AFT2 or AFT2019) [17]
• Founded on the concept of Local-Correlation-based Transition Modeling (LCTM) • Improvement on the γ-Re model [15,16] ◦ Need for the Re equation is removed • Exclusively dependent on the turbulence intermittency for triggering the transition from laminar to turbulent flow	• Founded on linear stability theory • Model computes progression of the amplification factor associated with streamwise instabilities • Coupled with an intermittency equation • Transition occurs once the maximum amplification ration of any instability in the boundary layer is reached, denoted as N_{crit} • N_{crit} can be computed from freestream turbulence intensity (Tu_{inf}) using Mack's relationship [17,18]

- Neither model considers impact of crossflow instabilities (Wing sweep > 15 degrees [8])
- SNLF wing analyzed under ULI efforts has a sweep of 12.5 degrees
  - Validates use of the models for this framework
- Implemented by Zhi Yang, who is a Research Scientist in the Mavriplis CFD Lab group [19]

2.2 Solvers

Two-Dimensional Analysis

Three-Dimensional Analysis

NSU2D [20]

2.2 Solvers

Two-Dimensional Analysis

Three-Dimensional Analysis

NSU2D [20]

- In house steady-state code that solves the compressible RANS equations in 2D
- Unstructured grids
- Nominally second-order accurate in space
- Efficient multigrid scheme to accelerate convergence
- Various other solver modules

2.2 Solvers

Two-Dimensional Analysis

Three-Dimensional Analysis

NSU2D [20]

- In house steady-state code that solves the compressible RANS equations in 2D
- Unstructured grids
- Nominally second-order accurate in space
- Efficient multigrid scheme to accelerate convergence
- Various other solver modules

- Various turbulence models available
  - Spalart-Allmaras turbulence model [21]
- Transition prediction
  - Coupled SA-AFT2 for free transition
  - N_{crit} is computed from an input of Tu_{inf}

2.2 Solvers

Two-Dimensional Analysis

Three-Dimensional Analysis

NSU2D [20]

- In house steady-state code that solves the compressible RANS equations in 2D
- Unstructured grids
- Nominally second-order accurate in space
- Efficient multigrid scheme to accelerate convergence
- Various other solver modules

- Various turbulence models available
  - Spalart-Allmaras turbulence model [21]
- Transition prediction
  - Coupled SA-AFT2 for free transition
  - N_{crit} is computed from an input of Tu_{inf}

- Grids generated with UMESH2D [22]

2.2 Solvers

Two-Dimensional Analysis

NSU2D [20]

- In house steady-state code that solves the compressible RANS equations in 2D
- Unstructured grids
- Nominally second-order accurate in space
- Efficient multigrid scheme to accelerate convergence
- Various other solver modules

- Various turbulence models available
    - Spalart-Allmaras turbulence model [21]
- Transition prediction
    - Coupled SA-AFT2 for free transition
    - N_{crit} is computed from an input of Tu_{inf}

- Grids generated with UMESH2D [22]

Three-Dimensional Analysis

NSU3D [23]

2.2 Solvers

Two-Dimensional Analysis

NSU2D [20]

- In house steady-state code that solves the compressible RANS equations in 2D
- Unstructured grids
- Nominally second-order accurate in space
- Efficient multigrid scheme to accelerate convergence
- Various other solver modules

- Various turbulence models available
    - Spalart-Allmaras turbulence model [21]
- Transition prediction
    - Coupled SA-AFT2 for free transition
    - N_{crit} is computed from an input of Tu_{inf}

- Grids generated with UMESH2D [22]

Three-Dimensional Analysis

NSU3D [23]

- In house steady-state code that solves the compressible RANS equations in 3D
- Unstructured, hybrid grids
- Extends accuracy and solver modules of NSU2D to 3D
- Extensively validated [24-26]

2.2 Solvers

Two-Dimensional Analysis

NSU2D [20]

- In house steady-state code that solves the compressible RANS equations in 2D
- Unstructured grids
- Nominally second-order accurate in space
- Efficient multigrid scheme to accelerate convergence
- Various other solver modules

- Various turbulence models available
  - Spalart-Allmaras turbulence model [21]
- Transition prediction
  - Coupled SA-AFT2 for free transition
  - N_{crit} is computed from an input of Tu_{inf}

- Grids generated with UMESH2D [22]

Three-Dimensional Analysis

NSU3D [23]

- In house steady-state code that solves the compressible RANS equations in 3D
- Unstructured, hybrid grids
- Extends accuracy and solver modules of NSU2D to 3D
- Extensively validated [24-26]

- Various turbulence models available
  - SA Turbulence model
- Transition prediction
  - Coupled SA-AFT2 or SA-Menter
  - N_{crit} computed from Tu_{inf}, or input directly

2.2 Solvers

Two-Dimensional Analysis

NSU2D [20]

- In house steady-state code that solves the compressible RANS equations in 2D
- Unstructured grids
- Nominally second-order accurate in space
- Efficient multigrid scheme to accelerate convergence
- Various other solver modules

- Various turbulence models available
    - Spalart-Allmaras turbulence model [21]
- Transition prediction
    - Coupled SA-AFT2 for free transition
    - N_{crit} is computed from an input of Tu_{inf}

- Grids generated with UMESH2D [22]

Three-Dimensional Analysis

NSU3D [23]

- In house steady-state code that solves the compressible RANS equations in 3D
- Unstructured, hybrid grids
- Extends accuracy and solver modules of NSU2D to 3D
- Extensively validated [24-26]

- Various turbulence models available
    - SA Turbulence model
- Transition prediction
    - Coupled SA-AFT2 or SA-Menter
    - N_{crit} computed from Tu_{inf}, or input directly

- Grids generated with Pointwise at UTK [22]

2.3 Validation Efforts

- Validation of the solver transition prediction models performed under ULI and reproduced in this work [27]

Results for the S204 Airfoil [28] at Mach =0.5 , Re = 12 Million, Tu_{inf} = 0.07 % (Ncrit = 9.0)

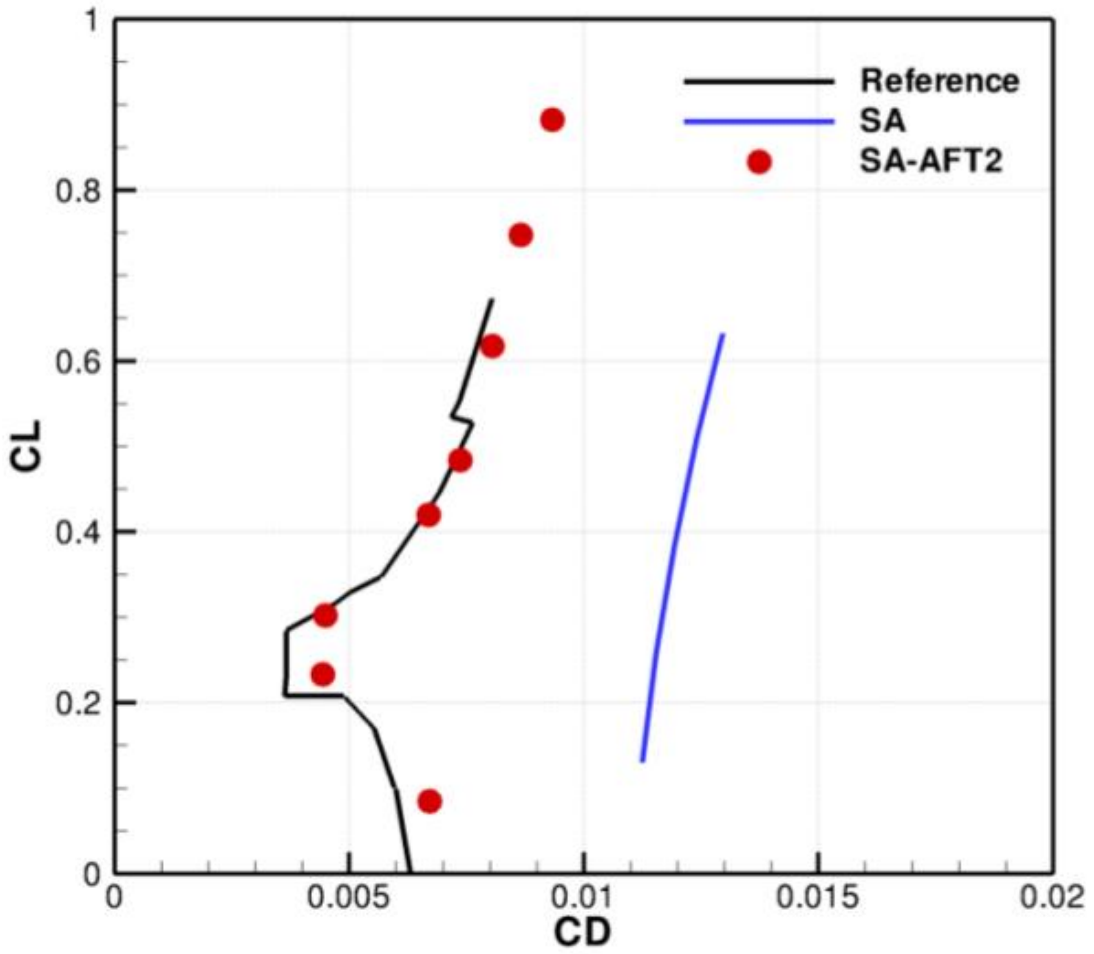

Results for Upper Surface of the TU Braunschweig [29] Sickle Wing at AOA = -2.6, Re = 2.5 Million

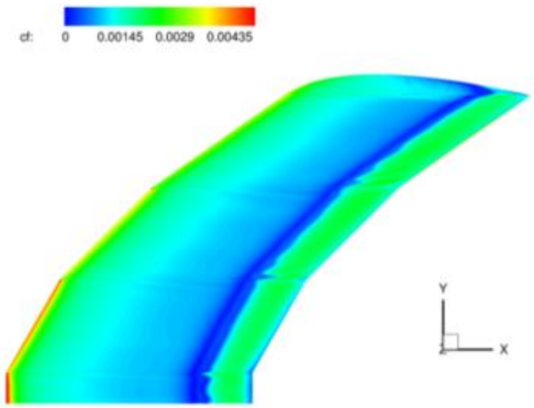

NSU3D-SA-AFT2

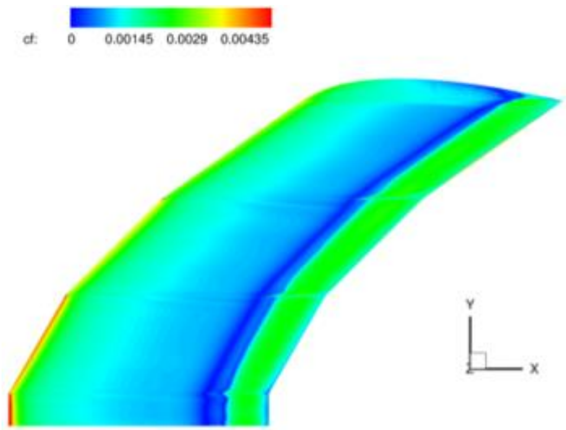

NSU3D-SA-Menter

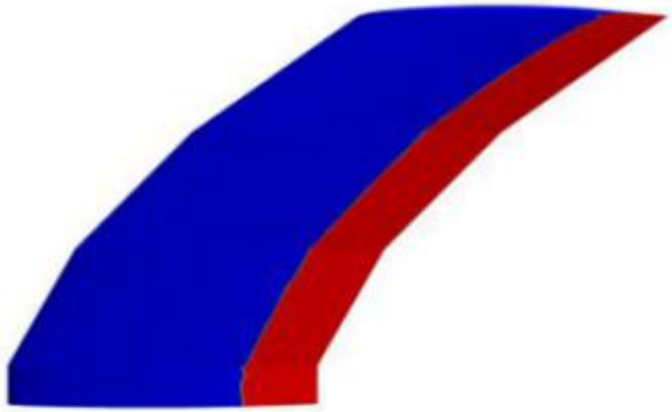

OVERFLOW-SA-AFT2 [17]

3. 2D Analysis of the S207 SNLF Airfoil

3.1 Computational Mesh for the S207 Airfoil Analysis

- Unstructured mesh was generated for the S207 SNLF Airfoil using UMESH2D
    - Part of the NSU2D software package

S207 SNLF Airfoil grid

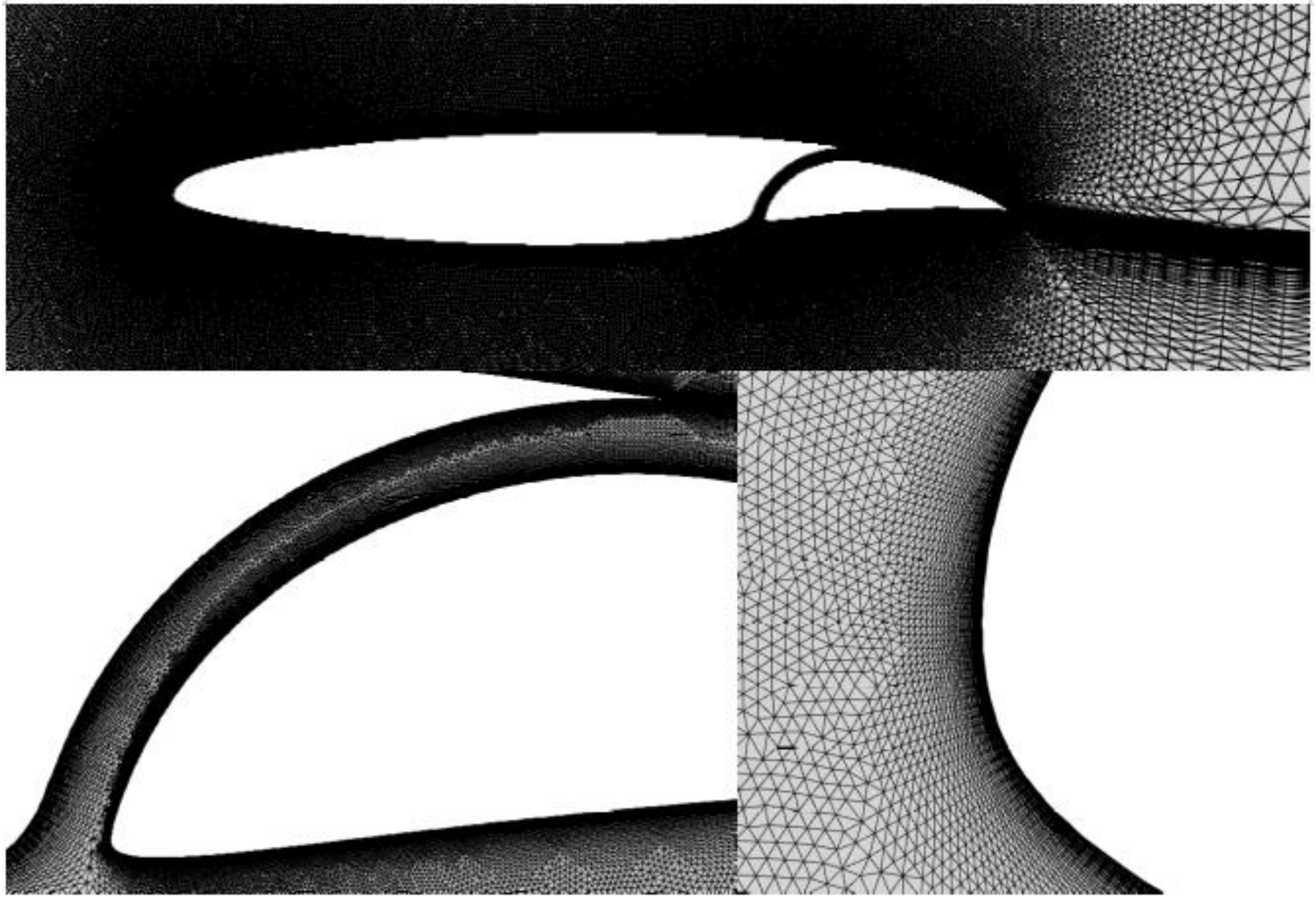

3.1 Computational Mesh for the S207 Airfoil Analysis

- Unstructured mesh was generated for the S207 SNLF Airfoil using UMESH2D
  - Part of the NSU2D software package

S207 SNLF Airfoil grid

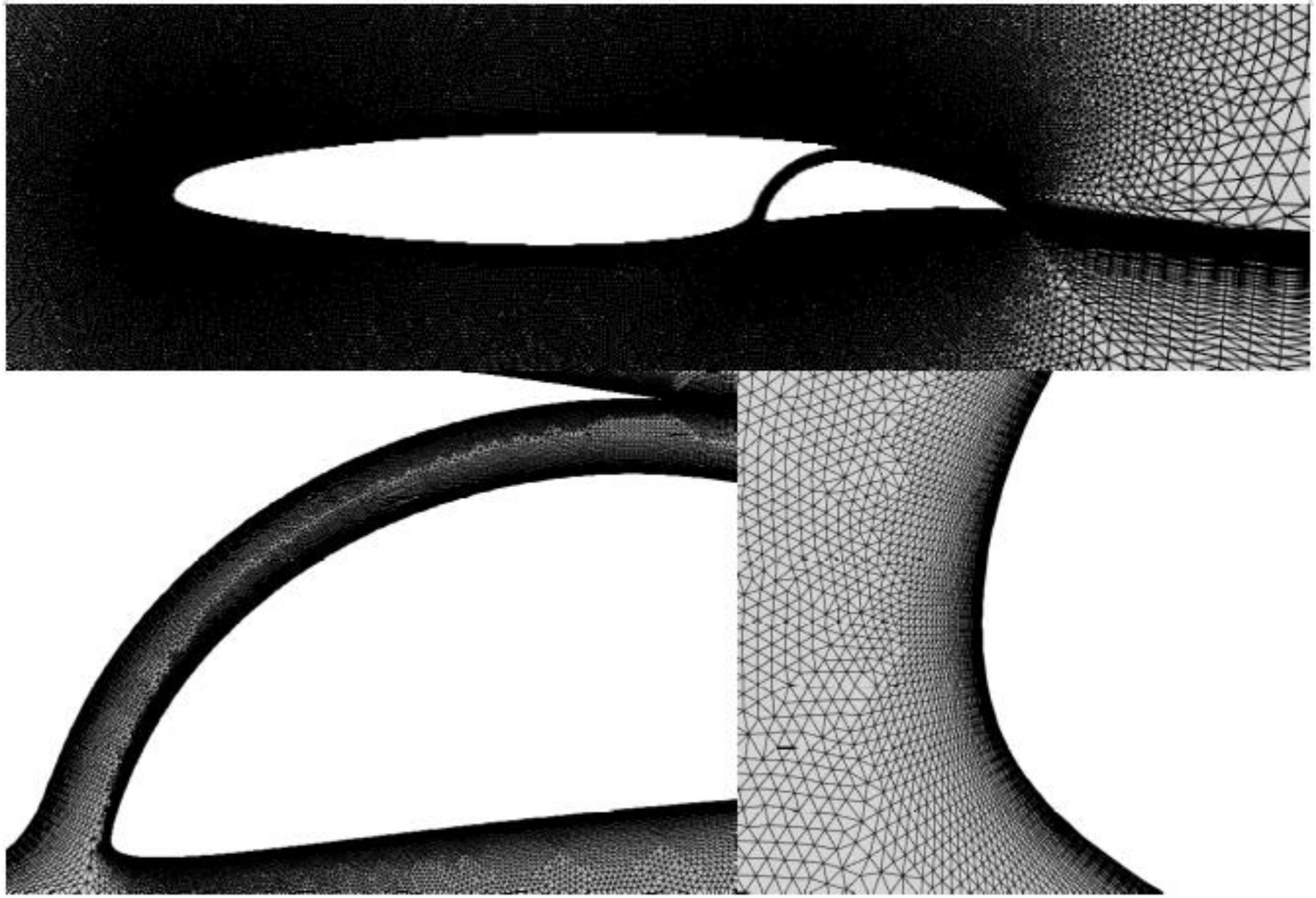

- Consists of 689326 triangular cells
- Far field boundaries are 1000 chord lengths away

3.1 Computational Mesh for the S207 Airfoil Analysis

- Unstructured mesh was generated for the S207 SNLF Airfoil using UMESH2D
  - Part of the NSU2D software package

S207 SNLF Airfoil grid

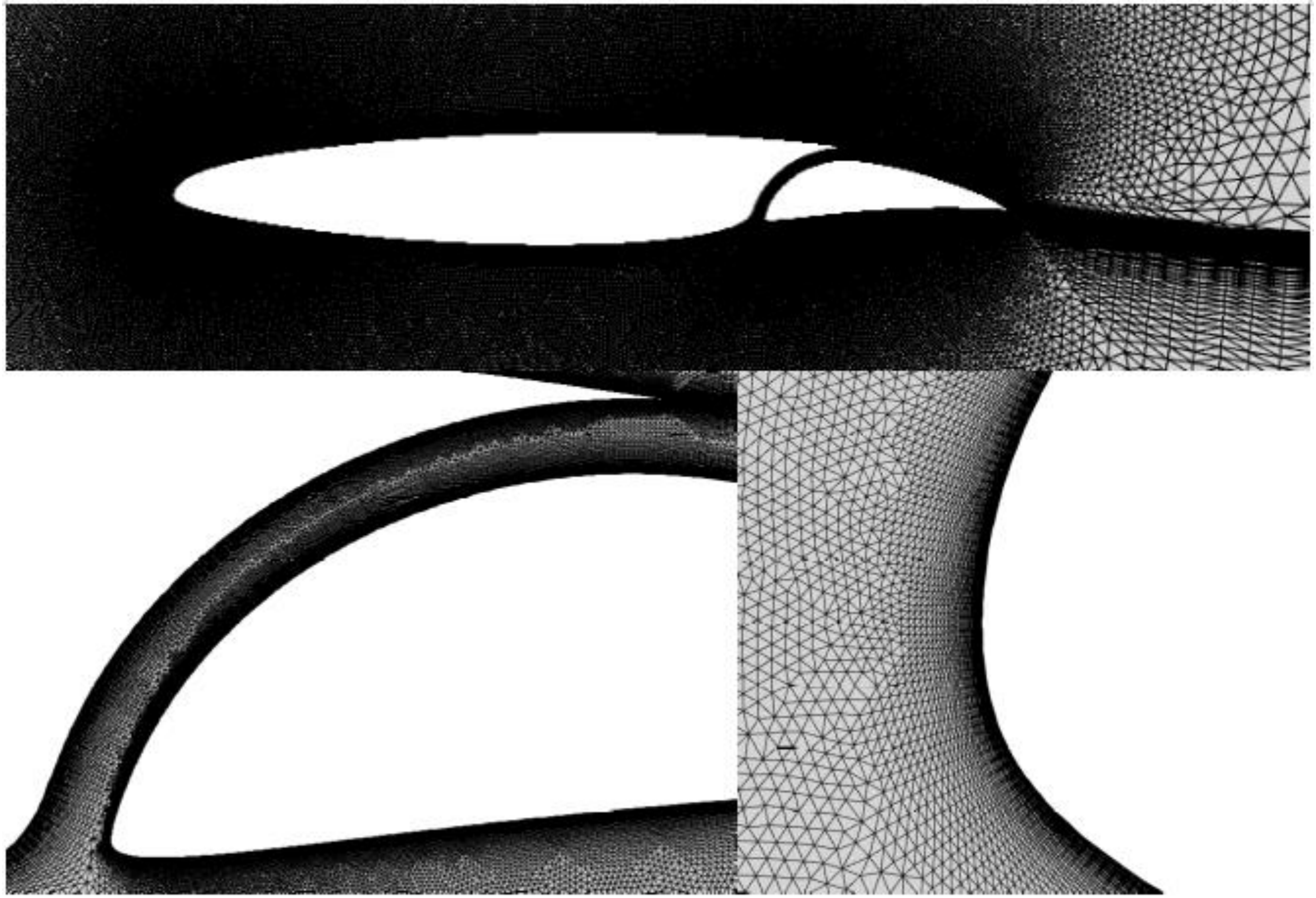

- Consists of 689326 triangular cells
- Far field boundaries are 1000 chord lengths away

- Both fore and aft elements have 2000 surface points
- Streamwise spacing at LE and TE is 0.02% chord length
- Normal wall-spacing for both element is set to 10^{-6}

3.1 Computational Mesh for the S207 Airfoil Analysis

- Unstructured mesh was generated for the S207 SNLF Airfoil using UMESH2D
  - Part of the NSU2D software package

S207 SNLF Airfoil grid

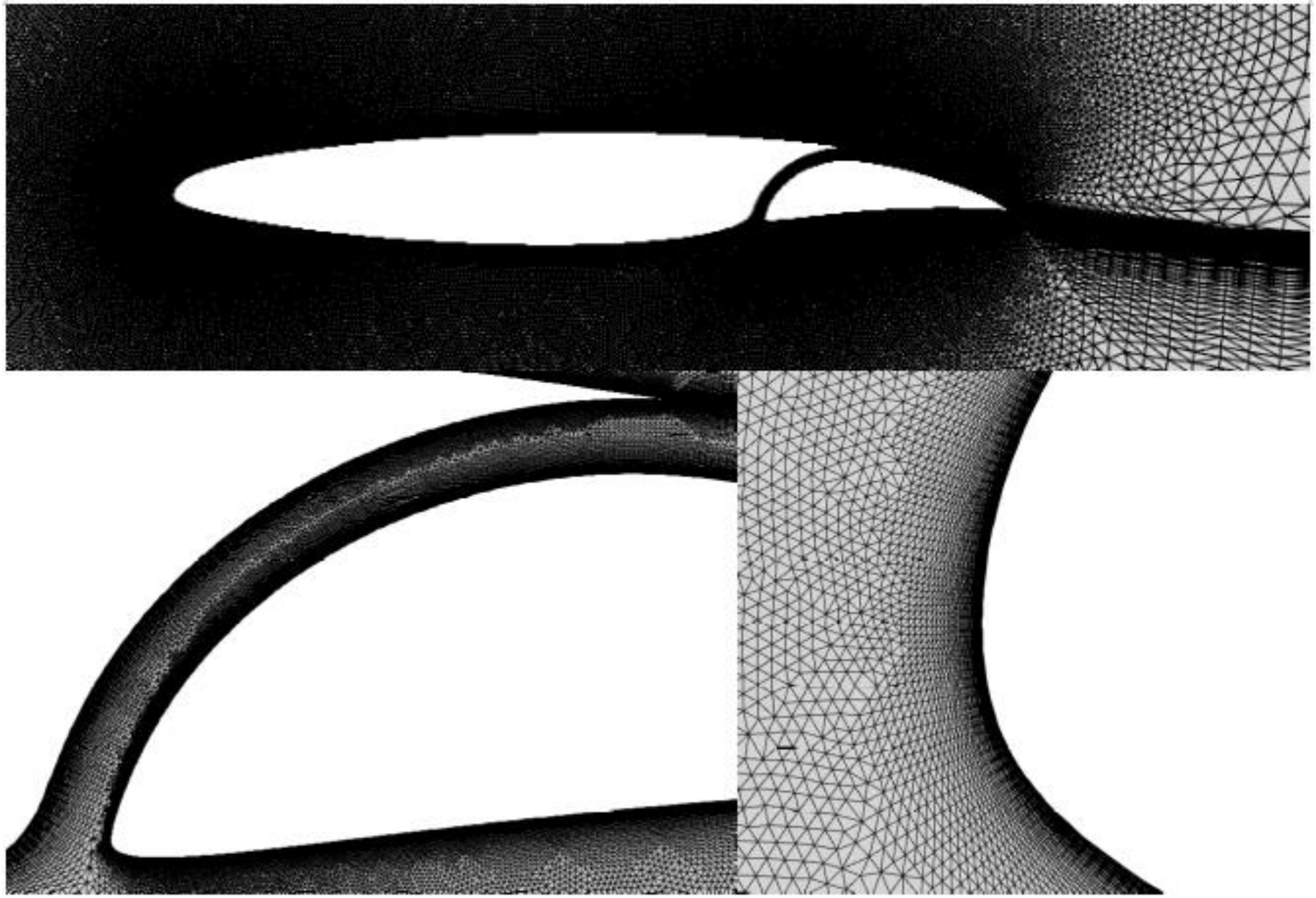

- Consists of 689326 triangular cells
- Far field boundaries are 1000 chord lengths away

- Both fore and aft elements have 2000 surface points
- Streamwise spacing at LE and TE is 0.02% chord length
- Normal wall-spacing for both element is set to 10^{-6}

- Growth rate of cells nearest the wing body set to 1.1 to capture expected thin laminar boundary layer

3.2 Simulations at Cruise

- Nominal angles of attack for the S207 airfoil are predominantly negative [10]
  - Mach = 0.7, AOA=-1.3°, Re=13.2 Million selected for establishing correspondence between NSU2D and original S207 Airfoil design report

S207 Airfoil Simulations Performed at Cruise

Simulation	Modeling	Cycles	Tu_∞	Trans. Freeze	Initial Condition
Run 0	SA	10000	NA	NA	Freestream
Run 1	SA-AFT2	10000	0.001%	3250	Run A
Run 2	SA-AFT2	20000	0.07%	3250	Run A

3.2 Simulations at Cruise

- Nominal angles of attack for the S207 airfoil are predominantly negative [10]
  - Mach = 0.7, AOA=-1.3°, Re=13.2 Million selected for establishing correspondence between NSU2D and original S207 Airfoil design report

S207 Airfoil Simulations Performed at Cruise

Simulation	Modeling	Cycles	Tu_∞	Trans. Freeze	Initial Condition
Run 0	SA	10000	NA	NA	Freestream
Run 1	SA-AFT2	10000	0.001%	3250	Run A
Run 2	SA-AFT2	20000	0.07%	3250	Run A

- Run 0: Fully turbulent simulation for comparison to free transition results, establish convergence prior to free transition

3.2 Simulations at Cruise

- Nominal angles of attack for the S207 airfoil are predominantly negative [10]
  - Mach = 0.7, AOA=-1.3°, Re=13.2 Million selected for establishing correspondence between NSU2D and original S207 Airfoil design report

S207 Airfoil Simulations Performed at Cruise

Simulation	Modeling	Cycles	Tu_{∞}	Trans. Freeze	Initial Condition
Run 0	SA	10000	NA	NA	Freestream
Run 1	SA-AFT2	10000	0.001%	3250	Run A
Run 2	SA-AFT2	20000	0.07%	3250	Run A

- Run 0: Fully turbulent simulation for comparison to free transition results, establish convergence prior to free transition
- Run 1: First successful free transitional run, freestream turbulence value is unrealistic

3.2 Simulations at Cruise

- Nominal angles of attack for the S207 airfoil are predominantly negative [10]
  - Mach = 0.7, AOA=-1.3°, Re=13.2 Million selected for establishing correspondence between NSU2D and original S207 Airfoil design report

S207 Airfoil Simulations Performed at Cruise

Simulation	Modeling	Cycles	Tu_∞	Trans. Freeze	Initial Condition
Run 0	SA	10000	NA	NA	Freestream
Run 1	SA-AFT2	10000	0.001%	3250	Run A
Run 2	SA-AFT2	20000	0.07%	3250	Run A

- Run 0: Fully turbulent simulation for comparison to free transition results, establish convergence prior to free transition
- Run 1: First successful free transitional run, freestream turbulence value is unrealistic
- Run 2: Free transitional run with a more realistic freestream turbulence value

3.2 Simulations at Cruise

NSU2D Results Compared to Original Design Data [8] for Mach = 0.7, Re = 13.2 Million, AOA= -1.3°

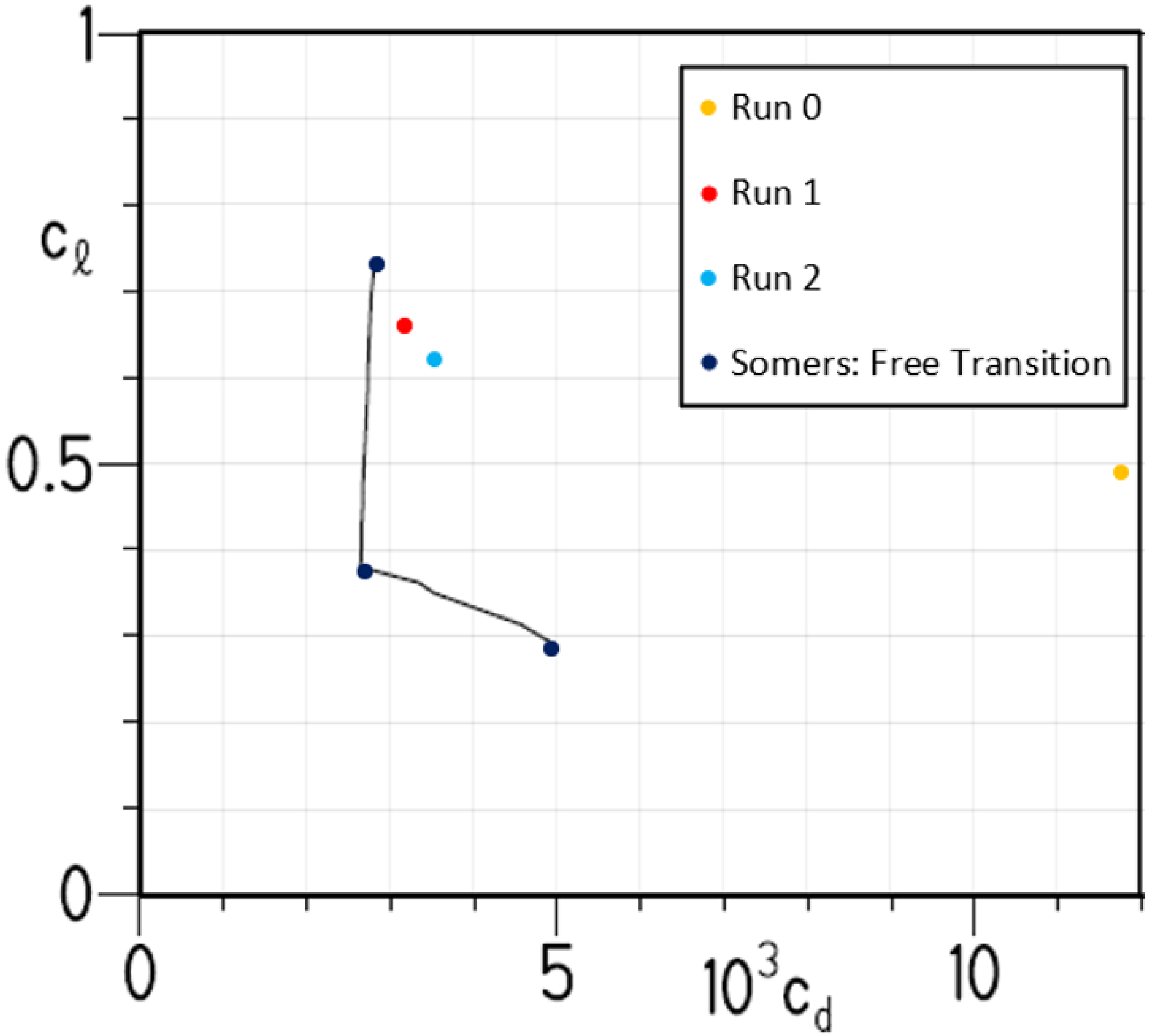

3.2 Simulations at Cruise

NSU2D Results Compared to Original Design Data [8] for Mach = 0.7, Re = 13.2 Million, AOA= -1.3°

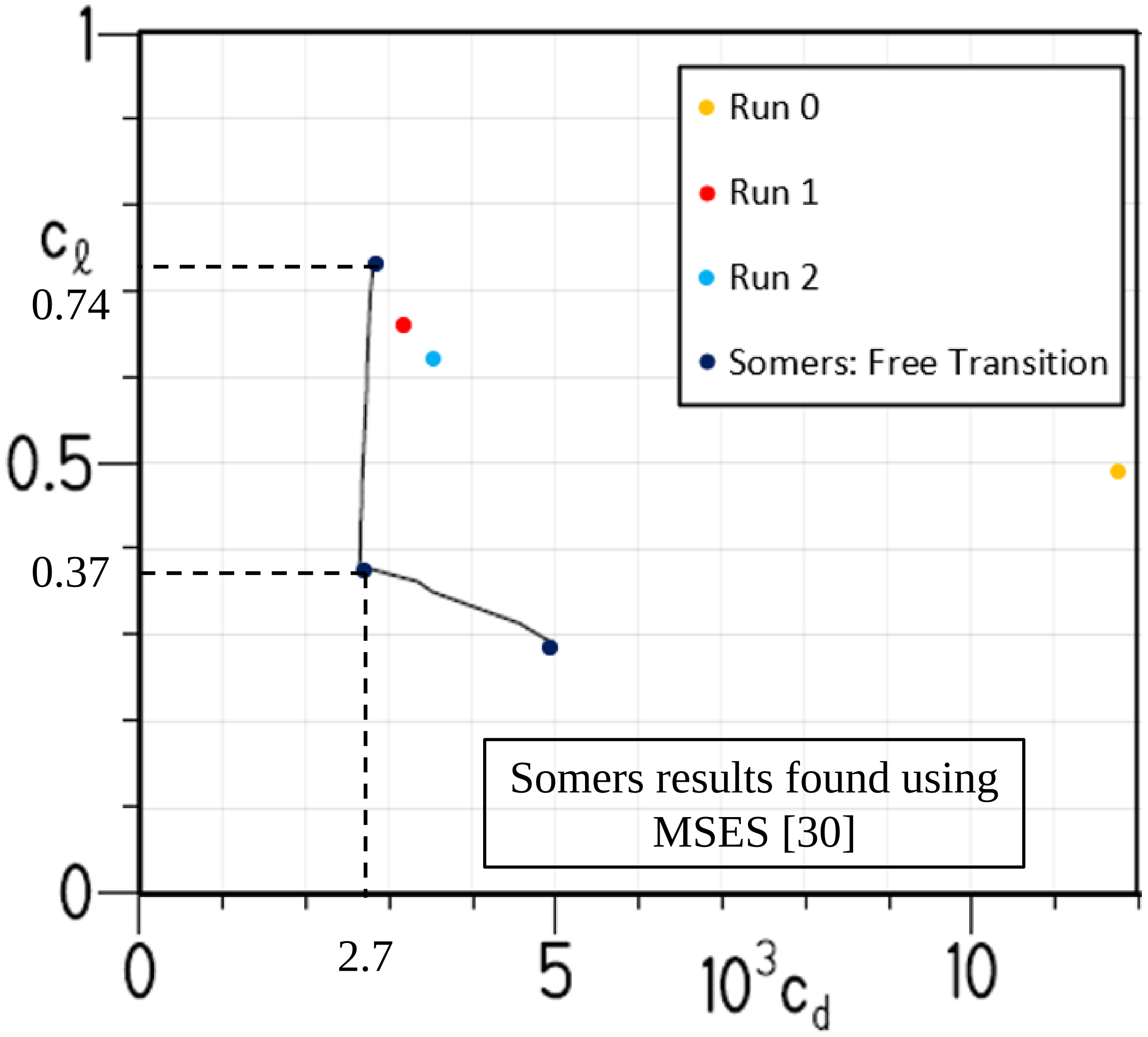

3.2 Simulations at Cruise

NSU2D Results Compared to Original Design Data [8] for Mach = 0.7, Re = 13.2 Million, AOA= -1.3°

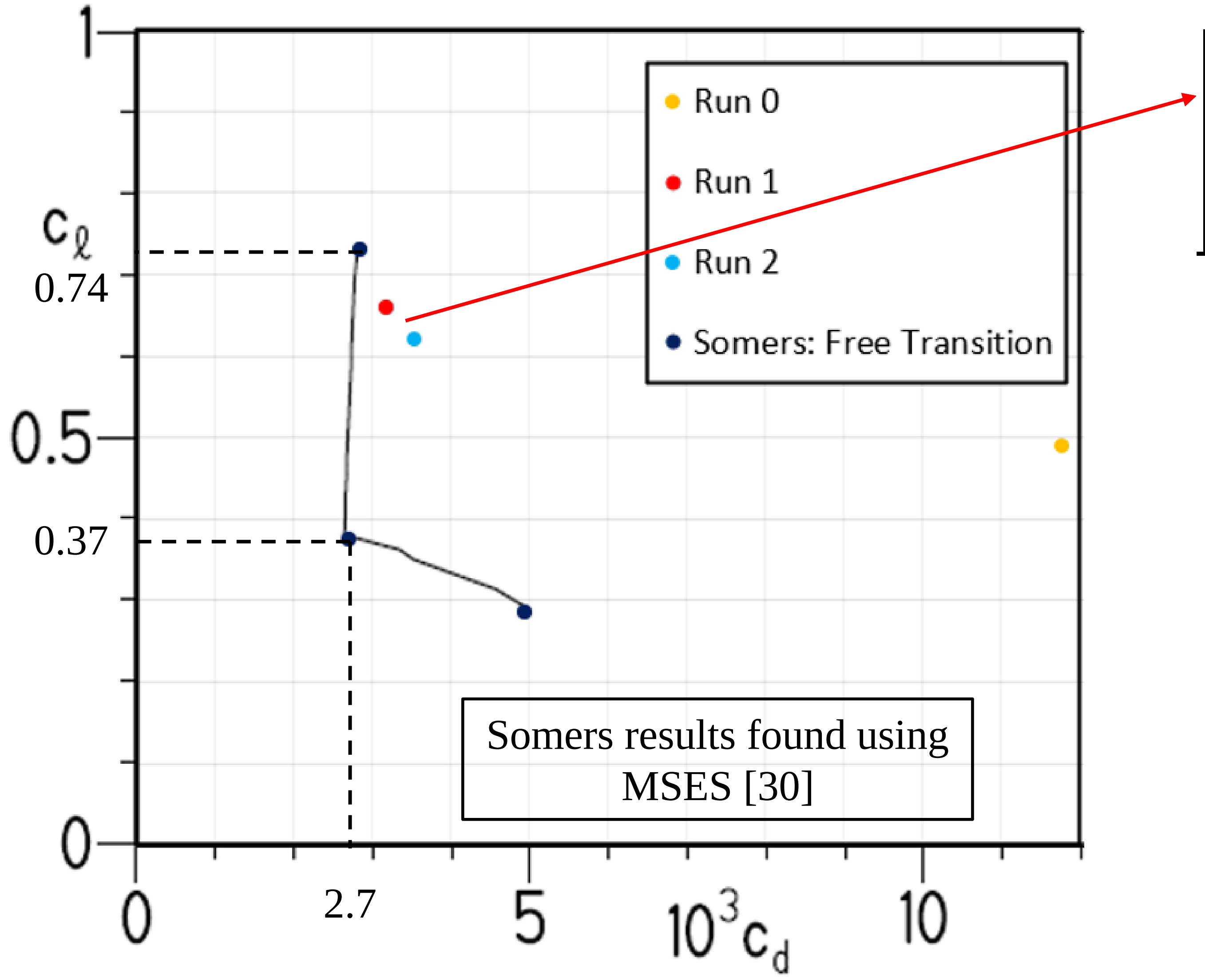

Run	C_L	C_D
0	0.488	0.0118
1	0.658	0.0032
2	0.620	0.0035

At most NSU2D-SA-AFT2 predicts 6 counts of drag more, and lift values are slightly lower than low drag bucket

3.2 Simulations at Cruise

NSU2D Results Compared to Original Design Data [8] for Mach = 0.7, Re = 13.2 Million, AOA= -1.3°

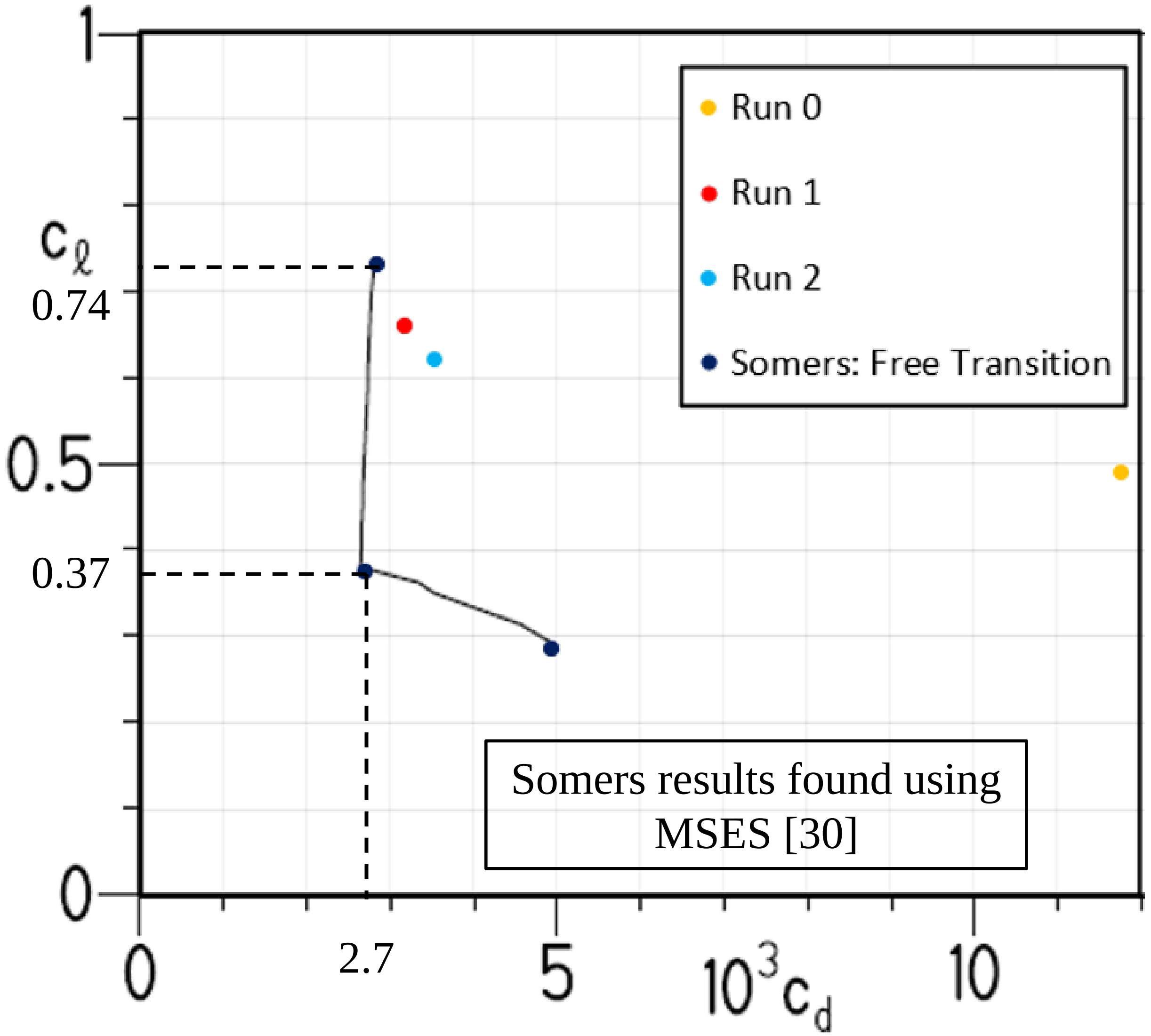

Run	C_L	C_D
0	0.488	0.0118
1	0.658	0.0032
2	0.620	0.0035

At most NSU2D-SA-AFT2 predicts 6 counts of drag more, and lift values are slightly lower than low drag bucket

2D Results agree well with MSES design metrics [8]

3.2 Simulations at Cruise

NSU2D Results Compared to Original Design Data [8] for Mach = 0.7, Re = 13.2 Million, AOA= -1.3°

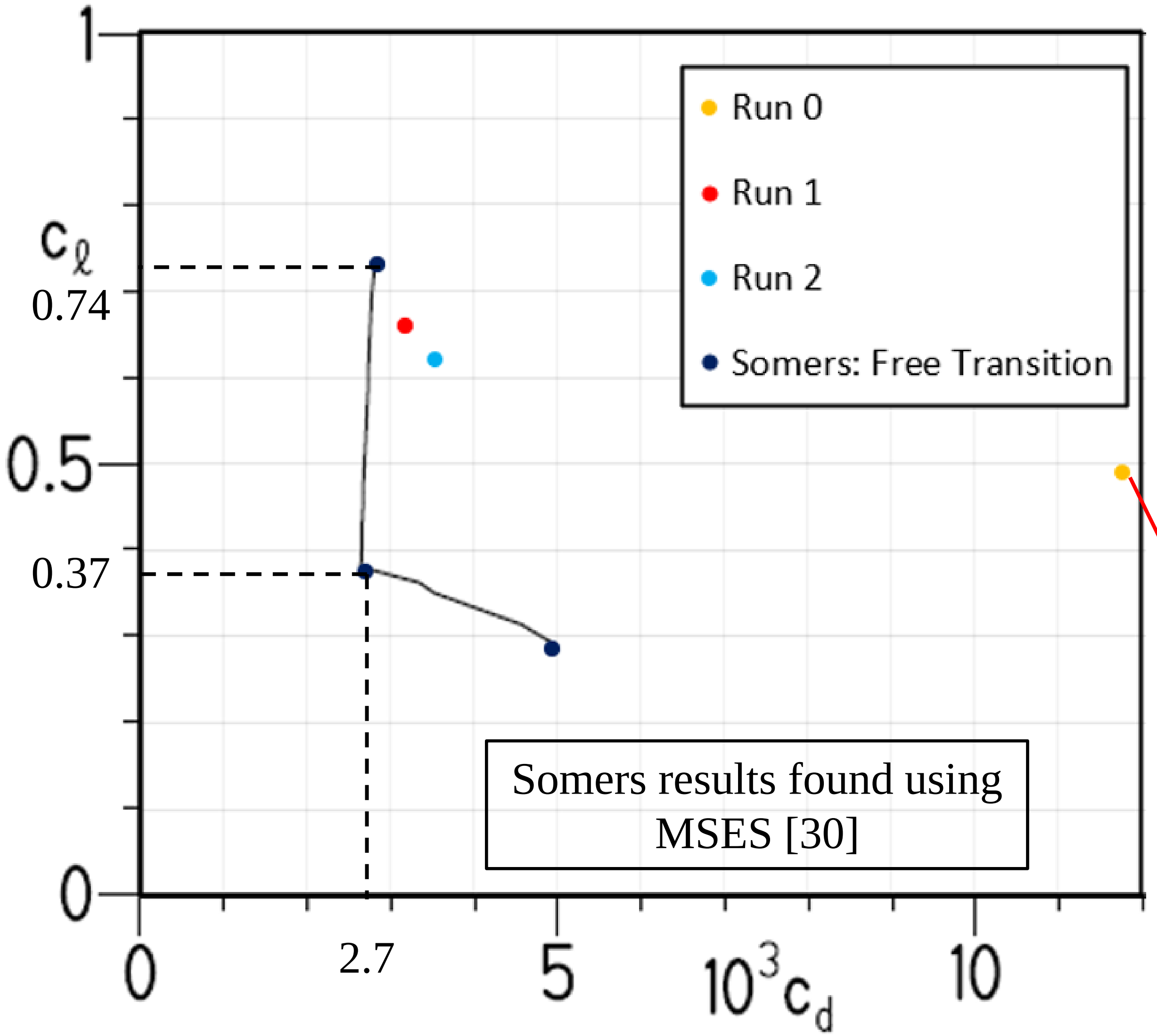

Run	C_L	C_D
0	0.488	0.0118
1	0.658	0.0032
2	0.620	0.0035

At most NSU2D-SA-AFT2 predicts 6 counts of drag more, and lift values are slightly lower than low drag bucket

2D Results agree well with MSES design metrics [8]

Differences between fully turbulent results and free transition results emphasize the usefulness of CFD in quantifying laminar flow

3.2 Simulations at Cruise

- The location of transition can be identified exactly through examination of skin friction drag profiles

Skin Friction Drag Profiles for S207 Fore Element at Mach = 0.7, Re = 13.2 Million, AOA = -1.3°

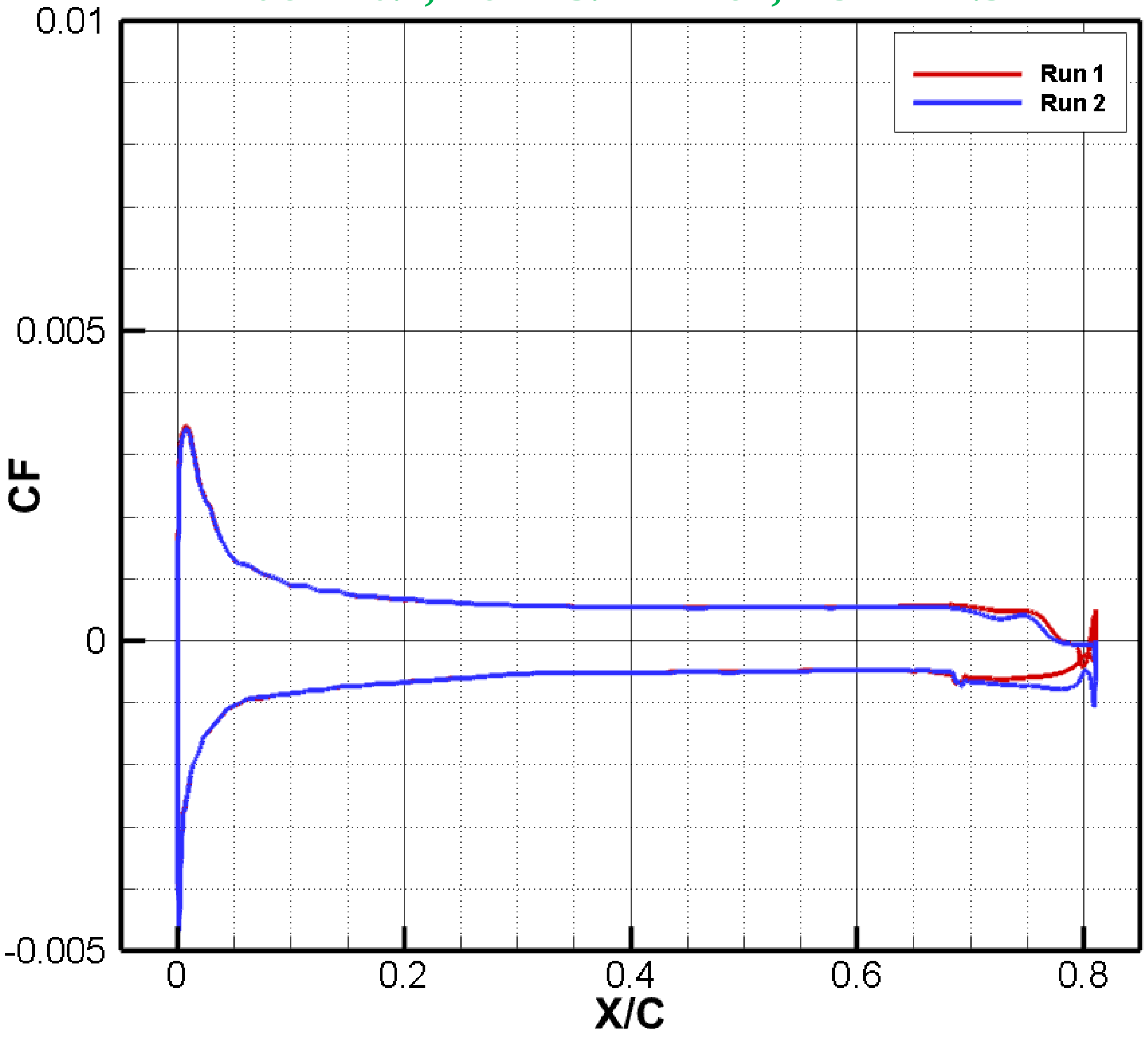

Skin Friction Drag Profiles for S207 Aft Element at Mach = 0.7, Re = 13.2 Million, AOA = -1.3°

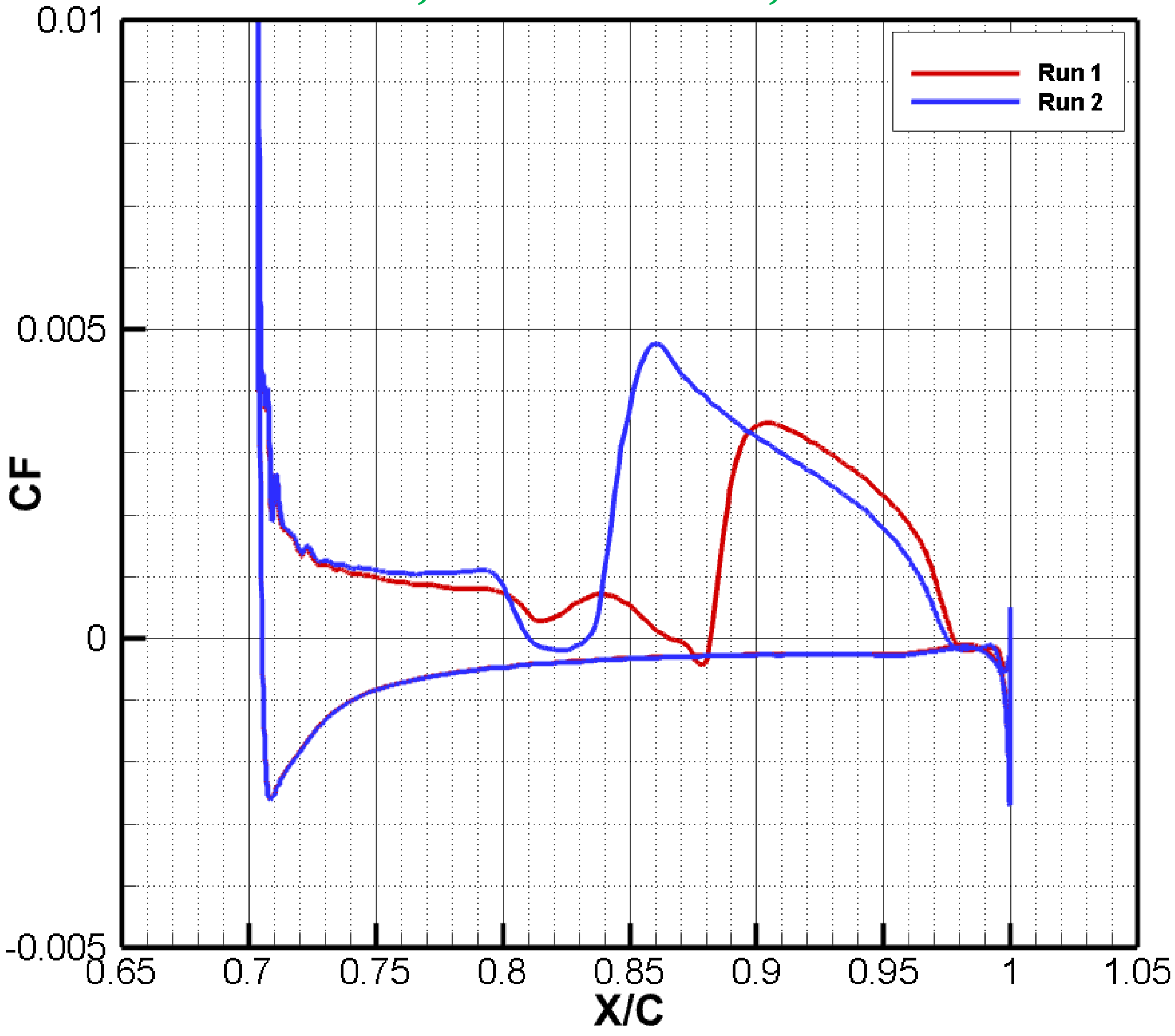

3.2 Simulations at Cruise

Note that –Cf is plotted on lower surface by convention

- The location of transition can be identified exactly through examination of skin friction drag profiles

Skin Friction Drag Profiles for S207 Fore Element at Mach = 0.7, Re = 13.2 Million, AOA = -1.3°

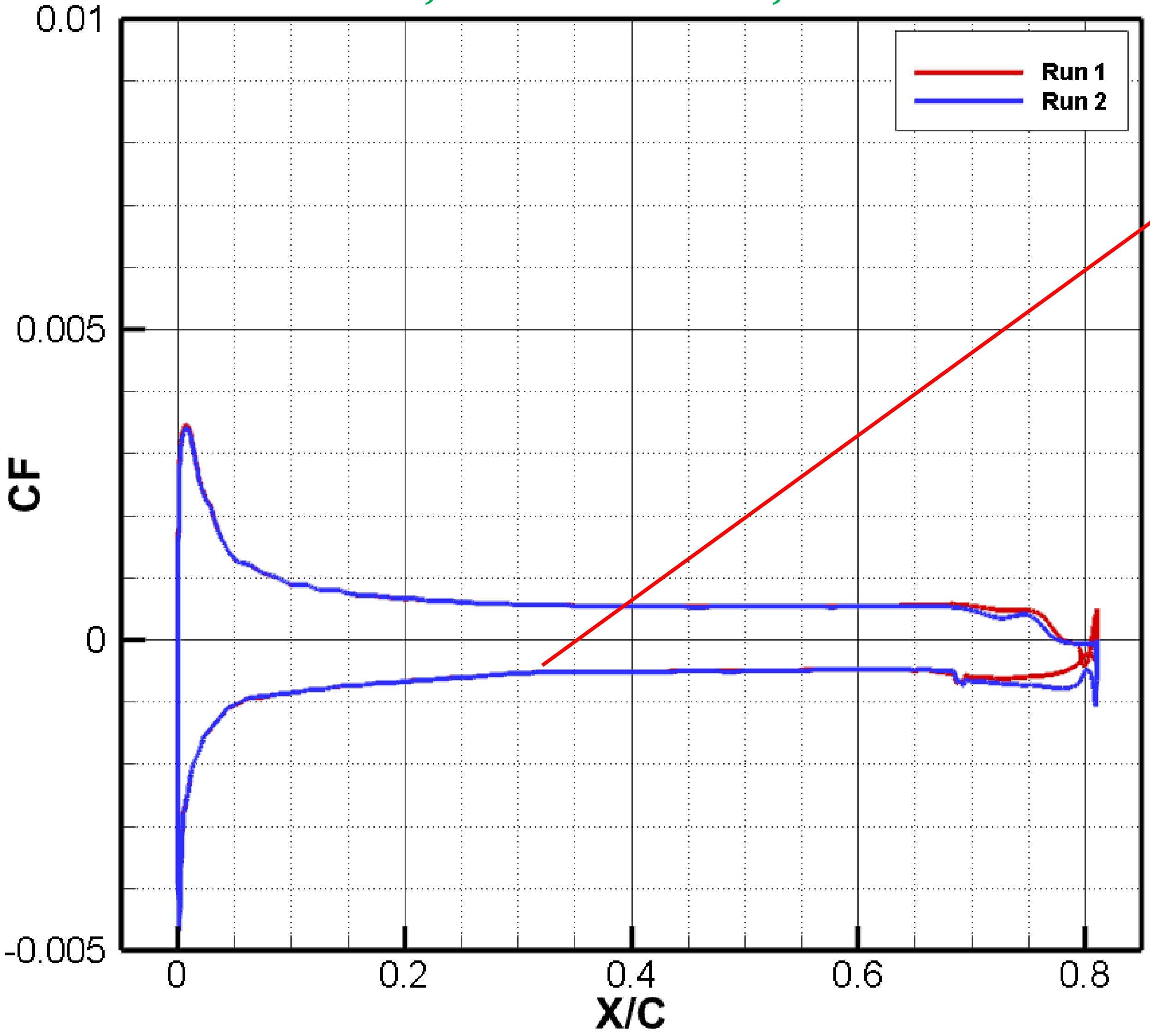

Skin Friction Drag Profiles for S207 Aft Element at Mach = 0.7, Re = 13.2 Million, AOA = -1.3°

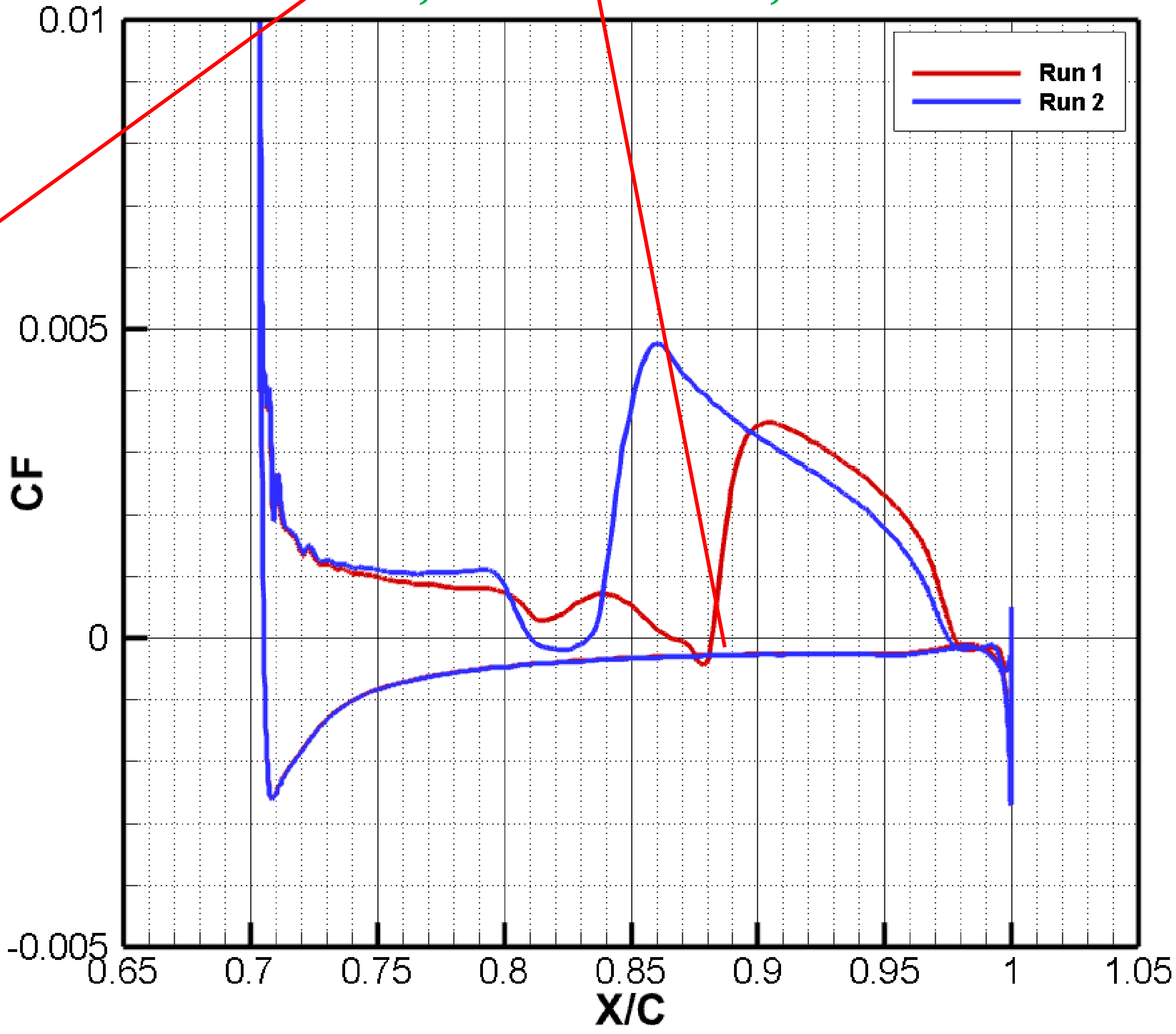

3.2 Simulations at Cruise

Note that –Cf is plotted on lower surface by convention

- The location of transition can be identified exactly through examination of skin friction drag profiles

Skin Friction Drag Profiles for S207 Fore Element at Mach = 0.7, Re = 13.2 Million, AOA = -1.3°

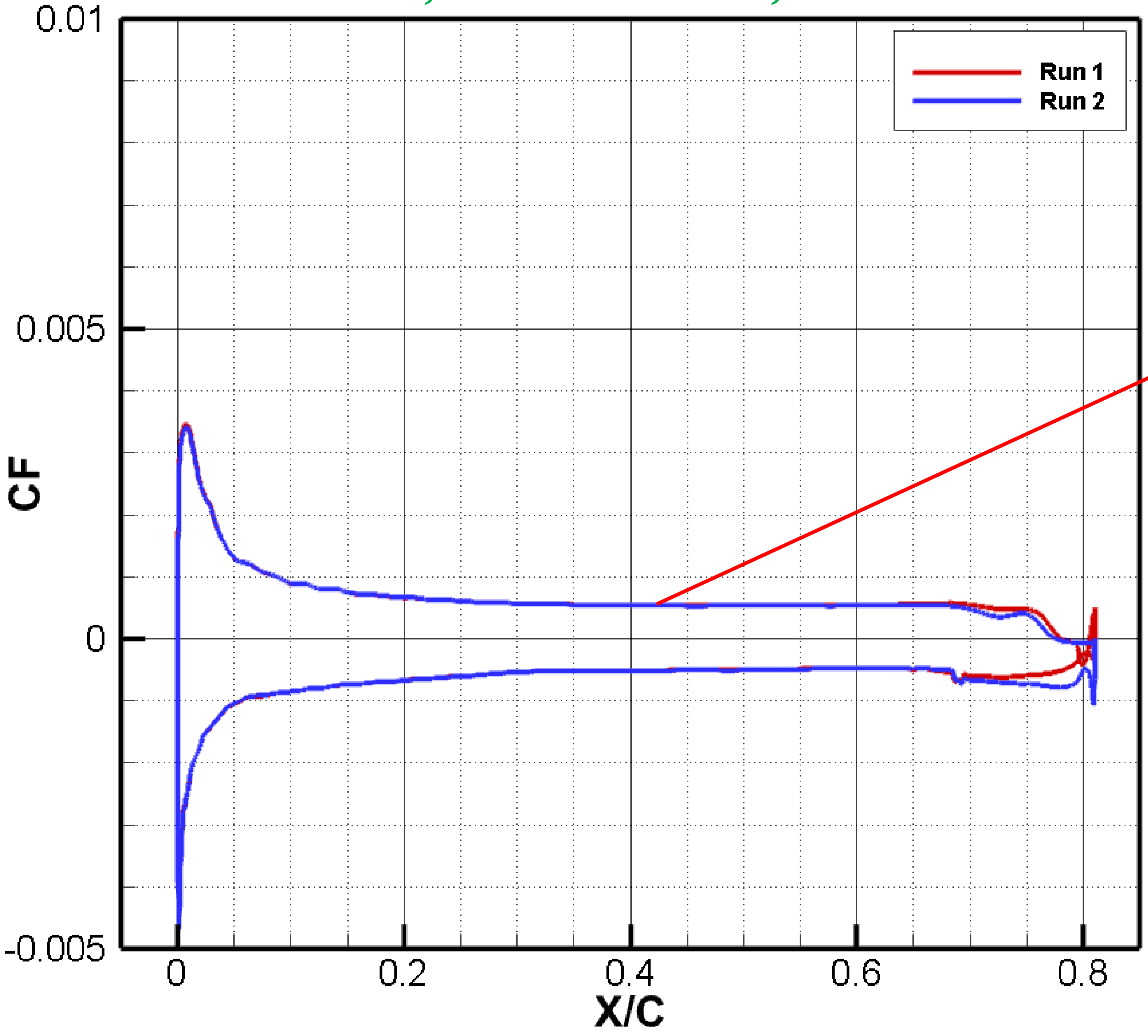

Skin Friction Drag Profiles for S207 Aft Element at Mach = 0.7, Re = 13.2 Million, AOA = -1.3°

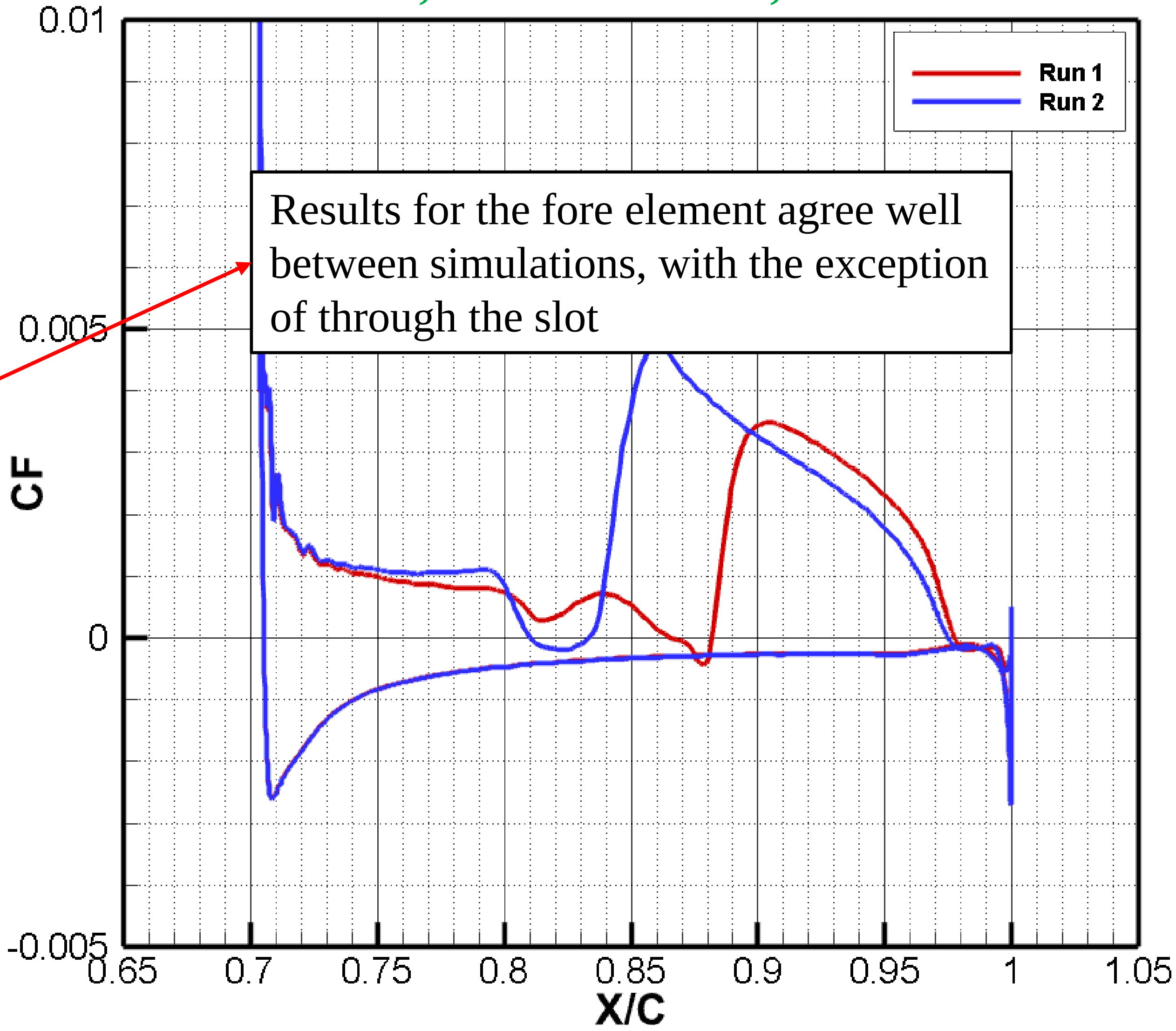

Results for the fore element agree well between simulations, with the exception of through the slot

3.2 Simulations at Cruise

Note that –Cf is plotted on lower surface by convention

- The location of transition can be identified exactly through examination of skin friction drag profiles

Skin Friction Drag Profiles for S207 Fore Element at Mach = 0.7, Re = 13.2 Million, AOA = -1.3°

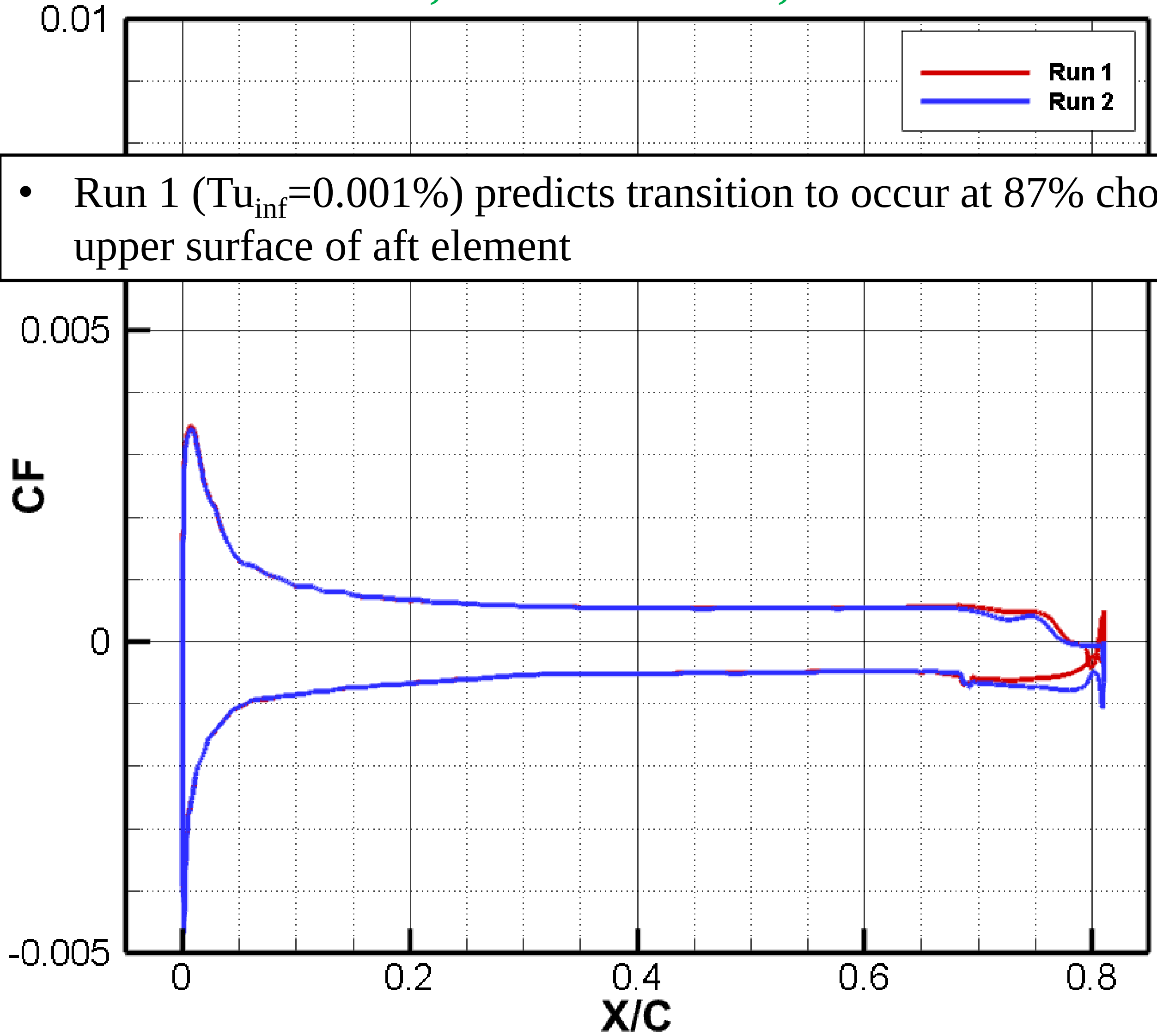

- Run 1 (Tu_{inf}=0.001%) predicts transition to occur at 87% chord on upper surface of aft element

Skin Friction Drag Profiles for S207 Aft Element at Mach = 0.7, Re = 13.2 Million, AOA = -1.3°

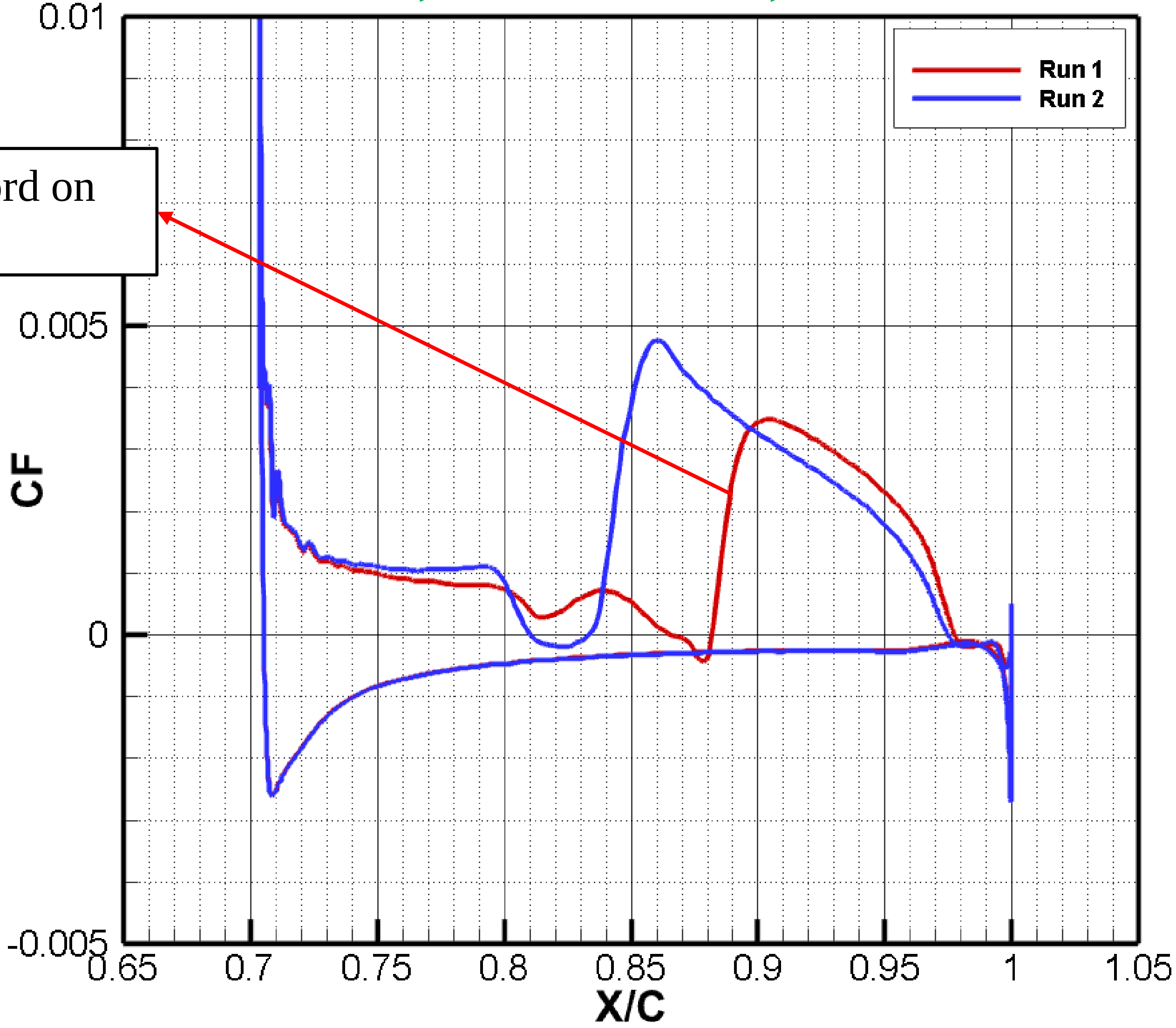

3.2 Simulations at Cruise

Note that –Cf is plotted on lower surface by convention

- The location of transition can be identified exactly through examination of skin friction drag profiles

Skin Friction Drag Profiles for S207 Fore Element at Mach = 0.7, Re = 13.2 Million, AOA = -1.3°

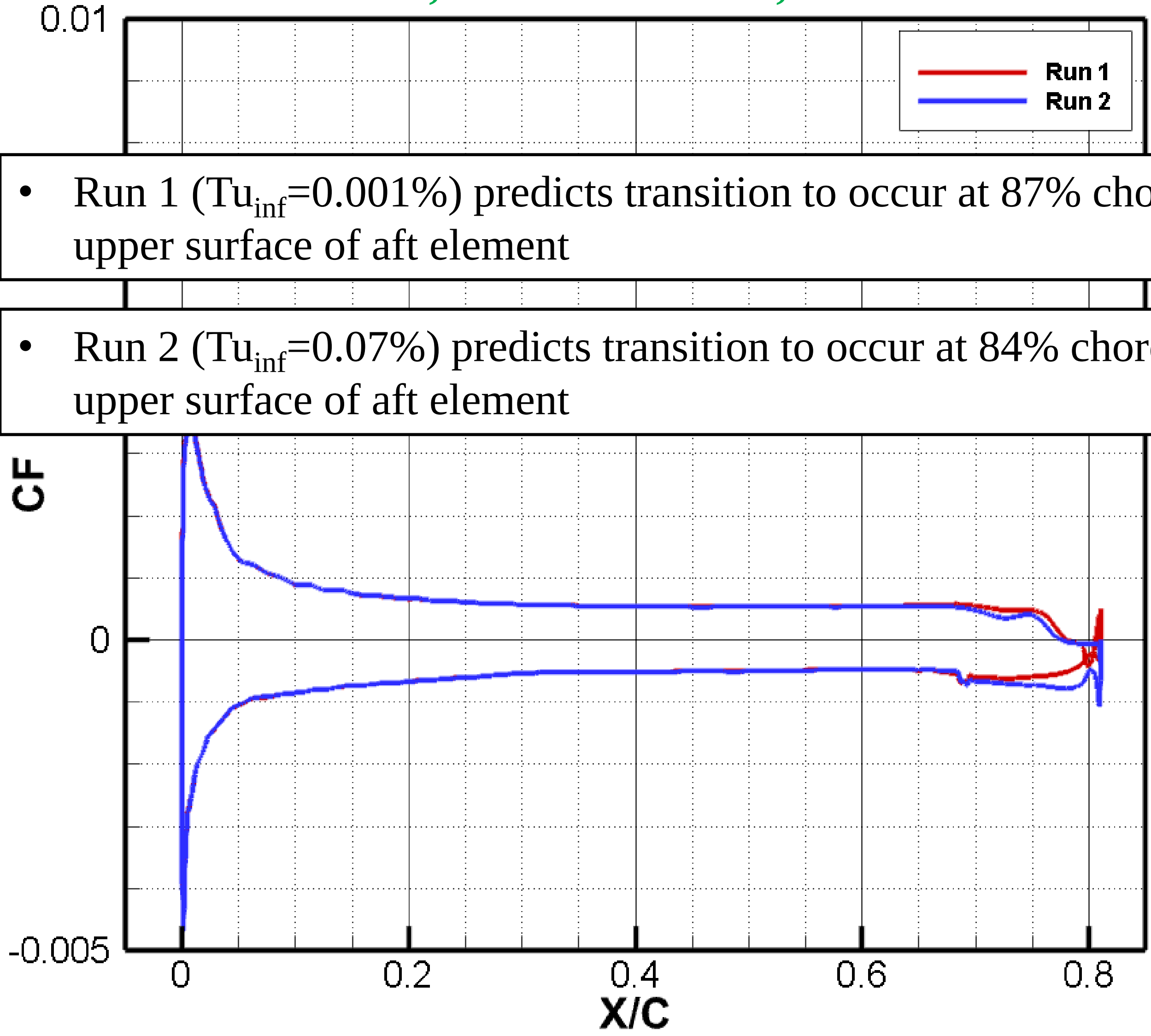

- Run 1 (Tu_{inf}=0.001%) predicts transition to occur at 87% chord on upper surface of aft element
- Run 2 (Tu_{inf}=0.07%) predicts transition to occur at 84% chord on upper surface of aft element

Skin Friction Drag Profiles for S207 Aft Element at Mach = 0.7, Re = 13.2 Million, AOA = -1.3°

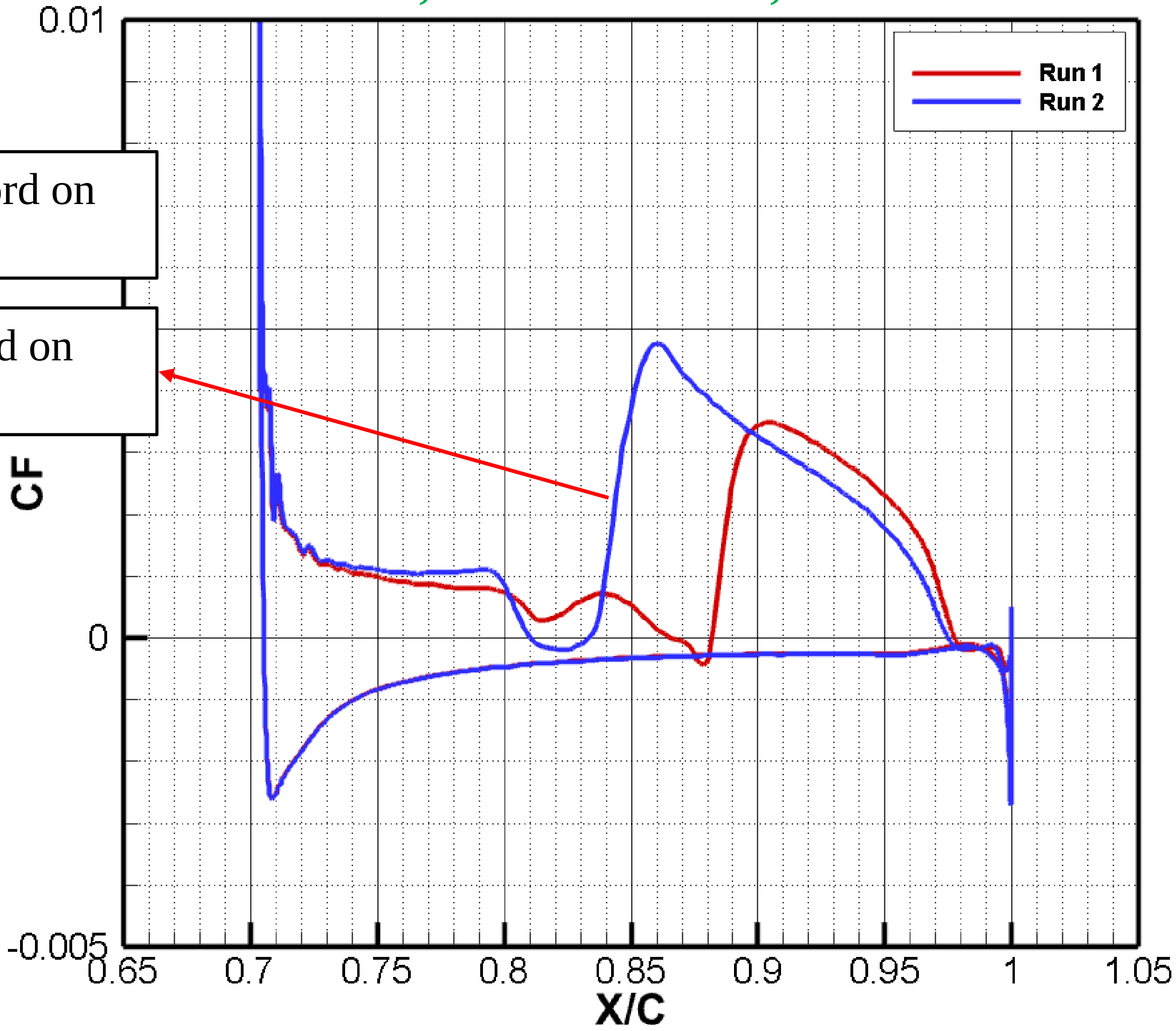

3.2 Simulations at Cruise

Note that –Cf is plotted on lower surface by convention

- The location of transition can be identified exactly through examination of skin friction drag profiles

Skin Friction Drag Profiles for S207 Fore Element at Mach = 0.7, Re = 13.2 Million, AOA = -1.3°

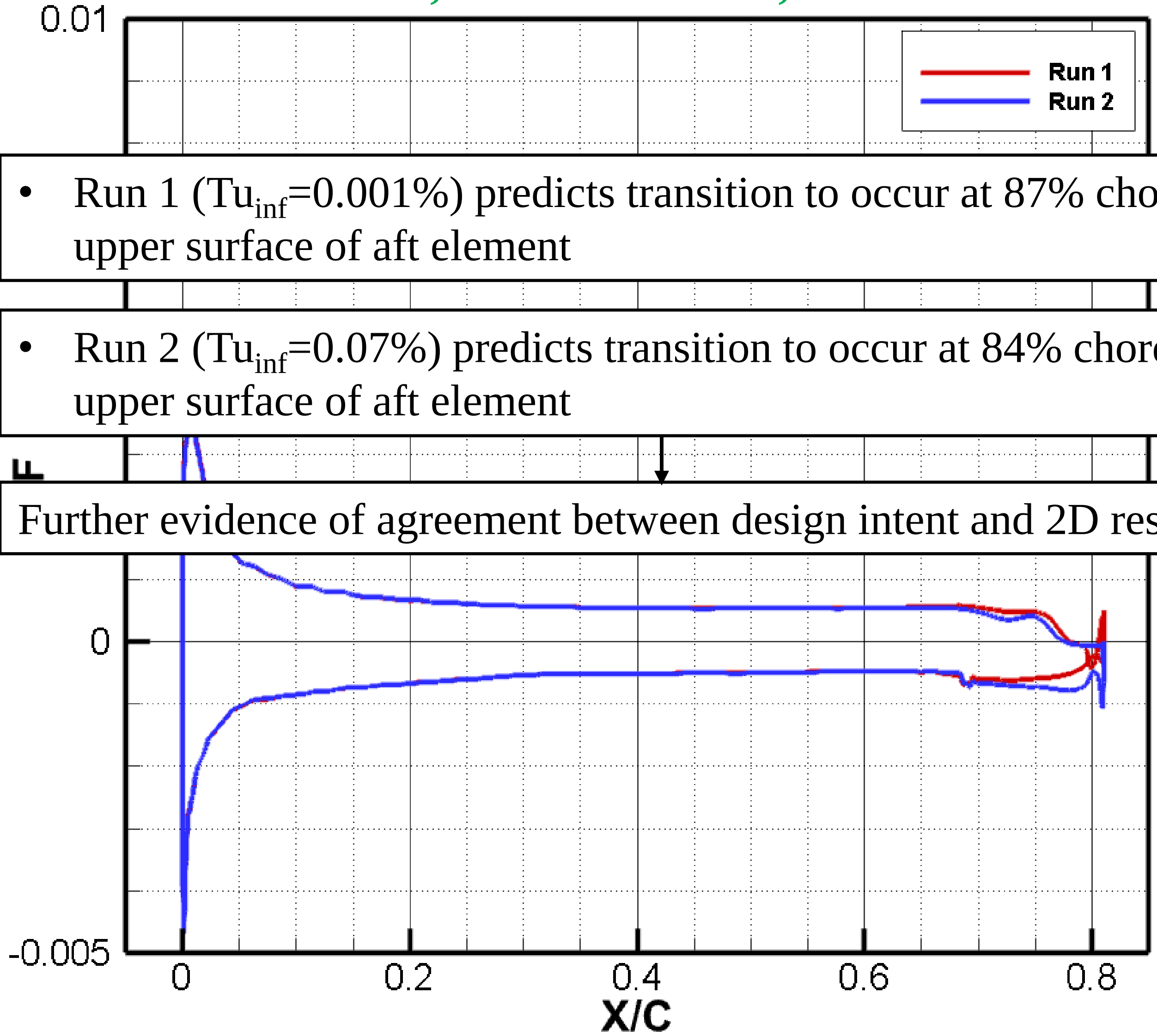

- Run 1 (Tu_{inf}=0.001%) predicts transition to occur at 87% chord on upper surface of aft element

- Run 2 (Tu_{inf}=0.07%) predicts transition to occur at 84% chord on upper surface of aft element

Further evidence of agreement between design intent and 2D results

Skin Friction Drag Profiles for S207 Aft Element at Mach = 0.7, Re = 13.2 Million, AOA = -1.3°

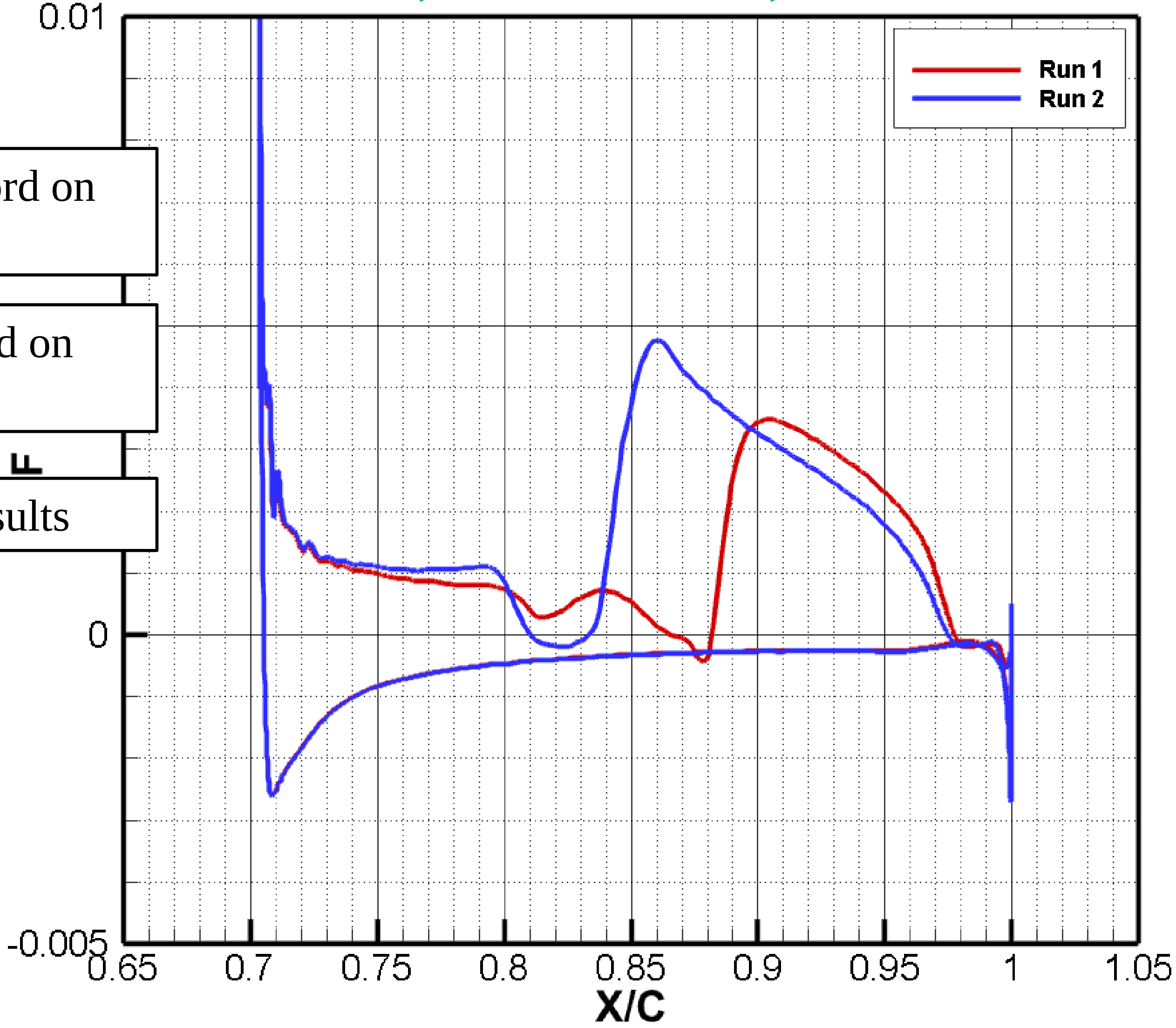

3.2 Simulations at Cruise

Note that –Cf is plotted on lower surface by convention

- The location of transition can be identified exactly through examination of skin friction drag profiles

Skin Friction Drag Profiles for S207 Fore Element at Mach = 0.7, Re = 13.2 Million, AOA = -1.3°

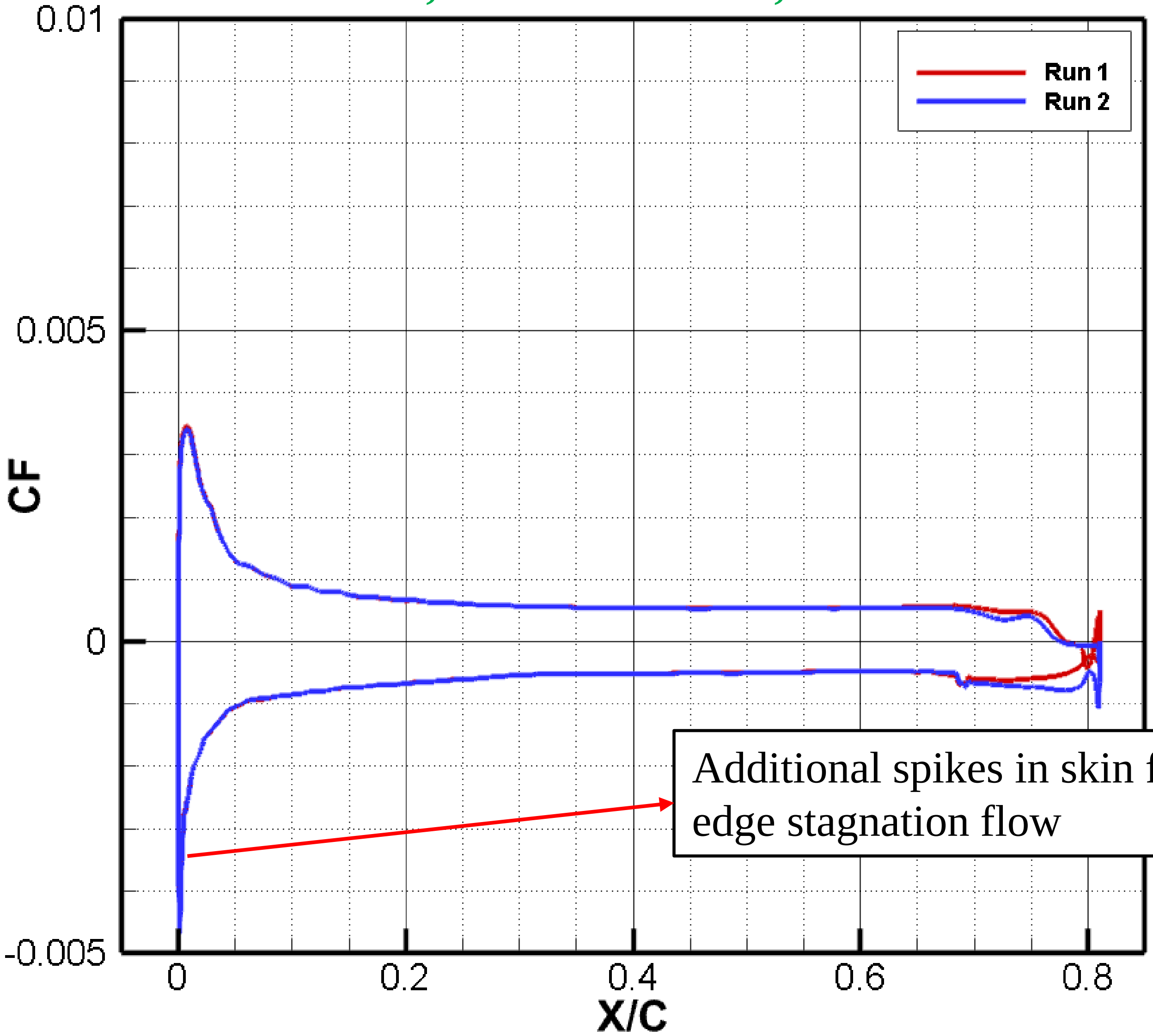

Skin Friction Drag Profiles for S207 Aft Element at Mach = 0.7, Re = 13.2 Million, AOA = -1.3°

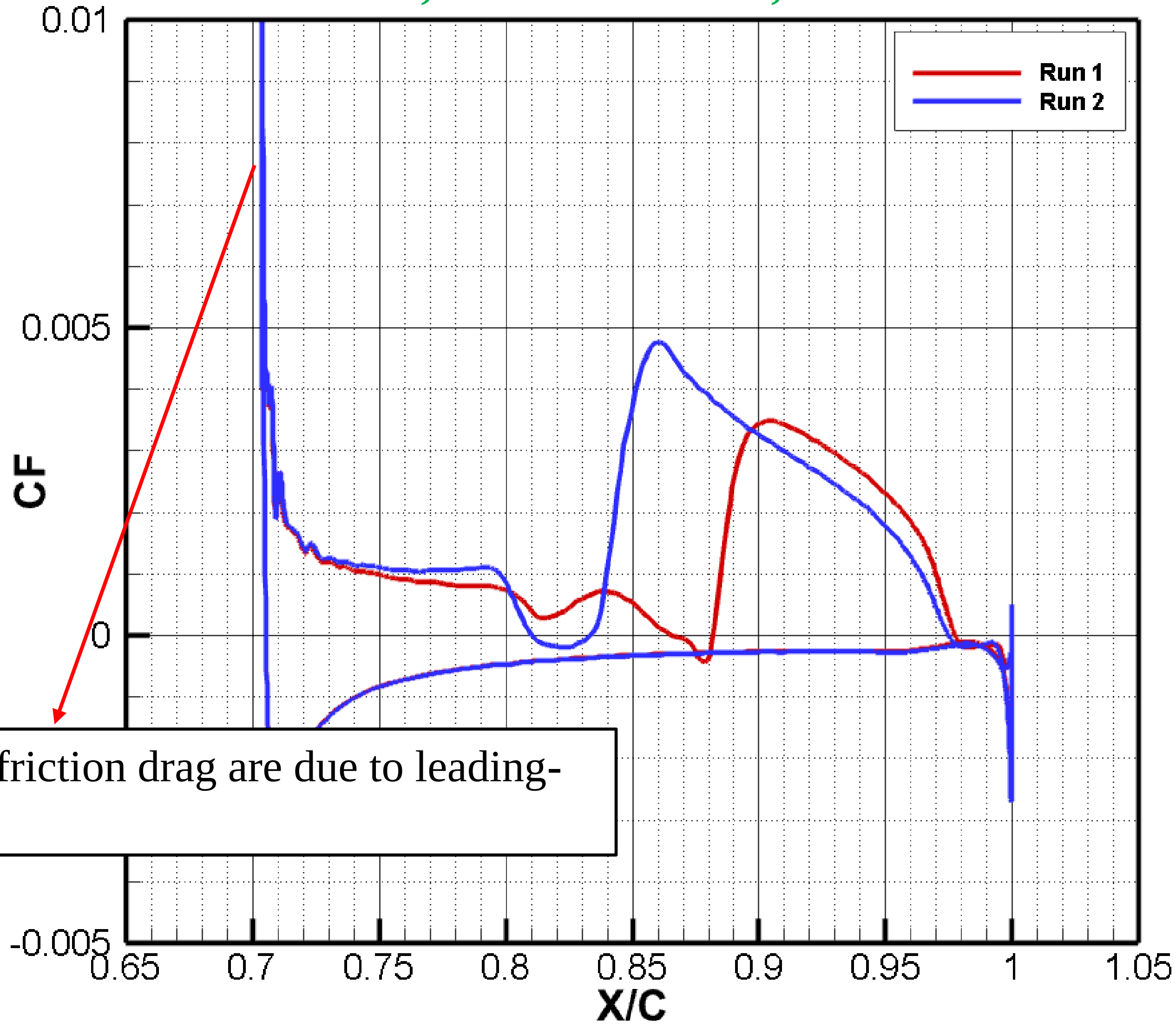

Additional spikes in skin friction drag are due to leading-edge stagnation flow

3.3 Sensitivity of Performance to Flap Position

- Performance of SNLF airfoils is sensitive to geometry changes, particularly in the slot
- Mach = 0.7, Re = 13.2e6, AOA = -1.3°
- Fully turbulent flow assumption used in all cases (i.e. no transition prediction model)
  - Easier to converge and offers quick insight to performance trends

Slot Sensitivity Study: Displacement Summary

Trans. Direction	Case Number	Trans. Magnitude
Horizontal	1a	-0.0055
	2a	-0.0050
	3a	-0.0025
	Baseline	0.0000
	5a	0.0025
	6a	0.0050
	7a	0.0100
	8a	0.0200
Vertical	1b	-0.0055
	2b	-0.0050
	3b	-0.0025
	Baseline	0.0000
	5b	0.0025
	6b	0.0050
	7b	0.0100
	8b	0.0200
Diagonal	1c	-0.0071
	2c	-0.0035
	Baseline	0.0000
	4c	0.0035
	5c	0.0071
	6c	0.0141
	7c	0.0283

3.3 Sensitivity of Performance to Flap Position

- Performance of SNLF airfoils is sensitive to geometry changes, particularly in the slot
- Mach = 0.7, Re = 13.2e6, AOA = -1.3°
- Fully turbulent flow assumption used in all cases (i.e. no transition prediction model)
  - Easier to converge and offers quick insight to performance trends

Slot Sensitivity Study: Displacement Summary

Trans. Direction	Case Number	Trans. Magnitude
	1a	-0.0055
	2a	-0.0050
	3a	-0.0025
Horizontal	Baseline	0.0000
	5a	0.0025
	6a	0.0050
	7a	0.0100
	8a	0.0200
	1b	-0.0055
	2b	-0.0050
	3b	-0.0025
Vertical	Baseline	0.0000
	5b	0.0025
	6b	0.0050
	7b	0.0100
	8b	0.0200
	1c	-0.0071
	2c	-0.0035
	Baseline	0.0000
Diagonal	4c	0.0035
	5c	0.0071
	6c	0.0141
	7c	0.0283

Negative values denote translations moved closer to the fore element

Positive values denote translations moved further from the fore element

3.3 Sensitivity of Performance to Flap Position

NSU2D-SA Flow Field Mach Contours for Horizontal Displacements (Case a)

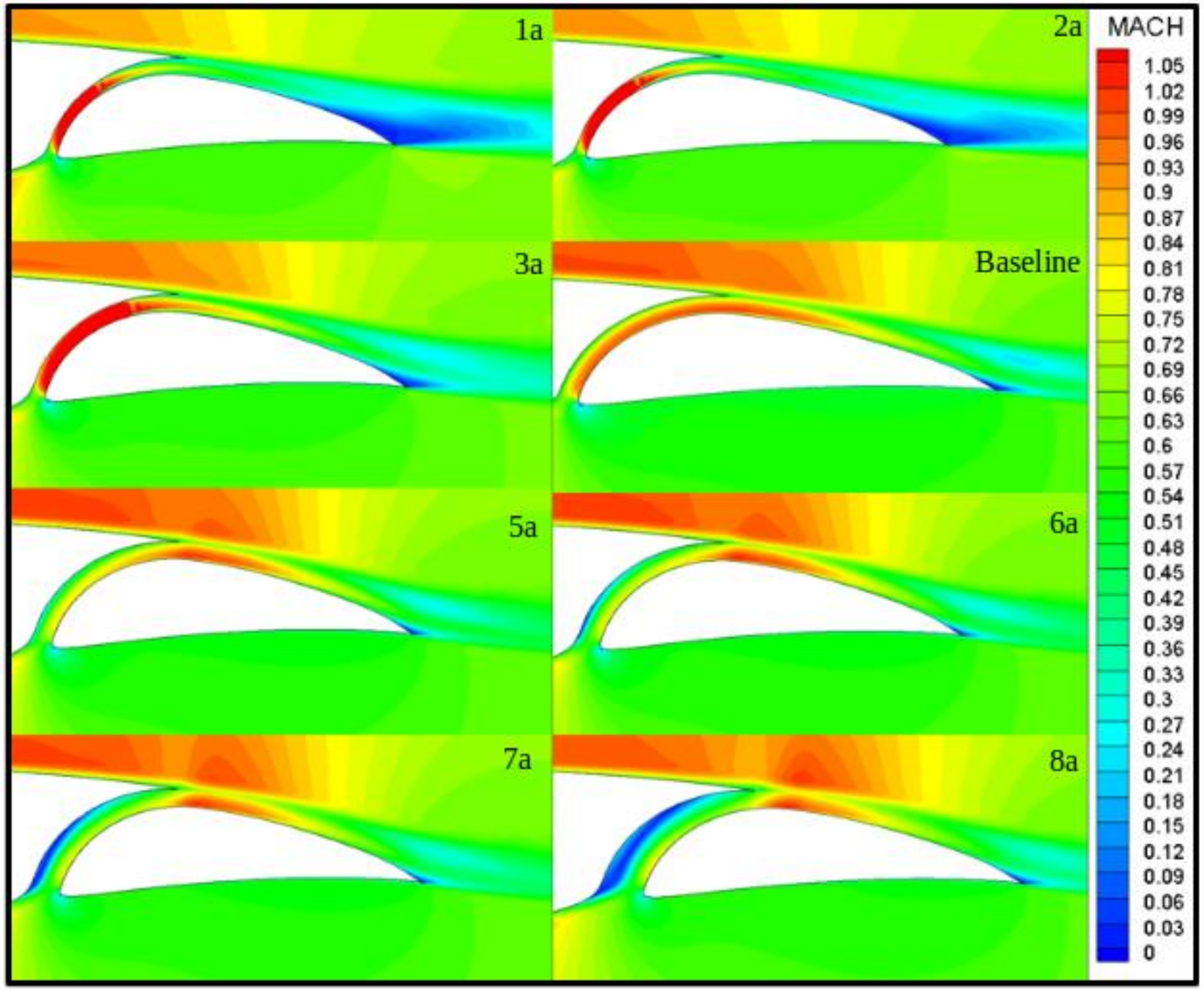

a) Shock wave formation for horz. narrowing, and flow separation on fore element through slot for horz. widening

3.3 Sensitivity of Performance to Flap Position

NSU2D-SA Flow Field Mach Contours for Vertical Displacements (Case b)

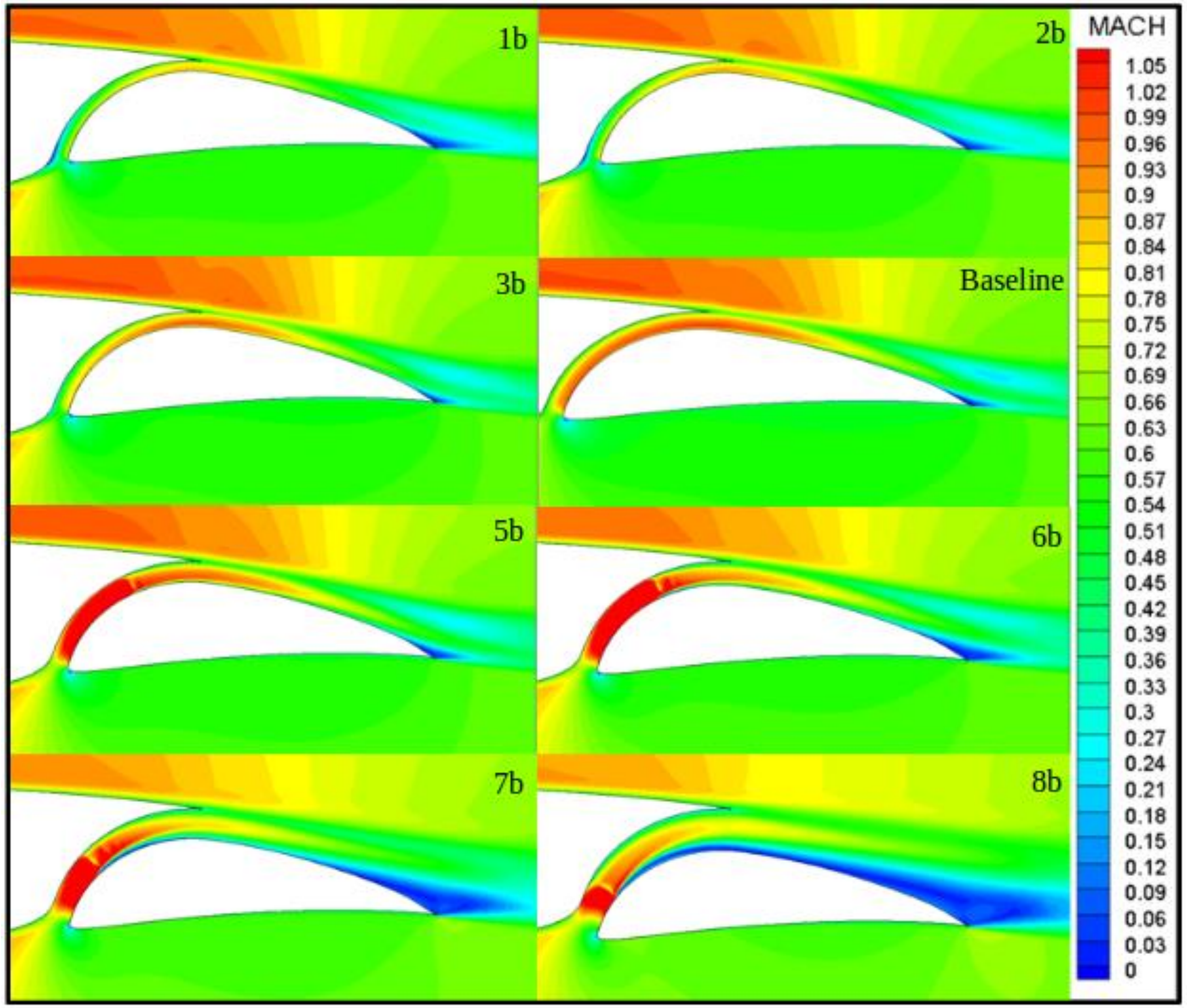

a) Shock wave formation for horz. narrowing, and flow separation on fore element through slot for horz. widening

b) Shock wave formation for vert. widening, reduced velocity for vert. narrowing

3.3 Sensitivity of Performance to Flap Position

NSU2D-SA Flow Field Mach Contours for Diagonal Displacements (Case c)

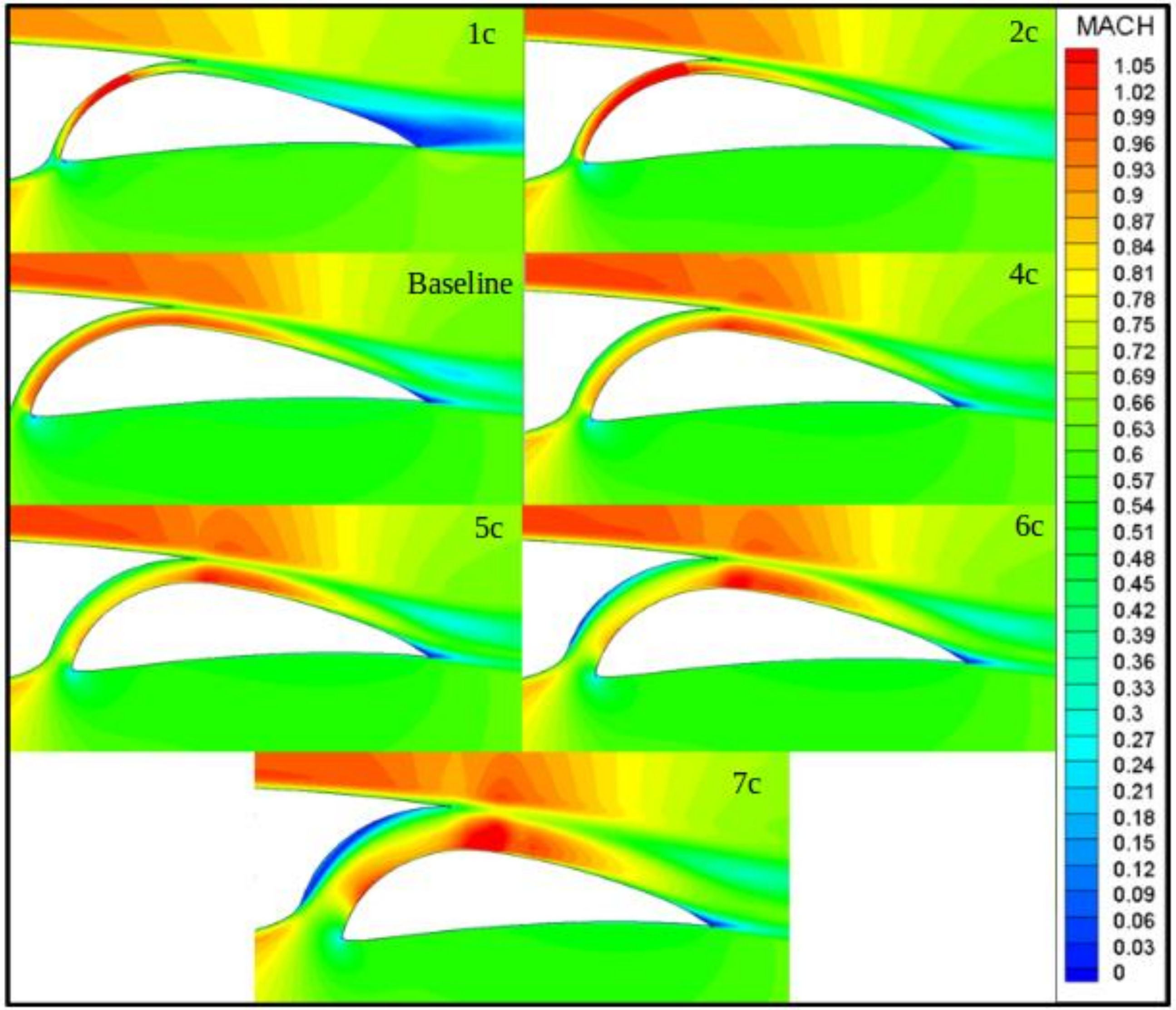

a) Shock wave formation for horz. narrowing, and flow separation on fore element through slot for horz. widening

b) Shock wave formation for vert. widening, reduced velocity for vert. narrowing

c) Severe flow separation at TE of aft element and shock wave formation for diagonal narrowing

3.3 Sensitivity of Performance to Flap Position

NSU2D-SA Flow Field Mach Contours for All Displacements

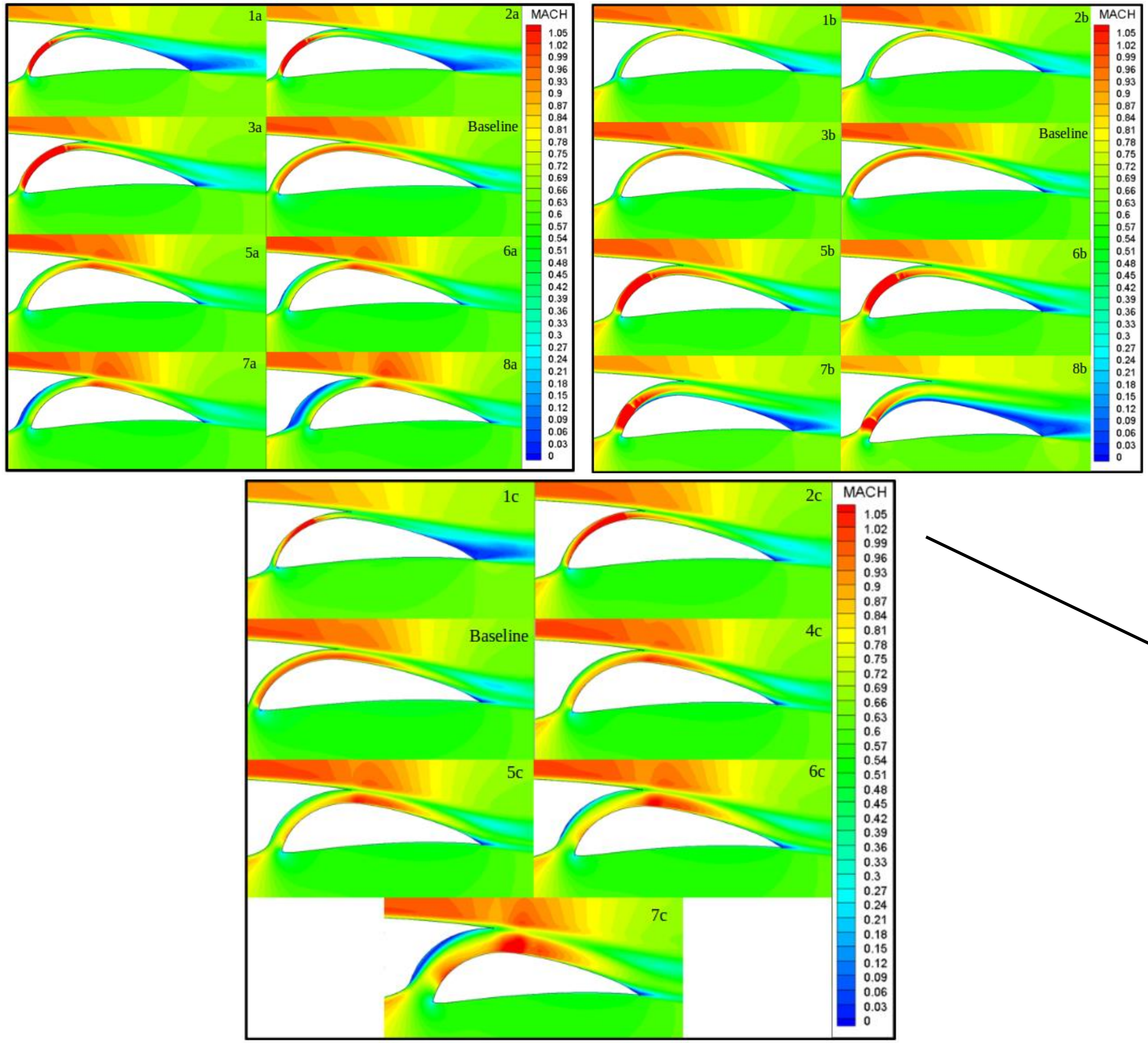

a) Shock wave formation for horz. narrowing, and flow separation on fore element through slot for horz. widening

b) Shock wave formation for vert. widening, reduced velocity for vert. narrowing

c) Severe flow separation at TE of aft element and shock wave formation for diagonal narrowing

Adequate flap displacements result in adverse flow behavior

3.3 Sensitivity of Performance to Flap Position

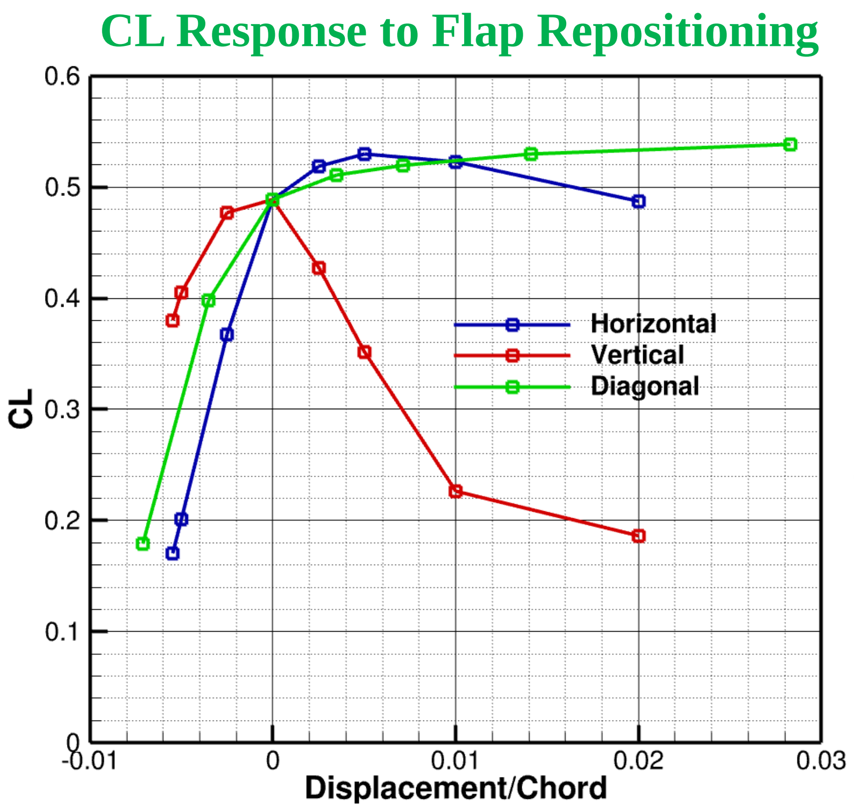

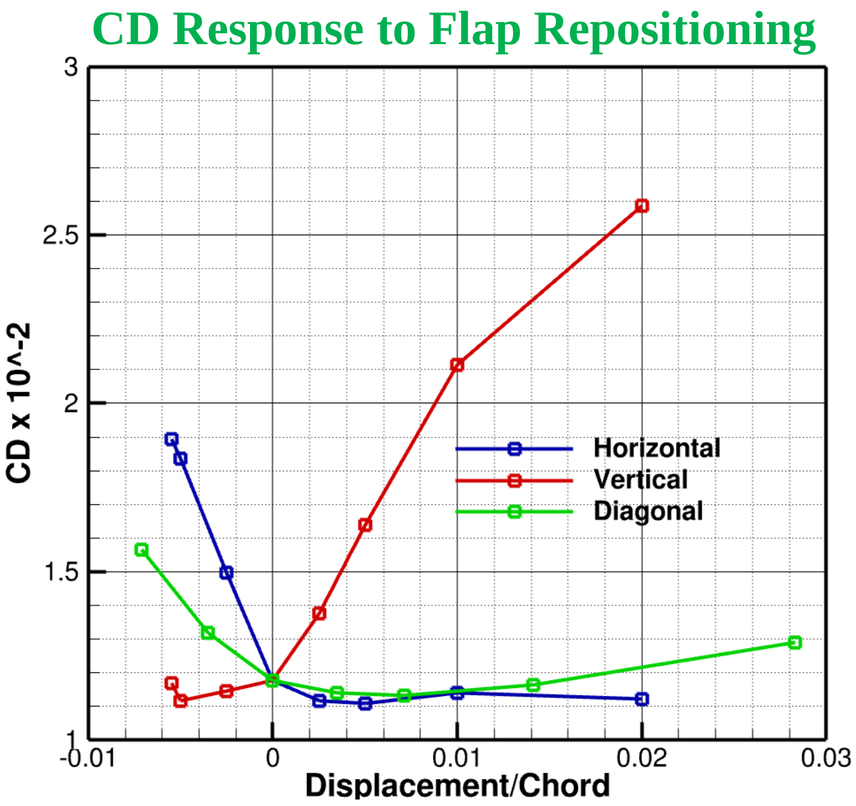

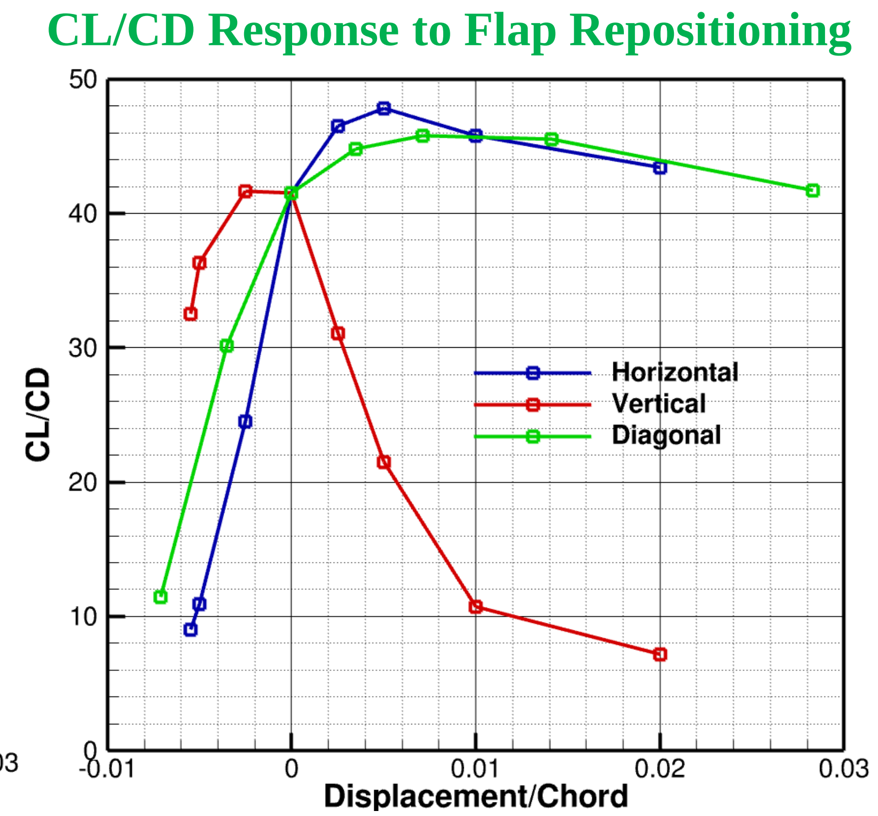

3.3 Sensitivity of Performance to Flap Position

CL Response to Flap Repositioning

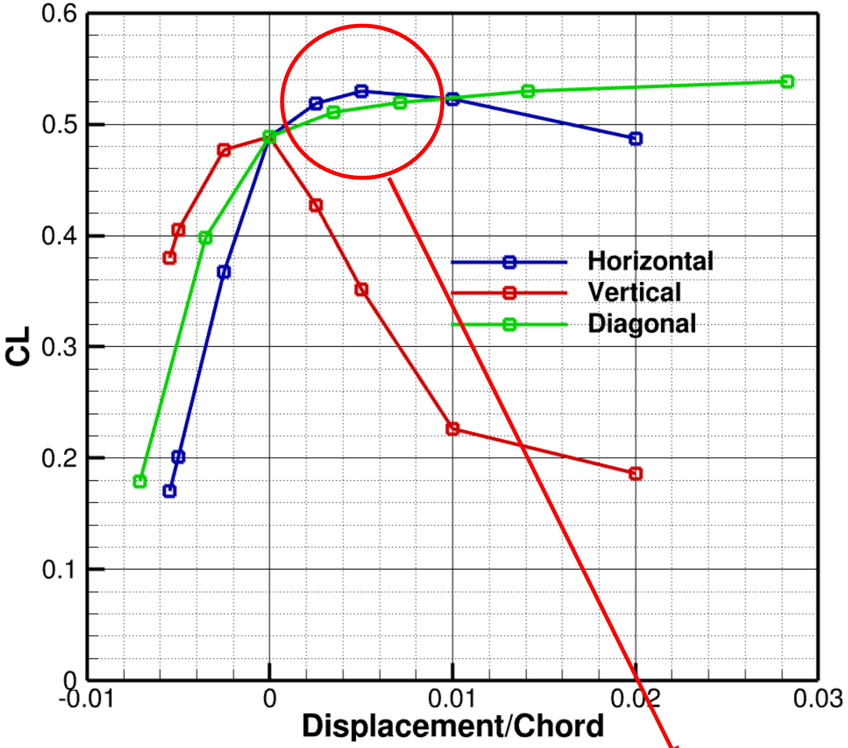

CD Response to Flap Repositioning

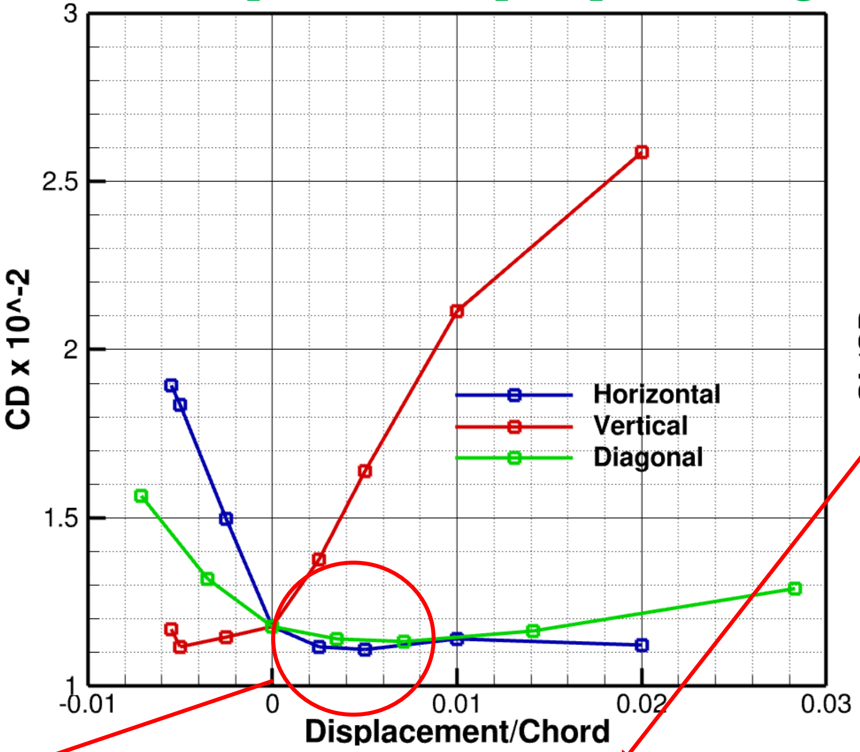

CL/CD Response to Flap Repositioning

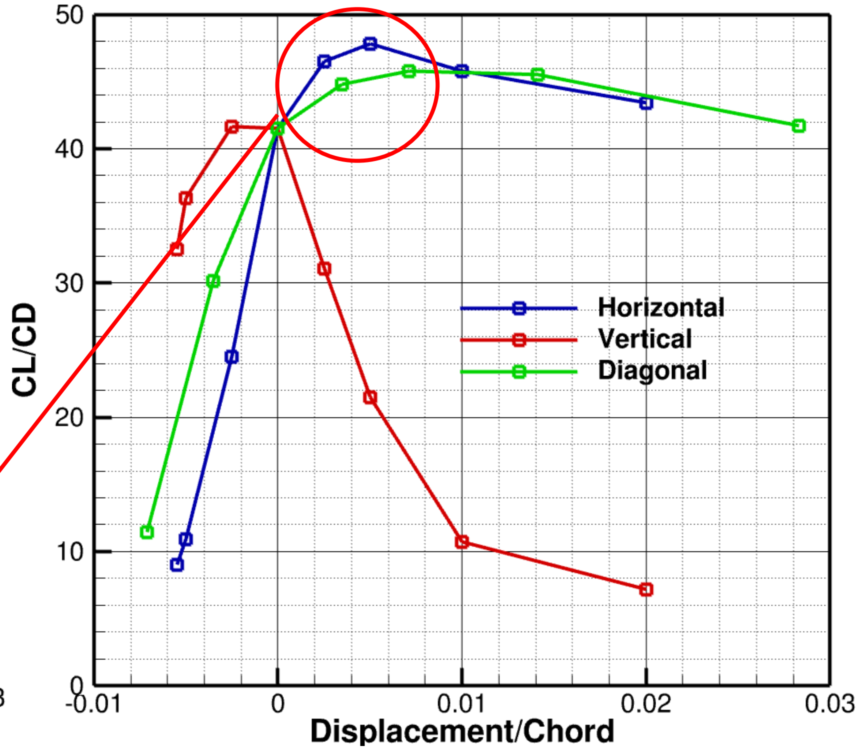

- Slight benefit for small horizontal and diagonal widening
  - Increase in lift coefficient and decrease in drag coefficient
  - Benefit not likely maintained across S207 operating conditions

3.3 Sensitivity of Performance to Flap Position

CL Response to Flap Repositioning

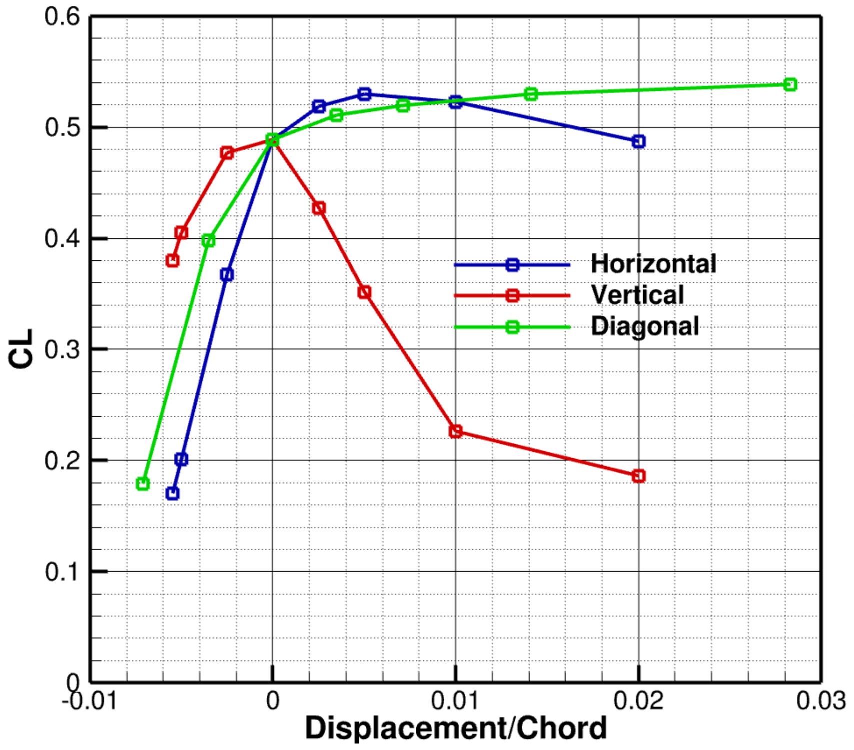

CD Response to Flap Repositioning

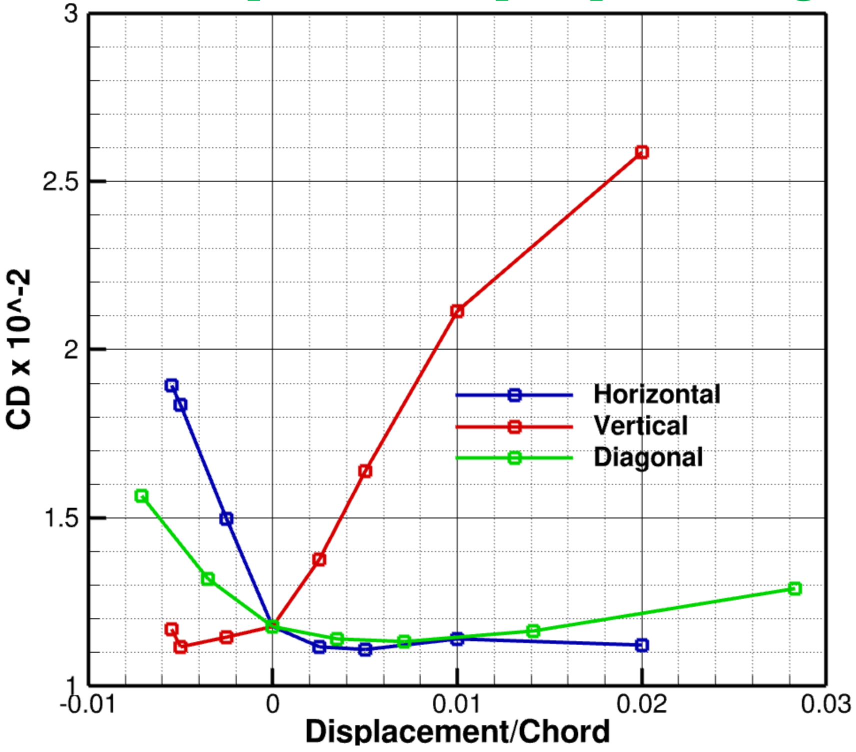

CL/CD Response to Flap Repositioning

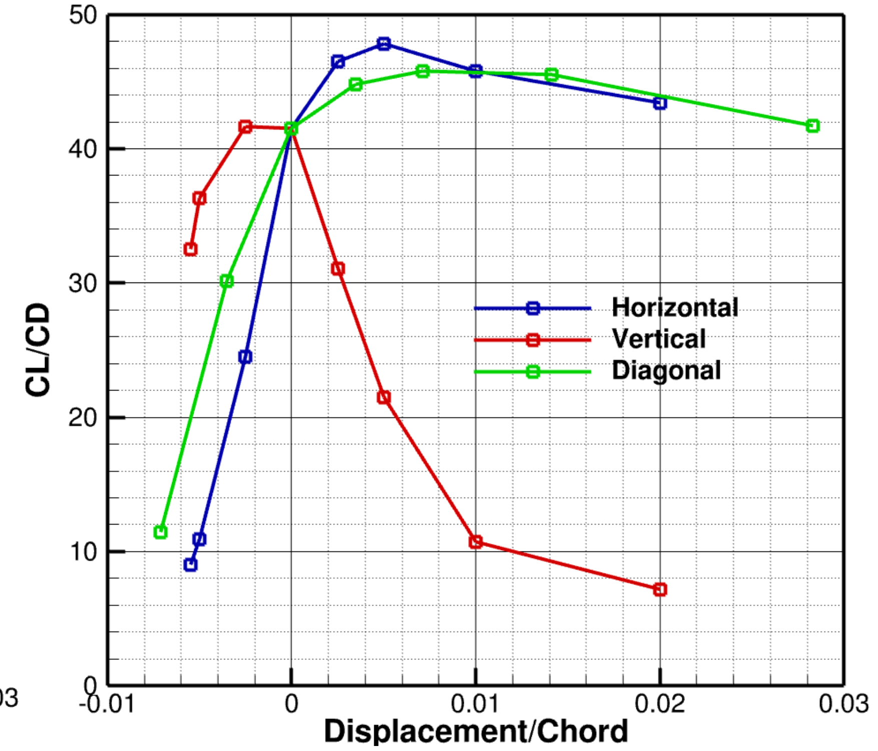

- Slight benefit for small horizontal and diagonal widening
  - Increase in lift coefficient and decrease in drag coefficient
  - Benefit not likely maintained across S207 operating conditions

- Flap Displacements should be no greater than 0.1% chord length to maintain S207 SNLF airfoil performance
  - This value is well above manufacturing tolerances
  - Preliminary structural analysis conducted at Penn State shows that the S207 wing box under gravitational loads predicts displacements below this limit [31]

4. 3D Analysis of an S207-Based Vehicle

4.1 The Geometry and Its Evolution

- Design of the S207 SNLF TTBW aircraft is based on the 2015 version of the Boeing SUGAR aircraft, which is the baseline comparison for the ULI project [32]
  - Wing was resized from 1477ft^2 to 1350ft^2 to account for the higher lift coefficient of the clean S207 airfoil [36]
  - All other planform properties such as sweep (12.5°) and aspect ratio were maintained

S207 Vehicle Geometry for Aerodynamic Analysis

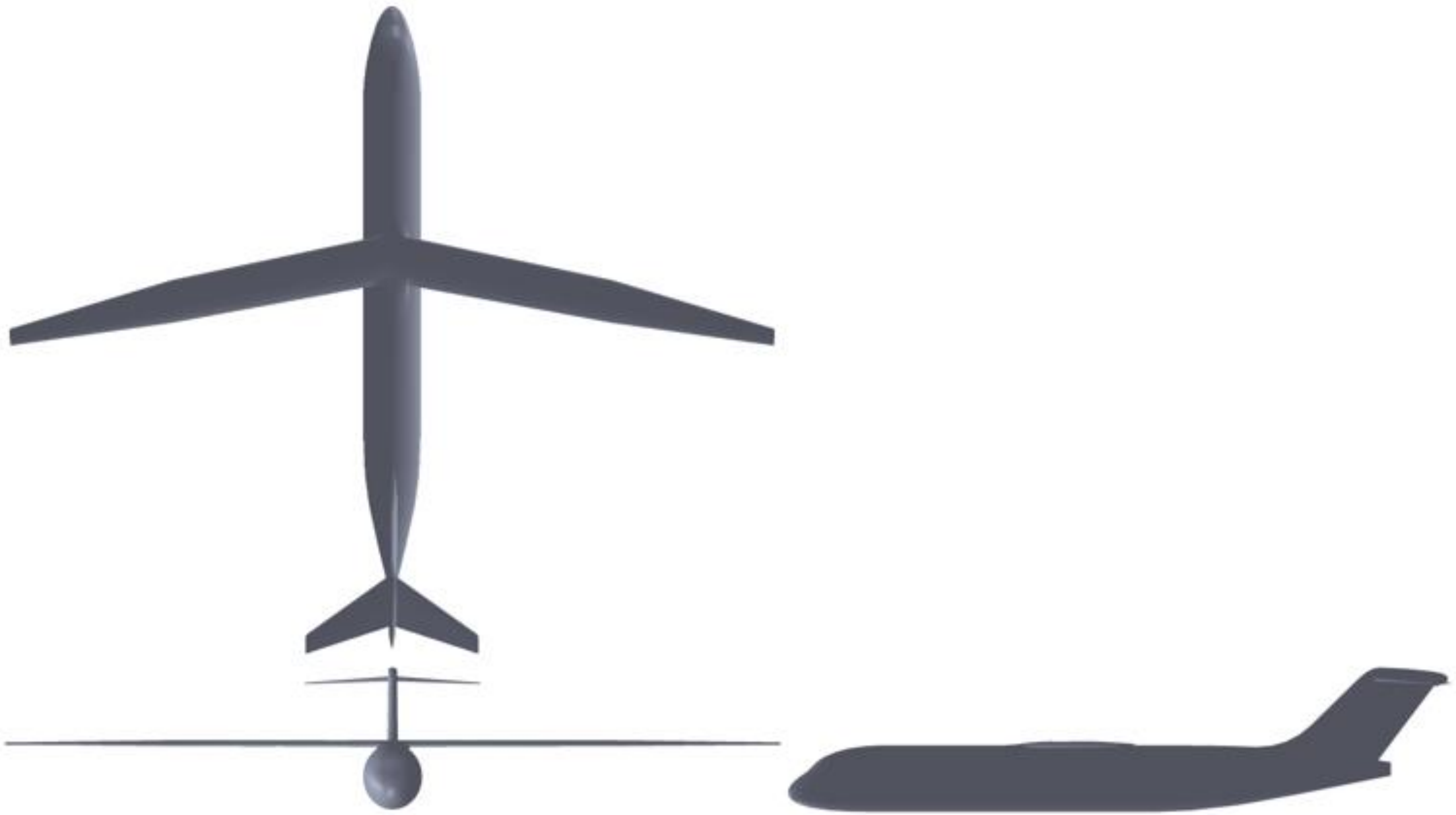

4.1 The Geometry and Its Evolution

- Design of the S207 SNLF TTBW aircraft is based on the 2015 version of the Boeing SUGAR aircraft, which is the baseline comparison for the ULI project [32]
  - Wing was resized from 1477ft^2 to 1350ft^2 to account for the higher lift coefficient of the clean S207 airfoil [36]
  - All other planform properties such as sweep (12.5°) and aspect ratio were maintained

S207 Vehicle Geometry for Aerodynamic Analysis

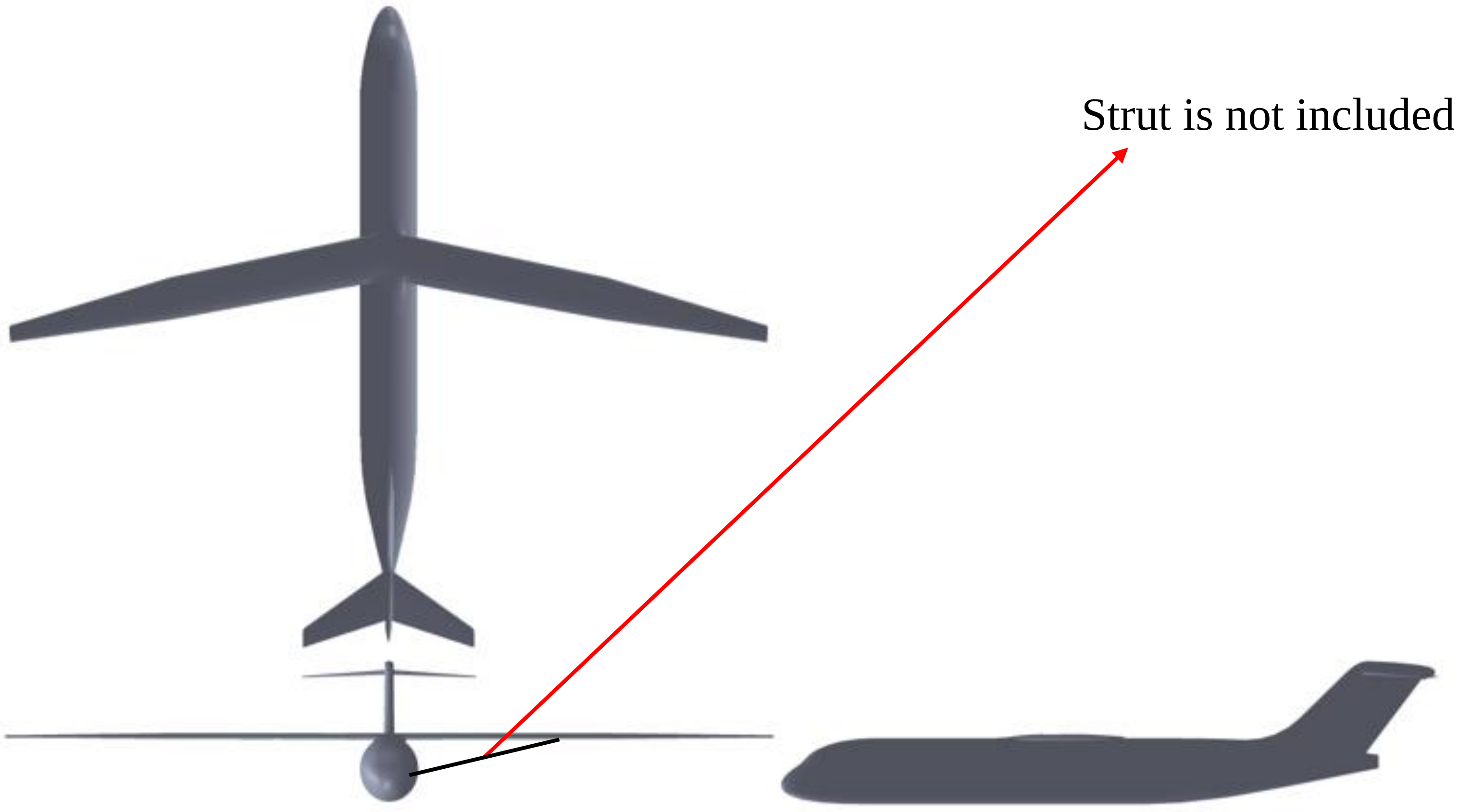

Strut is not included for current aerodynamic analysis

4.1 The Geometry and Its Evolution

- Three iterations of a half-span model of the S207 SNLF TTBW configuration were analyzed computationally
  - Subsequent geometries being developed upon discovery of errors in its predecessor
- Hybrid grids with prisms in the near-wall boundary layer regions and tetrahedral elements in the regions of inviscid flow
  - Generated with the Pointwise software at UTK
  - Meshing parameters held relatively constant between grids

Configuration 2 Grid

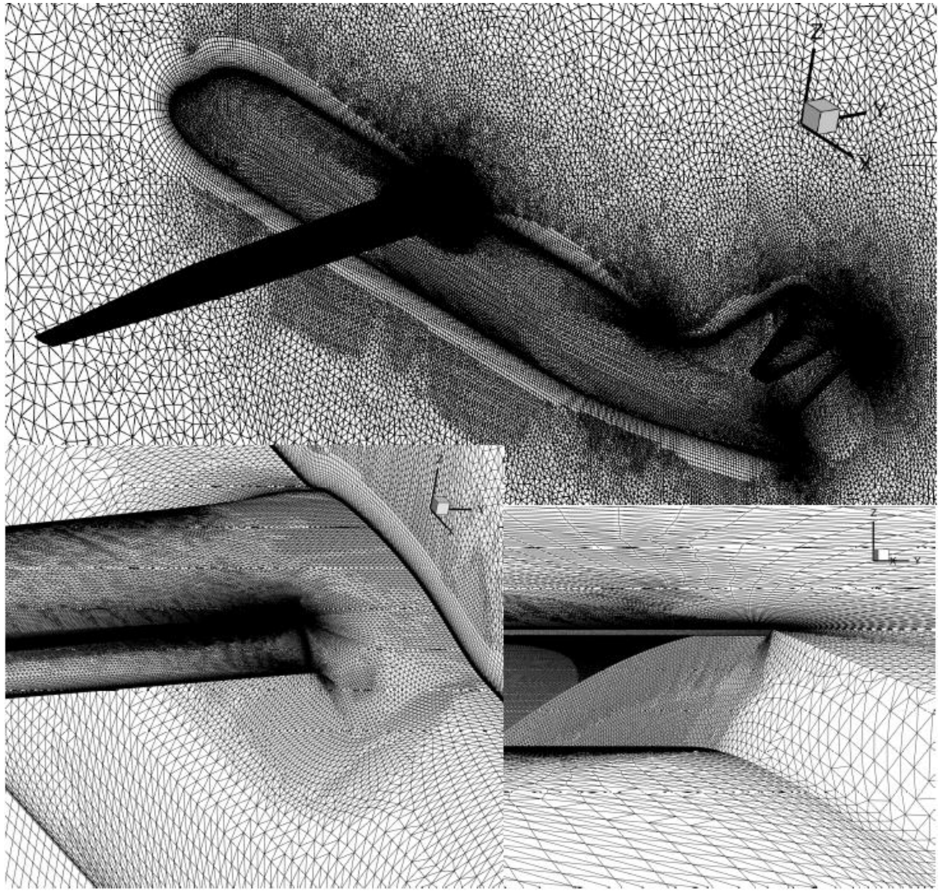

4.2 Results for the Initial Configuration

- Configuration 1 was used to develop a full set of drag polars requested by ULI associates at Boeing
    - Serves as input to their performance analysis
    - Mach number ranged from 0.200 to 0.750, angles of attack ranged from -2.0° to 5.0° (128 cases)
    - Every case was run using SA fully turbulent approach and SA-Menter free transition approach
    - Re = 1.4 million/ft with MAC=8.786ft, MAC-based Re=12.3 million

4.2 Results for the Initial Configuration

- Configuration 1 was used to develop a full set of drag polars requested by ULI associates at Boeing
  - Serves as input to their performance analysis
  - Mach number ranged from 0.200 to 0.750, angles of attack ranged from -2.0° to 5.0° (128 cases)
  - Every case was run using SA fully turbulent approach and SA-Menter free transition approach
  - Re = 1.4 million/ft with MAC=8.786ft, MAC-based Re=12.3 million

Configuration 1 Performance Polars

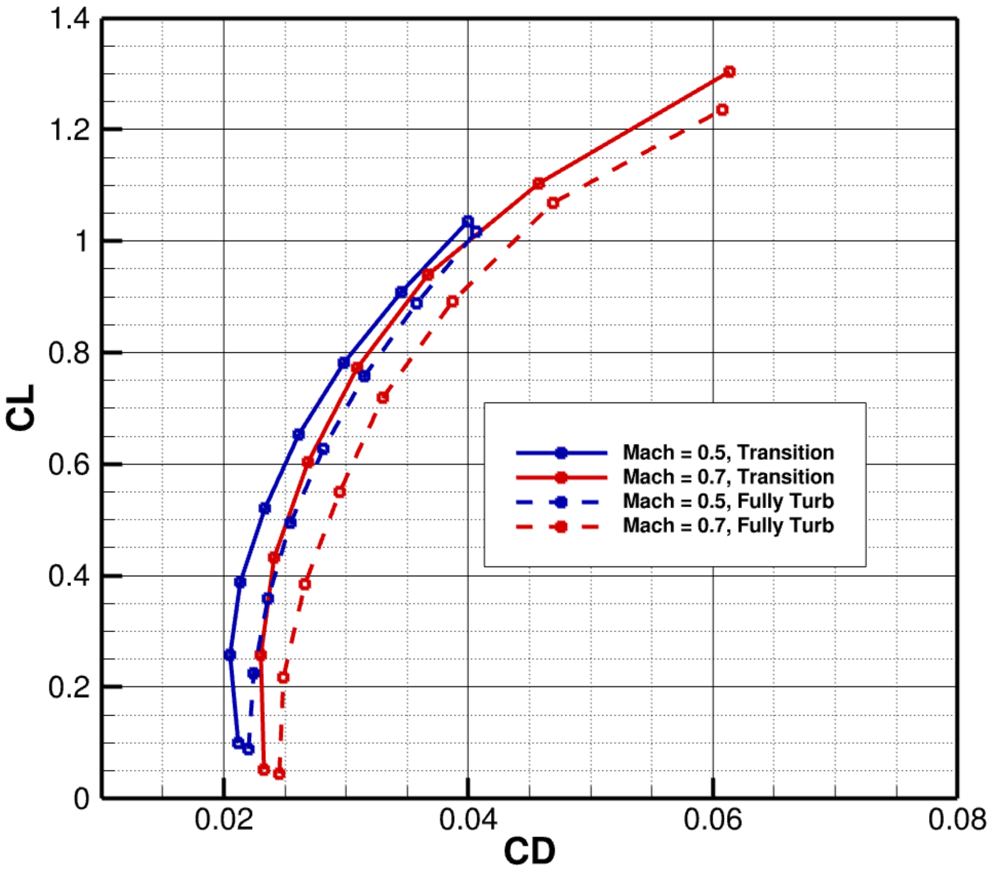

Configuration 1 Free Transition Spanwise Lift Distributions based on MAC

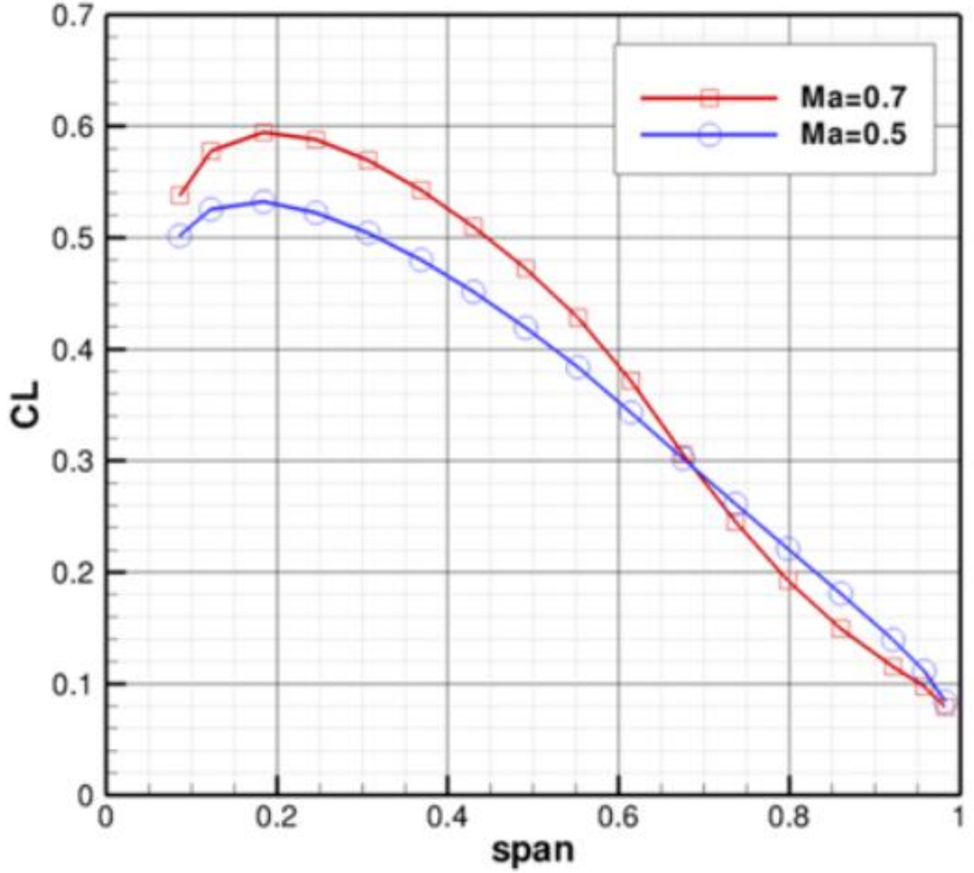

4.2 Results for the Initial Configuration

- Configuration 1 was used to develop a full set of drag polars requested by ULI associates at Boeing
  - Serves as input to their performance analysis
  - Mach number ranged from 0.200 to 0.750, angles of attack ranged from -2.0° to 5.0° (128 cases)
  - Every case was run using SA fully turbulent approach and SA-Menter free transition approach
  - Re = 1.4 million/ft with MAC=8.786ft, MAC-based Re=12.3 million

Configuration 1 Performance Polars

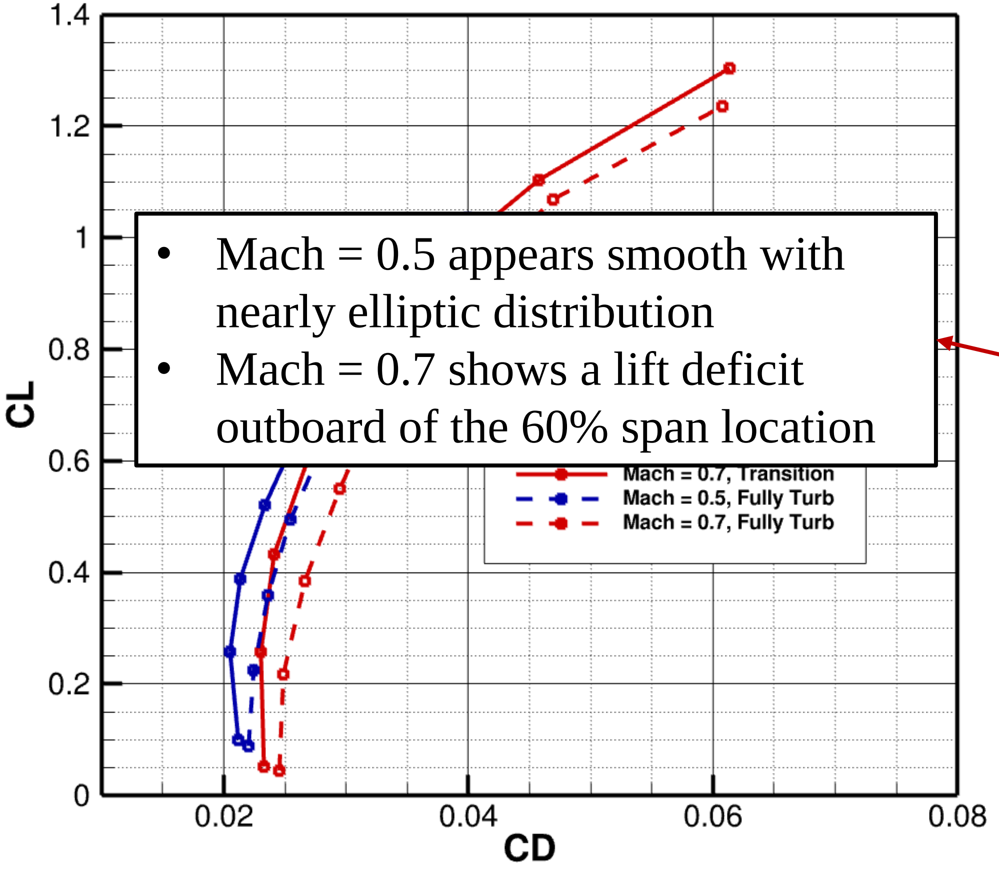

- Mach = 0.5 appears smooth with nearly elliptic distribution
- Mach = 0.7 shows a lift deficit outboard of the 60% span location

Configuration 1 Free Transition Spanwise Lift Distributions based on MAC

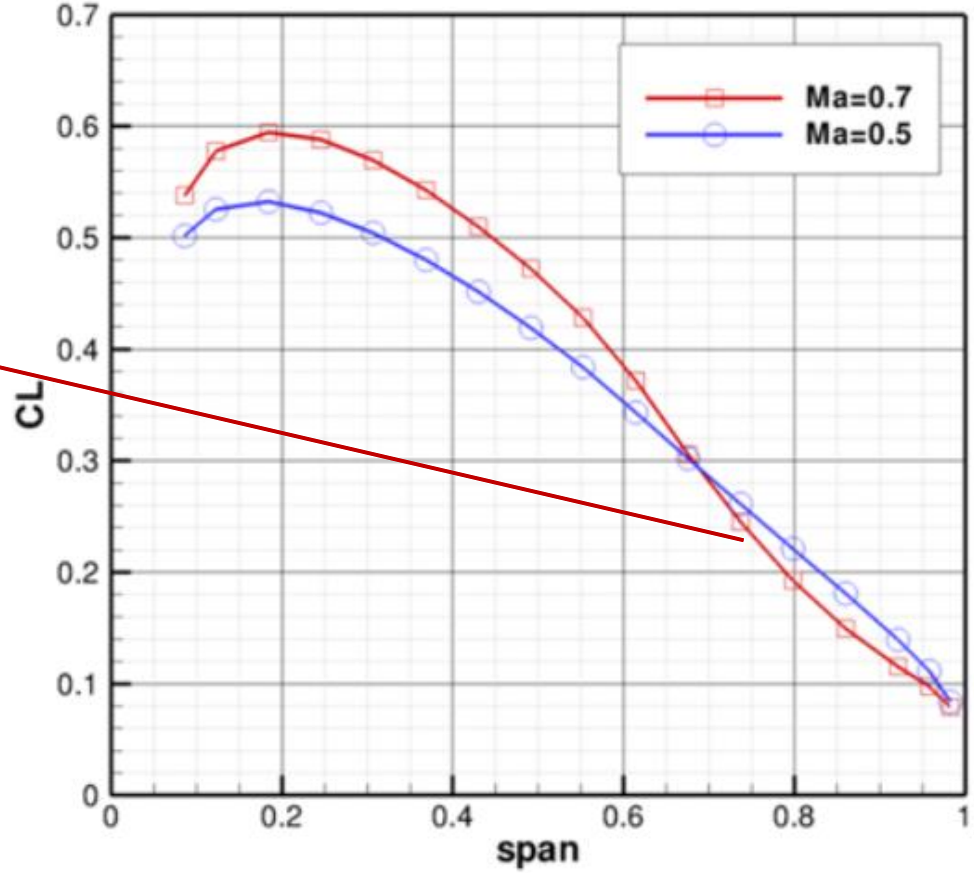

4.2 Results for the Initial Configuration

- This unexpected lift deficit in the outboard region of the wing was traced to the presence of a shock wave in the slot
  - Present in both fully turbulent and free transition runs

Fully Turbulent Mach Contour Distributions at Mach = 0.7, AOA = 0.0° for Configuration 1

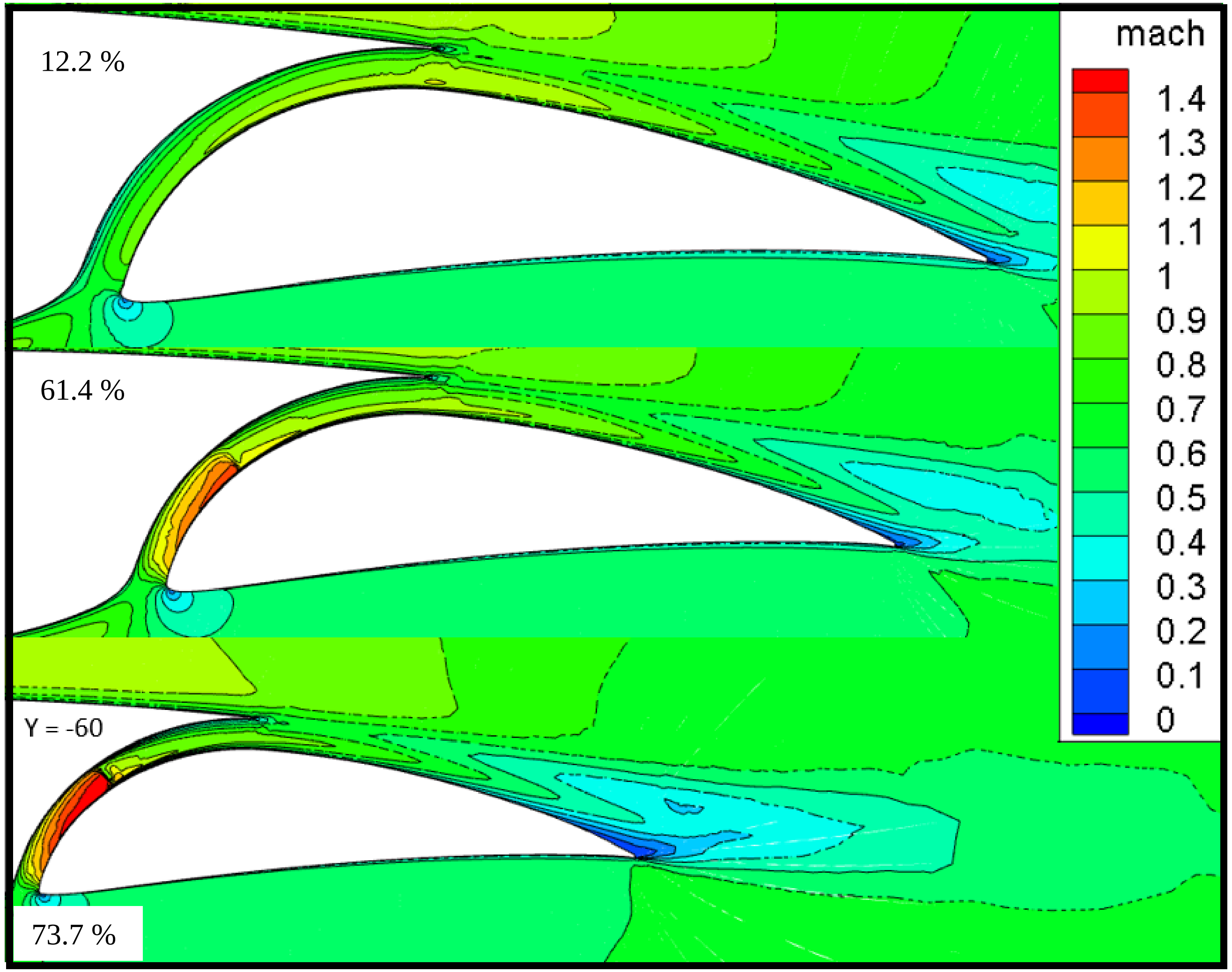

4.2 Results for the Initial Configuration

- This unexpected lift deficit in the outboard region of the wing was traced to the presence of a shock wave in the slot
  - Present in both fully turbulent and free transition runs

Fully Turbulent Mach Contour Distributions at Mach = 0.7, AOA = 0.0° for Configuration 1

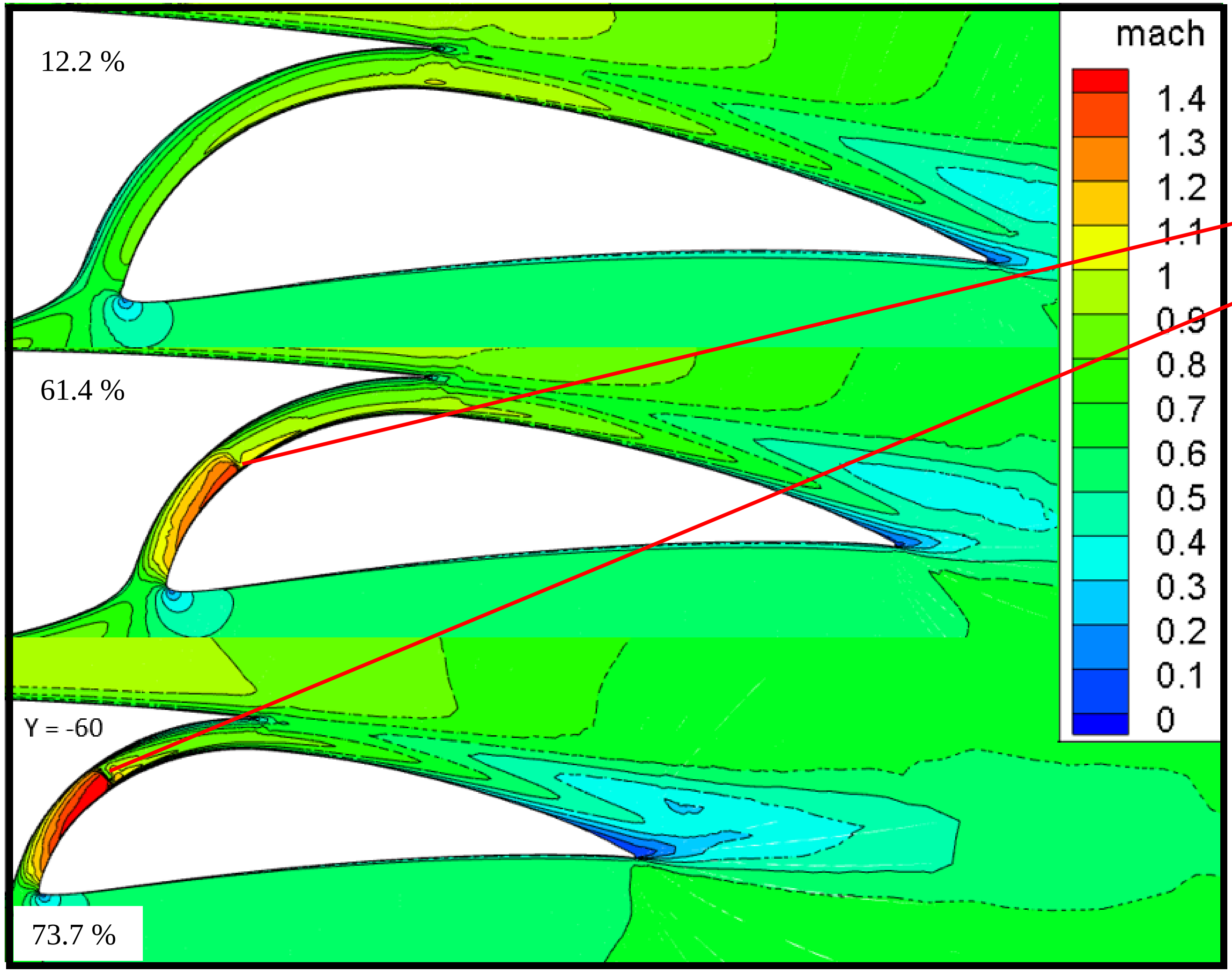

Pressure Coefficient Profile at Mach = 0.7, AOA =0.0° for Configuration 1 (Aft Element Removed)

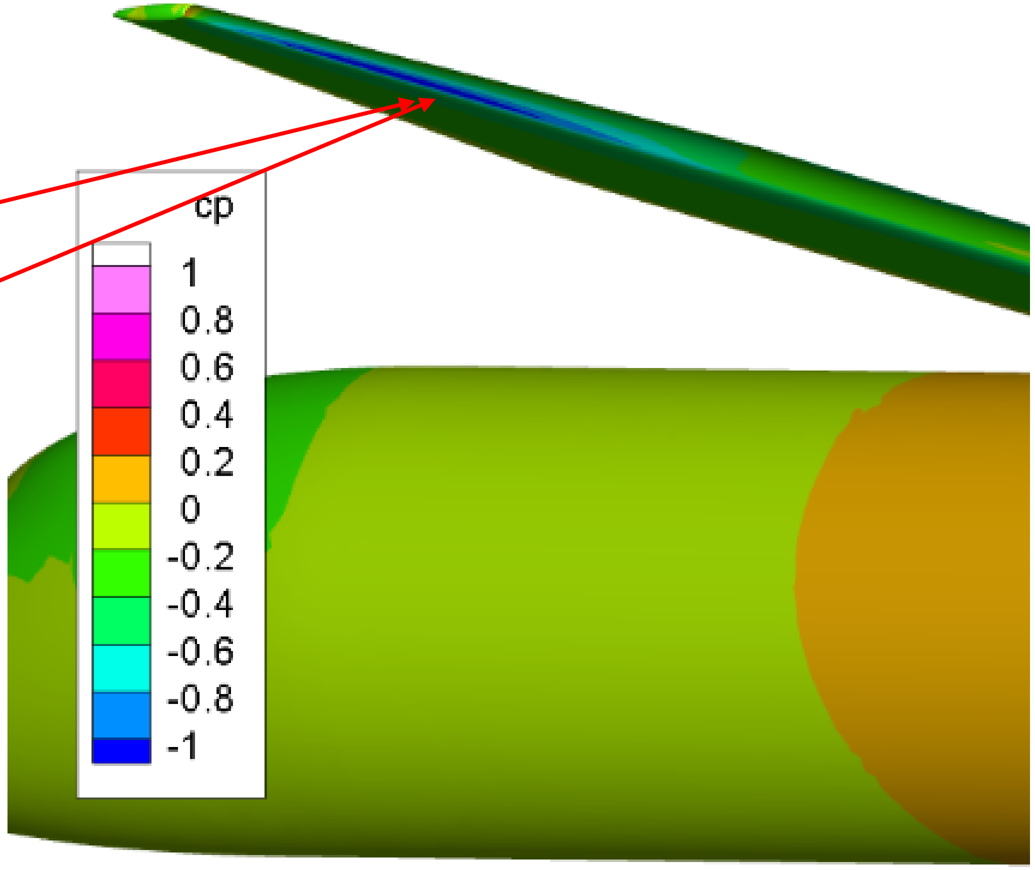

4.3 Shock Wave Elimination

- In the design of the aircraft wing, a sweep transformation was used on the S207 airfoil to define profiles parallel to the freestream [34,35]
  - A miscalculation was discovered, and its correction led to the generation of Configuration 2

Flap Differences Between Configuration and Configuration 2 at an Outboard Section

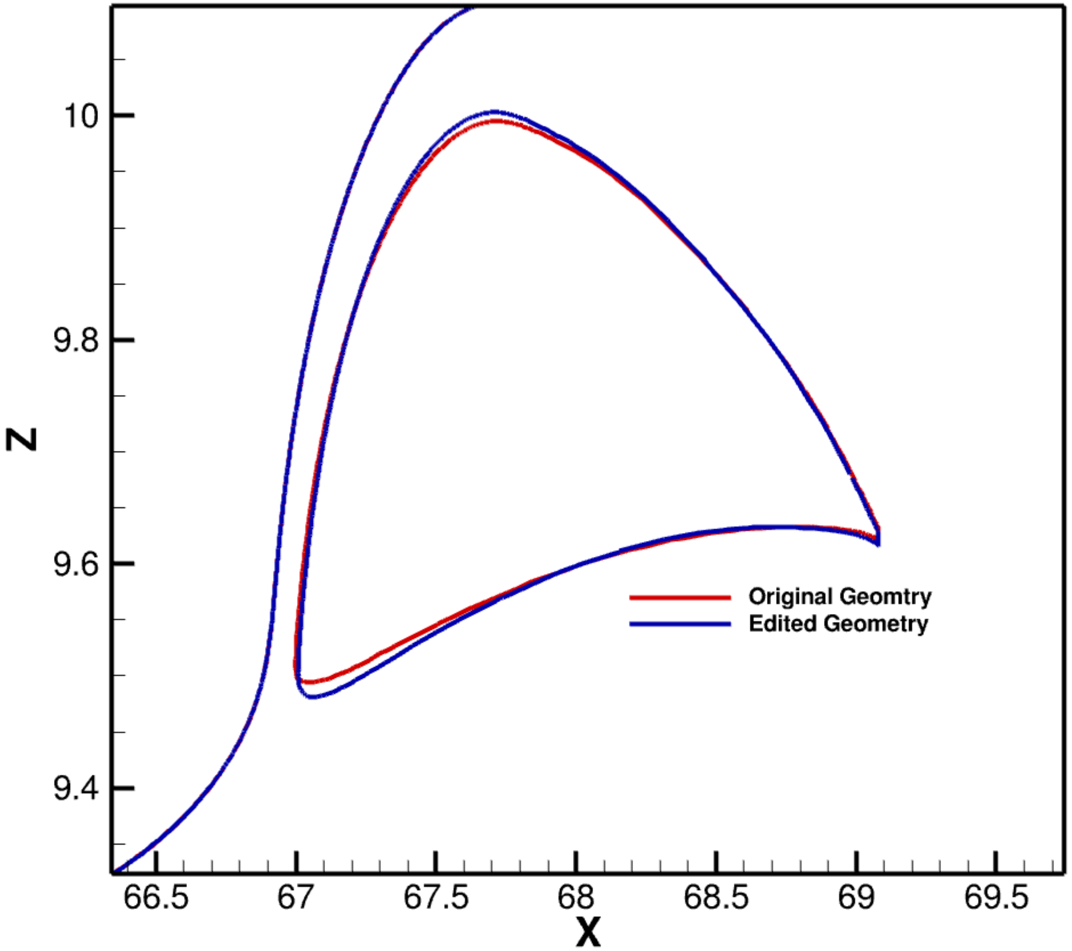

4.3 Shock Wave Elimination

- In the design of the aircraft wing, a sweep transformation was used on the S207 airfoil to define profiles parallel to the freestream [34,35]
  - A miscalculation was discovered, and its correction led to the generation of Configuration 2

Flap Differences Between Configuration and Configuration 2 at an Outboard Section

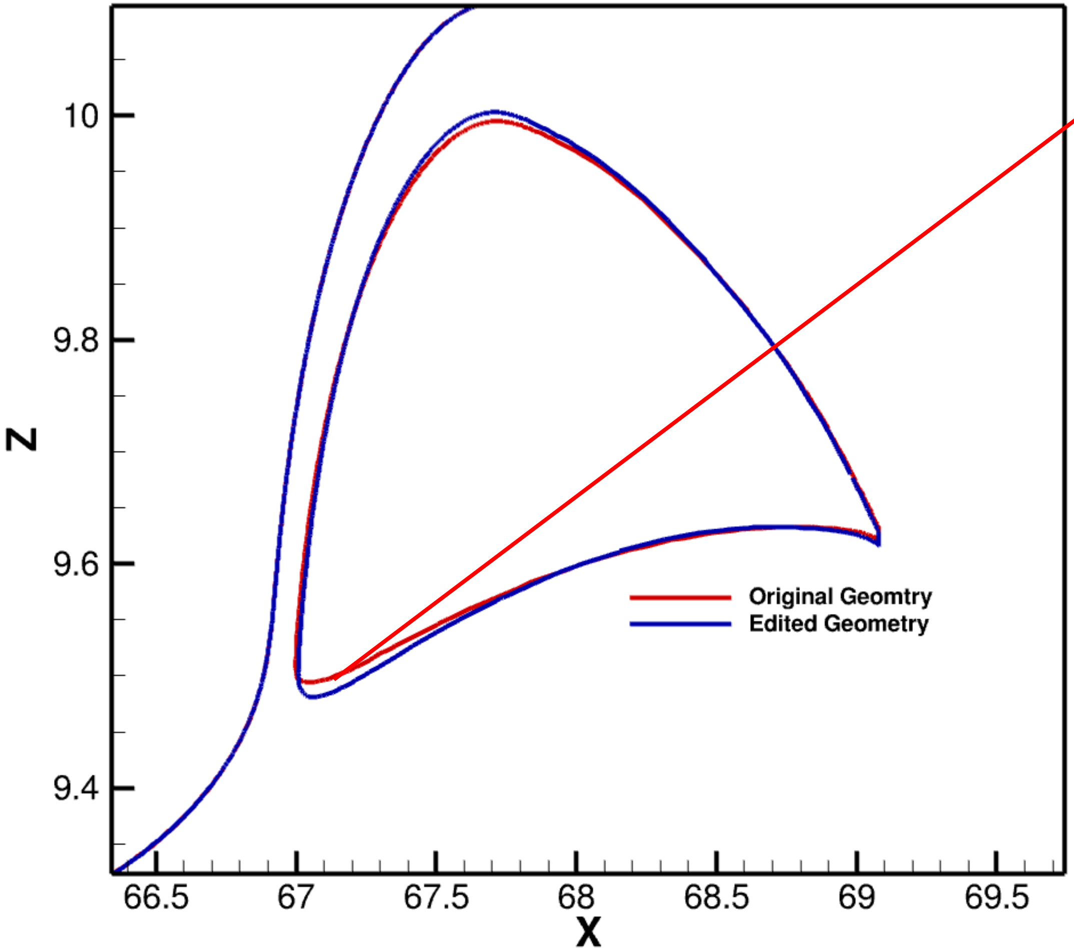

- Differences at the slot entrance were 0.13 inches in the horizontal direction and 0.16 inches in the vertical direction
  - Difference were within the range of 0.1% chord displacements found to be detrimental to airfoil performance

4.4 Initial Results for Configuration 3

- Configuration 2 was analyzed, but displayed early transition
- In light of the early transition on Configuration 2, further geometric modifications were made by the ULI members at UTK
    - Resulted in closer agreement between airfoil sections and the S207 airfoil 2D geometry
    - New geometry denoted Configuration 3

4.4 Initial Results for Configuration 3

- In light of the early transition on Configuration 2, further geometric modifications were made by the ULI members at UTK
  - Resulted in closer agreement between airfoil sections and the S207 airfoil 2D geometry
  - New geometry denoted Configuration 3

NSU2D-SA-Menter Free Transition Upper Surface C_{DF} for Configuration 3 at Mach = 0.7, AOA=-1.0°

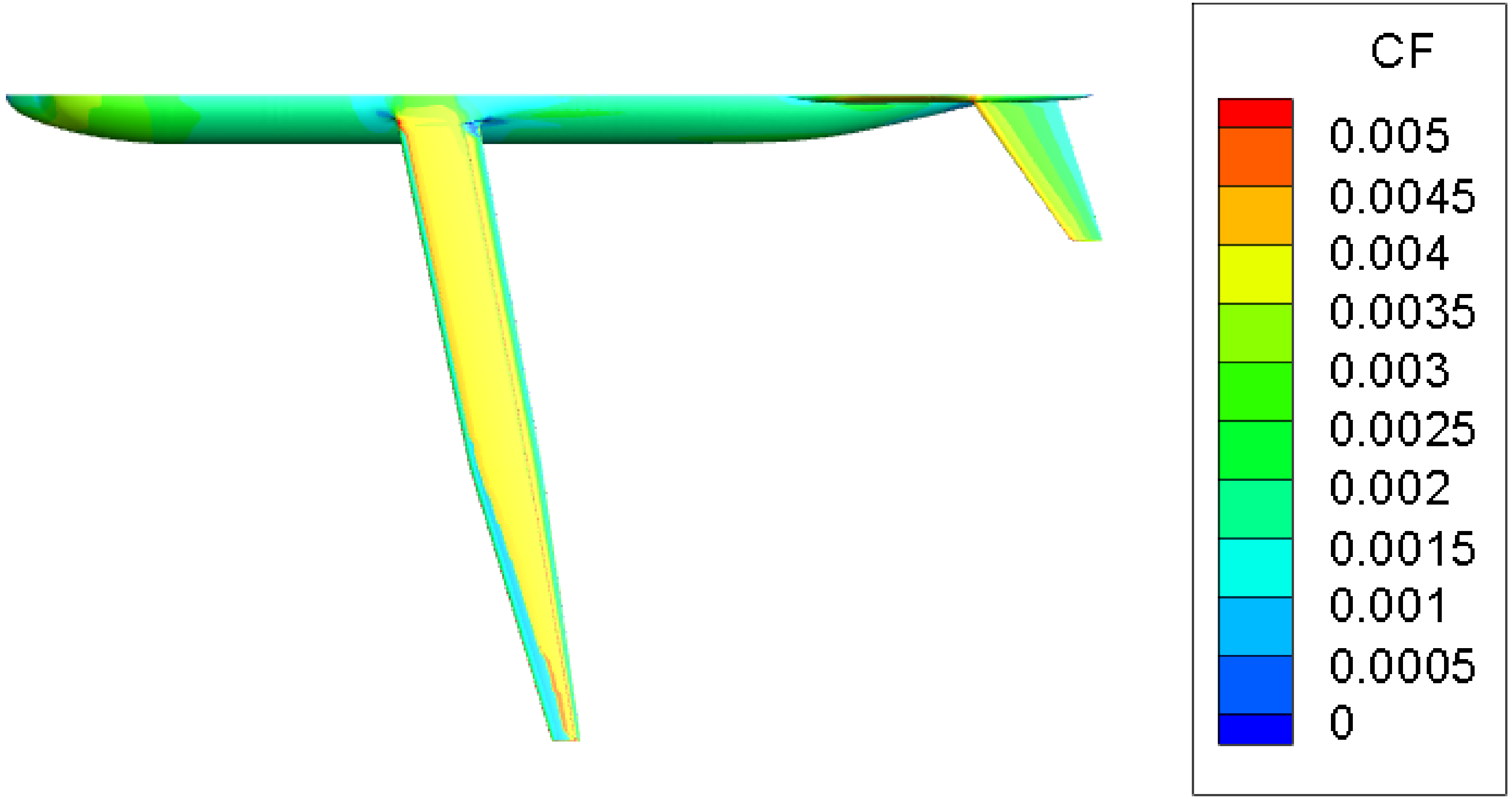

4.4 Initial Results for Configuration 3

- It was at this point that the decision was made to run the AFT2 transition model in place of the Menter model
- AFT2 model was used in 2D
- Rerun for Mach = 0.7, AOA = -1°

4.4 Initial Results for Configuration 3

- It was at this point that the decision was made to run the AFT2 transition model in place of the Menter model
- AFT2 model was used in 2D
- Rerun for Mach = 0.7, AOA = -1°

NSU2D-SA-AFT2 Free Transition Upper Surface C_{DF} for Configuration 3 at Mach = 0.7, AOA=-1.0°

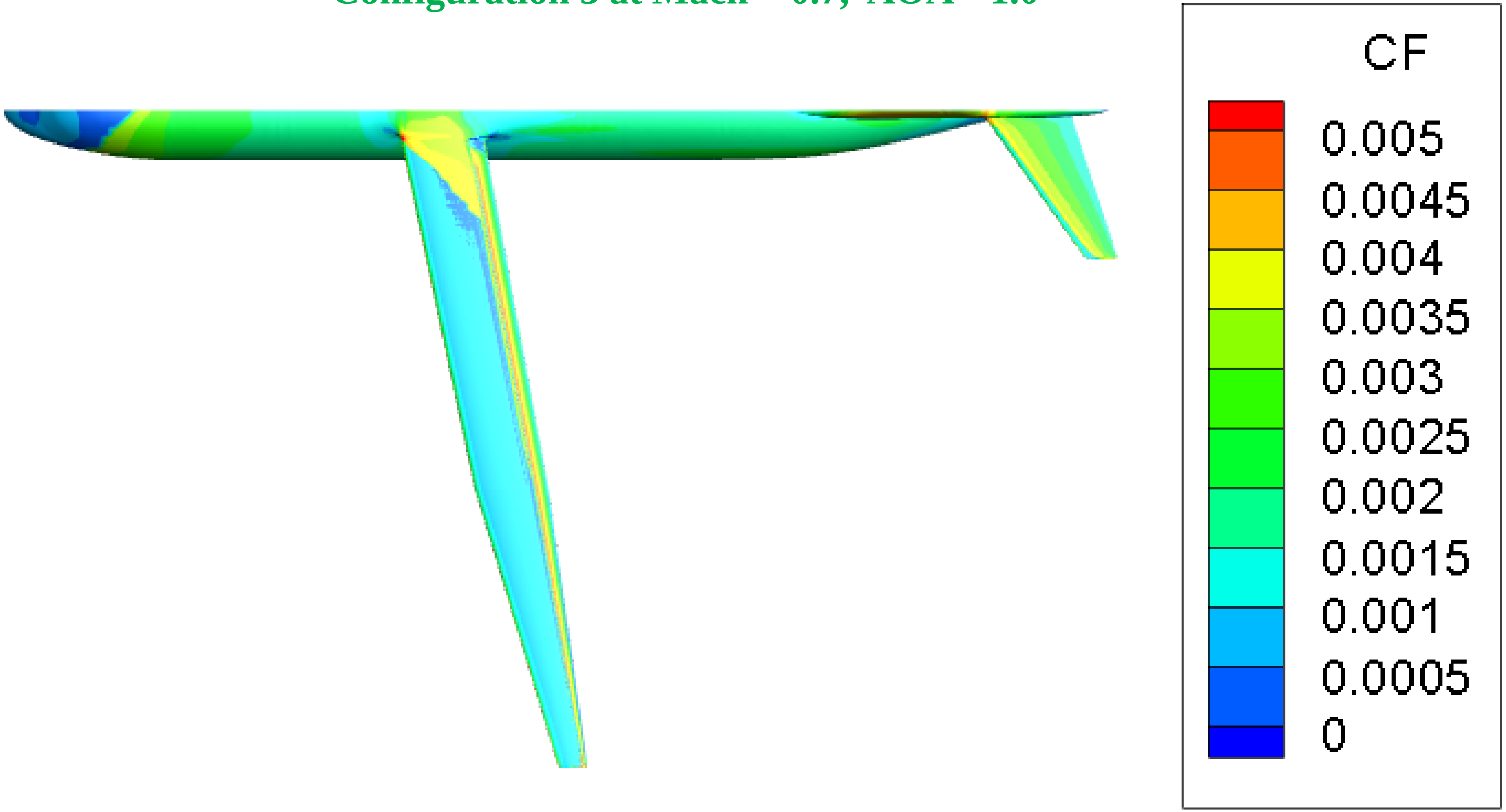

4.4 Initial Results for Configuration 3

- It was at this point that the decision was made to run the AFT2 transition model in place of the Menter model
- AFT2 model was used in 2D
- Rerun for Mach = 0.7, AOA = -1°

NSU2D-SA-AFT2 Free Transition Upper Surface C_{DF} for Configuration 3 at Mach = 0.7, AOA=-1.0°

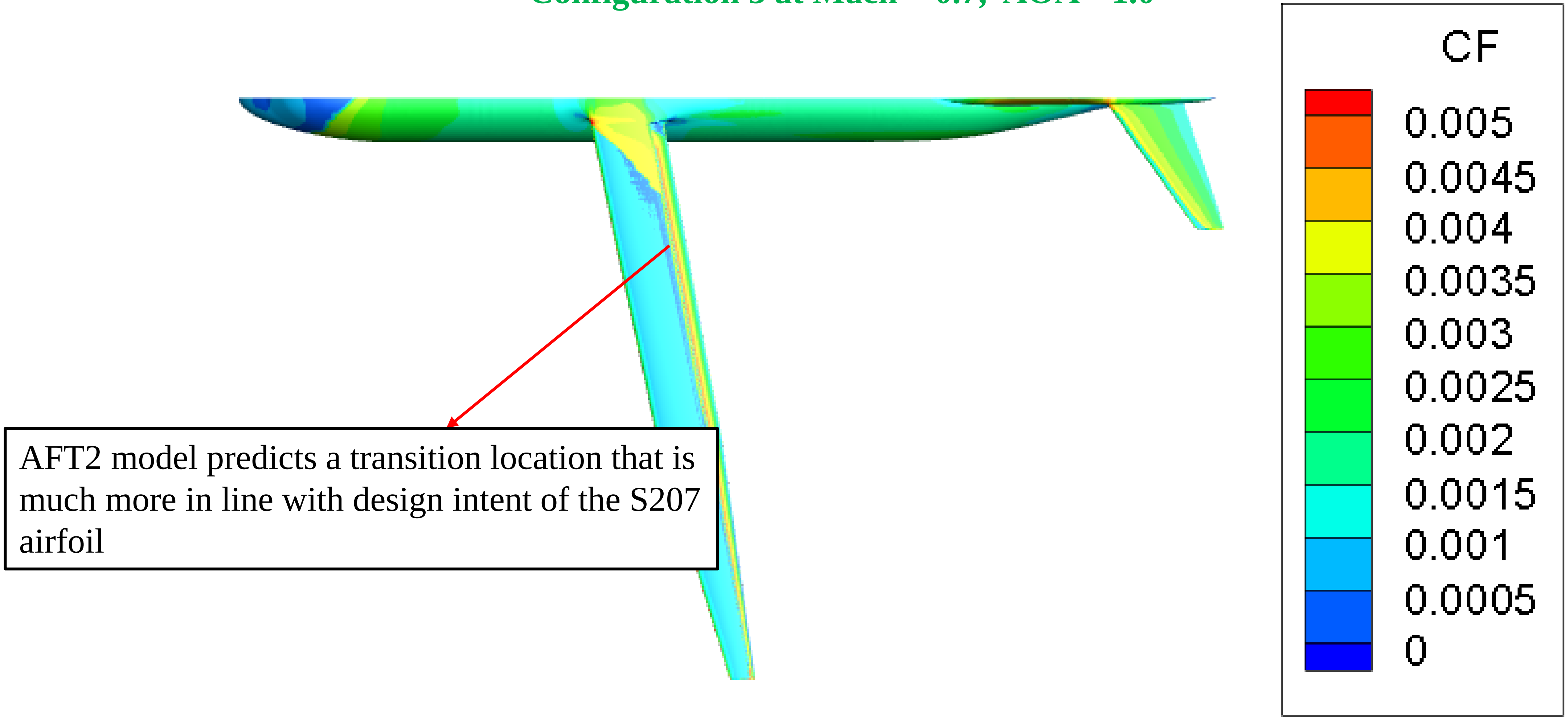

4.4 Initial Results for Configuration 3

- Two polars were developed initially for Configuration 3, Denoted Cases 1 and 2
  - Mach = 0.7273, Re = 12.3 Million, AOA = -2, -1, 0, 1, 1.5, 2.0, 2.5 degrees
  - Flow parameters and modeling details for both were requested by Boeing

S207 Partition Diagram

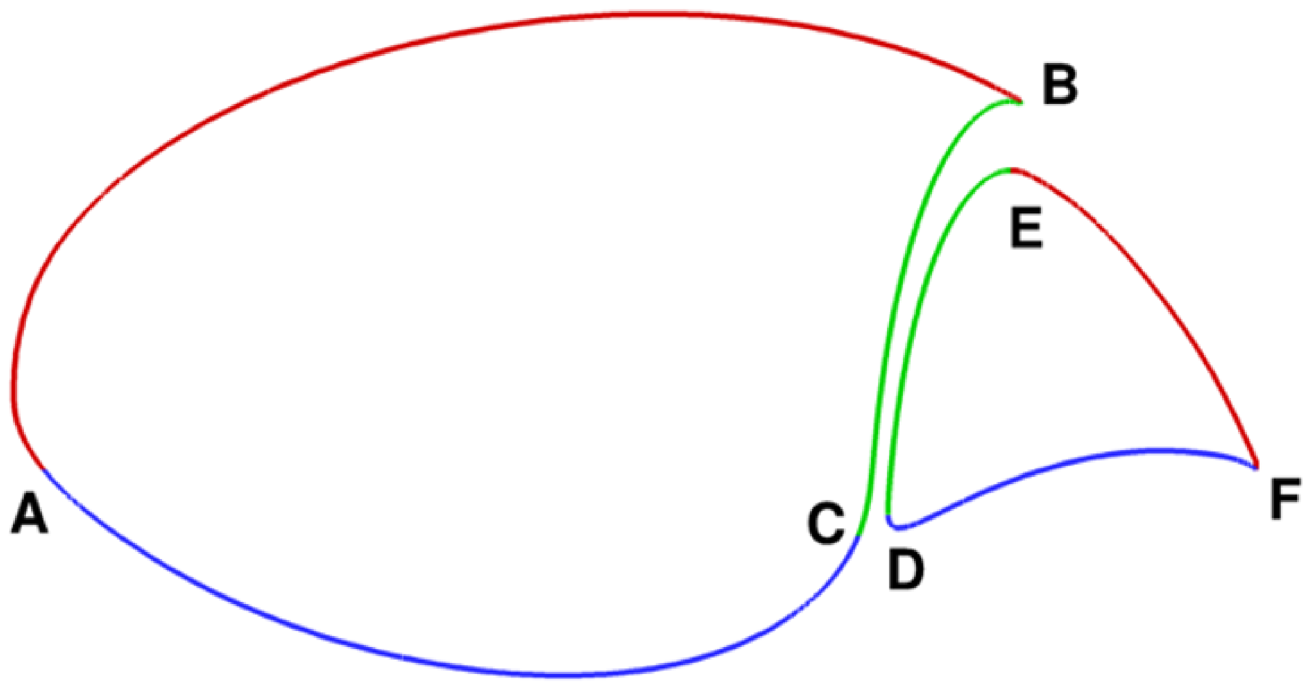

Cases 1 and 2 Modeling Summary

Case Number	Element	Segment	Modeling
1	Fore	AB	Free Transition
		AC	Free Transition
		CB	Free Transition
1	Aft	DE	Free Transition
		DF	Free Transition
		EF	Free Transition
2	Fore	AB	Free Transition
		AC	Fully Turbulent
		CB	Fully Turbulent
2	Aft	DE	Free Transition
		DF	Free Transition
		EF	Free Transition

4.4 Initial Results for Configuration 3

- Case 1 predicts higher lift and lower drag due to more laminar flow on the bottom surface of the wing

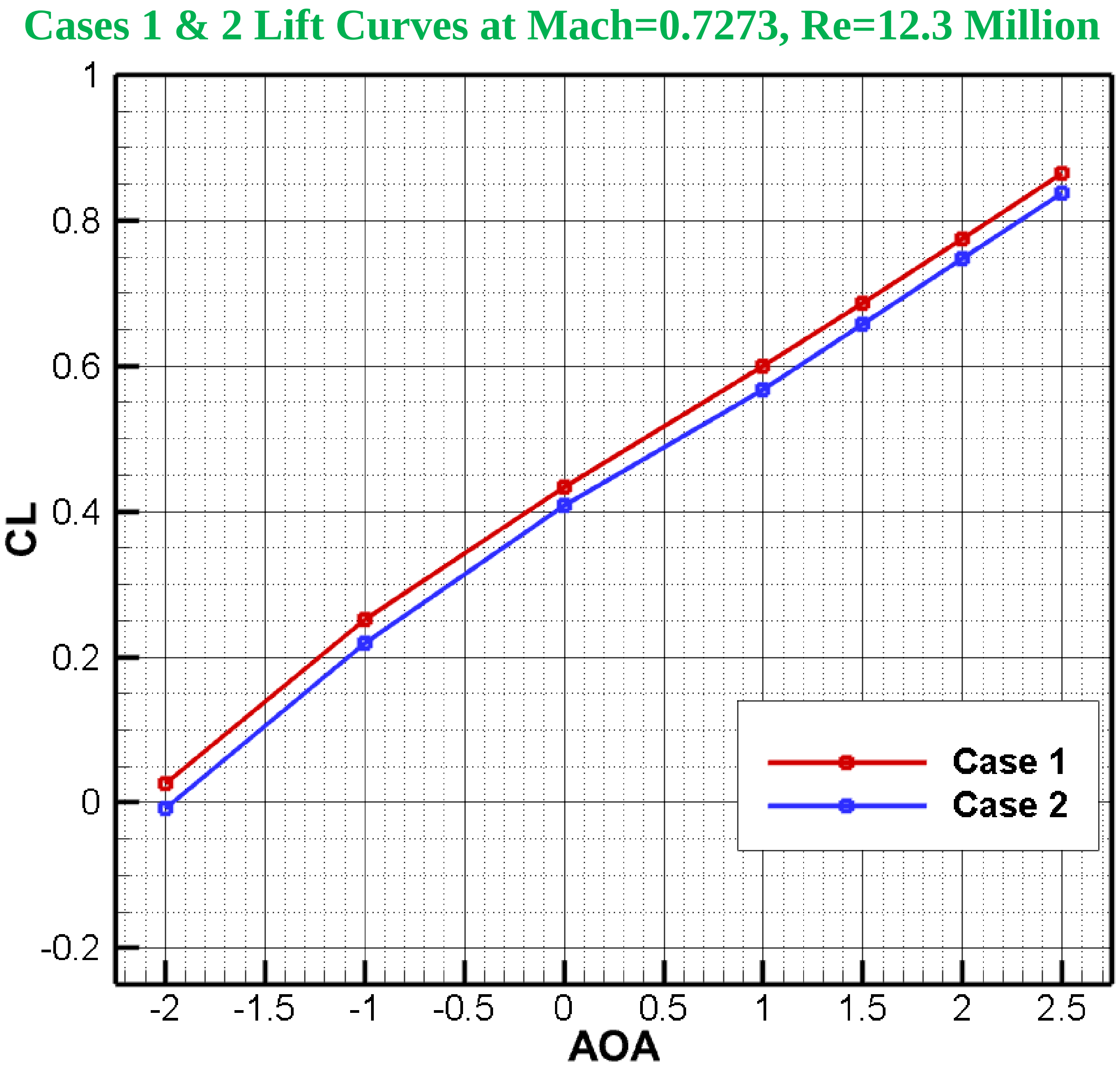

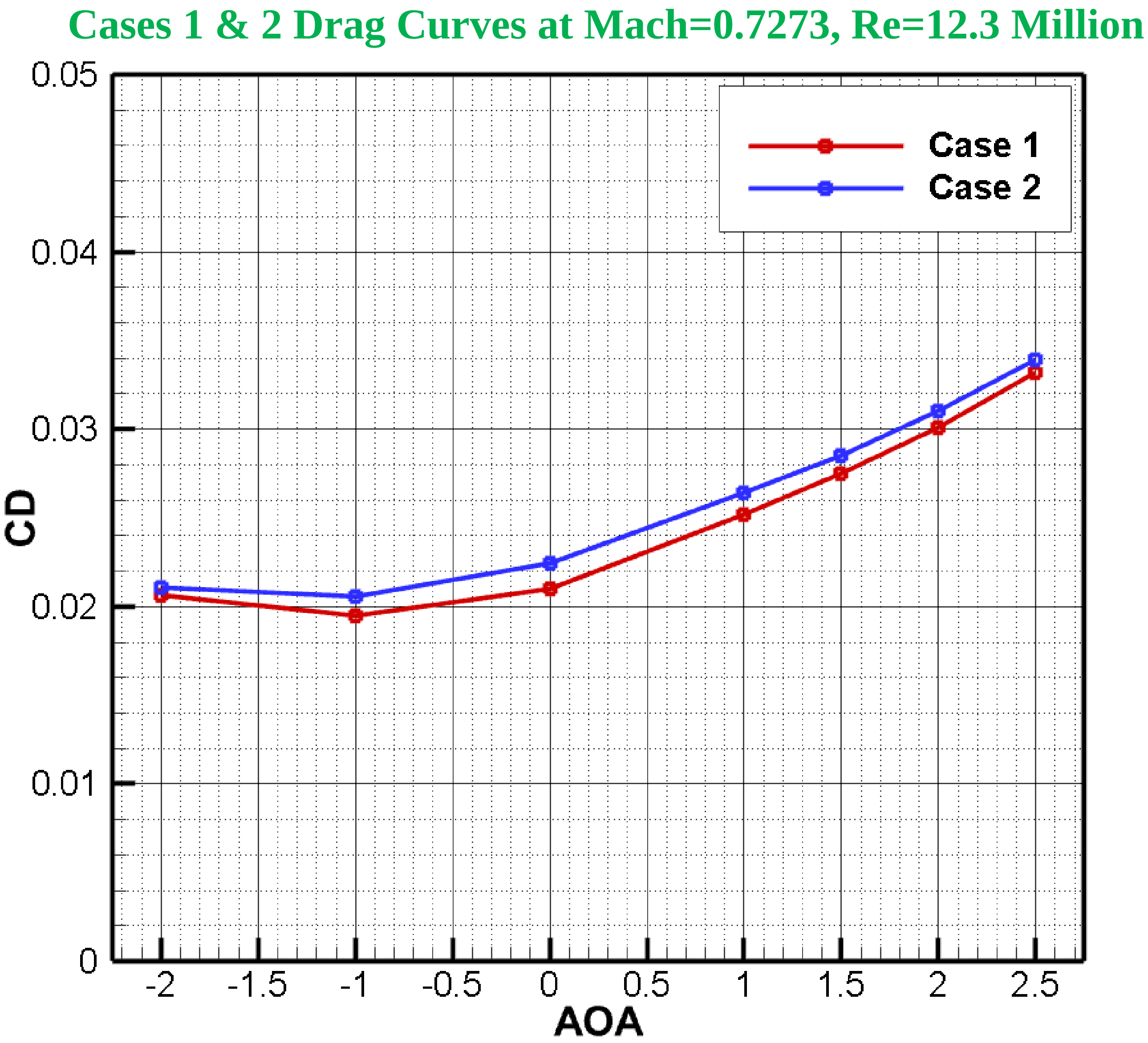

4.4 Initial Results for Configuration 3

- Examination of skin friction drag shows the formation of a low-drag bucket between -2° and 1°

Cases 1 & 2 C_{DF} at Mach=0.7273, Re=12.3 Million

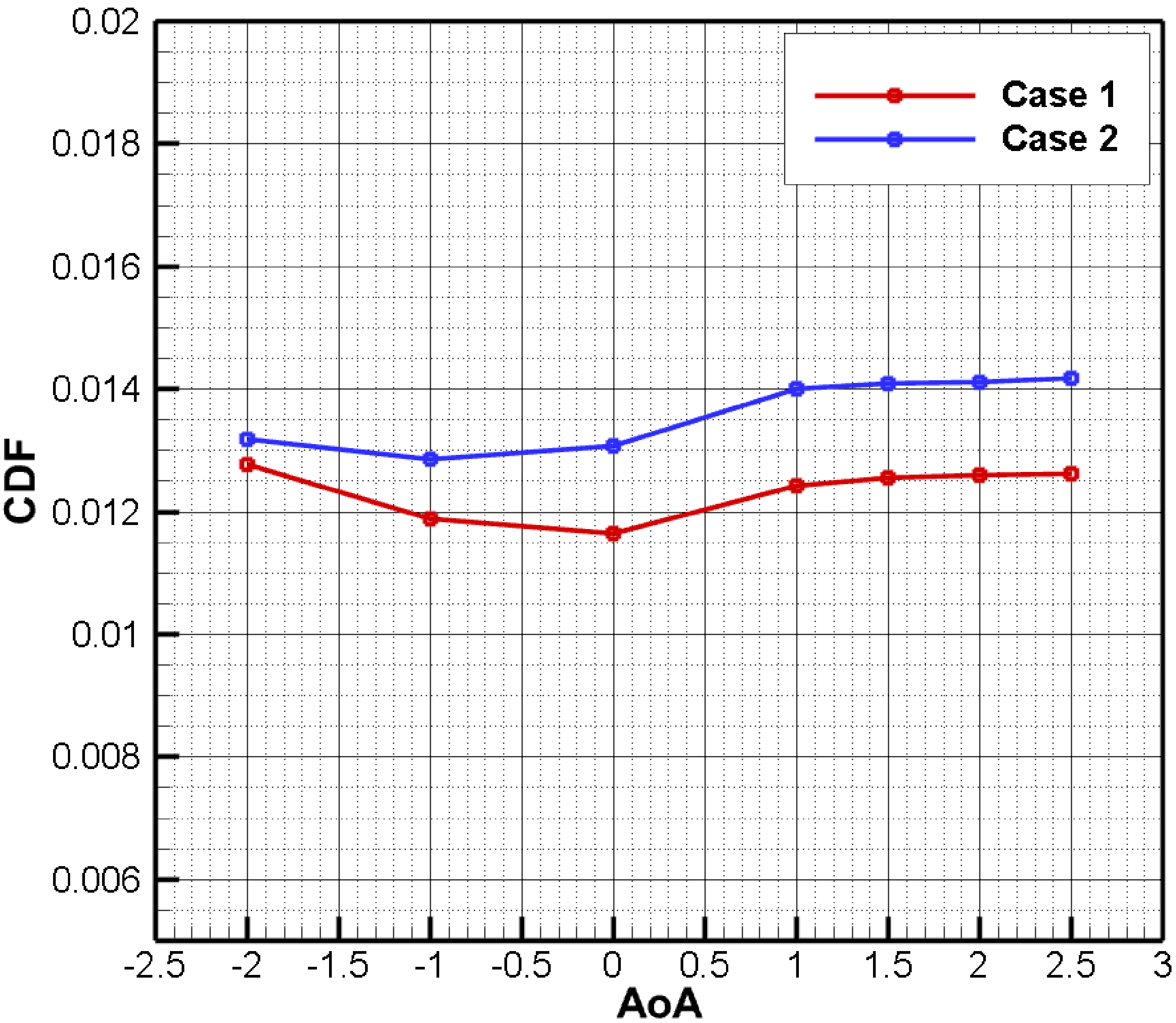

4.4 Initial Results for Configuration 3

- Examination of skin friction drag shows the formation of a low-drag bucket between -2° and 1°

Cases 1 & 2 C_{DF} at Mach=0.7273, Re=12.3 Million

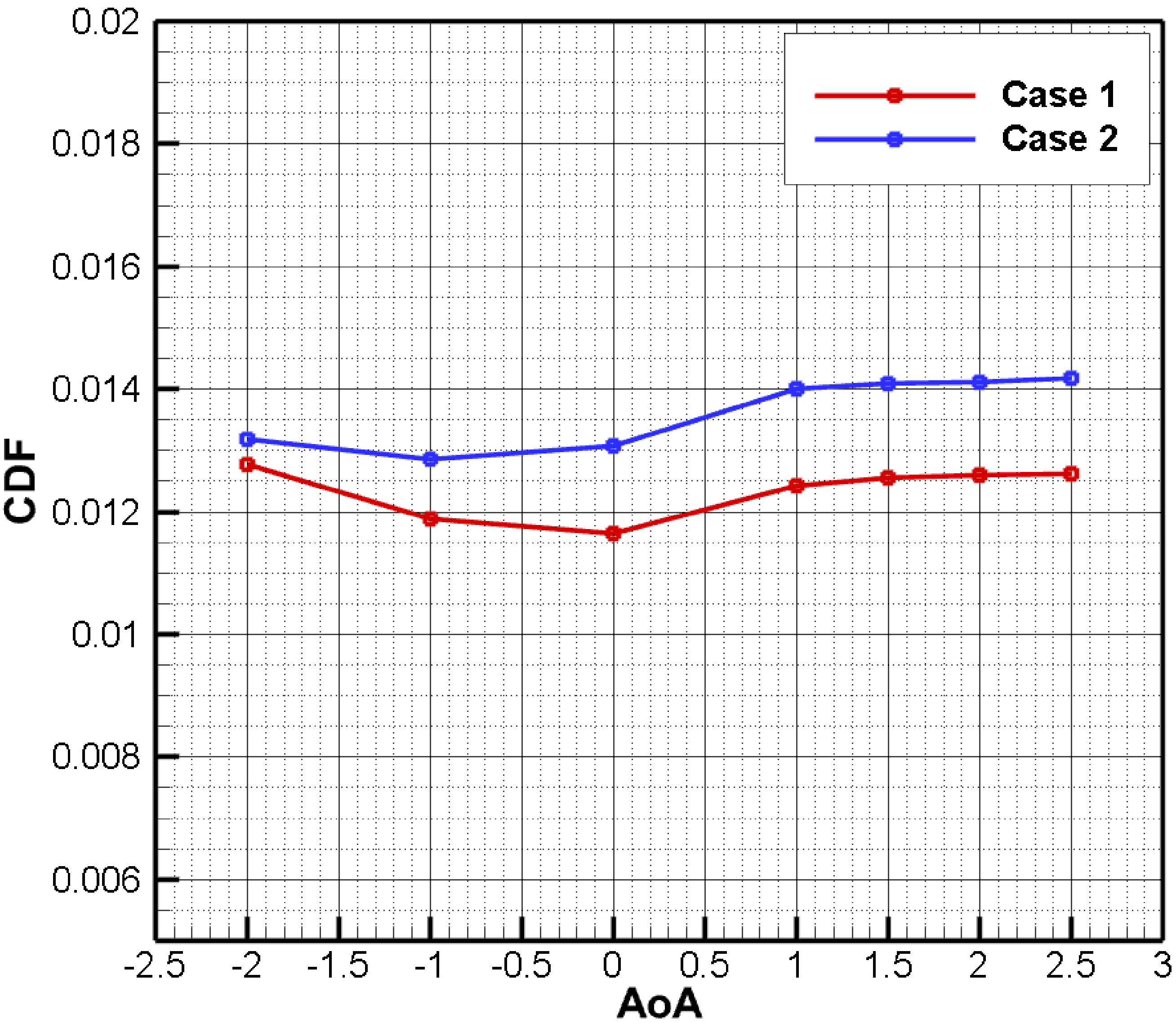

Case 1 Upper Surface C_{DF} at Mach=0.7273, Re=12.3 Million

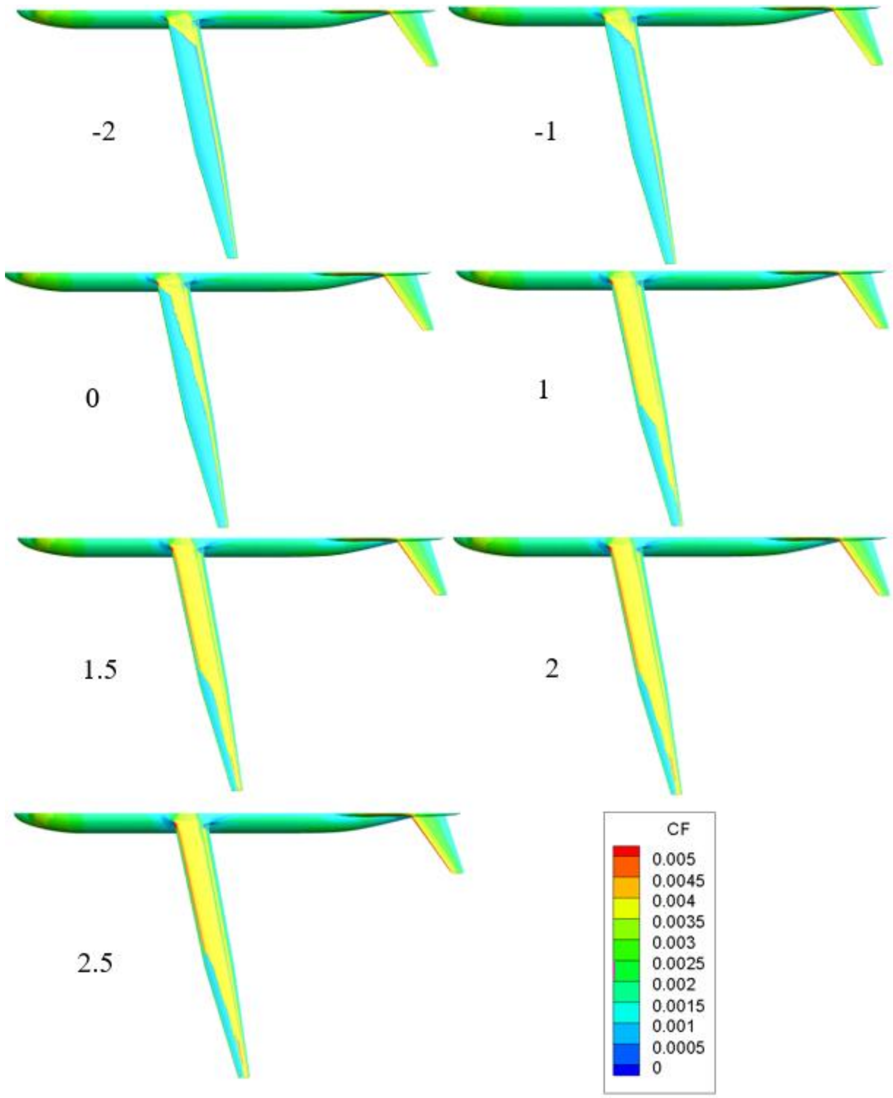

4.4 Initial Results for Configuration 3

- Examination of skin friction drag shows the formation of a low-drag bucket between -2° and 1°

Cases 1 & 2 C_{DF} at Mach=0.7273, Re=12.3 Million

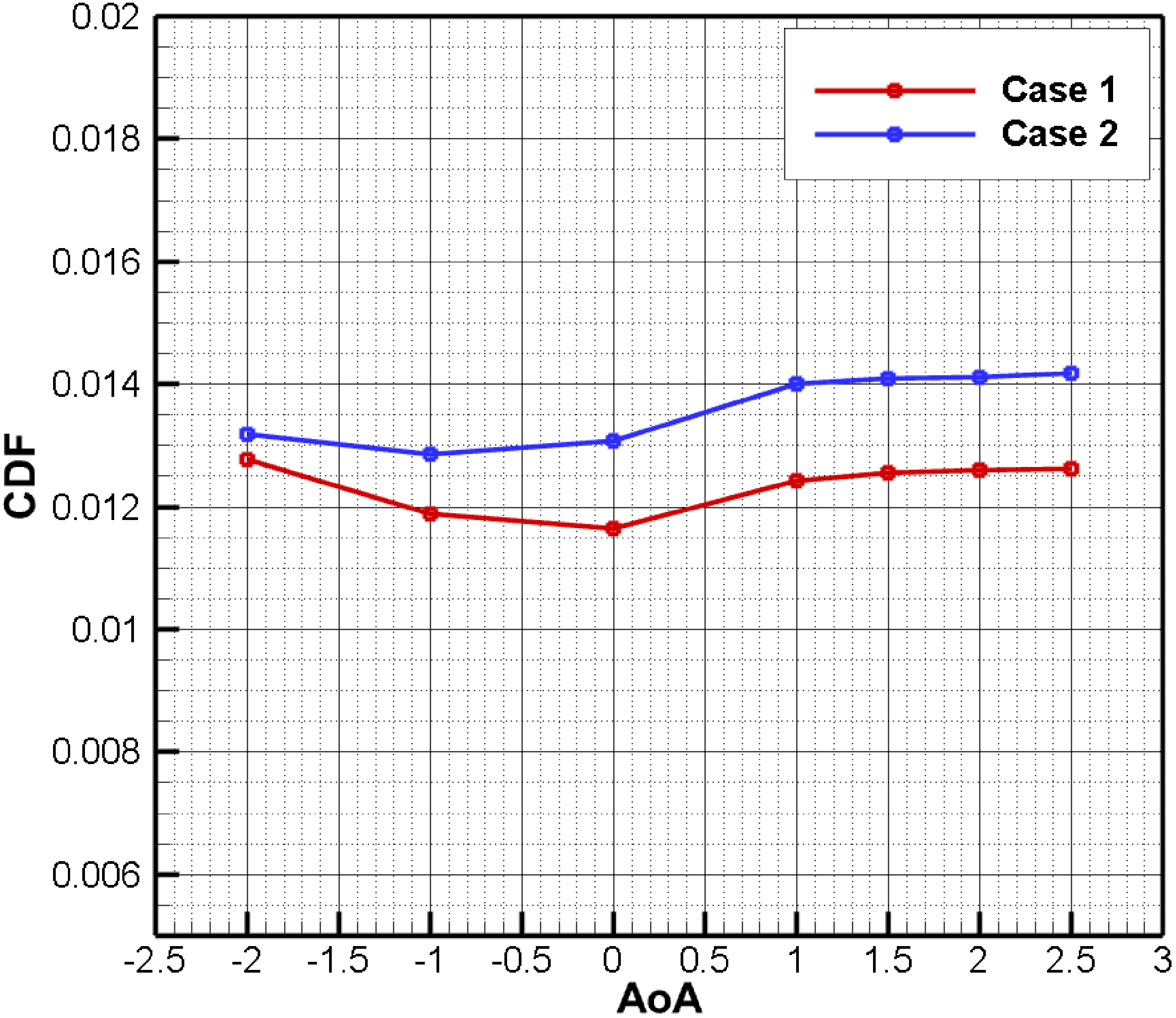

Case 1 Upper Surface C_{DF} at Mach=0.7273, Re=12.3 Million, AOA=0.0

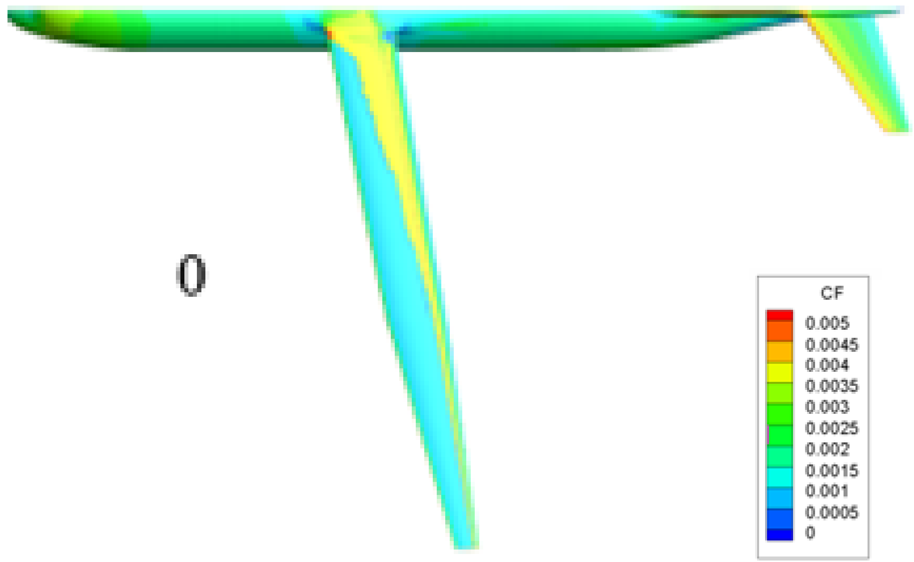

- Note the transition line for AOA=0 indicates lack of agreement with 2D design intent as transition seems to bleed from the fairing

4.4 Initial Results for Configuration 3

- Examination of skin friction drag shows the formation of a low-drag bucket between -2° and 1°

Cases 1 & 2 C_{DF} at Mach=0.7273, Re=12.3 Million

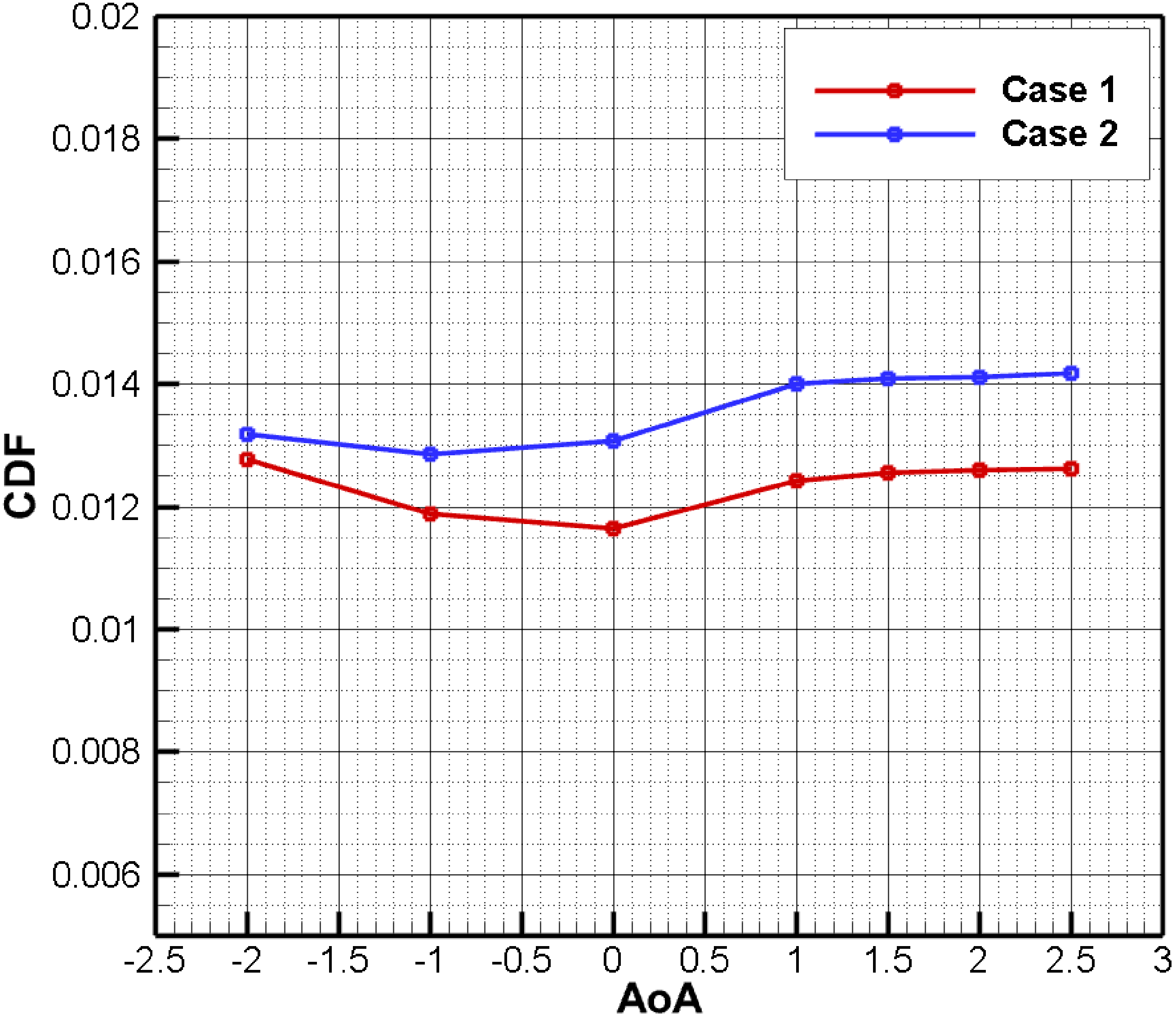

Case 1 Lower Surface C_{DF} at Mach=0.7273, Re=12.3 Million

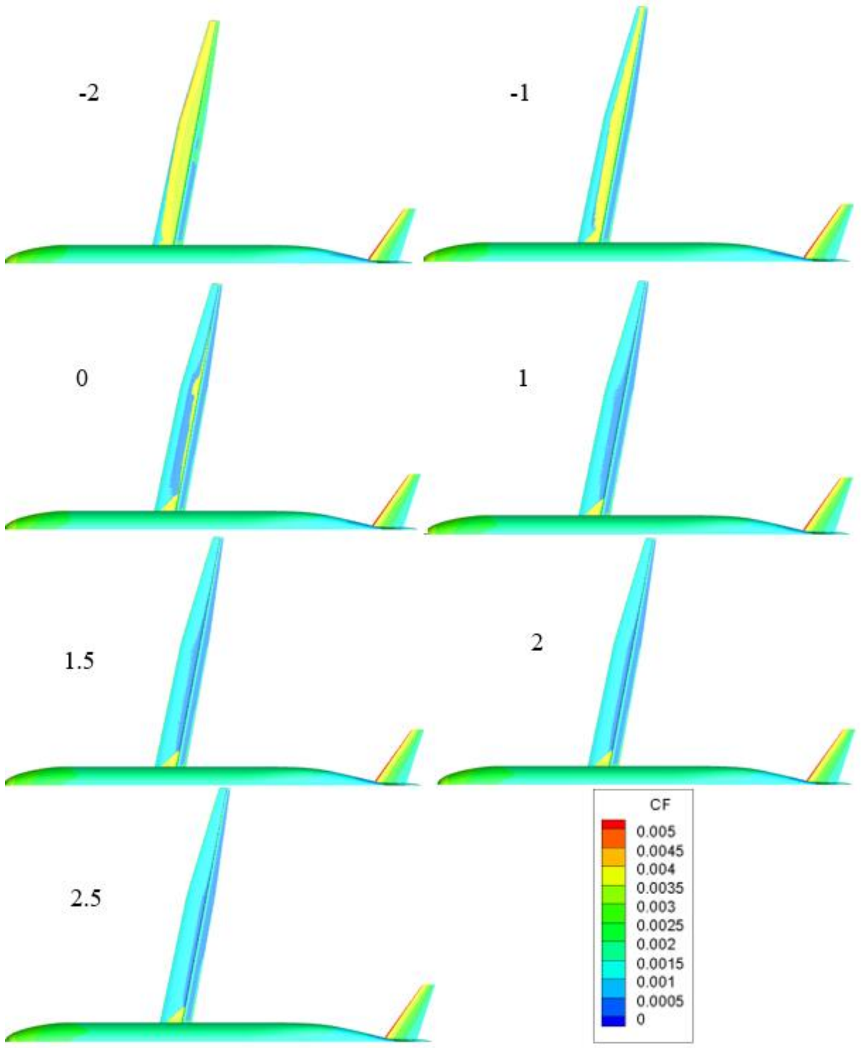

4.5 Polars for Configuration 3

- Full polars were developed for Configuration 3 using fully turbulent, Case 1, and Case 2 modeling
  - Fully turbulent runs and Case 1 Runs ranged from Mach = 0.200 to 0.750, and AOA = -2° to 5°
  - Number of runs for Case 2 specifics were reduced due to lack of computational resources
  - Requested and delivered to Boeing for input to their performance analysis

NSU3D-SA-AFT2 Free Transition (Entire Wing) Drag Polars for Re = 12.3 Million for Configuration 3

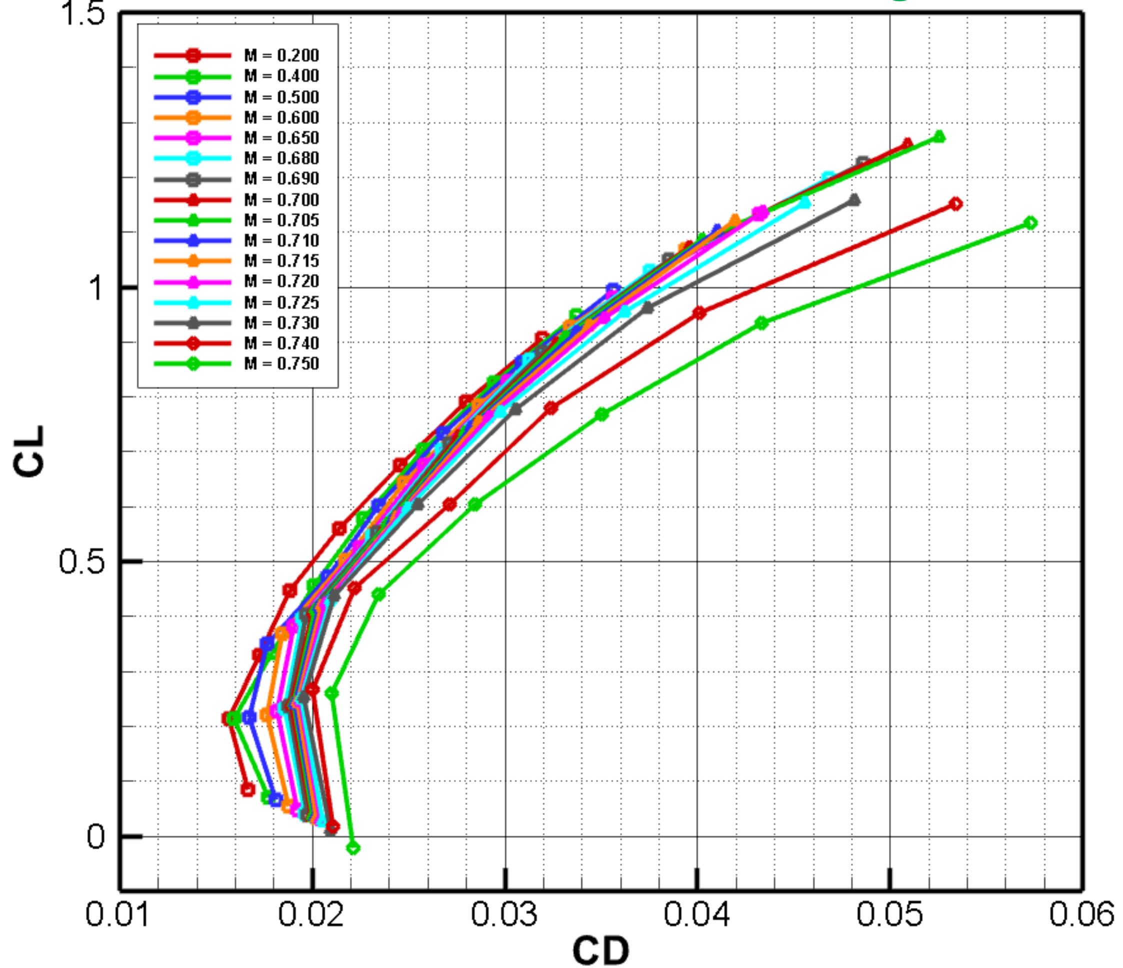

NSU3D-SA Fully Turbulent Drag Polars for Re = 12.3 Million for Configuration 3

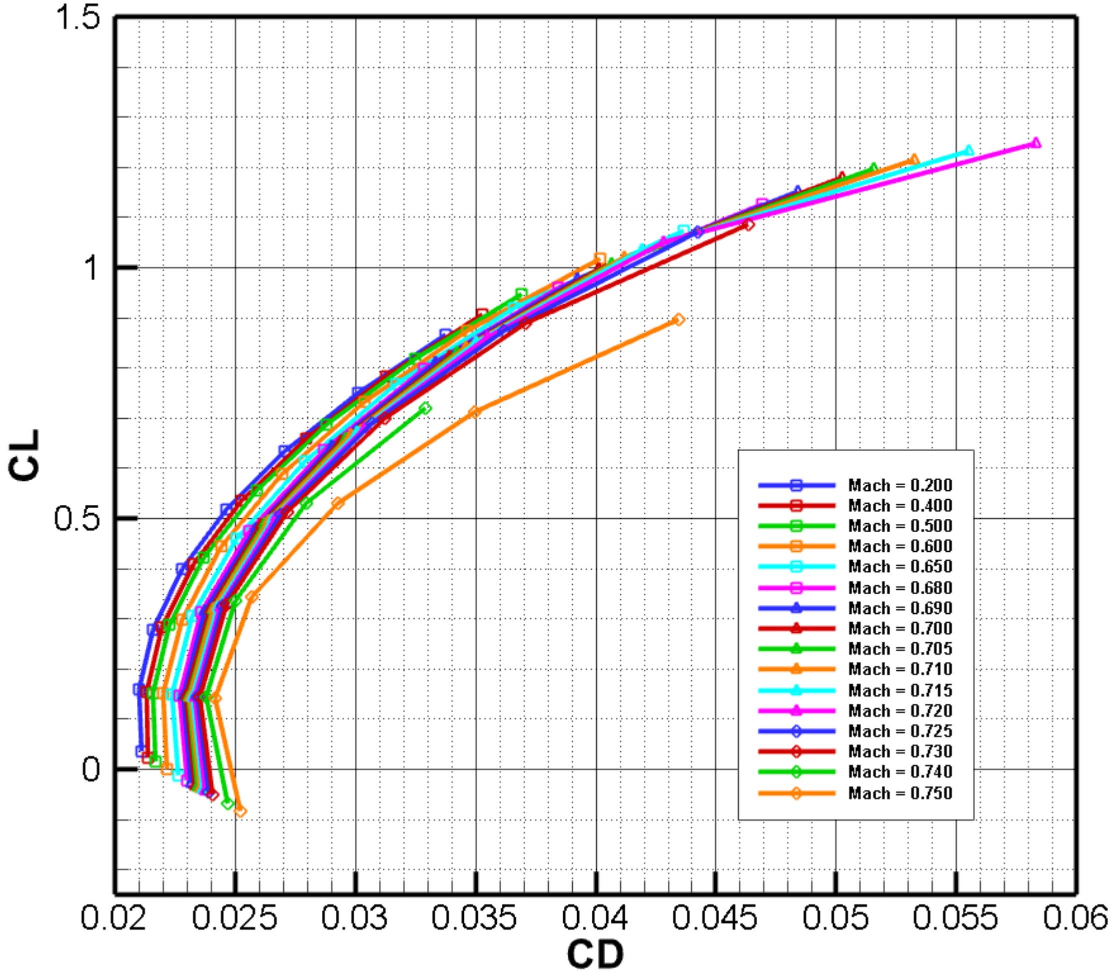

4.5 Polars for Configuration 3

- Full polars were developed for Configuration 3 using fully turbulent, Case 1, and Case 2 modeling
  - Fully turbulent runs and Case 1 Runs ranged from Mach = 0.200 to 0.750, and AOA = -2° to 5°
  - Number of runs for Case 2 specifics were reduced due to lack of computational resources
  - Requested and delivered to Boeing for input to their performance analysis

NSU3D-SA-AFT2 (Full Wing) Results Compared to NSU3D-SA Results for Configuration 3

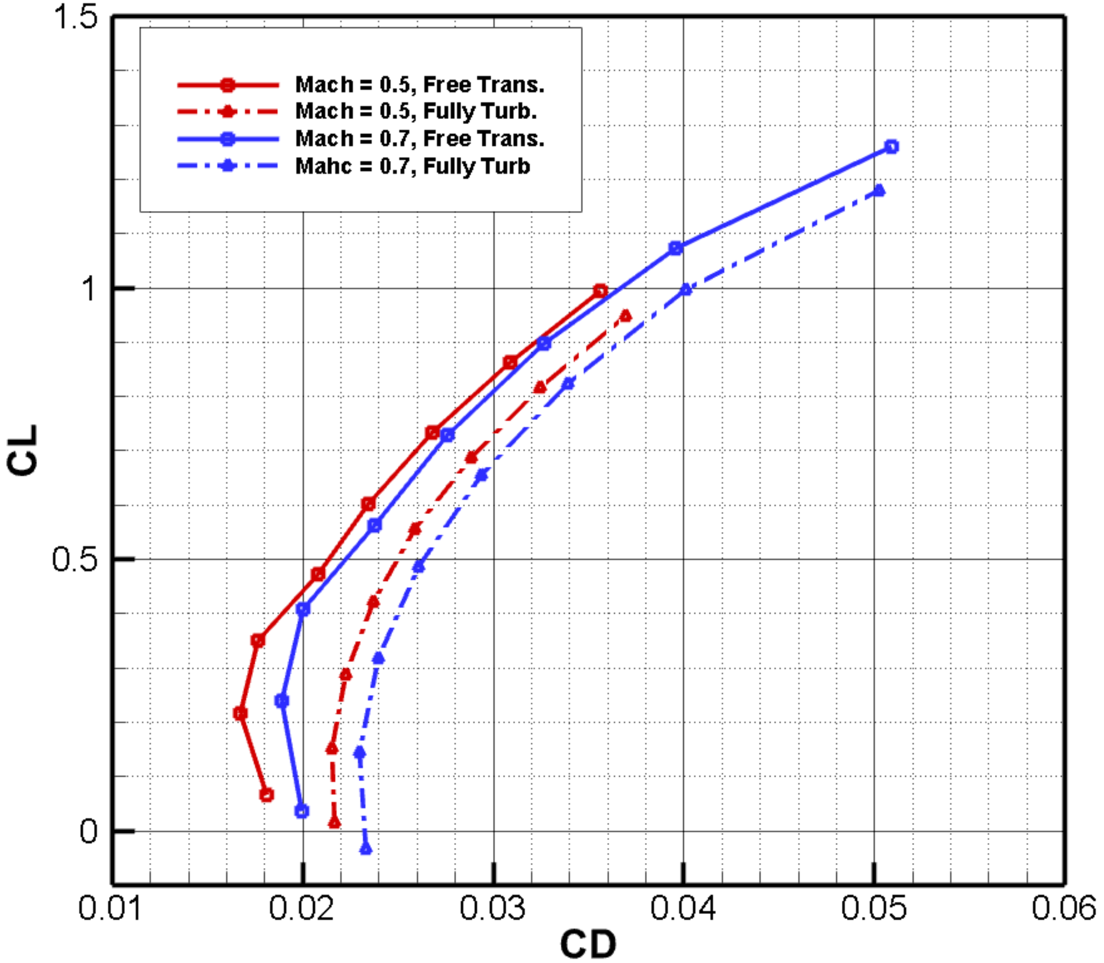

4.5 Polars for Configuration 3

- Full polars were developed for Configuration 3 using fully turbulent, Case 1, and Case 2 modeling
  - Fully turbulent runs and Case 1 Runs ranged from Mach = 0.200 to 0.750, and AOA = -2° to 5°
  - Number of runs for Case 2 specifics were reduced due to lack of computational resources
  - Requested and delivered to Boeing for input to their performance analysis

NSU3D-SA-AFT2 (Full Wing) Results Compared to NSU3D-SA Results for Configuration 3

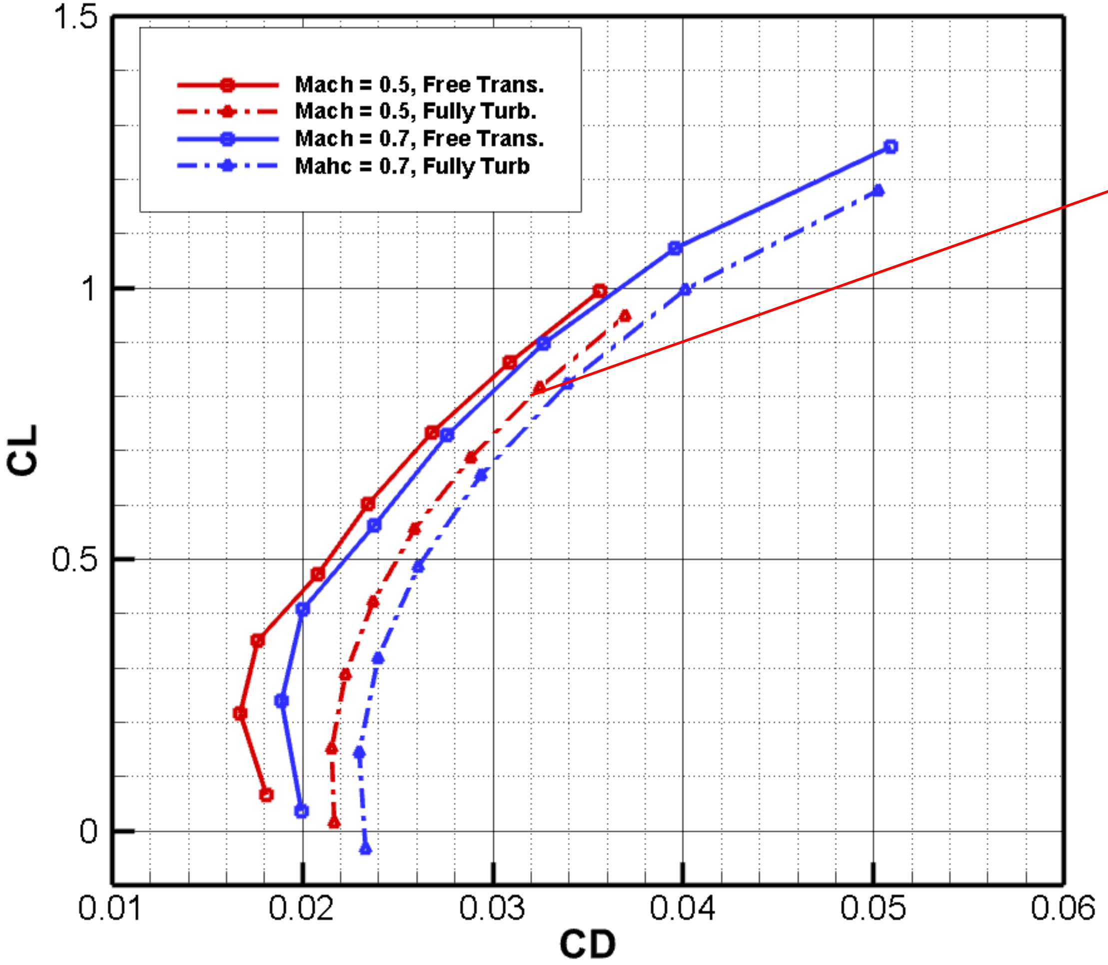

- Once again, free transition results predict higher lift coefficients and lower drag coefficients compared to fully turbulent runs

4.5 Polars for Configuration 3

- Full polars were developed for Configuration 3 using fully turbulent, Case 1, and Case 2 modeling
  - Fully turbulent runs and Case 1 Runs ranged from Mach = 0.200 to 0.750, and AOA = -2° to 5°
  - Number of runs for Case 2 specifics were reduced due to lack of computational resources
  - Requested and delivered to Boeing for input to their performance analysis

NSU3D-SA-AFT2 (Full Wing) Results Compared to NSU3D-SA Results for Configuration 3

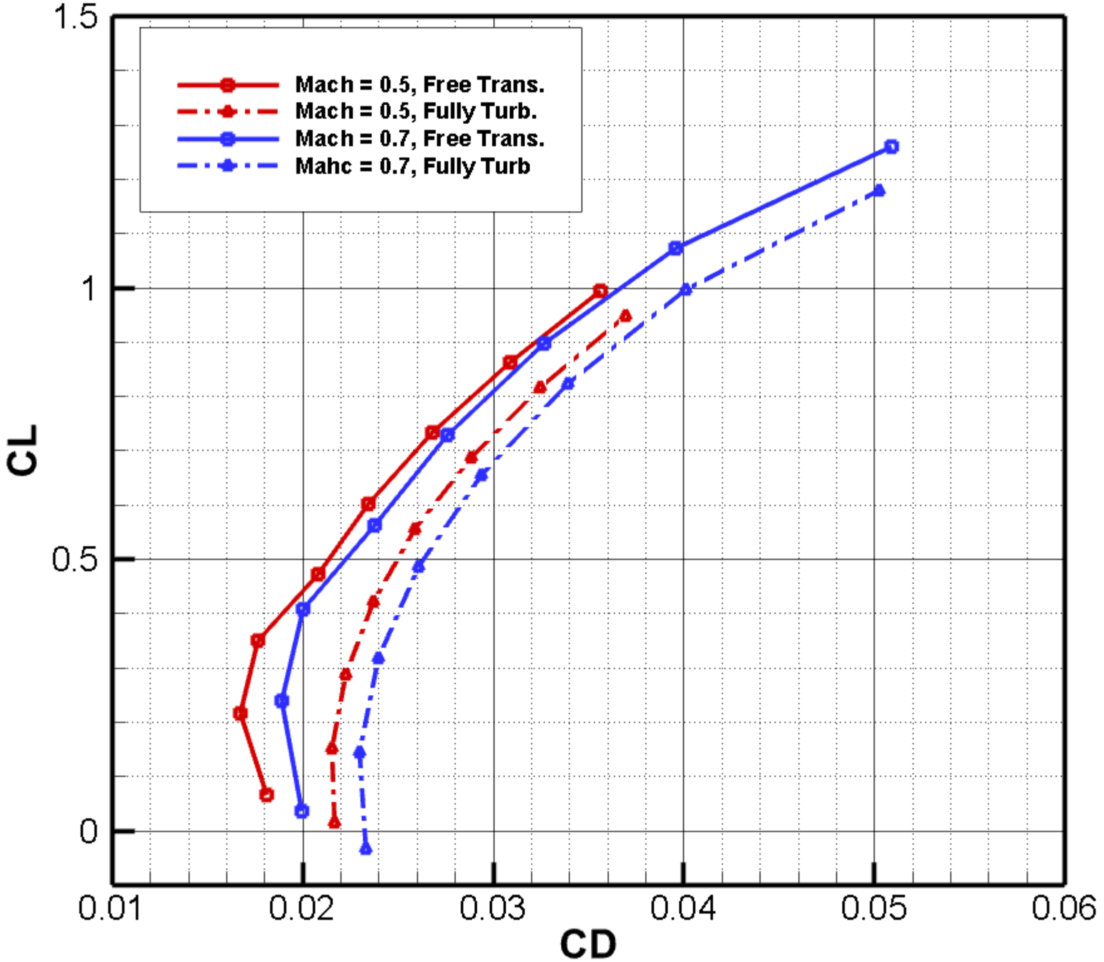

- Once again, free transition results predict higher lift coefficients and lower drag coefficients compared to fully turbulent runs

- Note that other data was provided to Boeing as well, such as pitching moment curves and pressure drag curves, but are excluded for brevity
- Runs that use Case 2 specifics have also been excluded, as quantification of differences was done in Section 4.4

4.5 Polars for Configuration 3

- Full polars were developed for Configuration 3 using fully turbulent, Case 1, and Case 2 modeling
  - Fully turbulent runs and Case 1 Runs ranged from Mach = 0.200 to 0.750, and AOA = -2° to 5°
  - Number of runs for Case 2 specifics were reduced due to lack of computational resources
  - Requested and delivered to Boeing for input to their performance analysis

NSU3D-SA Fully Turbulent CDF at Re = 12.3 Million

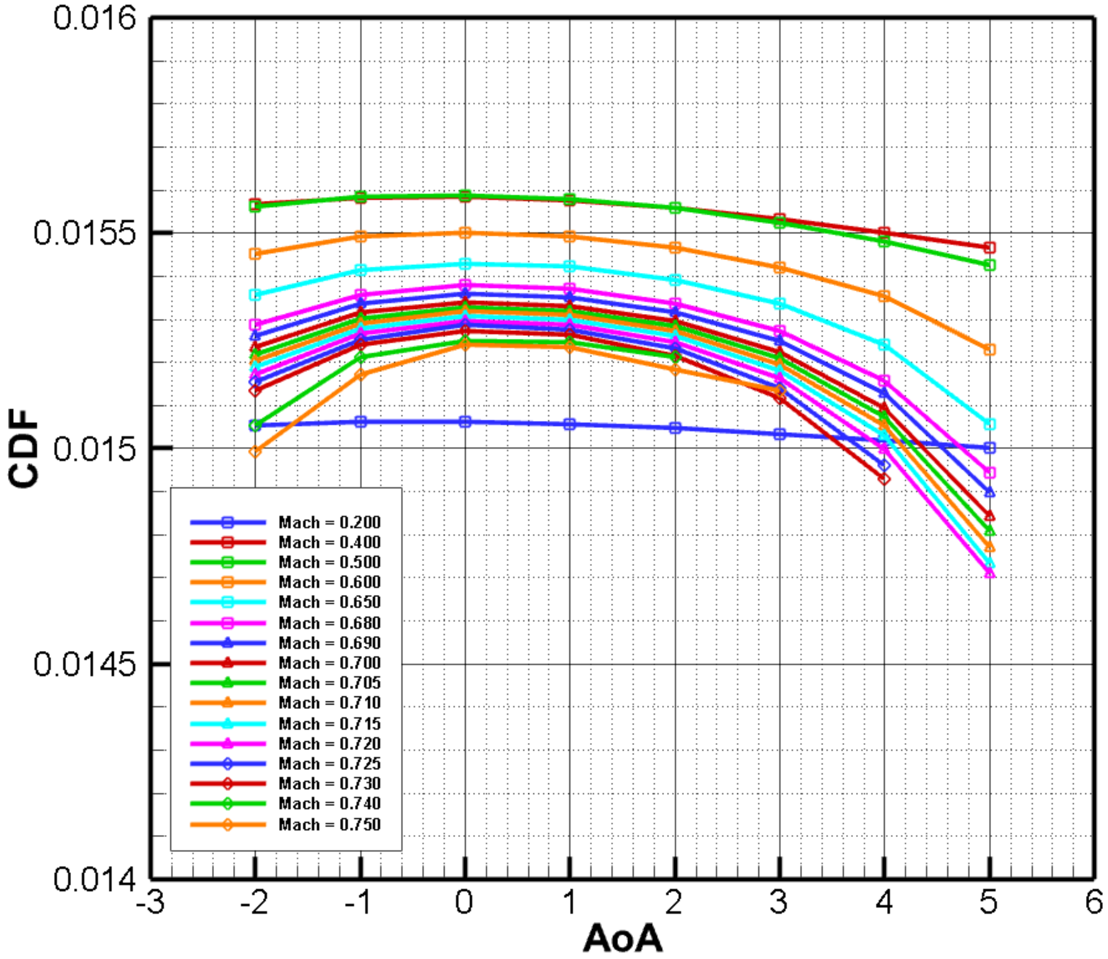

NSU3D-SA-AFT2 Free Transition CDF at Re = 12.3 Million

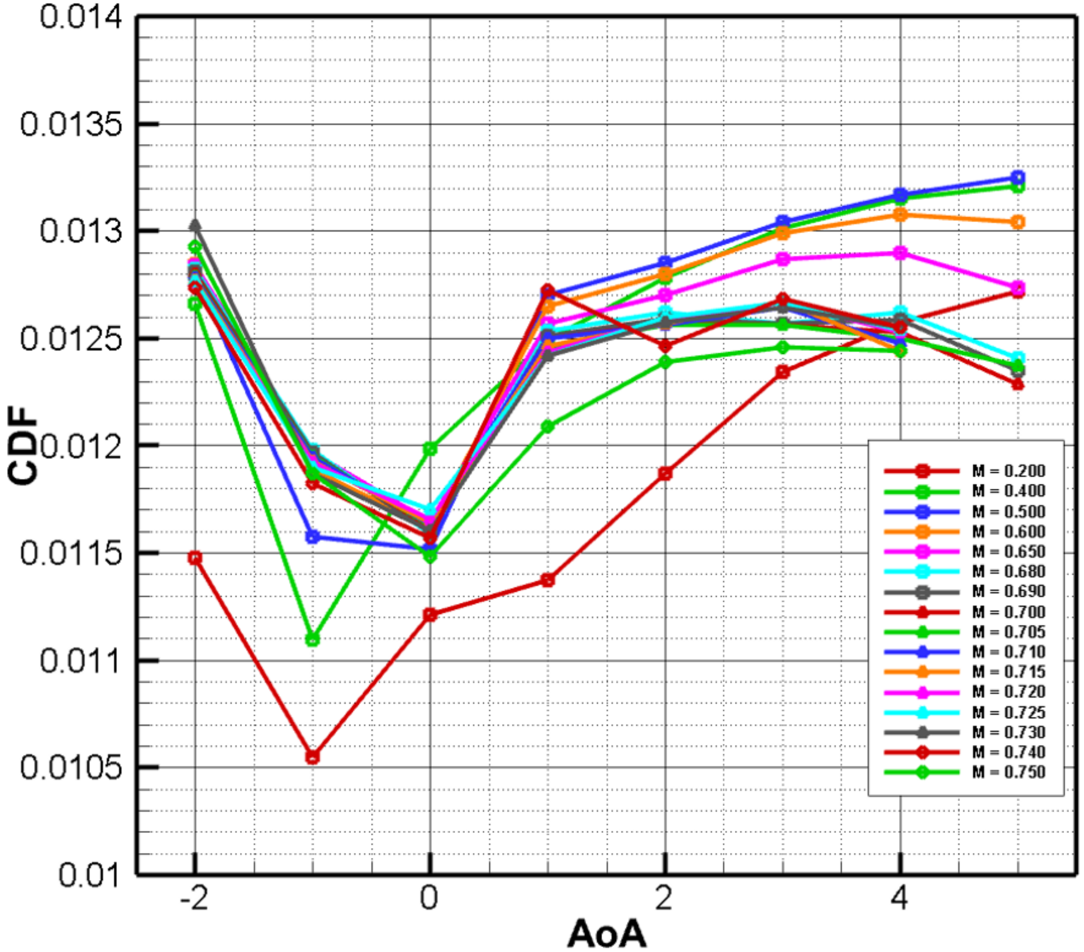

4.5 Polars for Configuration 3

- Full polars were developed for Configuration 3 using fully turbulent, Case 1, and Case 2 modeling
  - Fully turbulent runs and Case 1 Runs ranged from Mach = 0.200 to 0.750, and AOA = -2° to 5°
  - Number of runs for Case 2 specifics were reduced due to lack of computational resources
  - Requested and delivered to Boeing for input to their performance analysis

NSU3D-SA Fully Turbulent CDF at Re = 12.3 Million

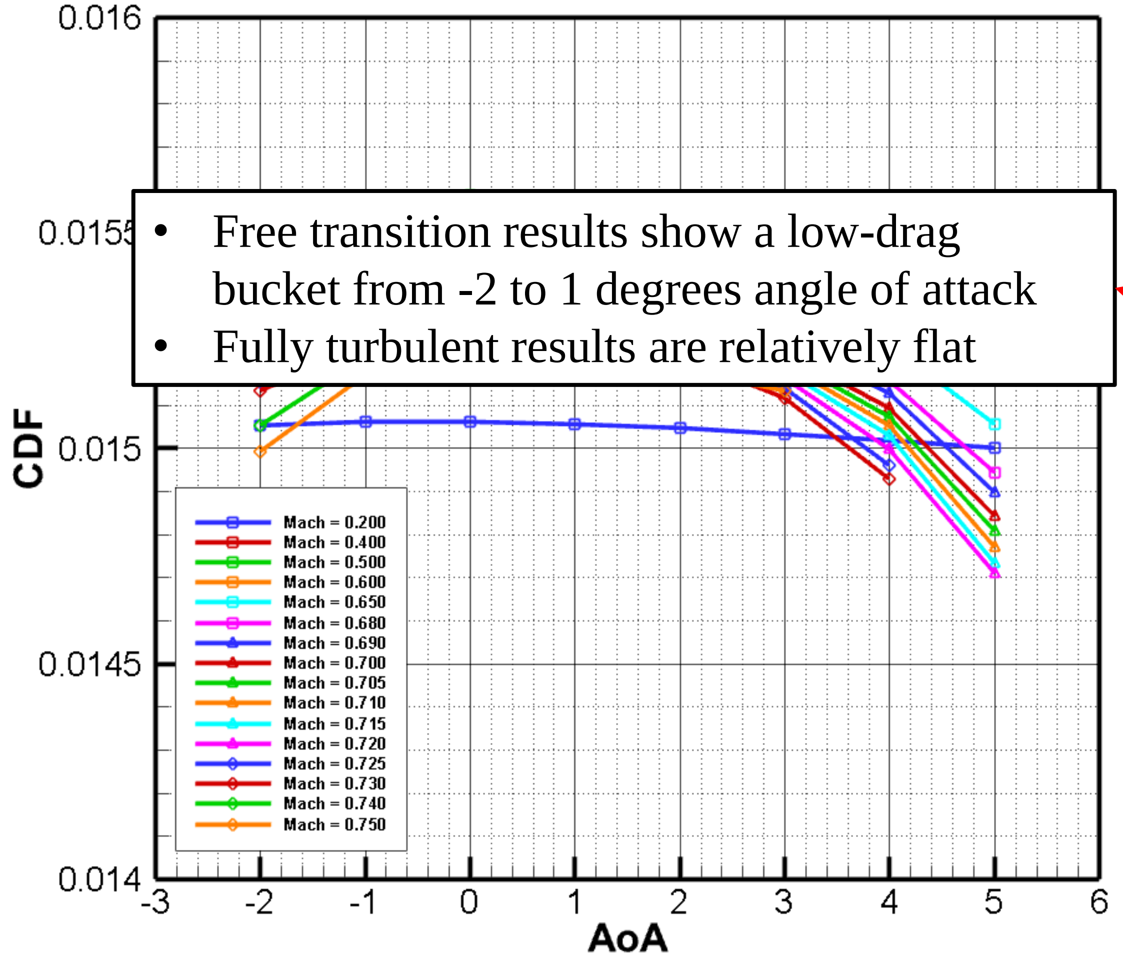

- Free transition results show a low-drag bucket from -2 to 1 degrees angle of attack
- Fully turbulent results are relatively flat

NSU3D-SA-AFT2 Free Transition CDF at Re = 12.3 Million

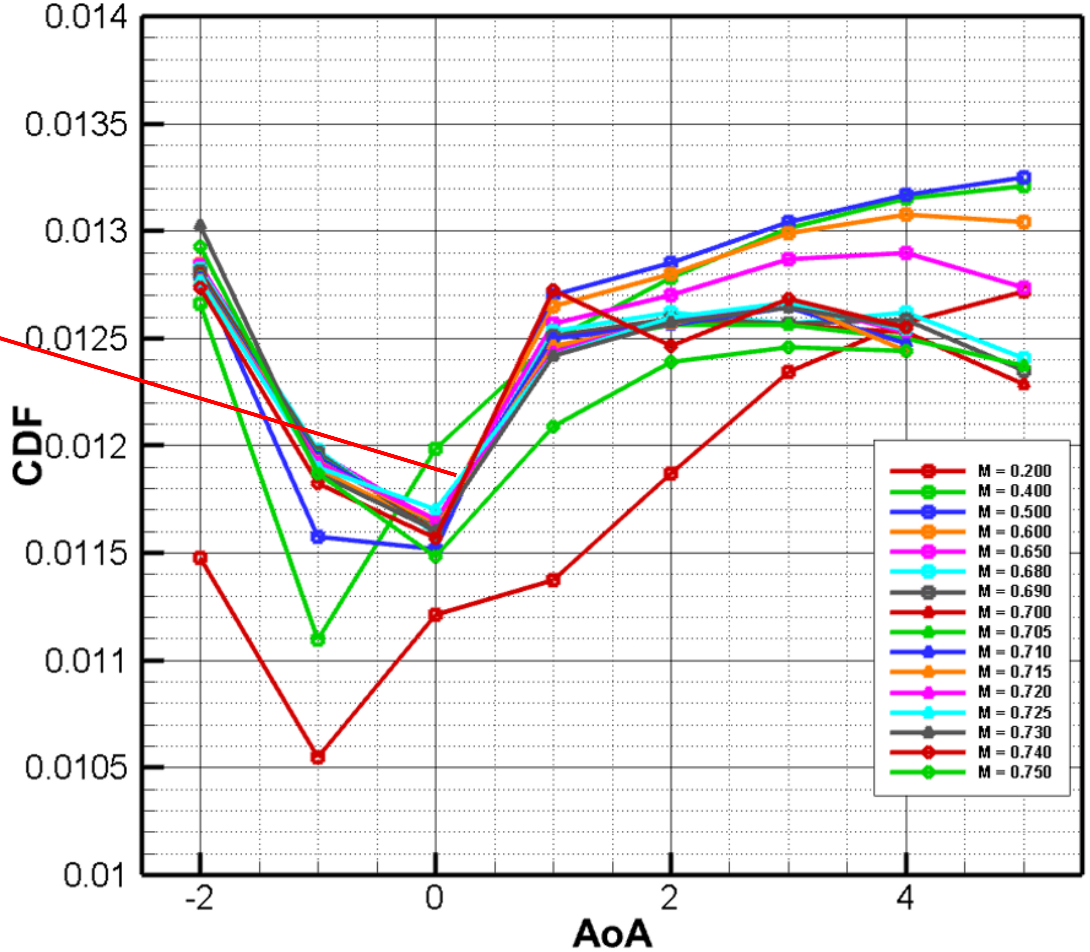

4.5 Polars for Configuration 3

- Comparisons of spanwise lift coefficient values to two-dimensional results were performed for Configuration 3

NSU3D-SA-AFT2 Free Transition Spanwise C_L Values Compared to NSU2D-SA-AFT2 Free Transition Results at Mach = 0.7, AOA = 0.0°

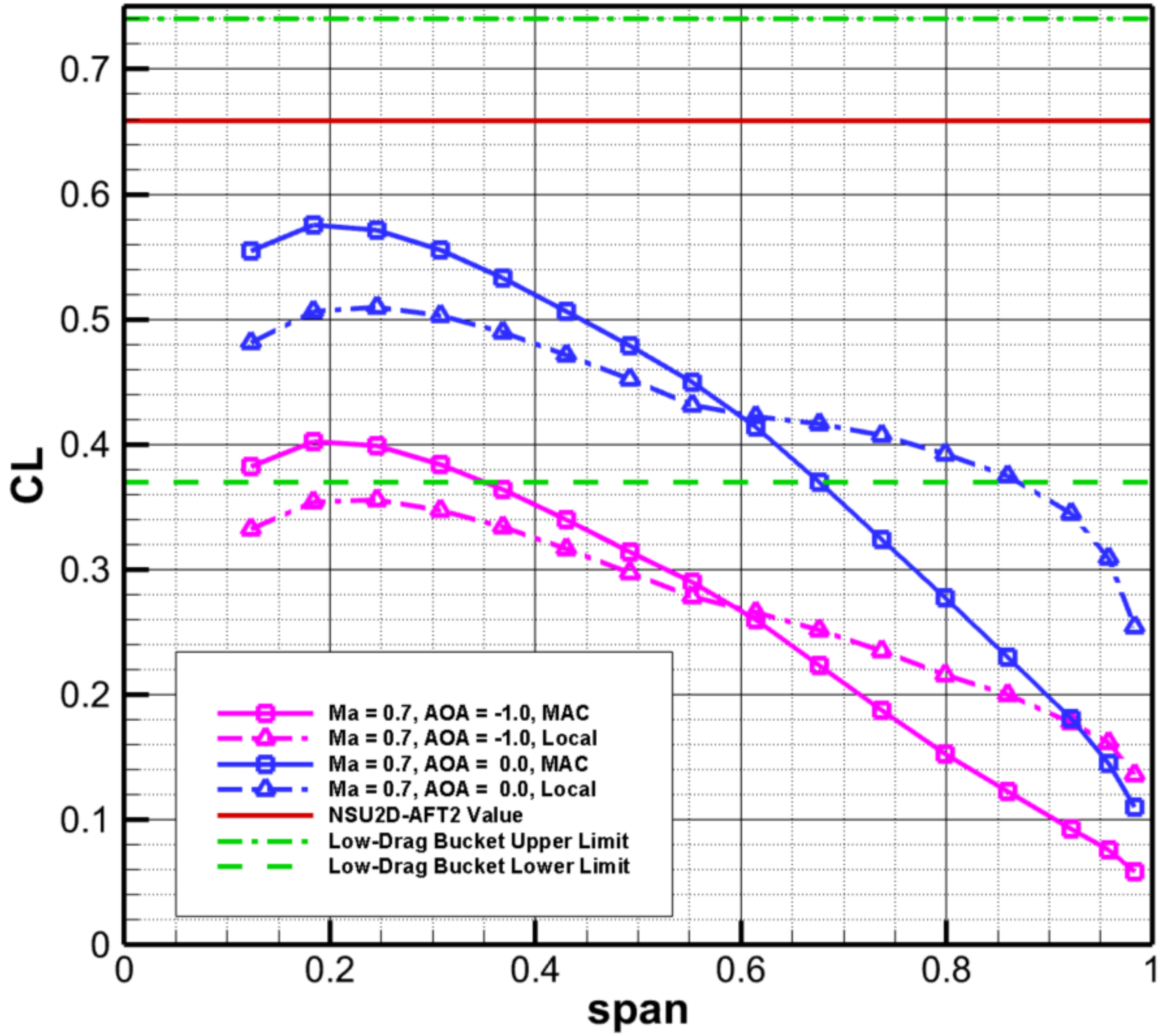

4.5 Polars for Configuration 3

- Comparisons of spanwise lift coefficient values to two-dimensional results were performed for Configuration 3

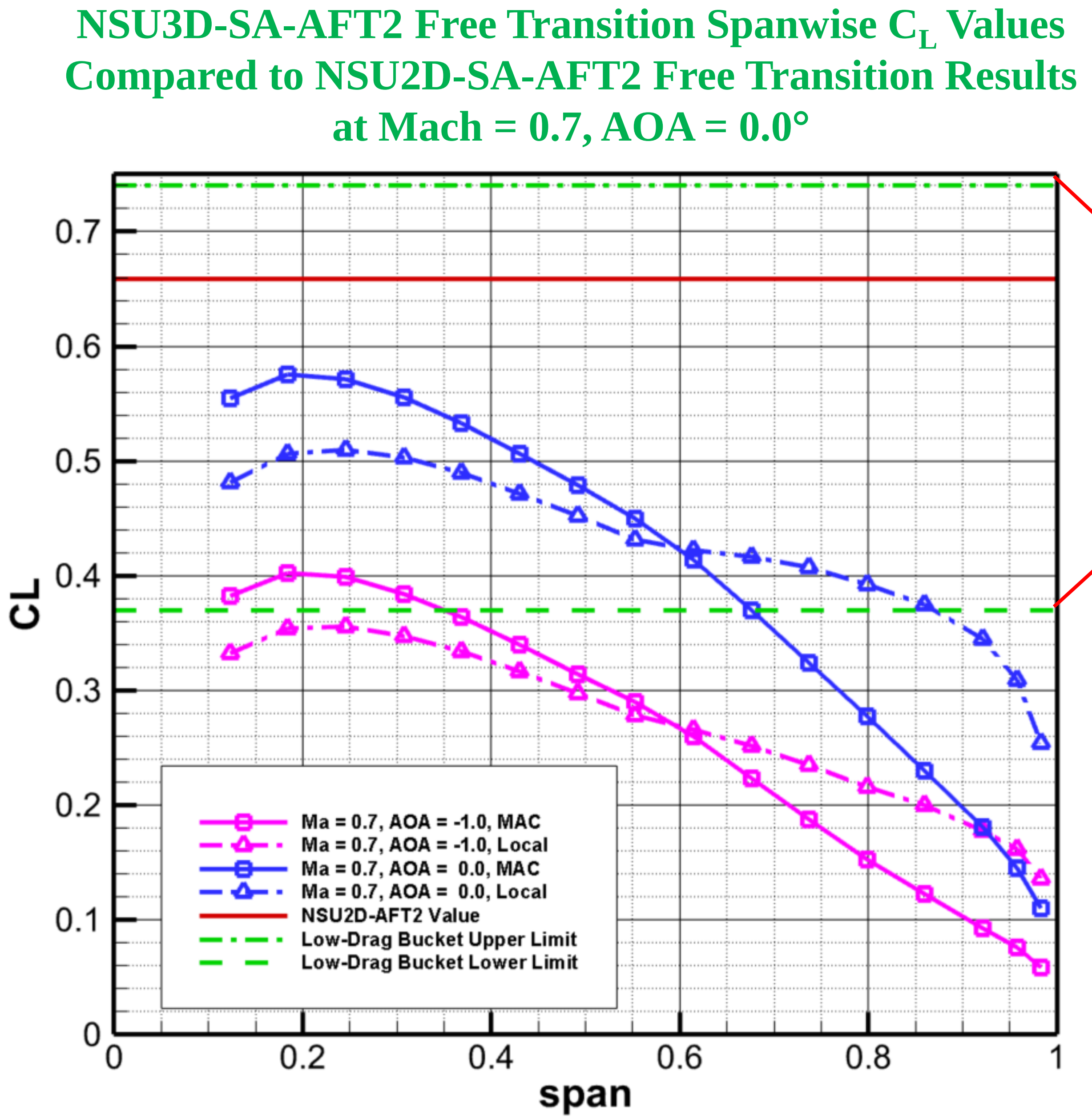

- Local chord-based values for Mach = 0.7 fall between the upper and lower limit of the low-drag bucket for the S207 airfoil [10]

4.5 Polars for Configuration 3

- Fully turbulent sectional surface pressure profiles were examined to further investigate alignment between two- and three-dimensional results

NSU3D-SA Fully Turbulent Cp Profile at 8.6% Span on Configuration 3 Compared to NSU2D-SA Fully Turbulent Cp Profile

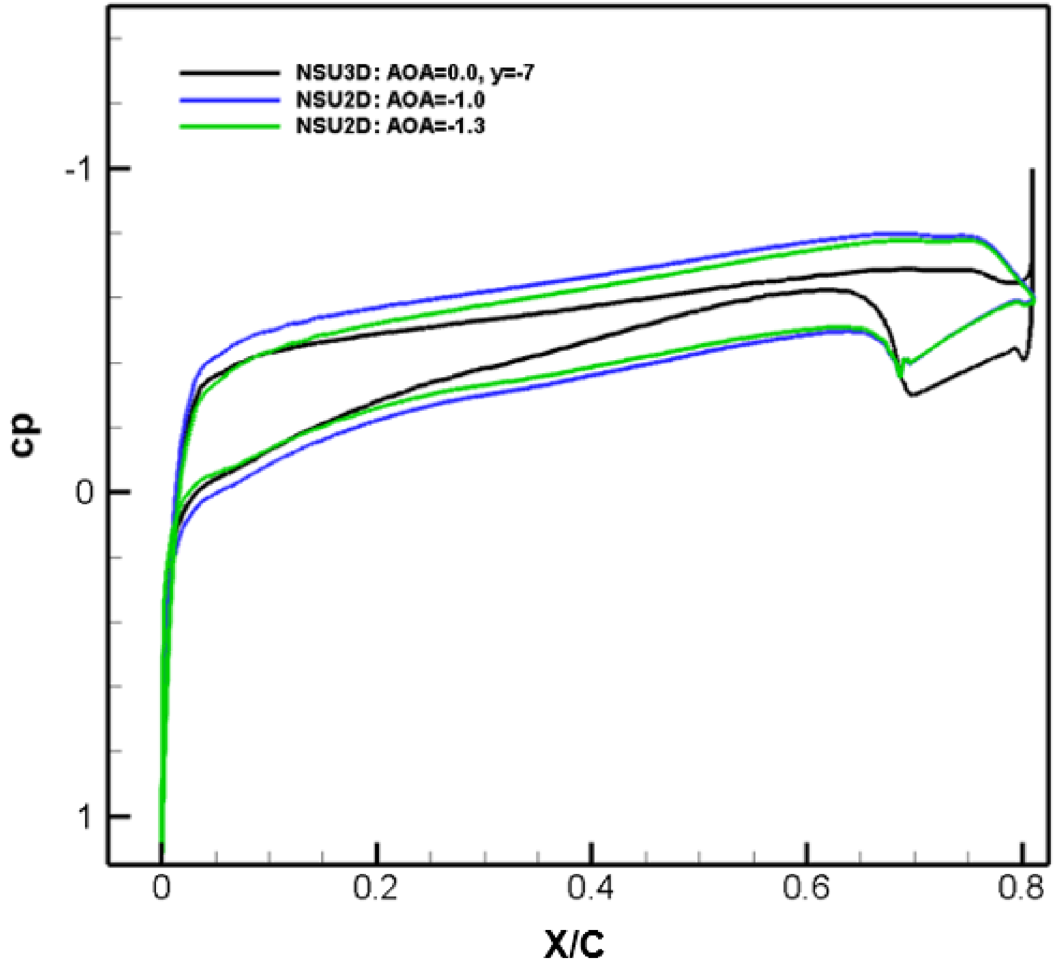

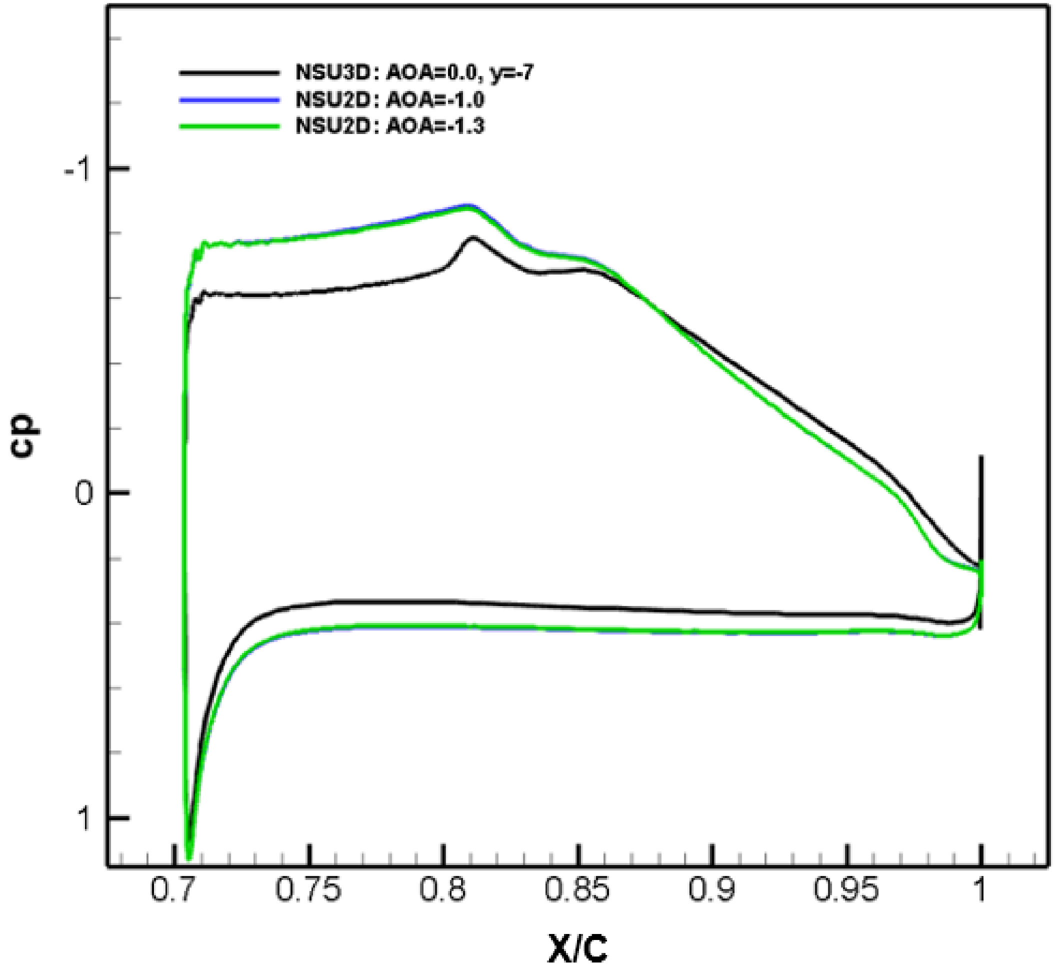

4.5 Polars for Configuration 3

- Fully turbulent sectional surface pressure profiles were examined to further investigate alignment between two- and three-dimensional results

NSU3D-SA Fully Turbulent Cp Profile at 8.6% Span on Configuration 3 Compared to NSU2D-SA Fully Turbulent Cp Profile

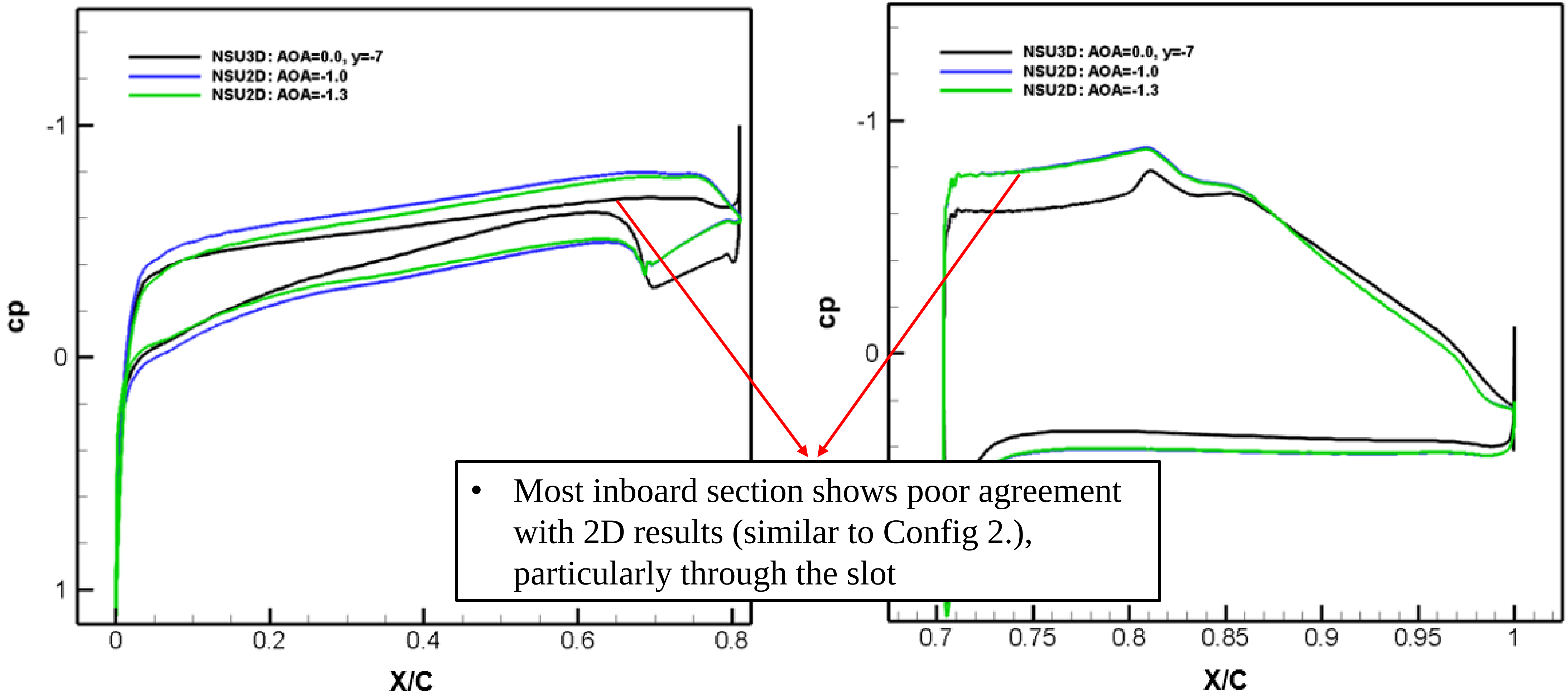

- Most inboard section shows poor agreement with 2D results (similar to Config 2.), particularly through the slot

4.5 Polars for Configuration 3

- Fully turbulent sectional surface pressure profiles were examined to further investigate alignment between two- and three-dimensional results

NSU3D-SA Fully Turbulent Cp Profile at 18.4% Span on Configuration 3 Compared to NSU2D-SA Fully Turbulent Cp Profile

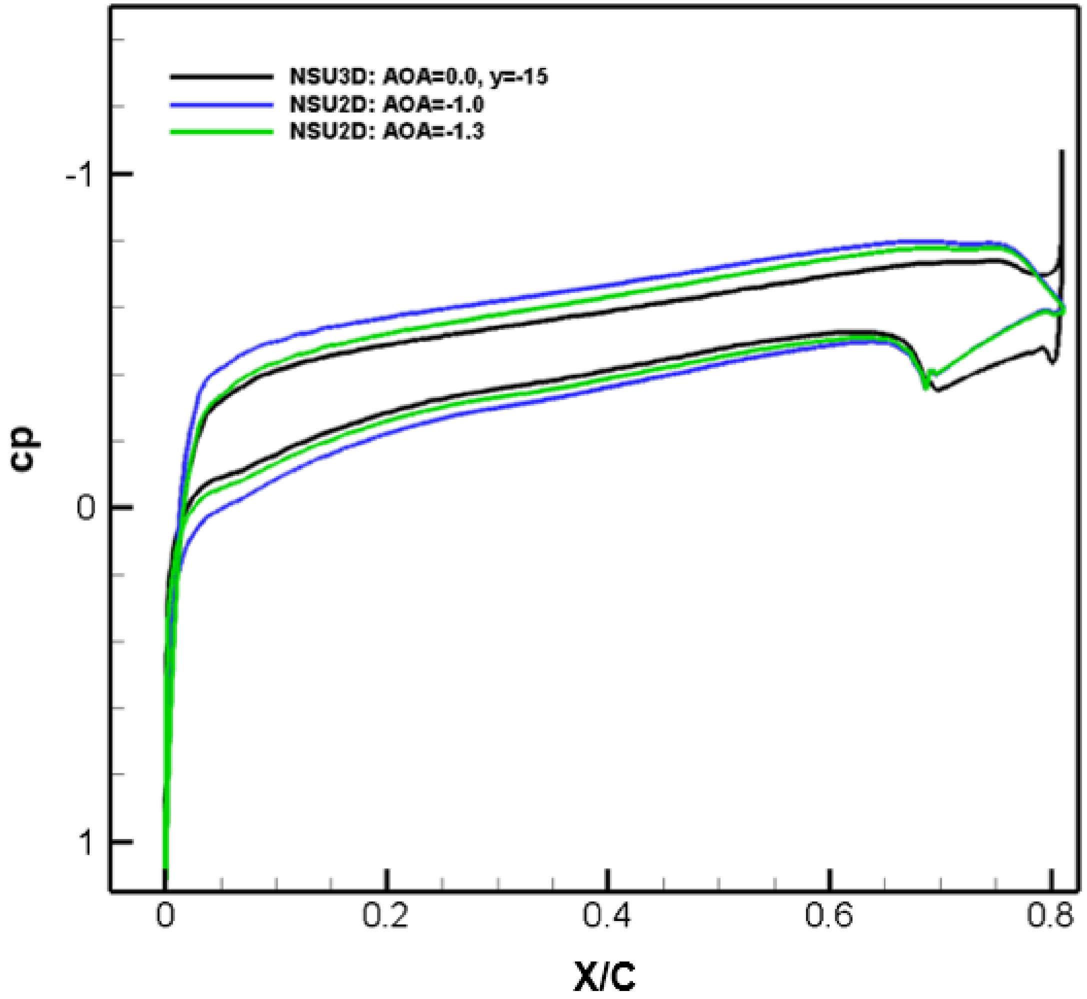

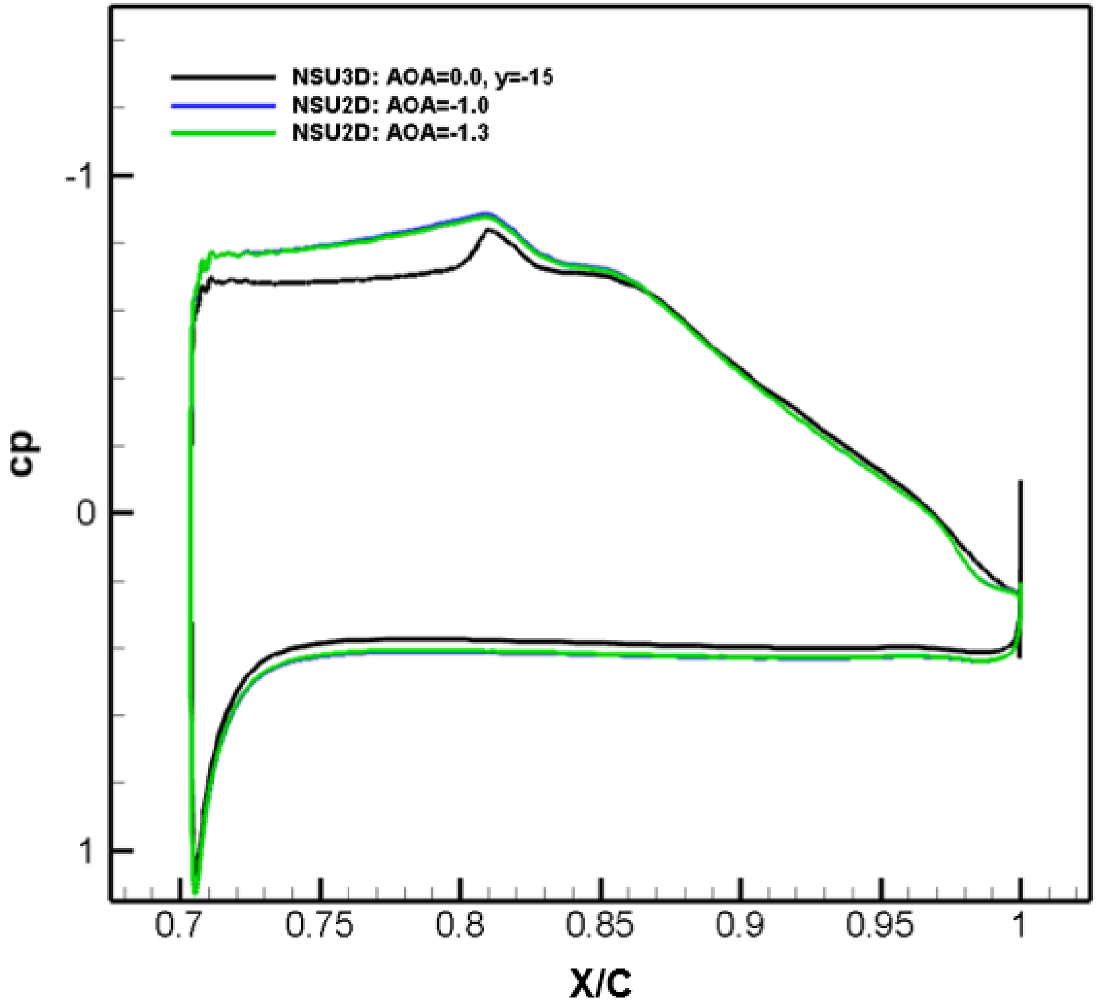

4.5 Polars for Configuration 3

- Fully turbulent sectional surface pressure profiles were examined to further investigate alignment between two- and three-dimensional results

NSU3D-SA Fully Turbulent Cp Profile at 18.4% Span on Configuration 3 Compared to NSU2D-SA Fully Turbulent Cp Profile

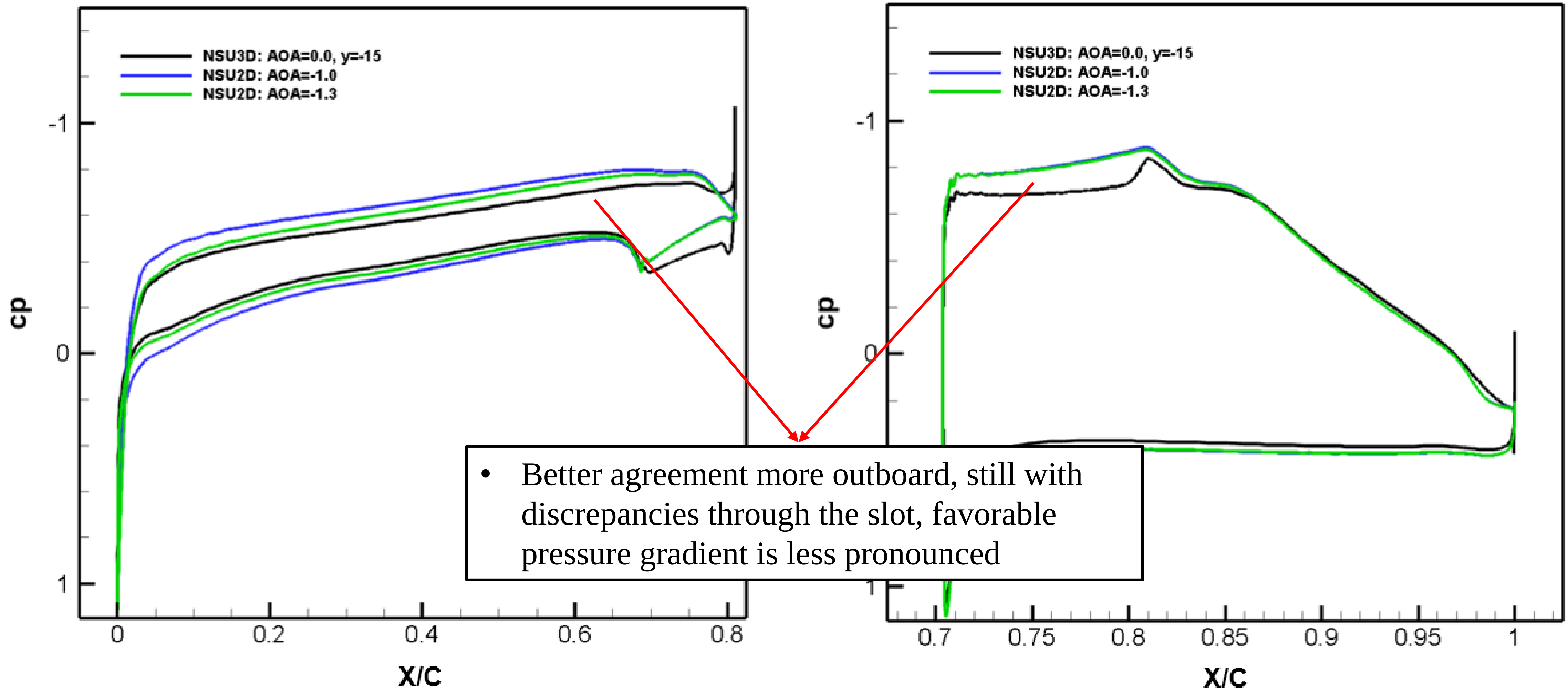

- Better agreement more outboard, still with discrepancies through the slot, favorable pressure gradient is less pronounced

4.5 Polars for Configuration 3

- Fully turbulent sectional surface pressure profiles were examined to further investigate alignment between two- and three-dimensional results

NSU3D-SA Fully Turbulent Cp Profile at 36.8% Span on Configuration 3 Compared to NSU2D-SA Fully Turbulent Cp Profile

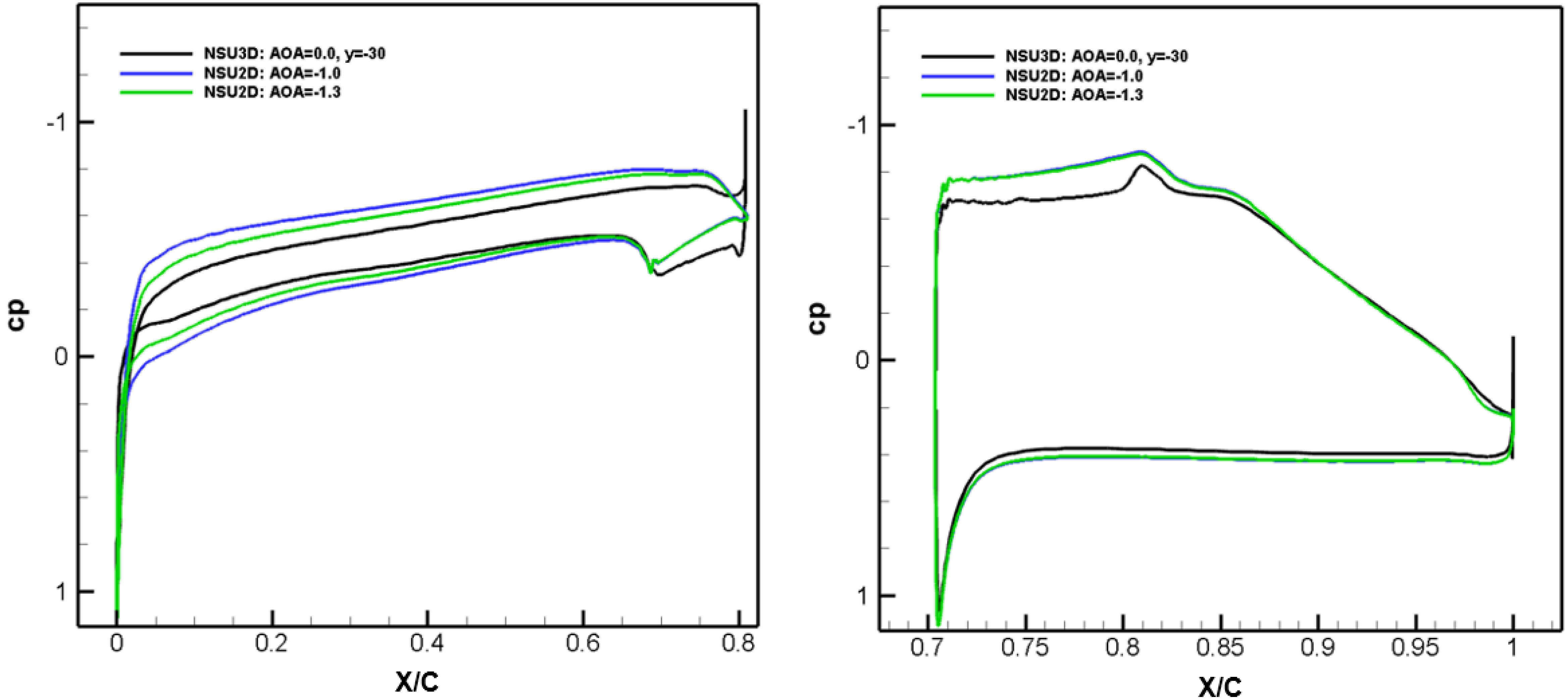

4.5 Polars for Configuration 3

- Fully turbulent sectional surface pressure profiles were examined to further investigate alignment between two- and three-dimensional results

NSU3D-SA Fully Turbulent Cp Profile at 36.8% Span on Configuration 3 Compared to NSU2D-SA Fully Turbulent Cp Profile

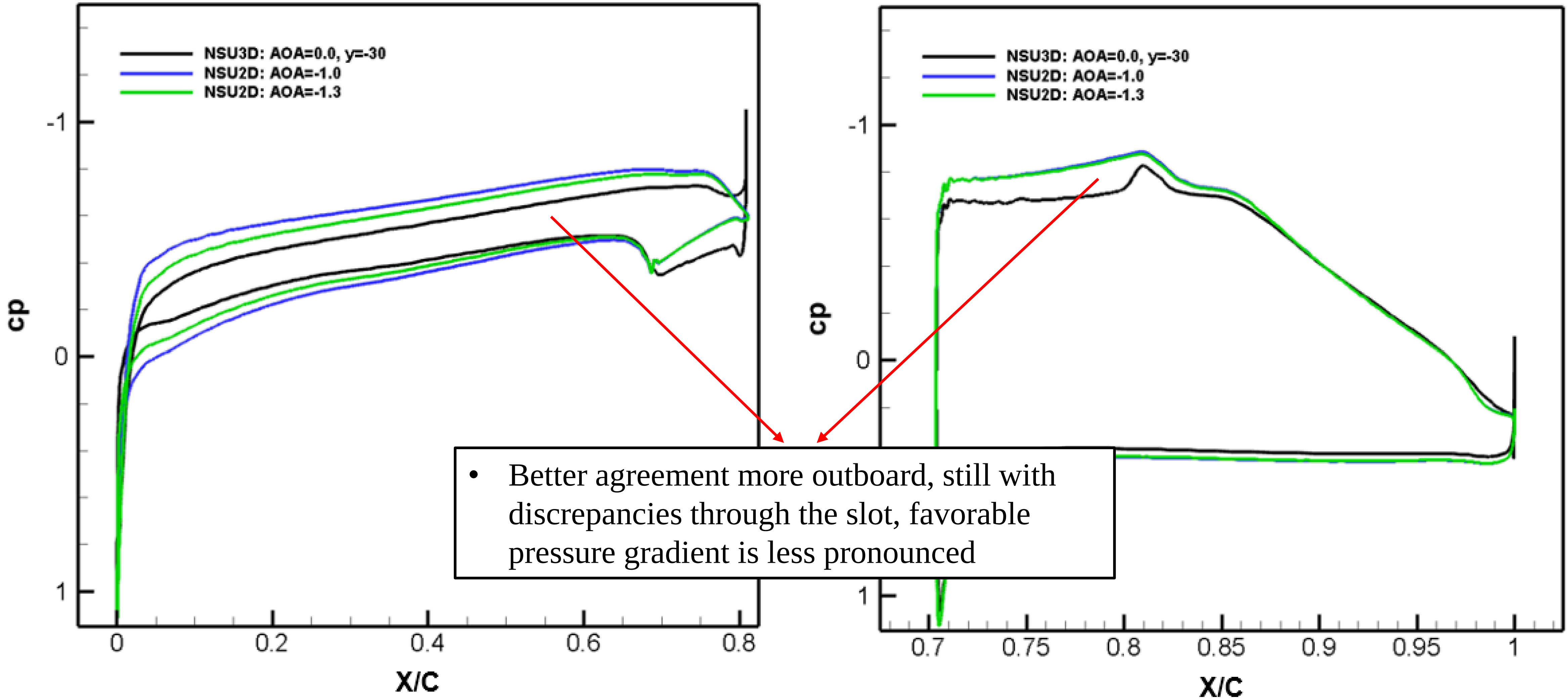

- Better agreement more outboard, still with discrepancies through the slot, favorable pressure gradient is less pronounced

5. Computational Results for the S207-Based Wind Tunnel Model

5.1 The NASA Ames Wind Tunnel Tests

- ULI efforts concerning the S207 SNLF airfoil included a capstone demonstration in the NASA Ames UWPT 11-ft transonic wind tunnel
  - Physical model of an S207-based swept wing was fabricated
  - February and March of 2022

S207 –Based Wind Tunnel Model

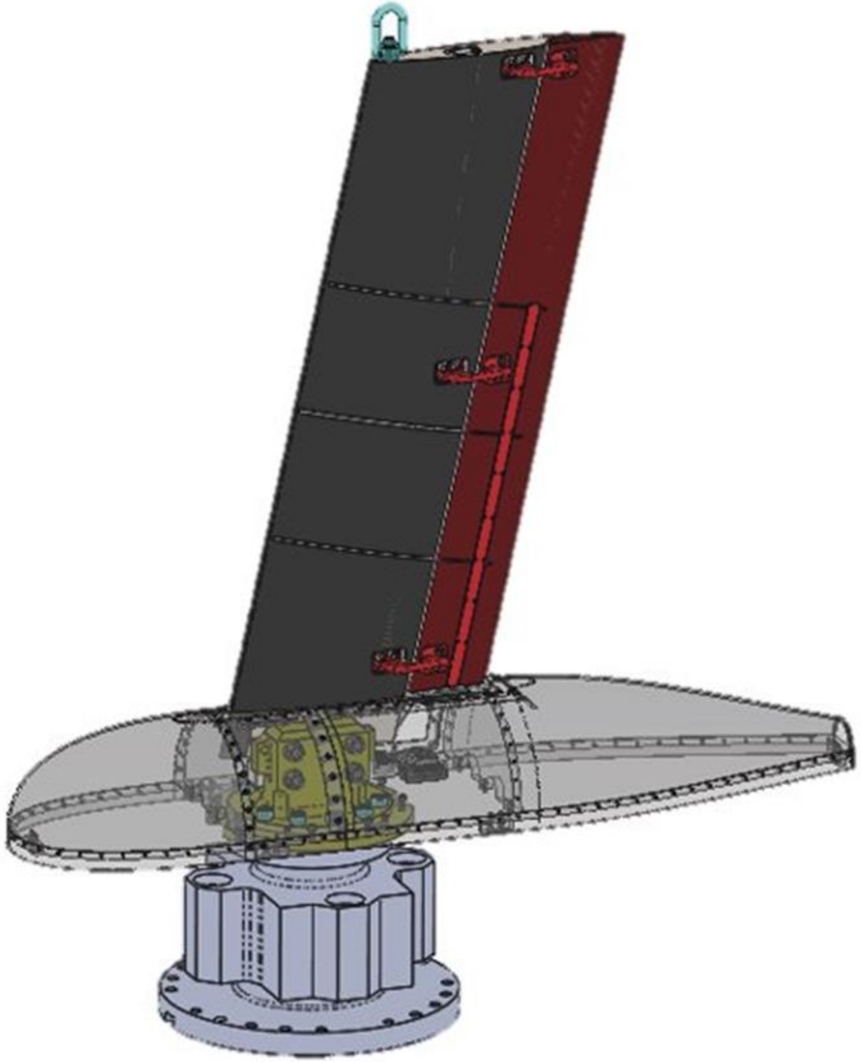

5.1 The NASA Ames Wind Tunnel Tests

- ULI efforts concerning the S207 SNLF airfoil included a capstone demonstration in the NASA Ames UWPT 11-ft transonic wind tunnel
  - Physical model of an S207-based swept wing was fabricated
  - February and March of 2022

- 12.5 degrees of sweep
- 2ft chord

S207 –Based Wind Tunnel Model

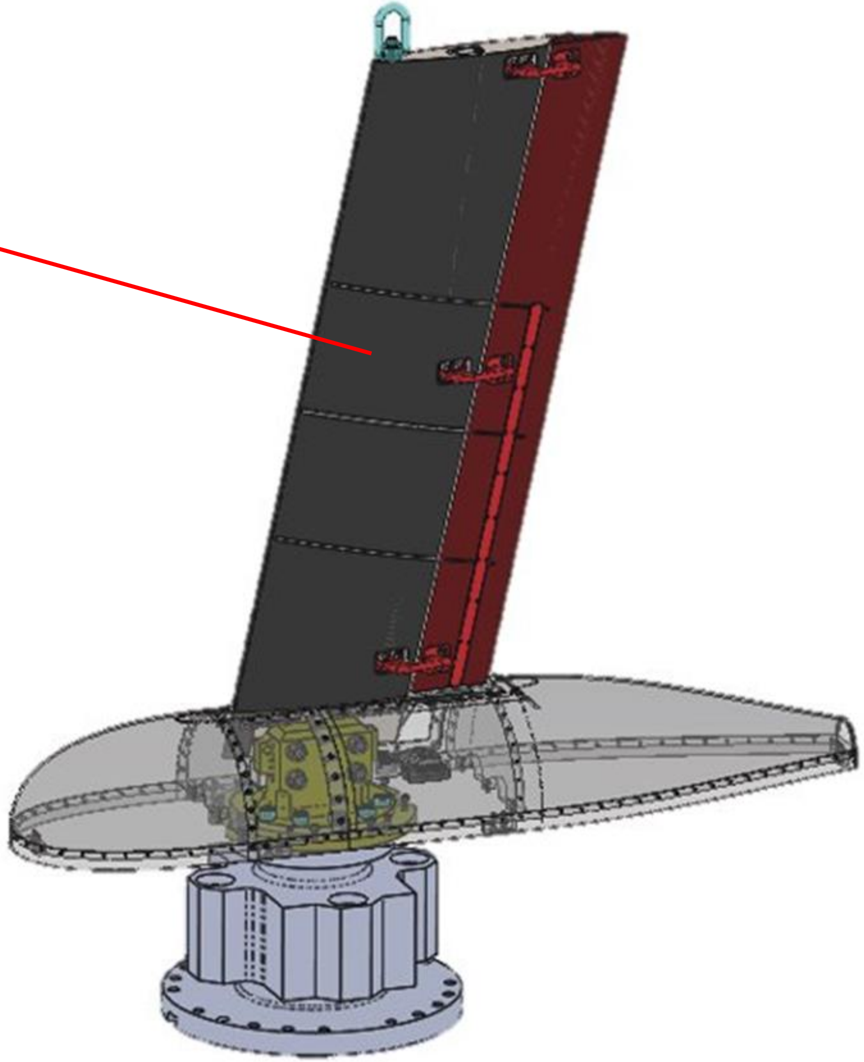

5.1 The NASA Ames Wind Tunnel Tests

- ULI efforts concerning the S207 SNLF airfoil included a capstone demonstration in the NASA Ames UWPT 11-ft transonic wind tunnel
  - Physical model of an S207-based swept wing was fabricated
  - February and March of 2022

- 12.5 degrees of sweep
- 2ft chord

- Three connectors attaching aft element to fore, and other bracketing
  - Flap is adjustable

S207 –Based Wind Tunnel Model

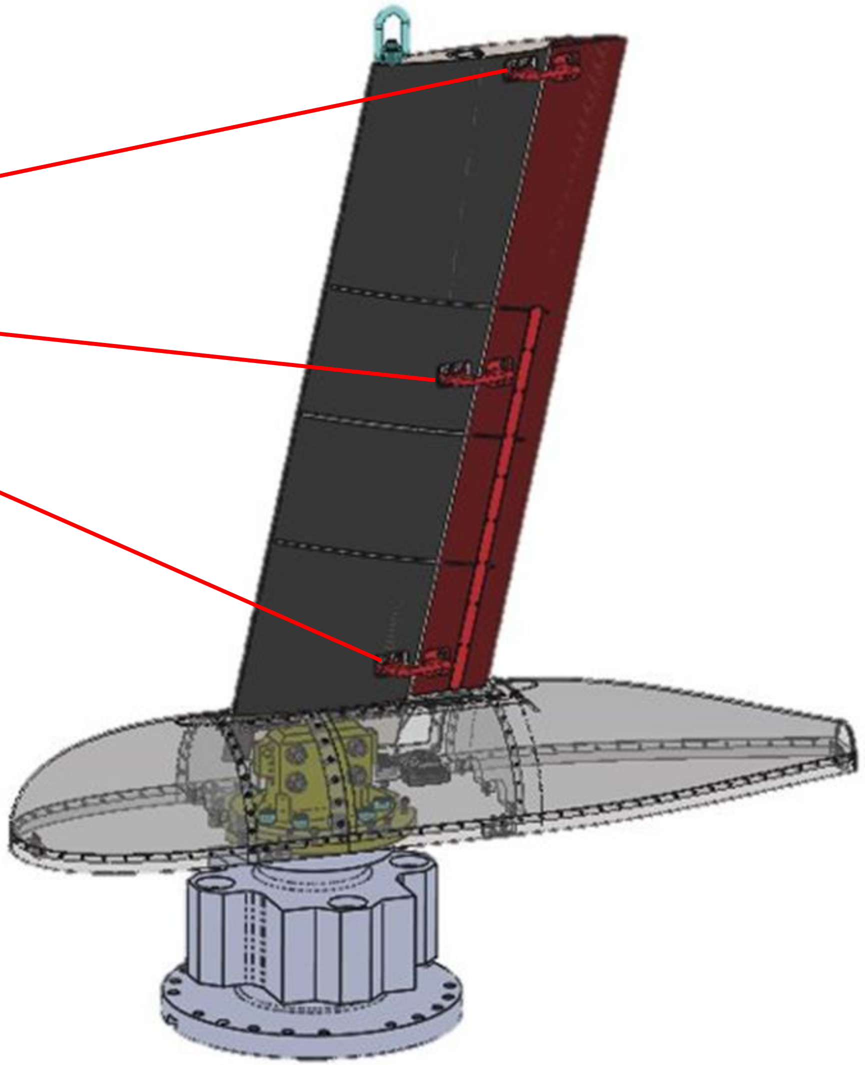

5.1 The NASA Ames Wind Tunnel Tests

- ULI efforts concerning the S207 SNLF airfoil included a capstone demonstration in the NASA Ames UWPT 11-ft transonic wind tunnel
  - Physical model of an S207-based swept wing was fabricated
  - February and March of 2022

- 12.5 degrees of sweep
- 2ft chord

- Three connectors attaching aft element to fore, and other bracketing
  - Flap is adjustable

- Rotation clockwise or counterclockwise

S207 –Based Wind Tunnel Model

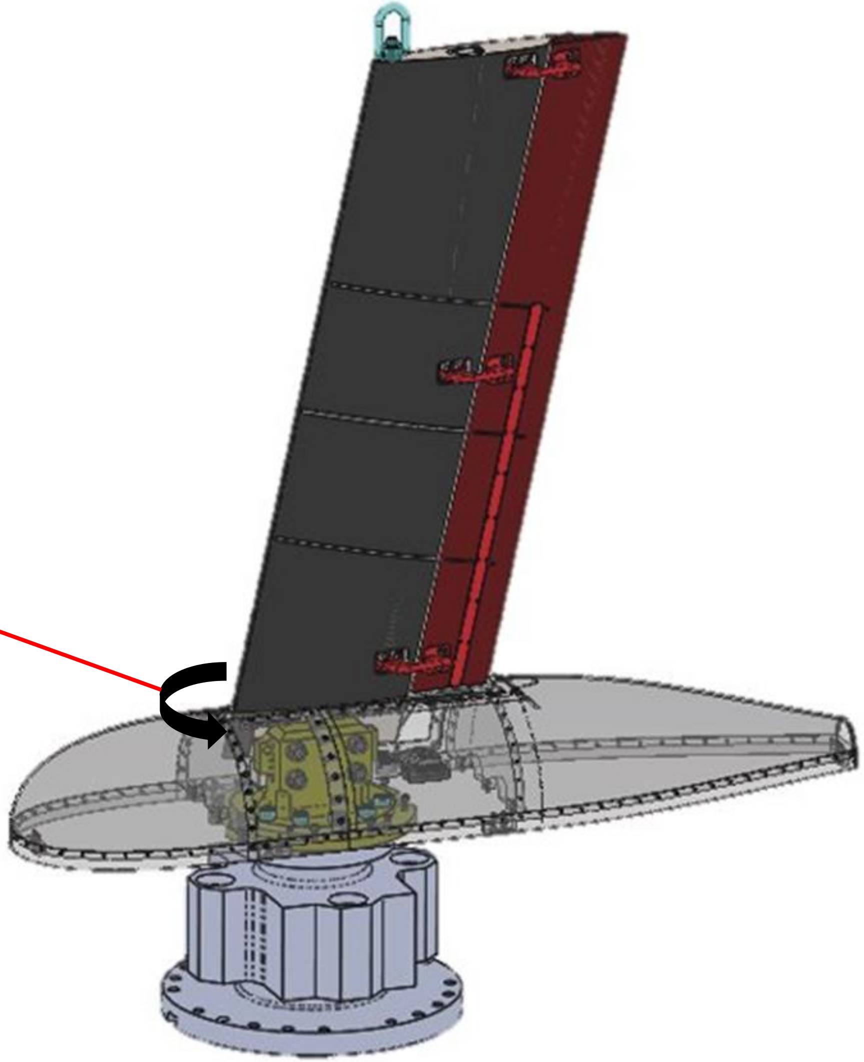

5.1 The NASA Ames Wind Tunnel Tests

- ULI efforts concerning the S207 SNLF airfoil included a capstone demonstration in the NASA Ames UWPT 11-ft transonic wind tunnel
  - Physical model of an S207-based swept wing was fabricated
  - February and March of 2022

- 12.5 degrees of sweep
- 2ft chord

- Three connectors attaching aft element to fore, and other bracketing
  - Flap is adjustable

- Rotation clockwise or counterclockwise

- Fiberglass fairing, rotates with wing

S207 –Based Wind Tunnel Model

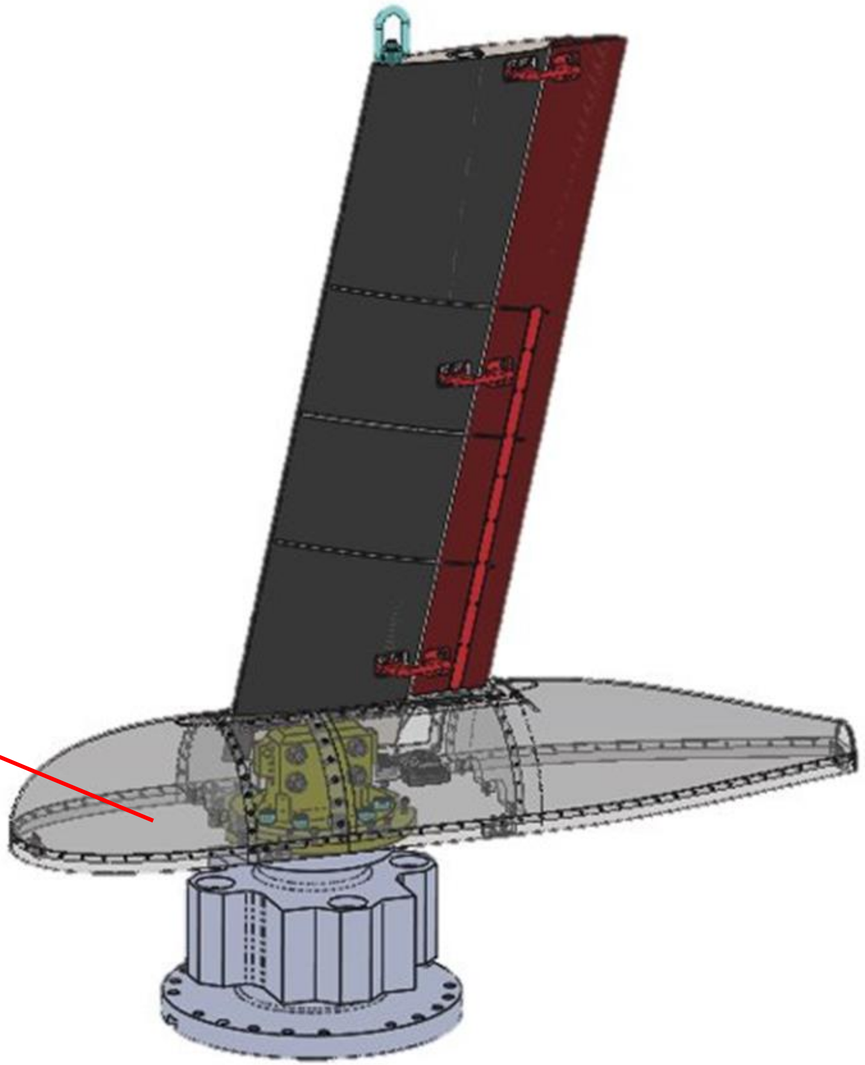

5.1 The NASA Ames Wind Tunnel Tests

- ULI efforts concerning the S207 SNLF airfoil included a capstone demonstration in the NASA Ames UWPT 11-ft transonic wind tunnel
  - Physical model of an S207-based swept wing was fabricated
  - February and March of 2022

- 12.5 degrees of sweep
- 2ft chord

- Three connectors attaching aft element to fore, and other bracketing
  - Flap is adjustable

- Rotation clockwise or counterclockwise

- Fiberglass fairing, rotates with wing

- Three rows of pressure ports at increasing spanwise location
  - L1 : Inboard
  - L2 : Midboard
  - L3 : Outboard

S207 –Based Wind Tunnel Model

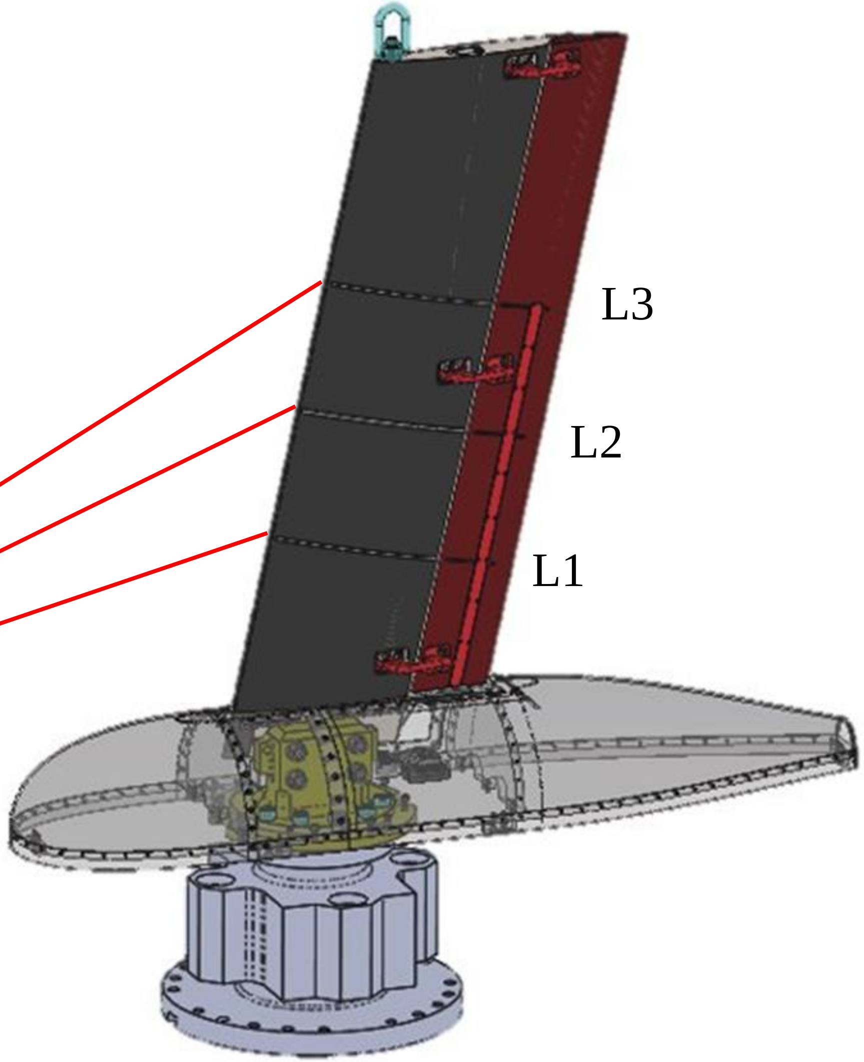

5.1 The NASA Ames Wind Tunnel Tests

S207 –Based Wind Tunnel Model Installation

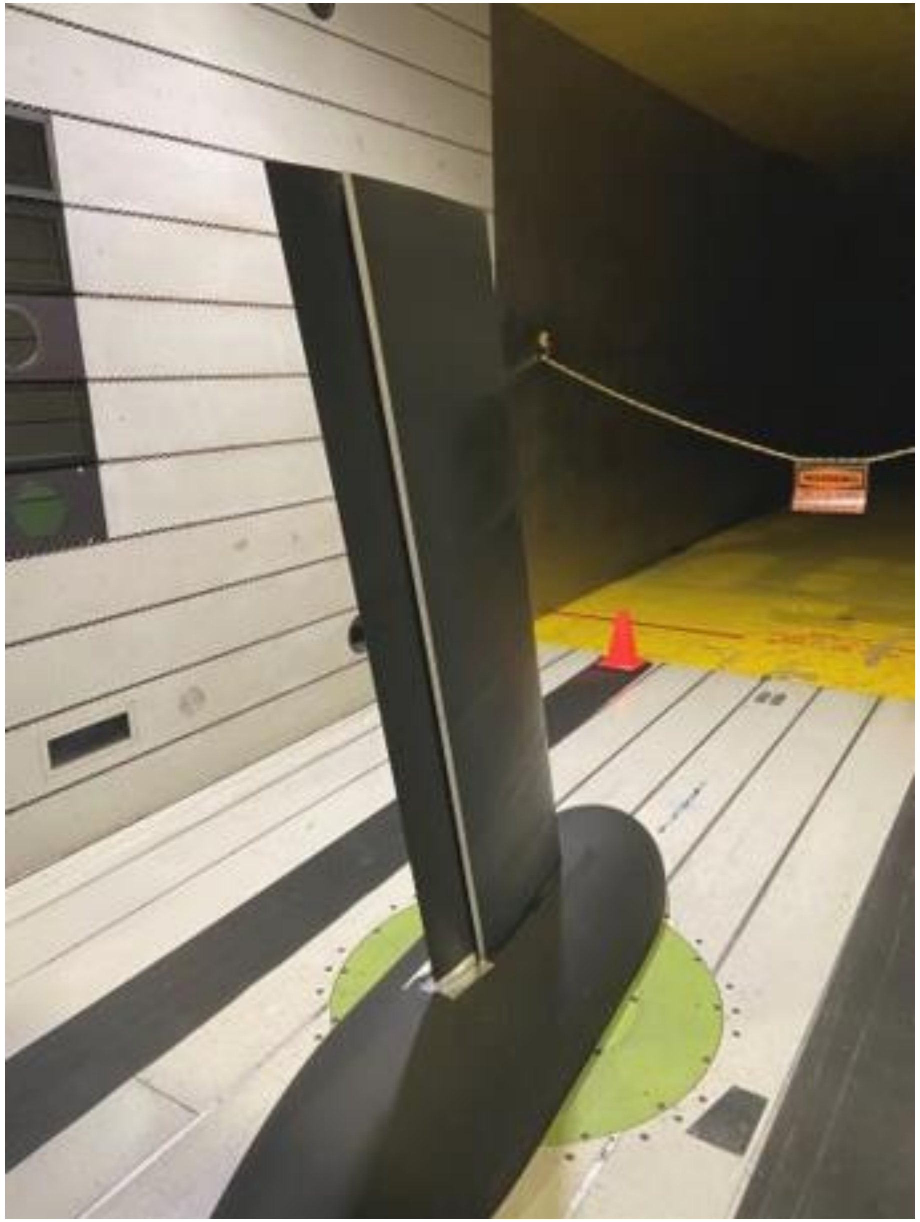

5.1 The NASA Ames Wind Tunnel Tests

- Model was painted matte black in anticipation of infrared (IR) thermography analysis

IR Flow (Left to Right) For Mach = 0.699, AOA=-0.002°, Re=12.93 Million

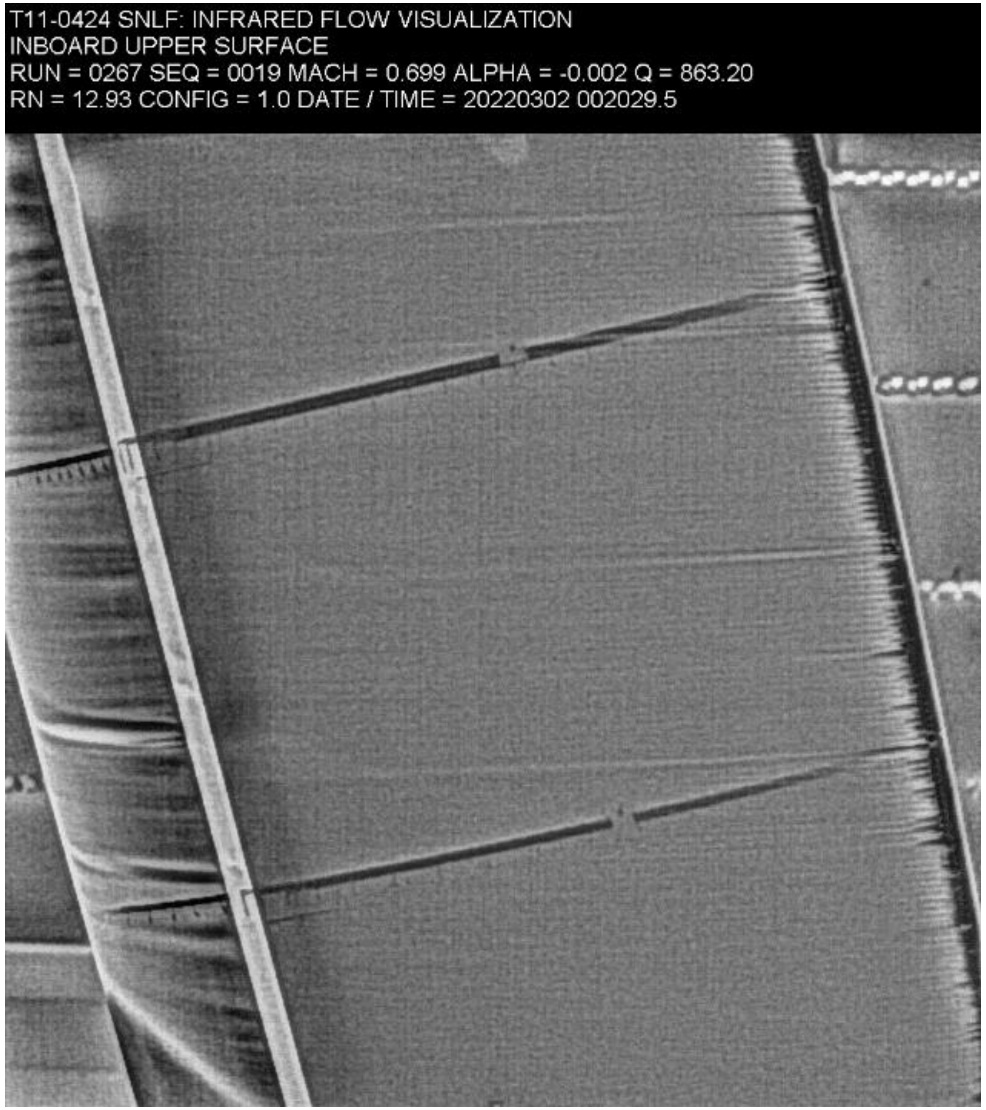

5.1 The NASA Ames Wind Tunnel Tests

- Model was painted matte black in anticipation of infrared (IR) thermography analysis

IR Flow (Left to Right) For Mach = 0.699, AOA=-0.002°, Re=12.93 Million

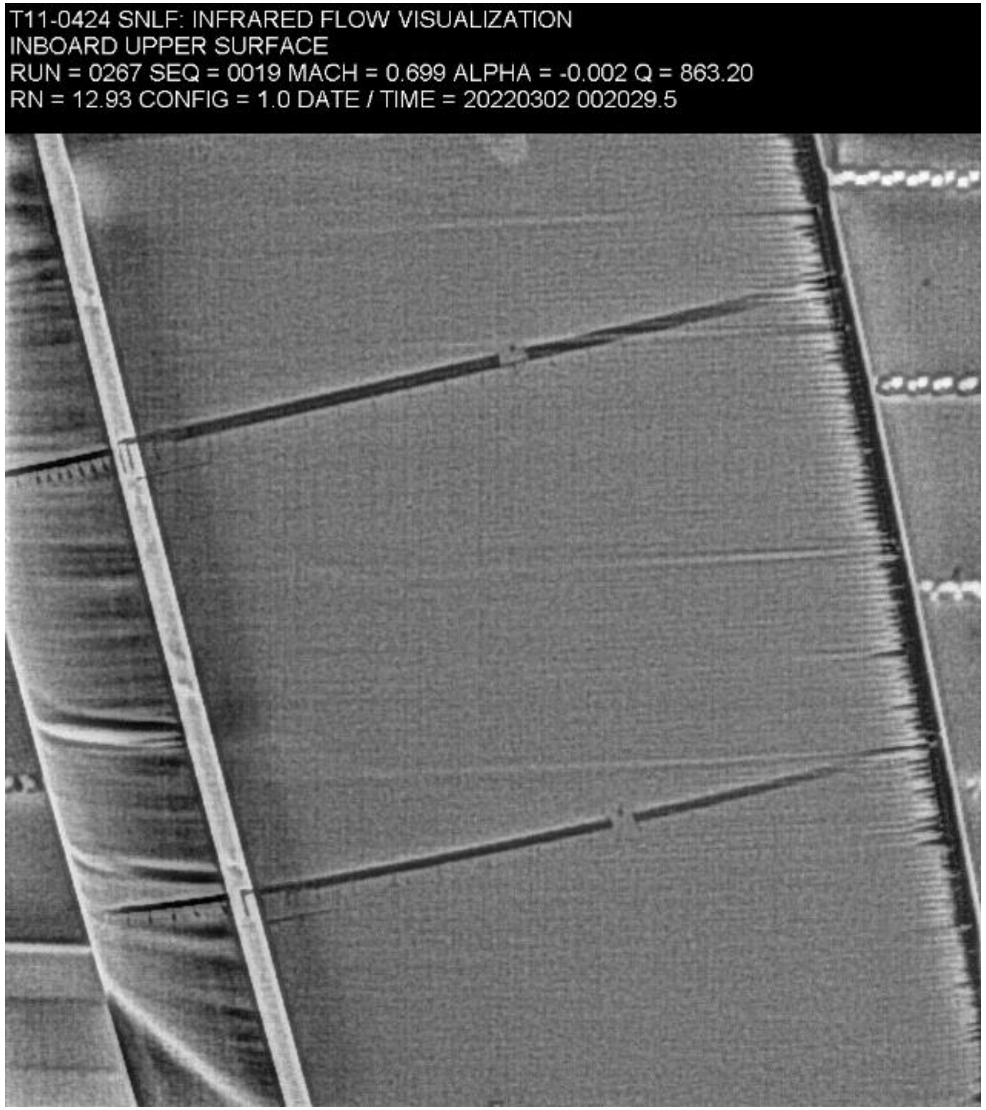

IR Flow (Left to Right) For Mach = 0.699, AOA=-1.000°, Re=12.95 Million

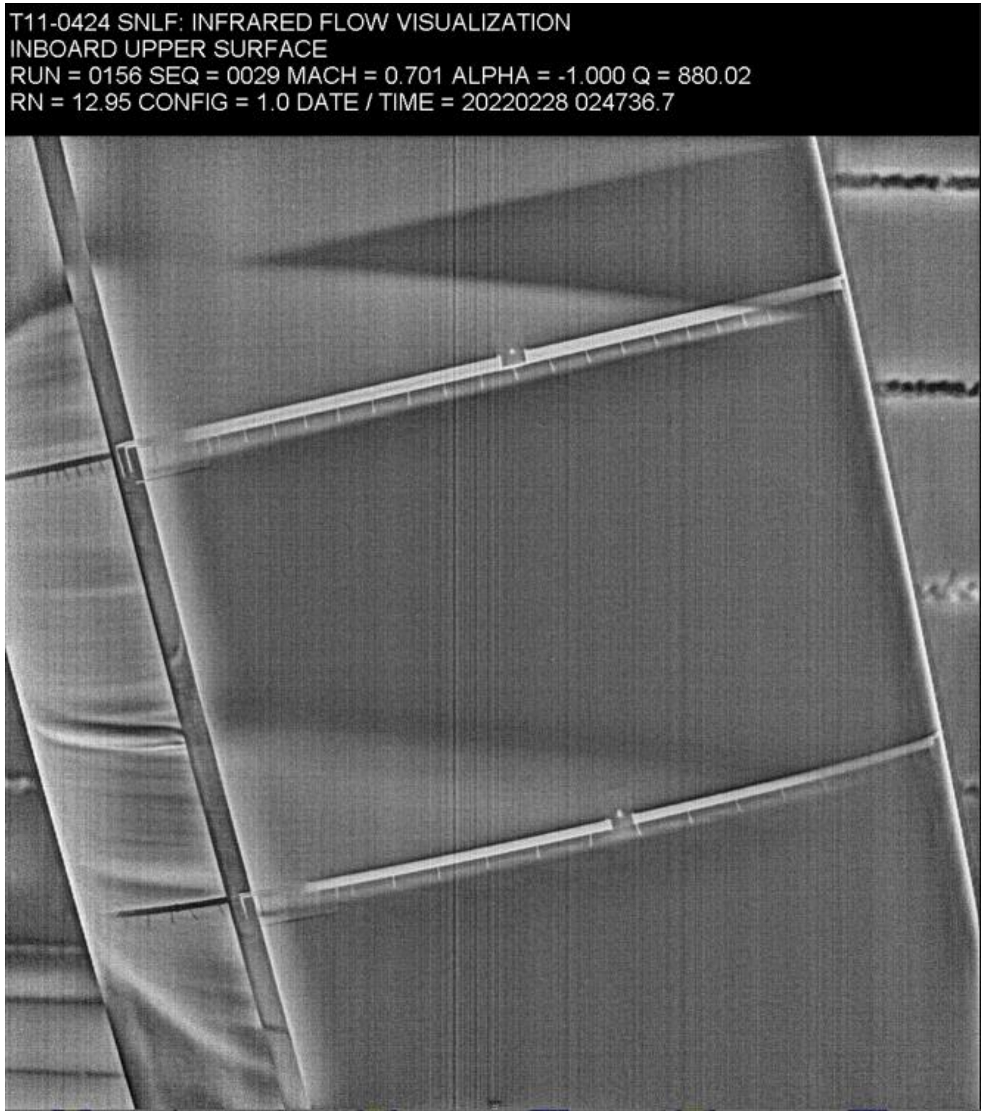

5.1 The NASA Ames Wind Tunnel Tests

- Model was painted matte black in anticipation of infrared (IR) thermography analysis

IR Flow (Left to Right) For Mach = 0.699, AOA=-0.002°, Re=12.93 Million

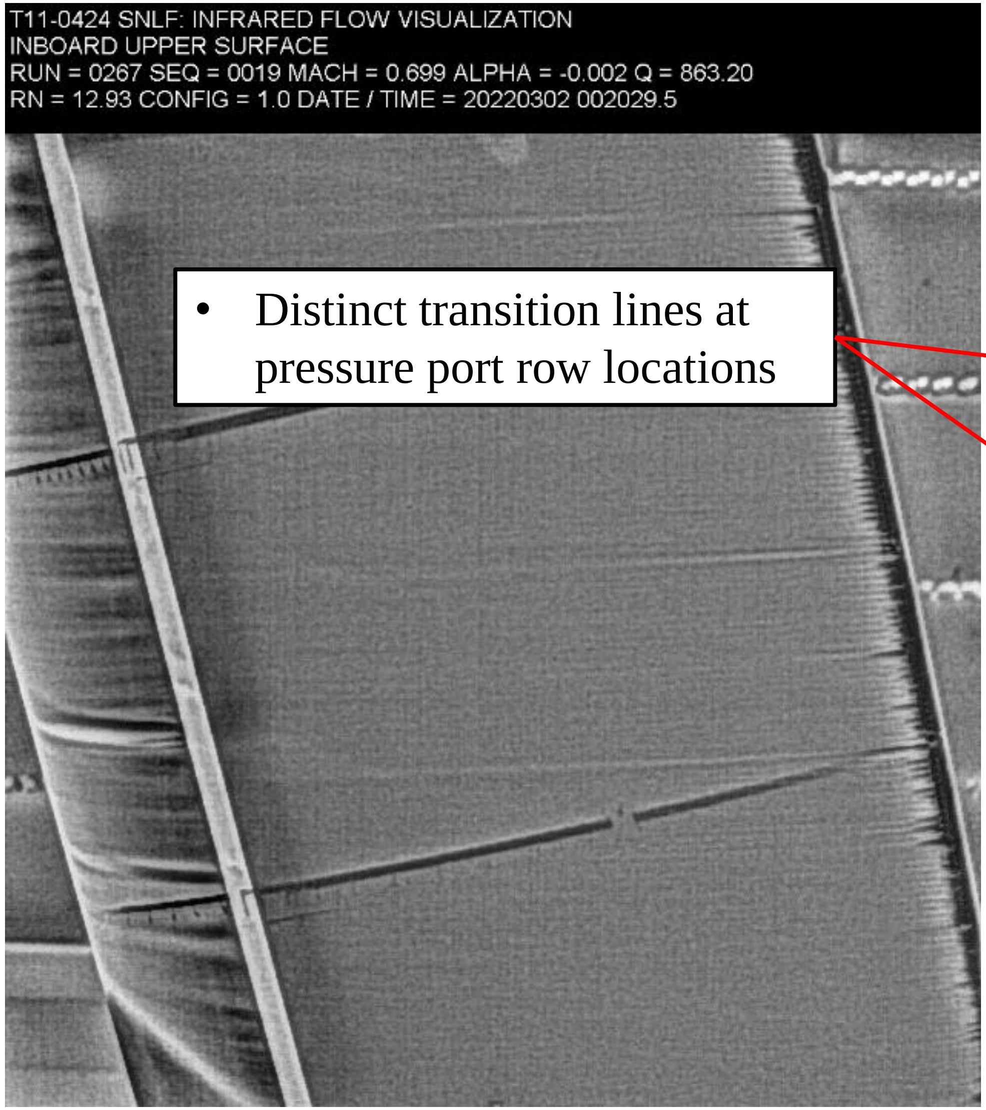

- Distinct transition lines at pressure port row locations

IR Flow (Left to Right) For Mach = 0.699, AOA=-1.000°, Re=12.95 Million

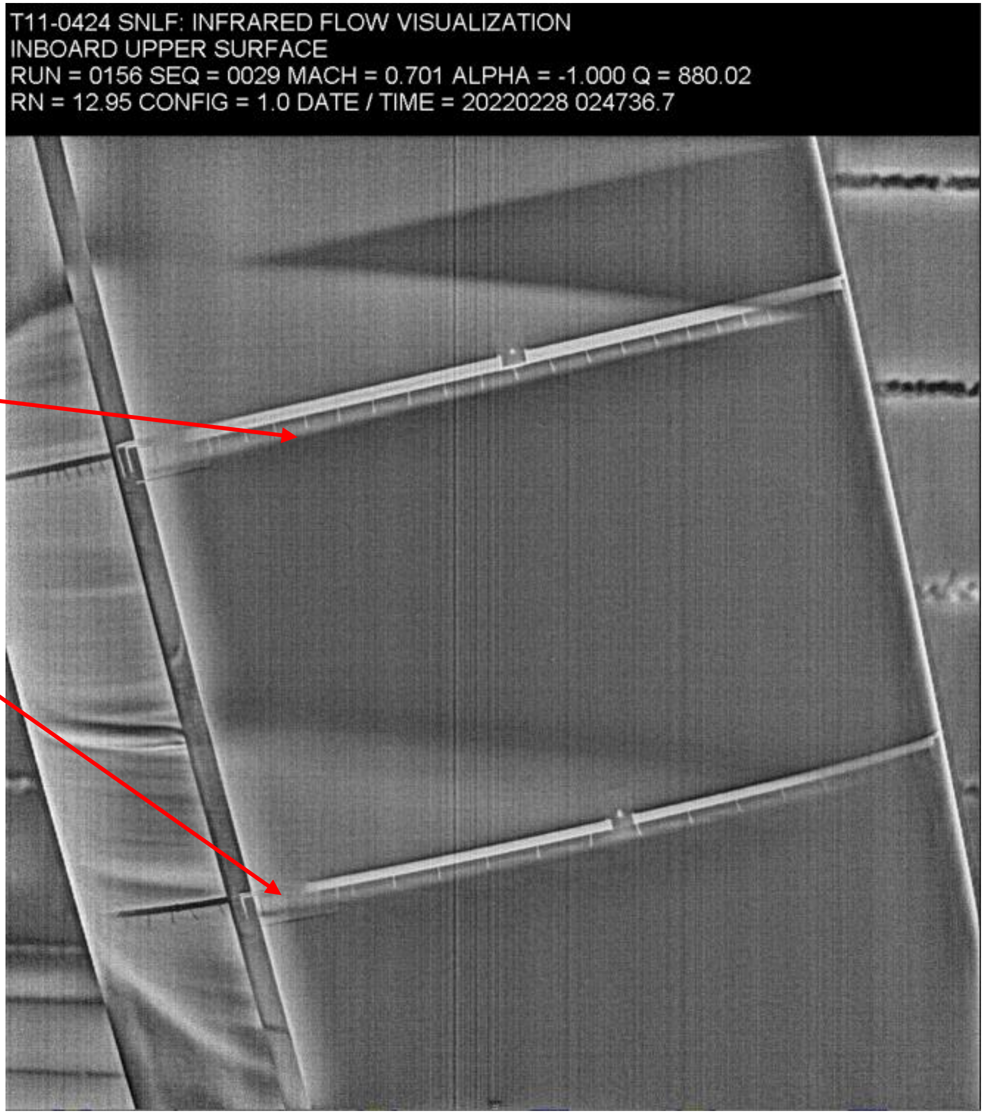

5.1 The NASA Ames Wind Tunnel Tests

- Model was painted matte black in anticipation of infrared (IR) thermography analysis

IR Flow (Left to Right) For Mach = 0.699, AOA=-0.002°, Re=12.93 Million

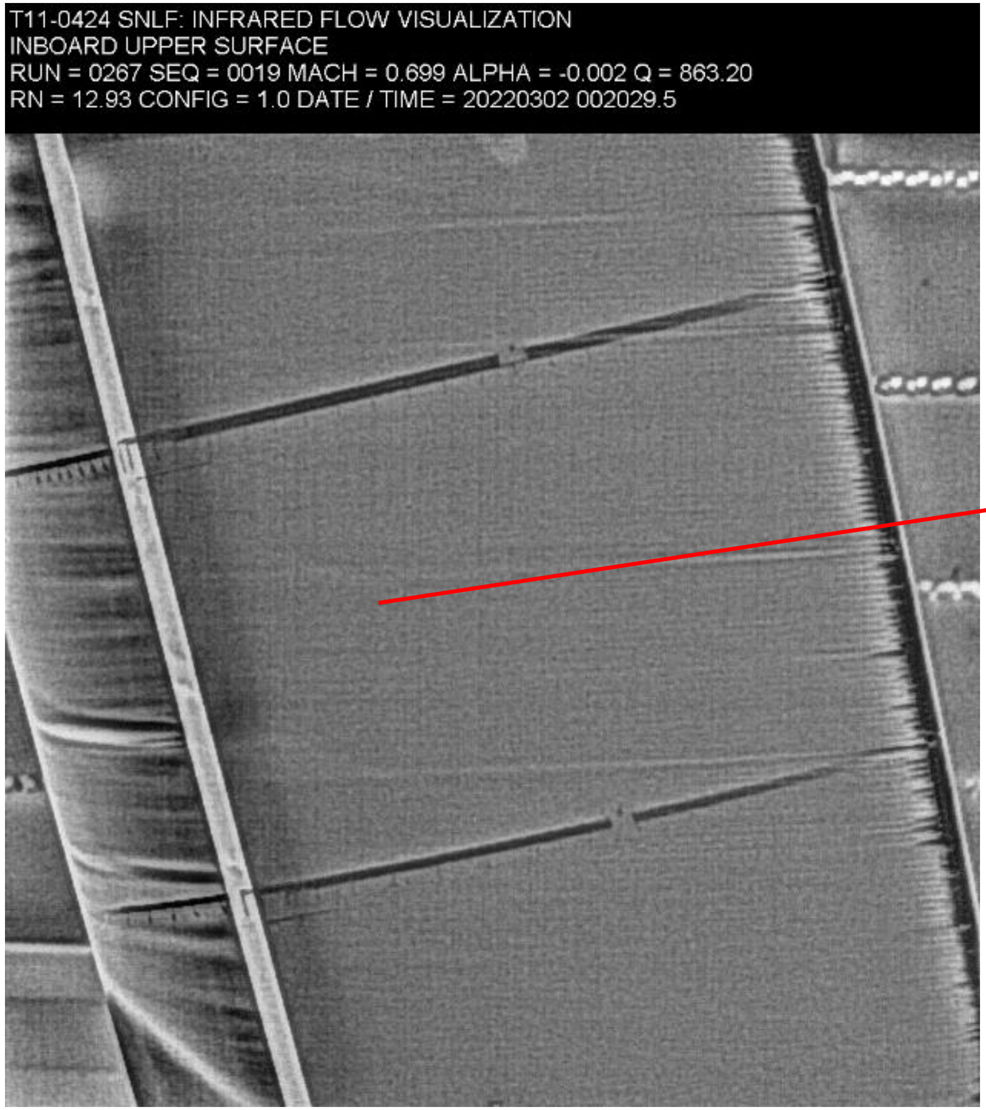

IR Flow (Left to Right) For Mach = 0.699, AOA=-1.000°, Re=12.95 Million

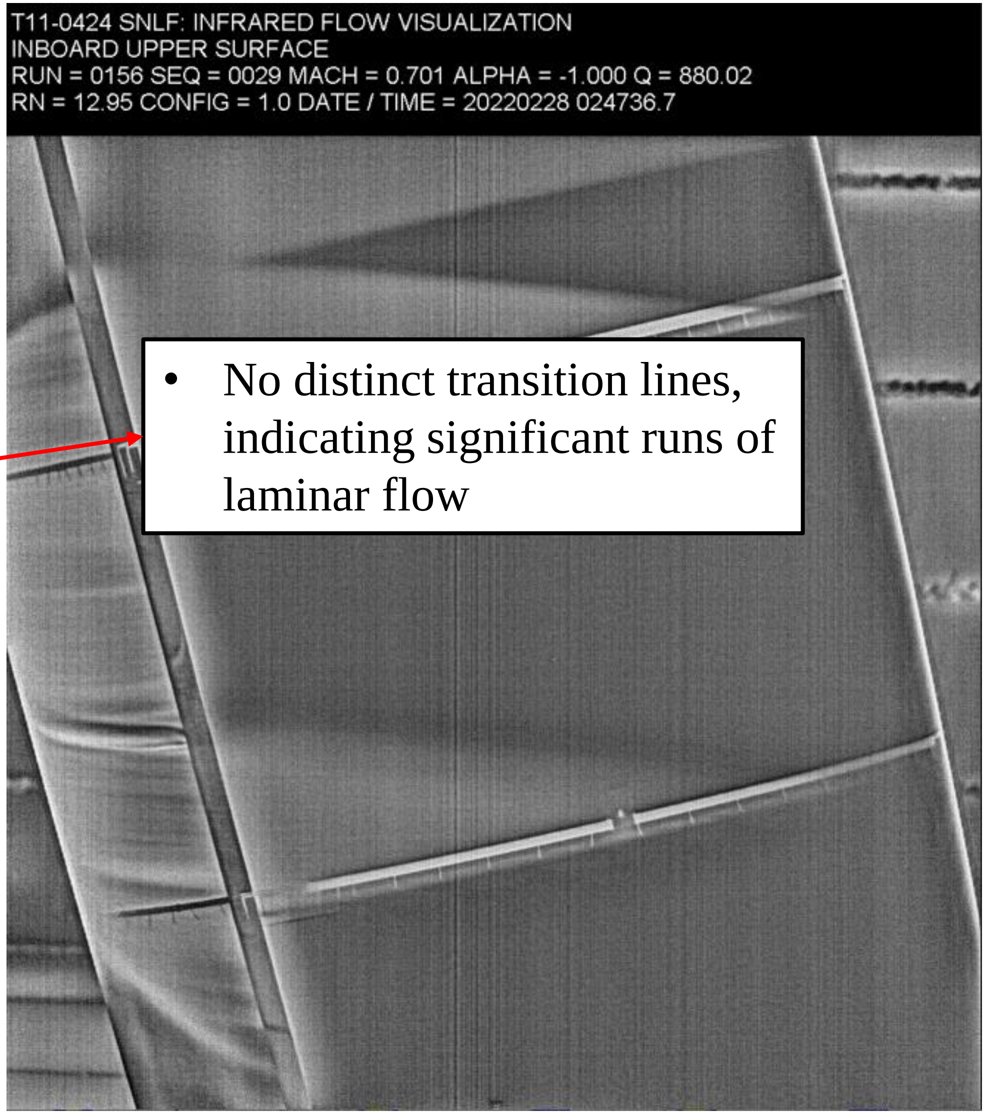

- No distinct transition lines, indicating significant runs of laminar flow

5.1 The NASA Ames Wind Tunnel Tests

- Model was painted matte black in anticipation of infrared (IR) thermography analysis

IR Flow (Left to Right) For Mach = 0.699, AOA=-0.002°, Re=12.93 Million

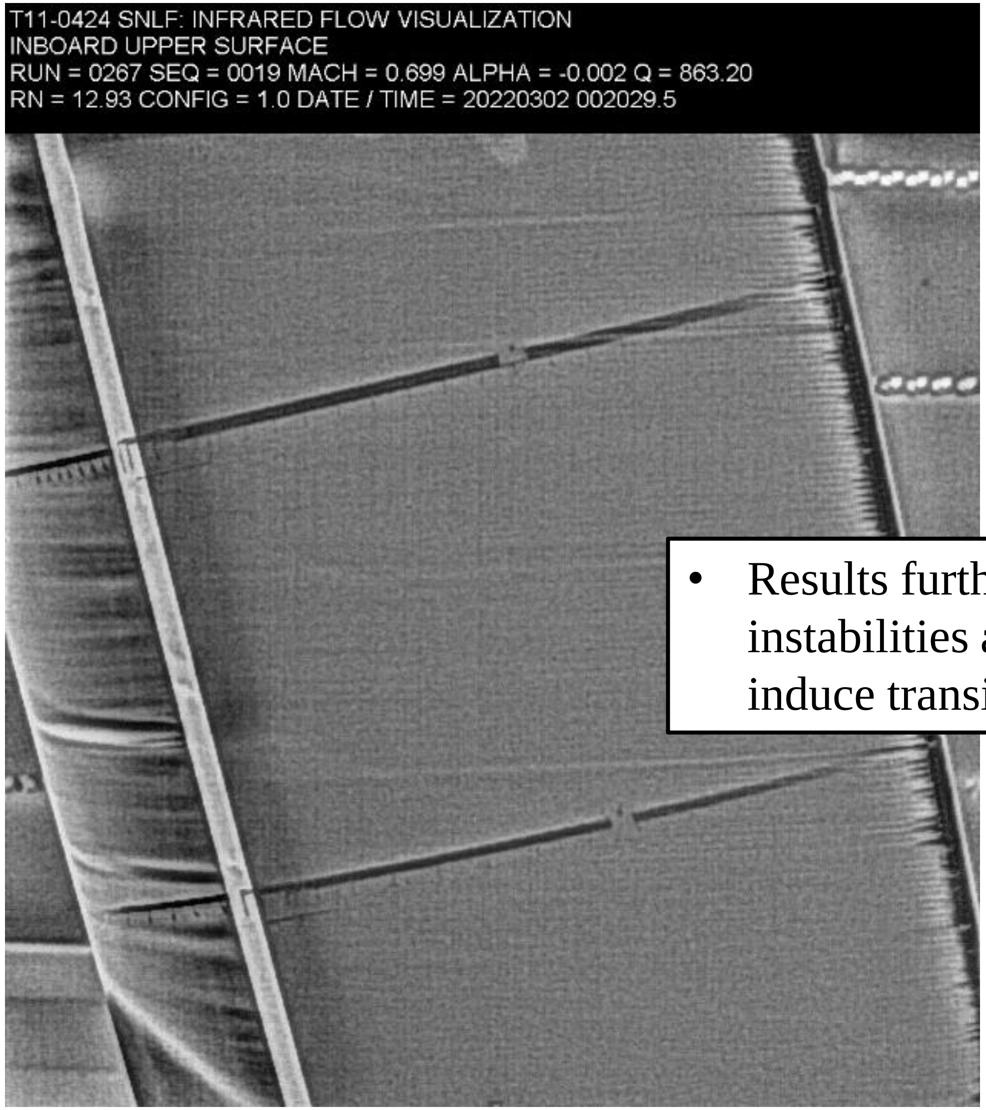

IR Flow (Left to Right) For Mach = 0.699, AOA=-1.000°, Re=12.95 Million

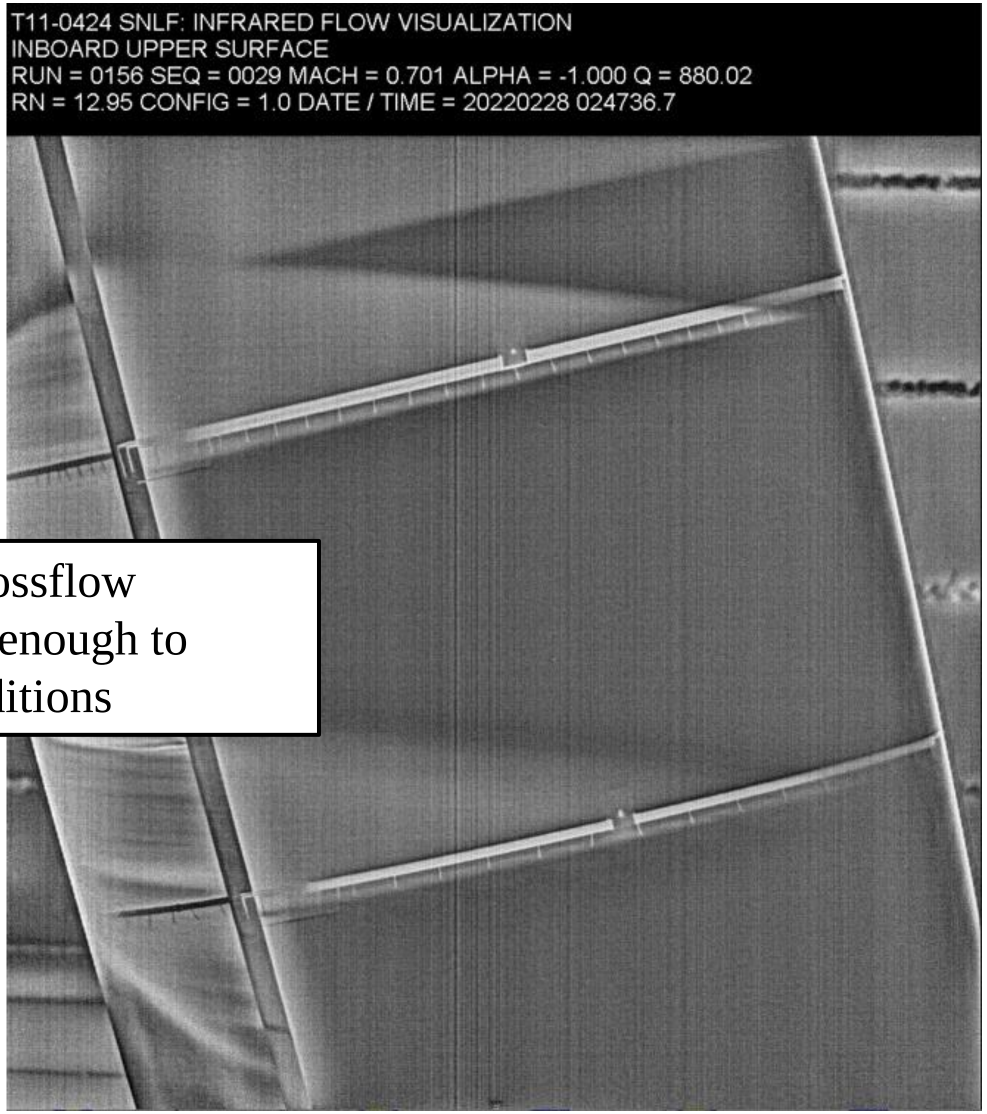

- Results further indicate that crossflow instabilities are not significant enough to induce transition at cruise conditions

5.2 Wind Tunnel Model Grid

- Wind tunnel model campaign was supported with CFD simulations completed on a wind tunnel model grid
    - Representative of experimental setup
    - Generated using Pointwise at UTK

Wing-Fairing Junction Model Grid

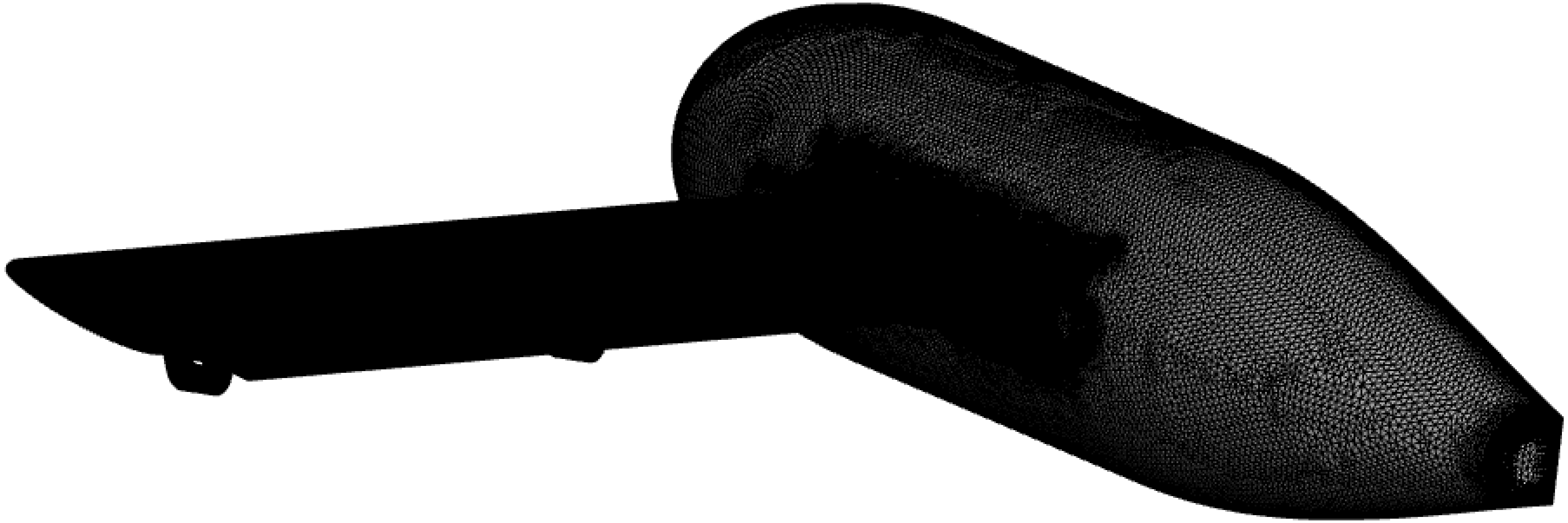

5.2 Wind Tunnel Model Grid

- Wind tunnel model campaign was supported with CFD simulations completed on a wind tunnel model grid
  - Representative of experimental setup
  - Generated using Pointwise at UTK

Wing-Fairing Junction Model Grid

- Unstructured with 168877277 nodes

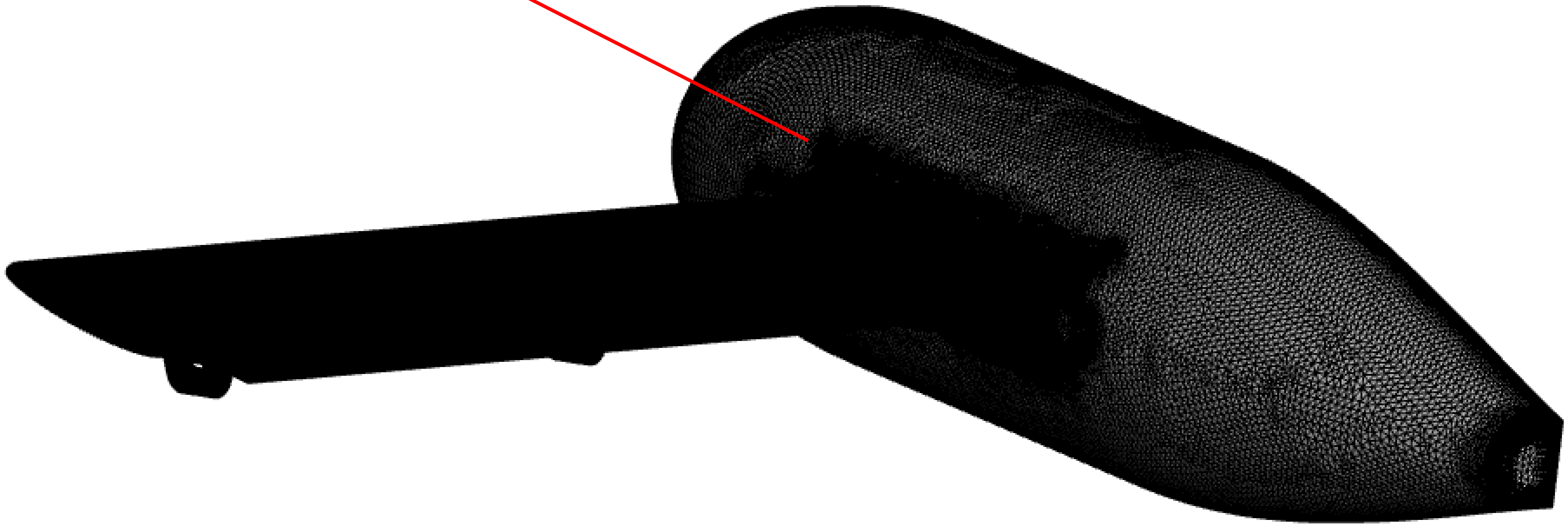

5.2 Wind Tunnel Model Grid

- Wind tunnel model campaign was supported with CFD simulations completed on a wind tunnel model grid
  - Representative of experimental setup
  - Generated using Pointwise at UTK

Wing-Fairing Junction Model Grid

- Unstructured with 168877277 nodes

- Refinement in region of the slot

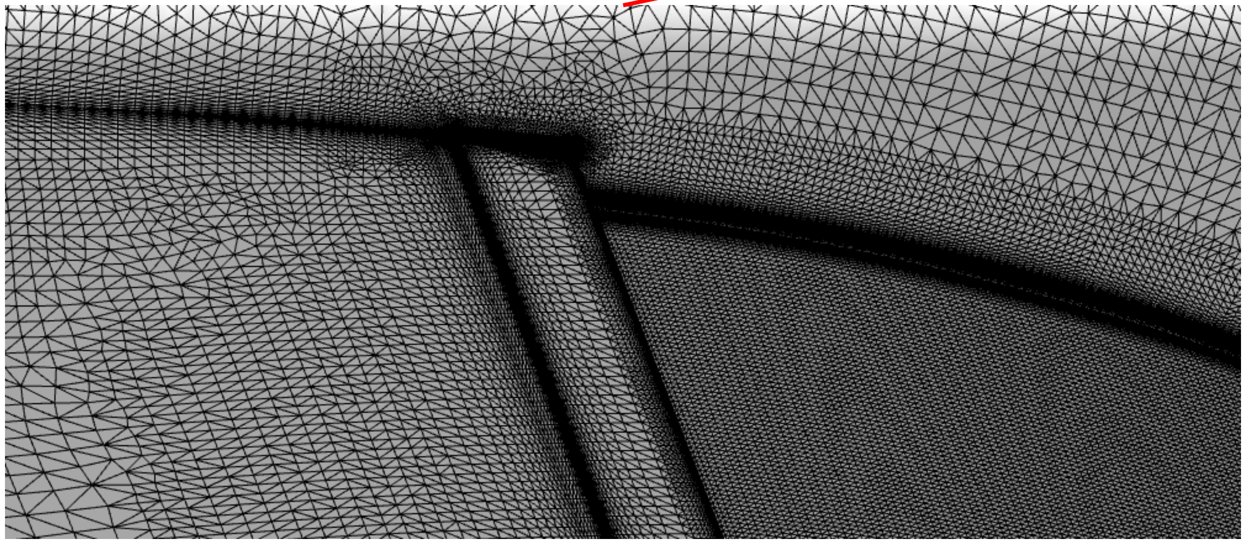

5.2 Wind Tunnel Model Grid

- Wind tunnel model campaign was supported with CFD simulations completed on a wind tunnel model grid
  - Representative of experimental setup
  - Generated using Pointwise at UTK

Entire Computational Domain

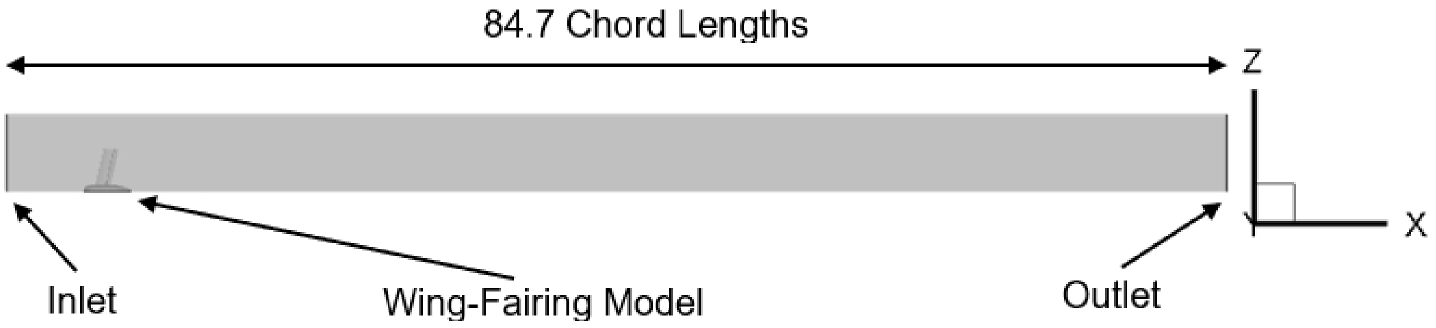

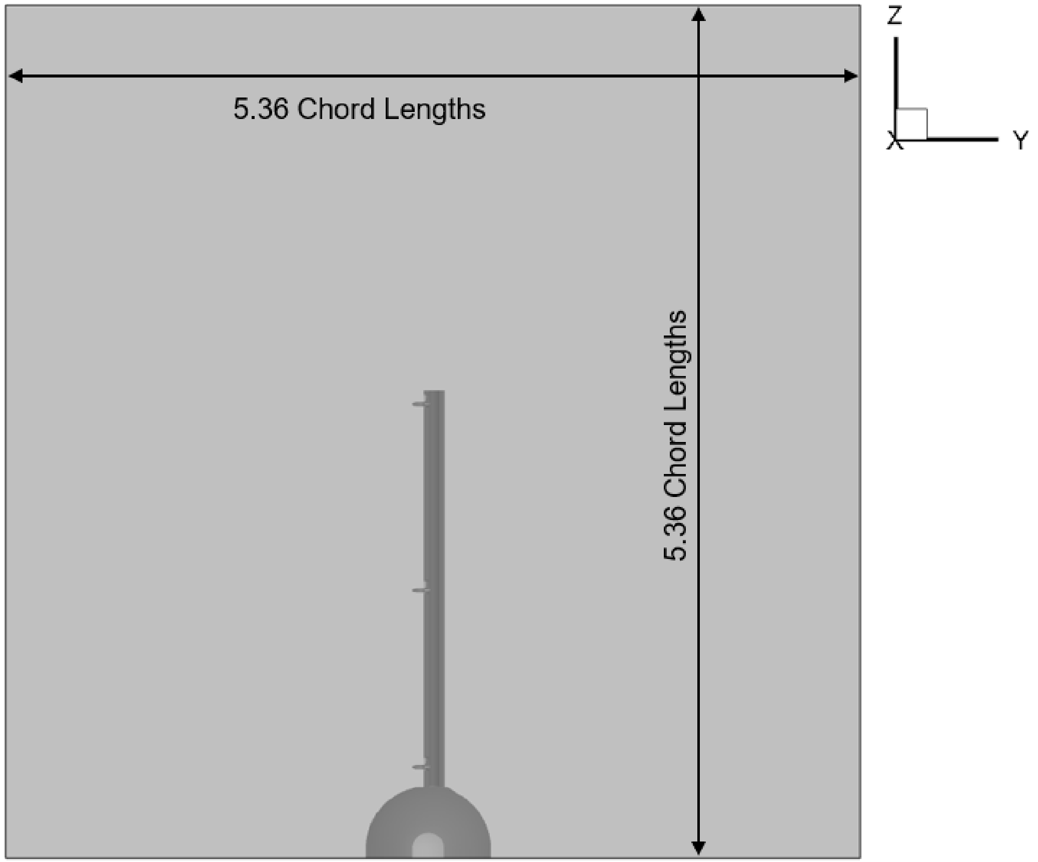

5.3 Computational Results for the Wind Tunnel Model

- Mach number of 0.7, AOA=0.0°, Re=12 Million
- N_{crit}=6 used, more accurate of wind tunnel results

NSU3D-SA-AFT2 Free Transition N_{crit}=6 Wind Tunnel Simulation Convergence History

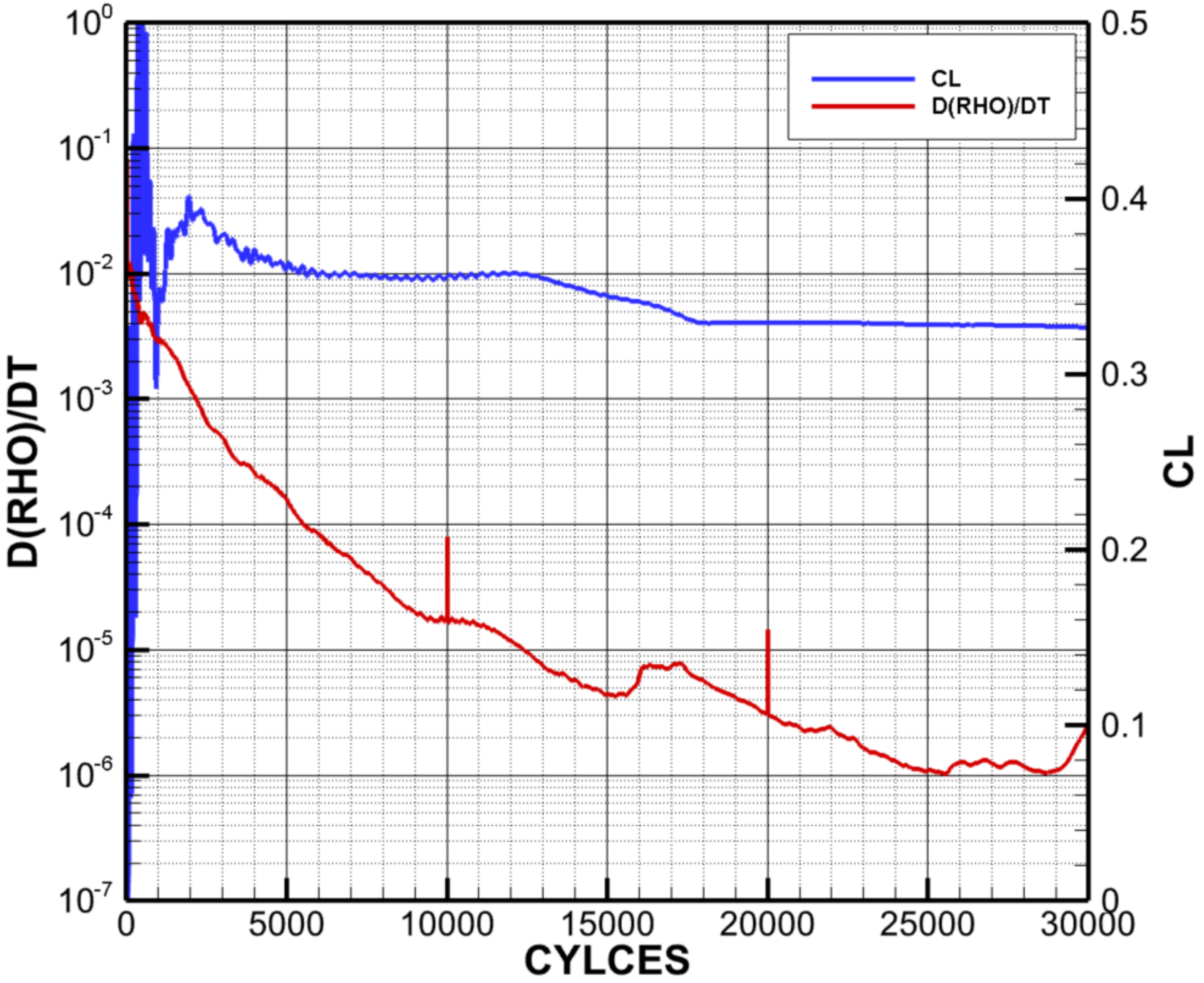

5.3 Computational Results for the Wind Tunnel Model

- Mach number of 0.7, AOA=0.0°, Re=12 Million
- N_{crit}=6 used, more accurate of wind tunnel results

NSU3D-SA-AFT2 Free Transition N_{crit}=6 Wind Tunnel Simulation Convergence History

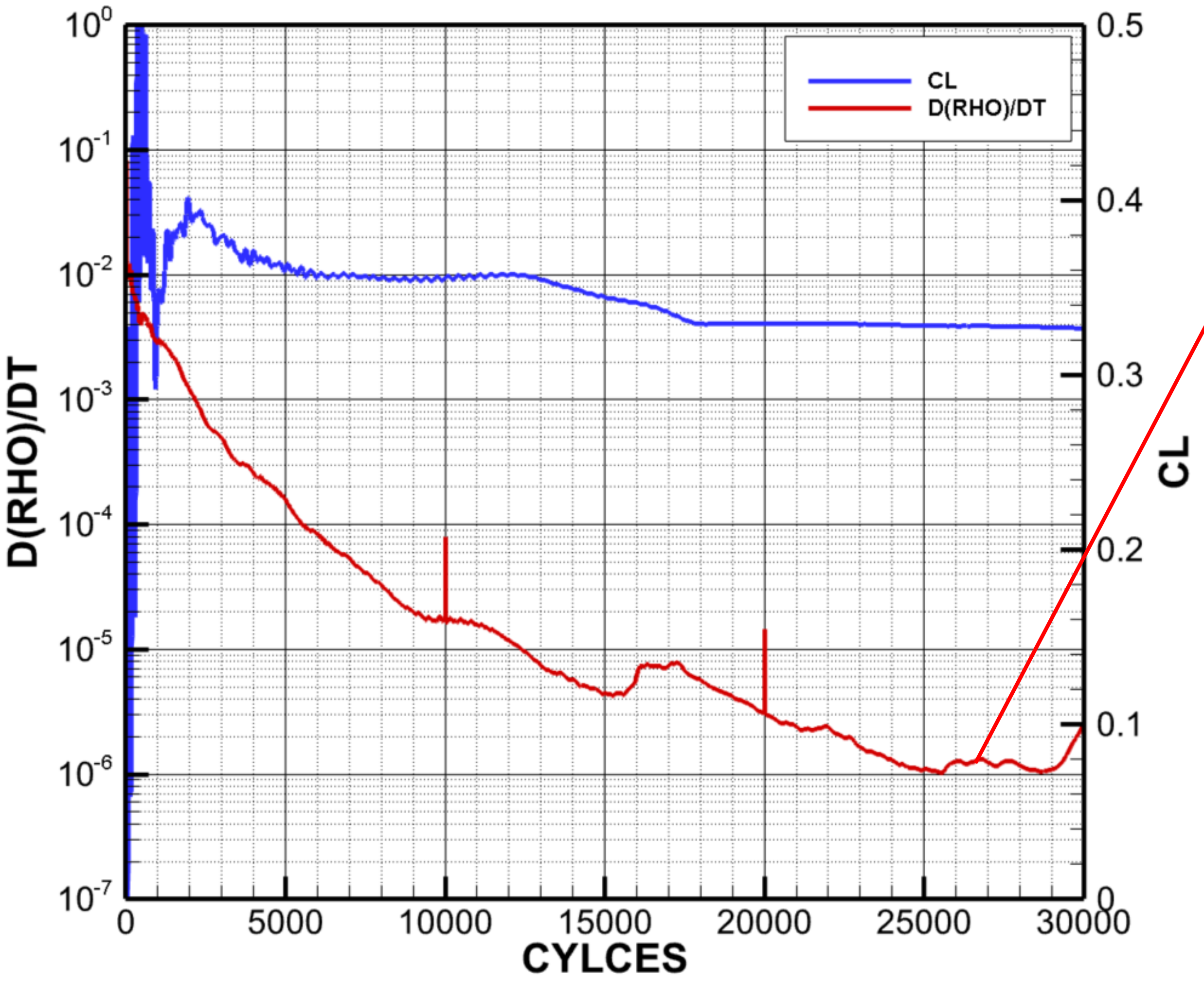

- Grid is very slow to converge due to grid size and application of transition prediction model.
  - Took roughly 25 to 30 hours to run

5.3 Computational Results for the Wind Tunnel Model

- Mach number of 0.7, AOA=0.0°, Re=12 Million
- N_{crit}=6 used, more accurate of wind tunnel results

NSU3D-SA-AFT2 Free Transition N_{crit}=6 Wind Tunnel Simulation Convergence History

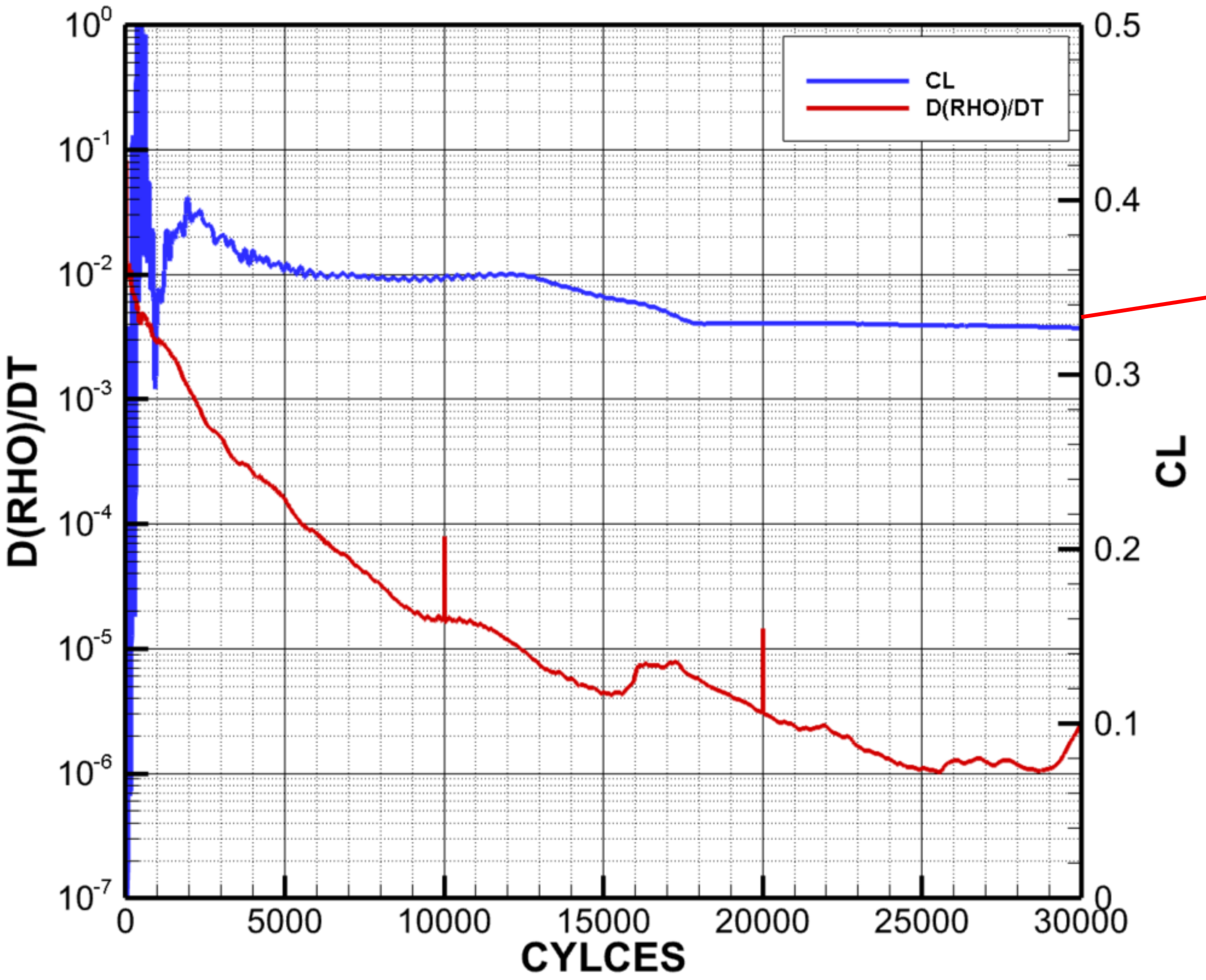

- Grid is very slow to converge due to grid size and application of transition prediction model.
  - Took roughly 25 to 30 hours to run

- CL = 0.32

5.3 Computational Results for the Wind Tunnel Model

- Skin friction drag contours at various stages in the simulation examined to investigate the behavior or the transition line

NSU3D-SA-AFT2 Free Transition Upper Surface Skin Friction Drag Profile for N_{crit}=6.0 at 10000 Cyc

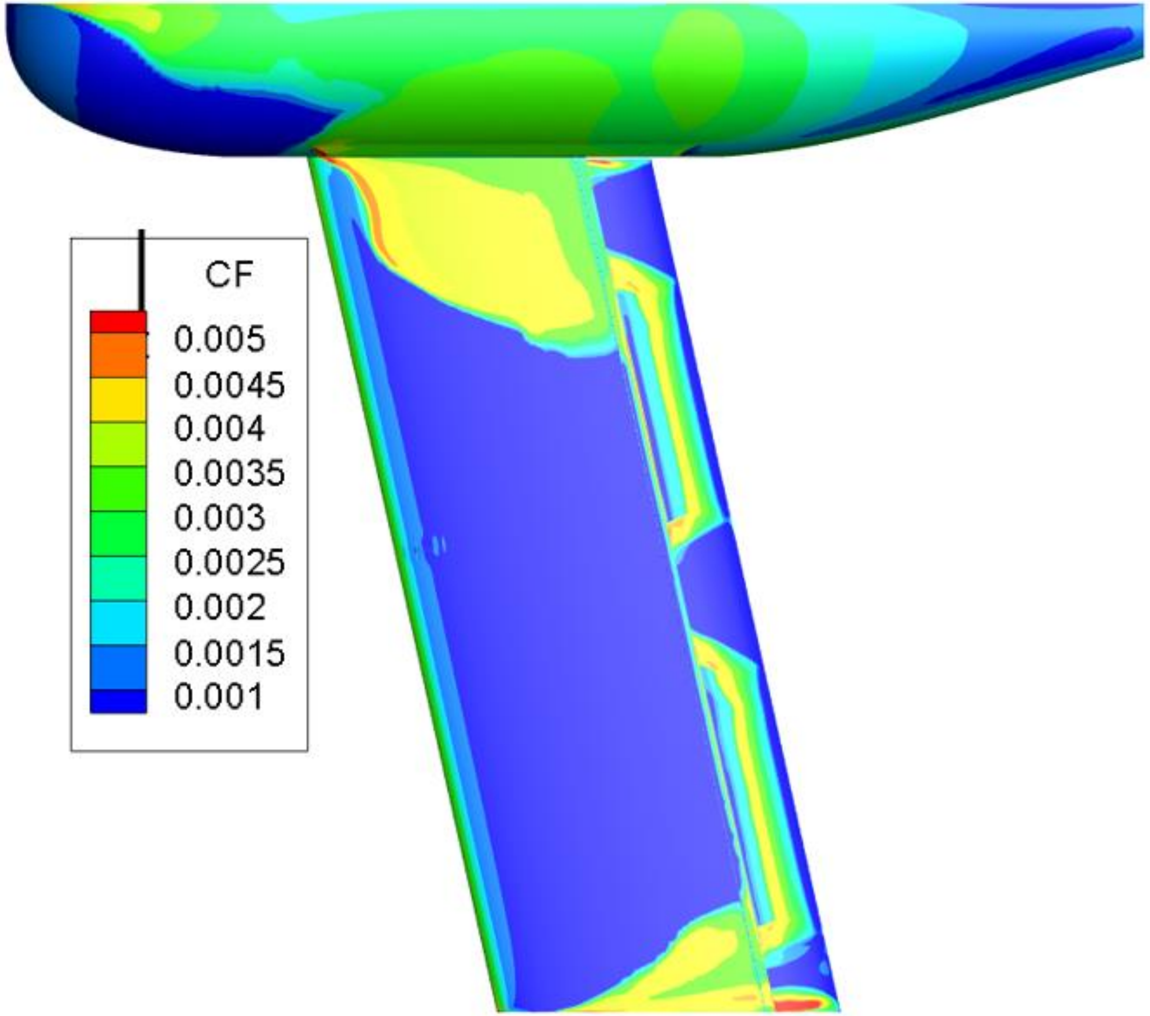

NSU3D-SA-AFT2 Free Transition Lower Surface Skin Friction Drag Profile for N_{crit}=6.0 at 10000 Cyc

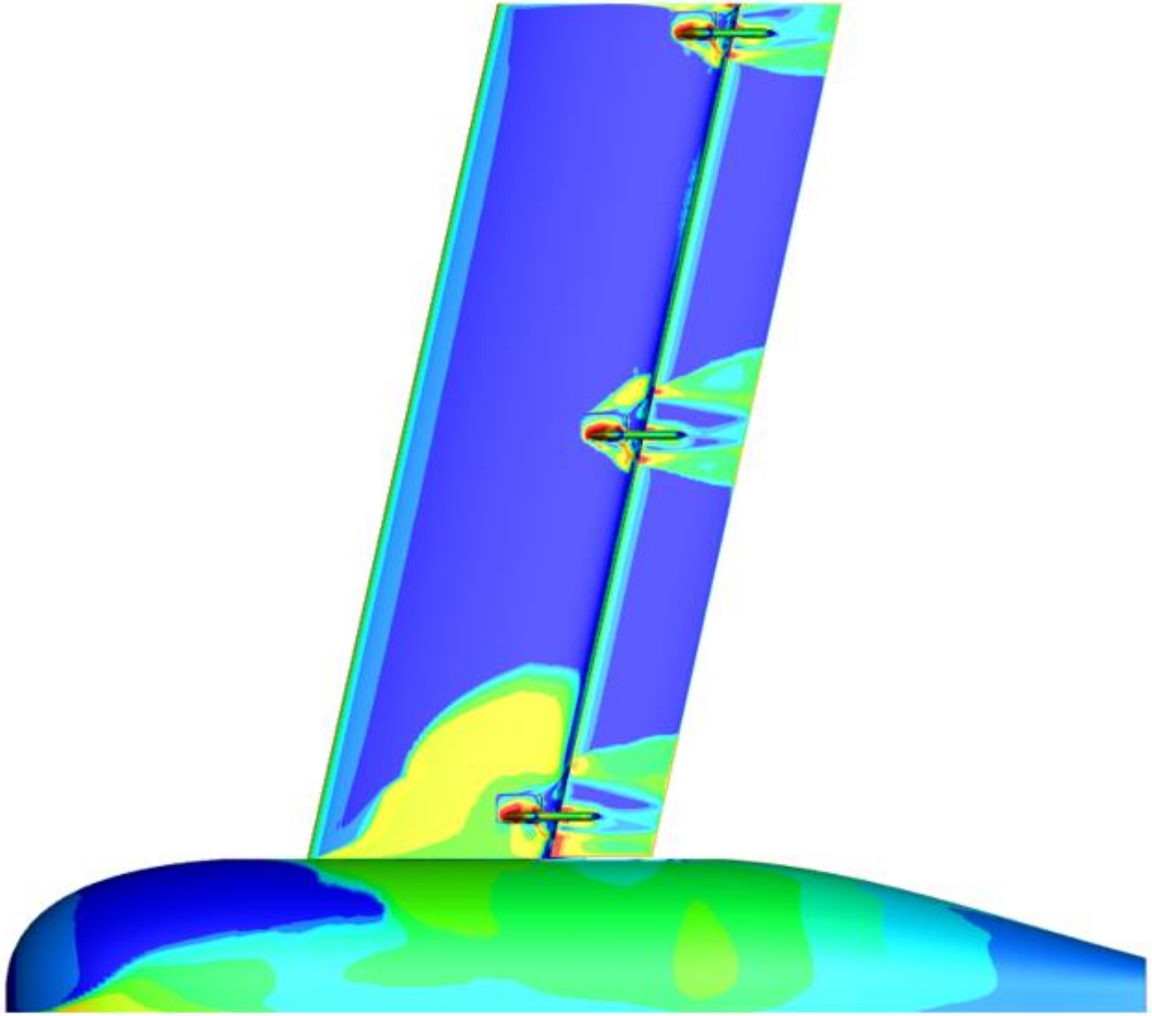

5.3 Computational Results for the Wind Tunnel Model

- Skin friction drag contours at various stages in the simulation examined to investigate the behavior or the transition line

NSU3D-SA-AFT2 Free Transition Upper Surface Skin Friction Drag Profile for N_{crit}=6.0 at 30000 Cyc

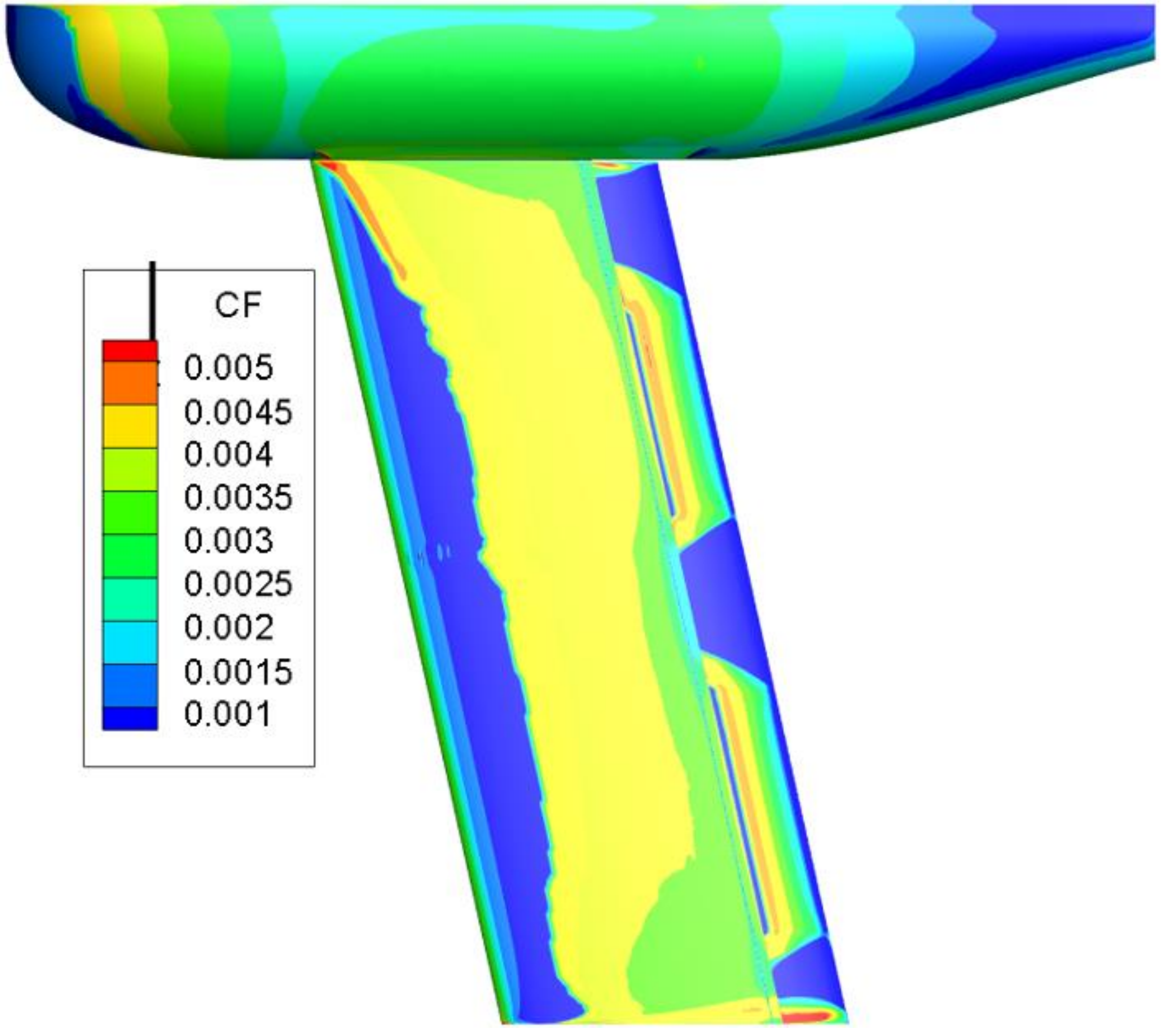

NSU3D-SA-AFT2 Free Transition Lower Surface Skin Friction Drag Profile for N_{crit}=6.0 at 30000 Cyc

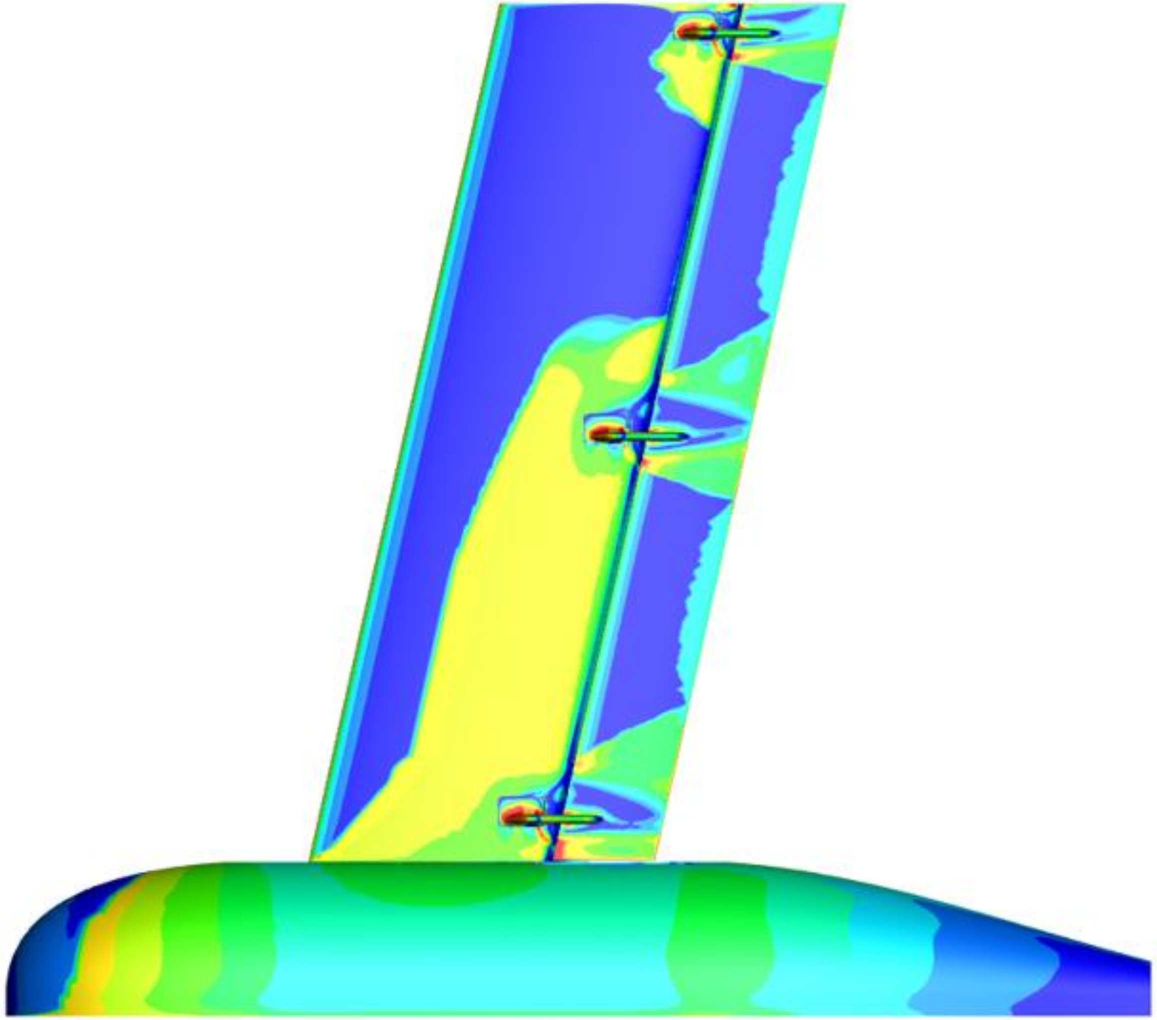

5.3 Computational Results for the Wind Tunnel Model

- Skin friction drag contours at various stages in the simulation examined to investigate the behavior or the transition line

NSU3D-SA-AFT2 Free Transition Upper Surface Skin Friction Drag Profile for N_{crit}=6.0 at 30000 Cyc

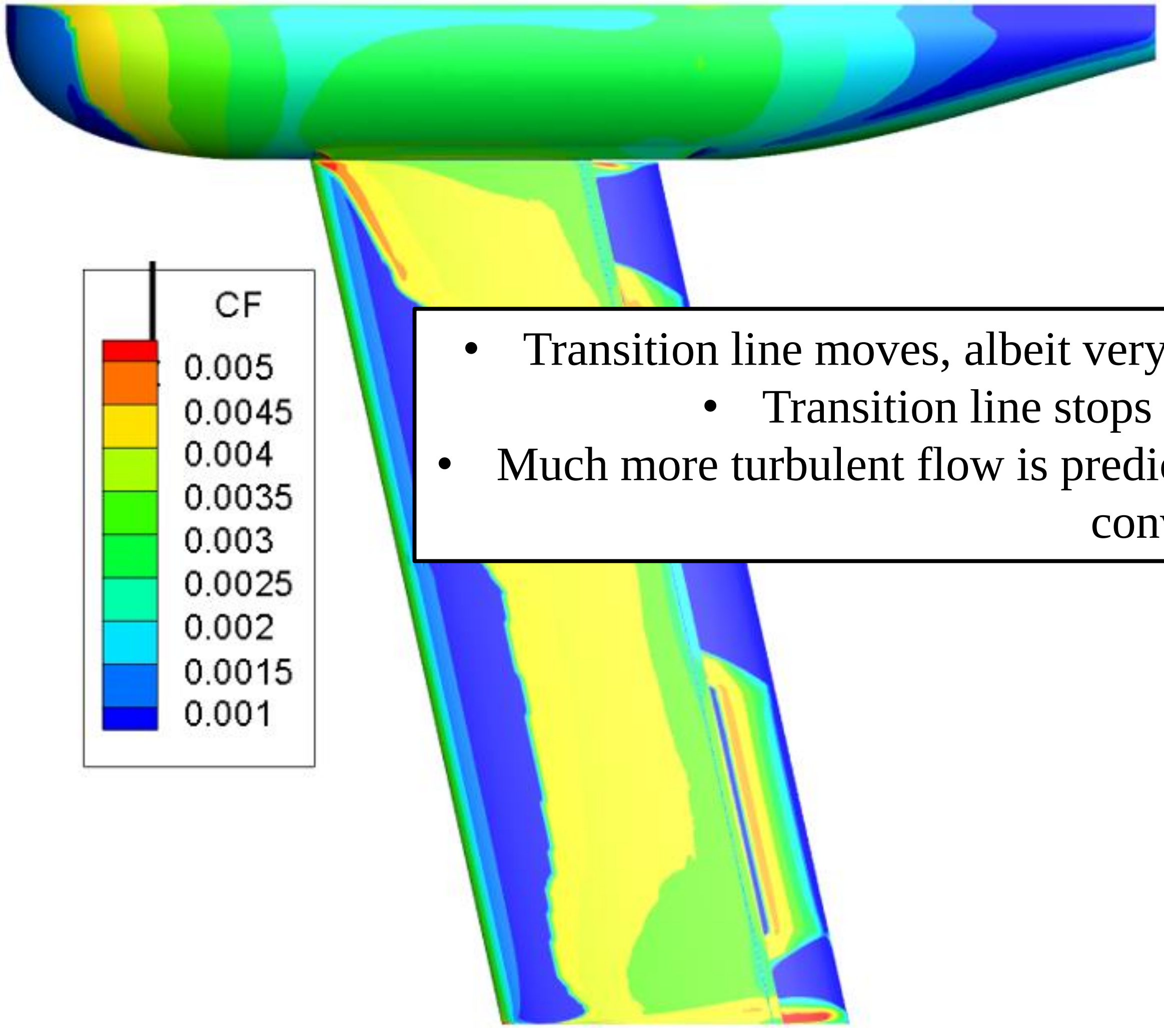

NSU3D-SA-AFT2 Free Transition Lower Surface Skin Friction Drag Profile for N_{crit}=6.0 at 30000 Cyc

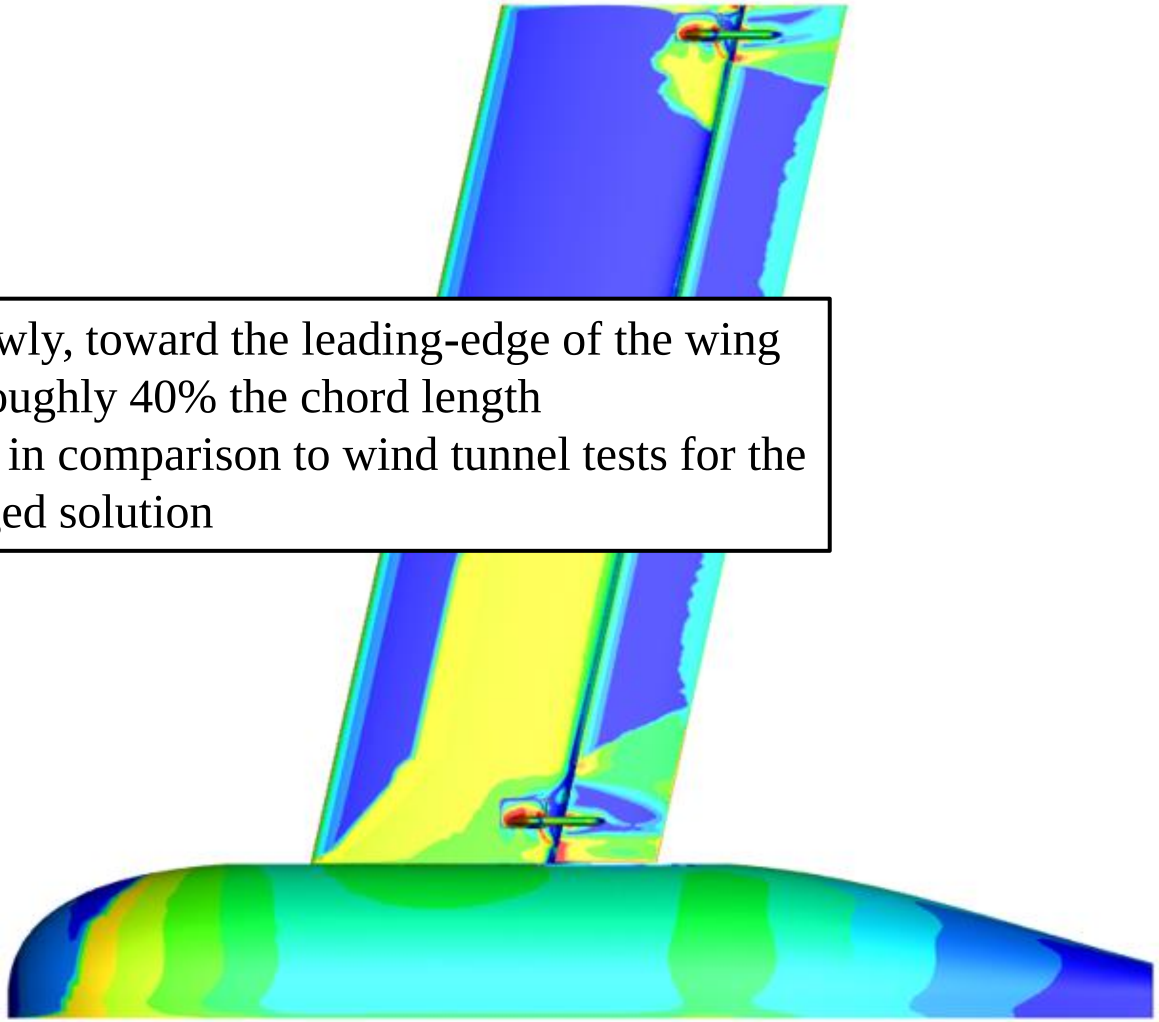

- Transition line moves, albeit very slowly, toward the leading-edge of the wing
- Transition line stops at roughly 40% the chord length
- Much more turbulent flow is predicted in comparison to wind tunnel tests for the converged solution

5.3 Computational Results for the Wind Tunnel Model

- To investigate differences further, surface pressure profile comparisons were made pressure port data
- Two wind tunnel runs were conducted at flow conditions close to Mach=0.7, AOA=0
  - The run data was post-processed and provided by ULI associates at Texas A&M

Relevant Wind Tunnel Runs Summary

Run	Mach	Reynolds Number	Angle of Attack
204	0.7013	12.95 Million	-0.0001
297	0.6994	12.93 Million	-0.0002

5.3 Computational Results for the Wind Tunnel Model

- To investigate differences further, surface pressure profile comparisons were made pressure port data
- Two wind tunnel runs were conducted at flow conditions close to Mach=0.7, AOA=0
  - The run data was post-processed and provided by ULI associates at Texas A&M

Pressure Profile Comparisons Between Wind Tunnel Tests L1 Pressure Port Data and NSU2D-SA-AFT2 Free Transition N_{crit}=6 Simulation

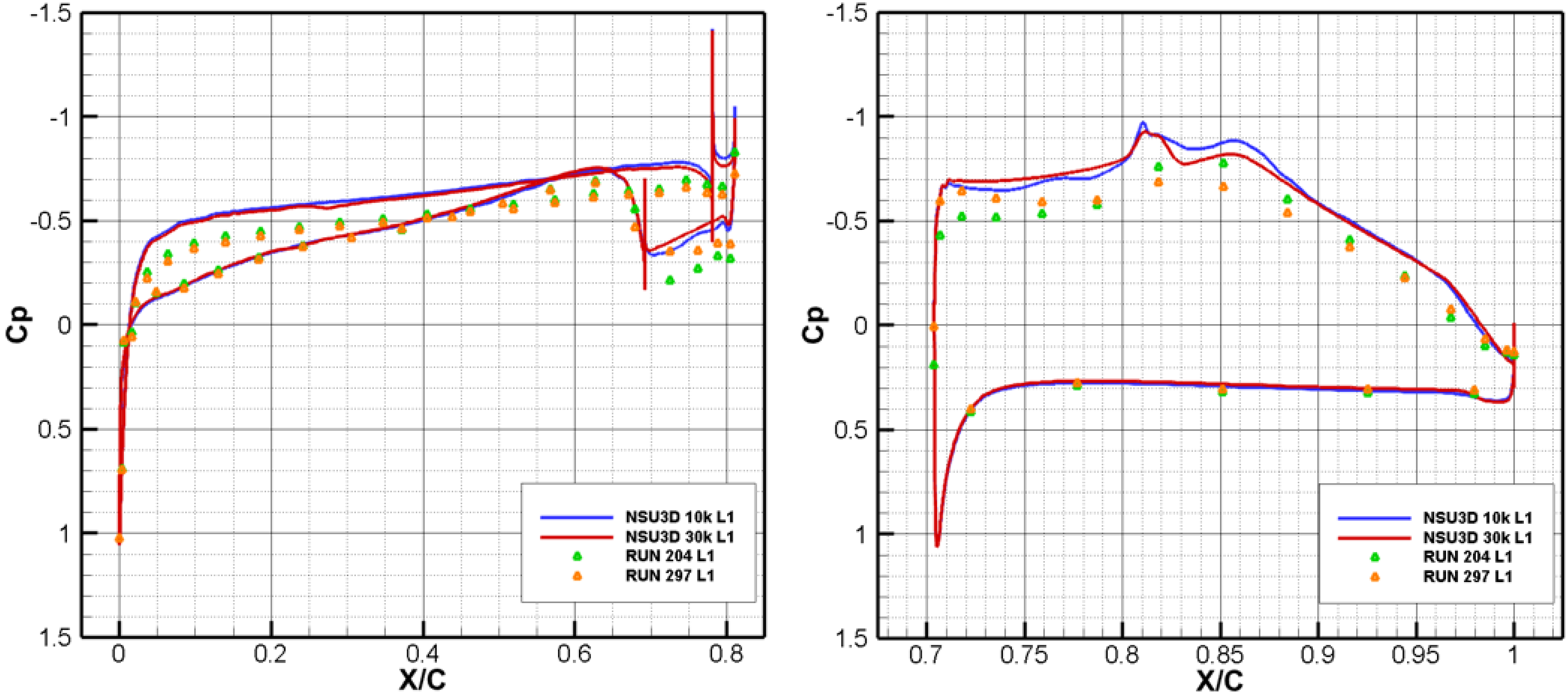

5.3 Computational Results for the Wind Tunnel Model

- To investigate differences further, surface pressure profile comparisons were made pressure port data
- Two wind tunnel runs were conducted at flow conditions close to Mach=0.7, AOA=0
  - The run data was post-processed and provided by ULI associates at Texas A&M

Pressure Profile Comparisons Between Wind Tunnel Tests L1 Pressure Port Data and NSU2D-SA-AFT2 Free Transition N_{crit}=6 Simulation

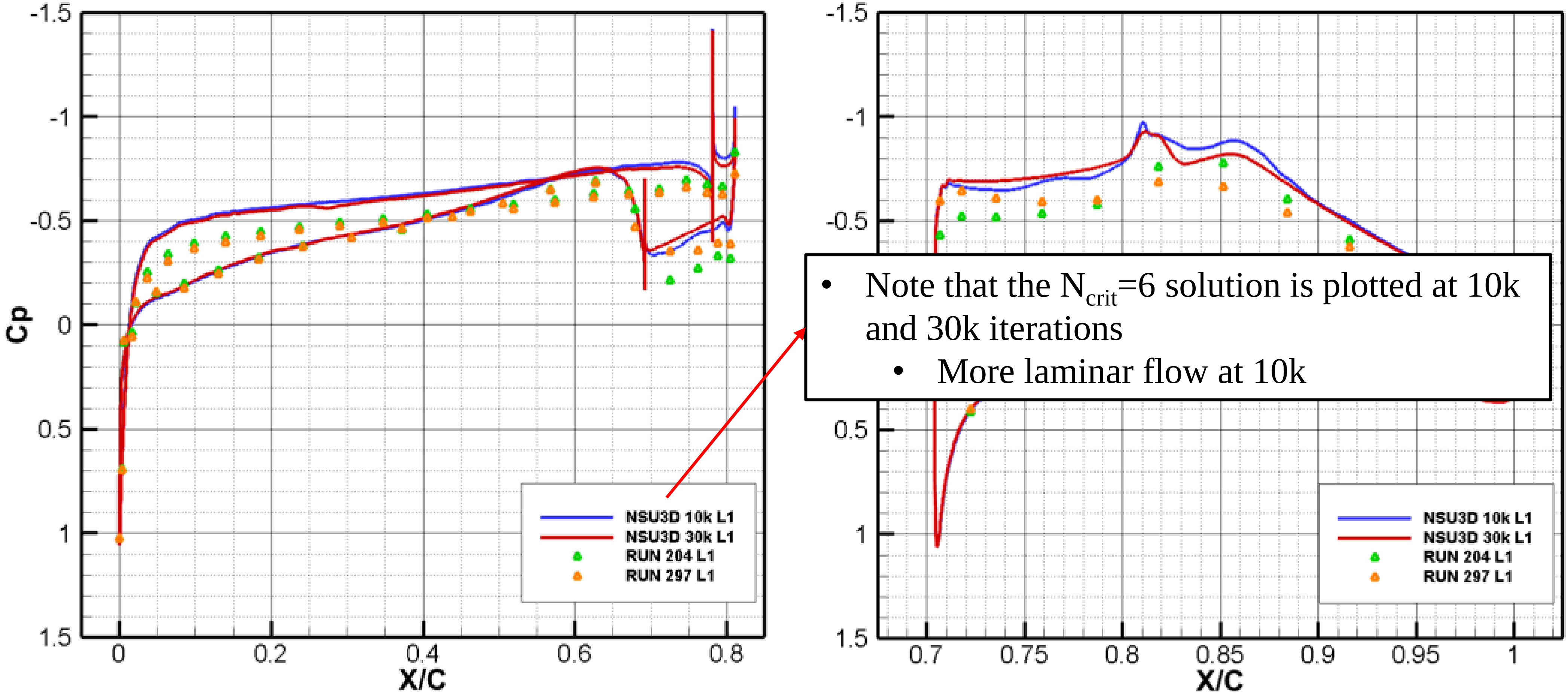

- Note that the N_{crit}=6 solution is plotted at 10k and 30k iterations
  - More laminar flow at 10k

5.3 Computational Results for the Wind Tunnel Model

- To investigate differences further, surface pressure profile comparisons were made pressure port data
- Two wind tunnel runs were conducted at flow conditions close to Mach=0.7, AOA=0
  - The run data was post-processed and provided by ULI associates at Texas A&M

Pressure Profile Comparisons Between Wind Tunnel Tests L1 Pressure Port Data and NSU2D-SA-AFT2 Free Transition N_{crit}=6 Simulation

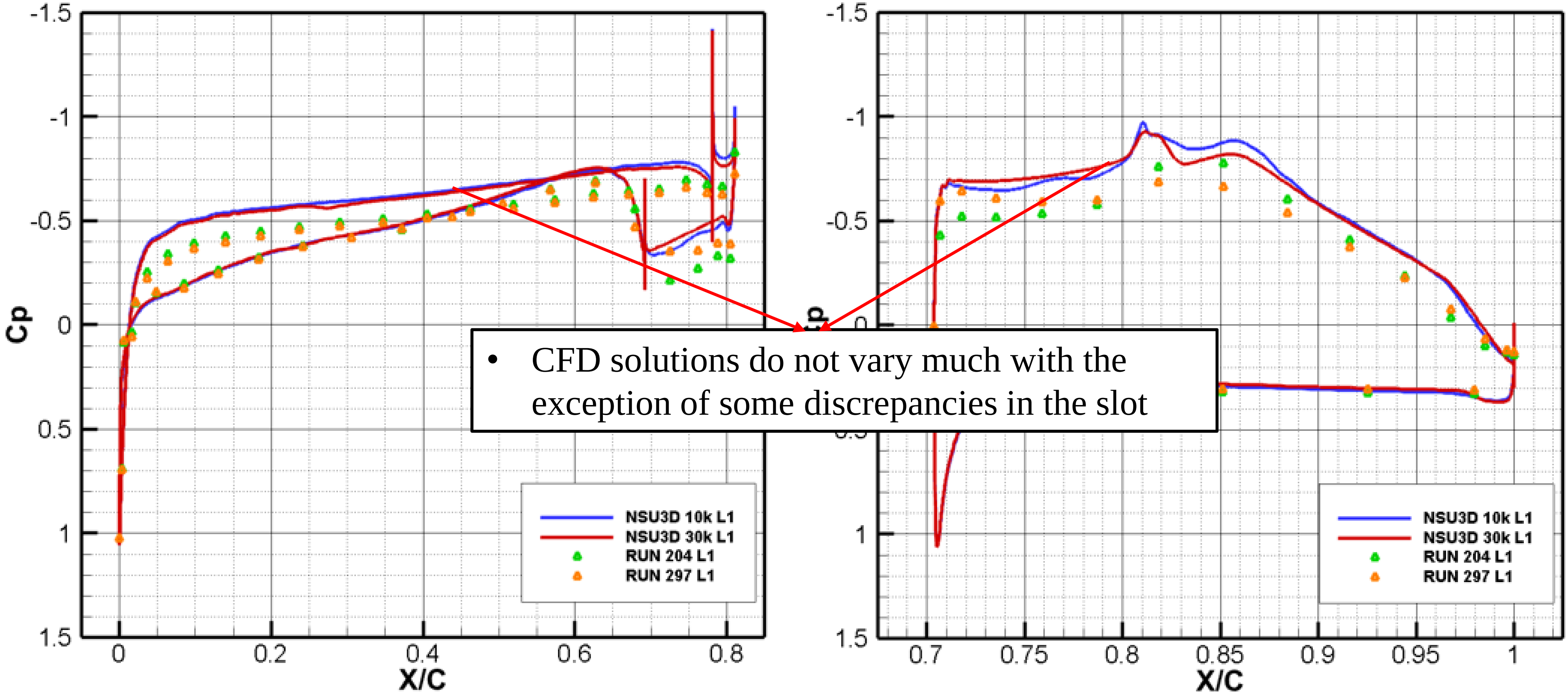

- CFD solutions do not vary much with the exception of some discrepancies in the slot

5.3 Computational Results for the Wind Tunnel Model

- To investigate differences further, surface pressure profile comparisons were made pressure port data
- Two wind tunnel runs were conducted at flow conditions close to Mach=0.7, AOA=0
  - The run data was post-processed and provided by ULI associates at Texas A&M

Pressure Profile Comparisons Between Wind Tunnel Tests L1 Pressure Port Data and NSU2D-SA-AFT2 Free Transition N_{crit}=6 Simulation

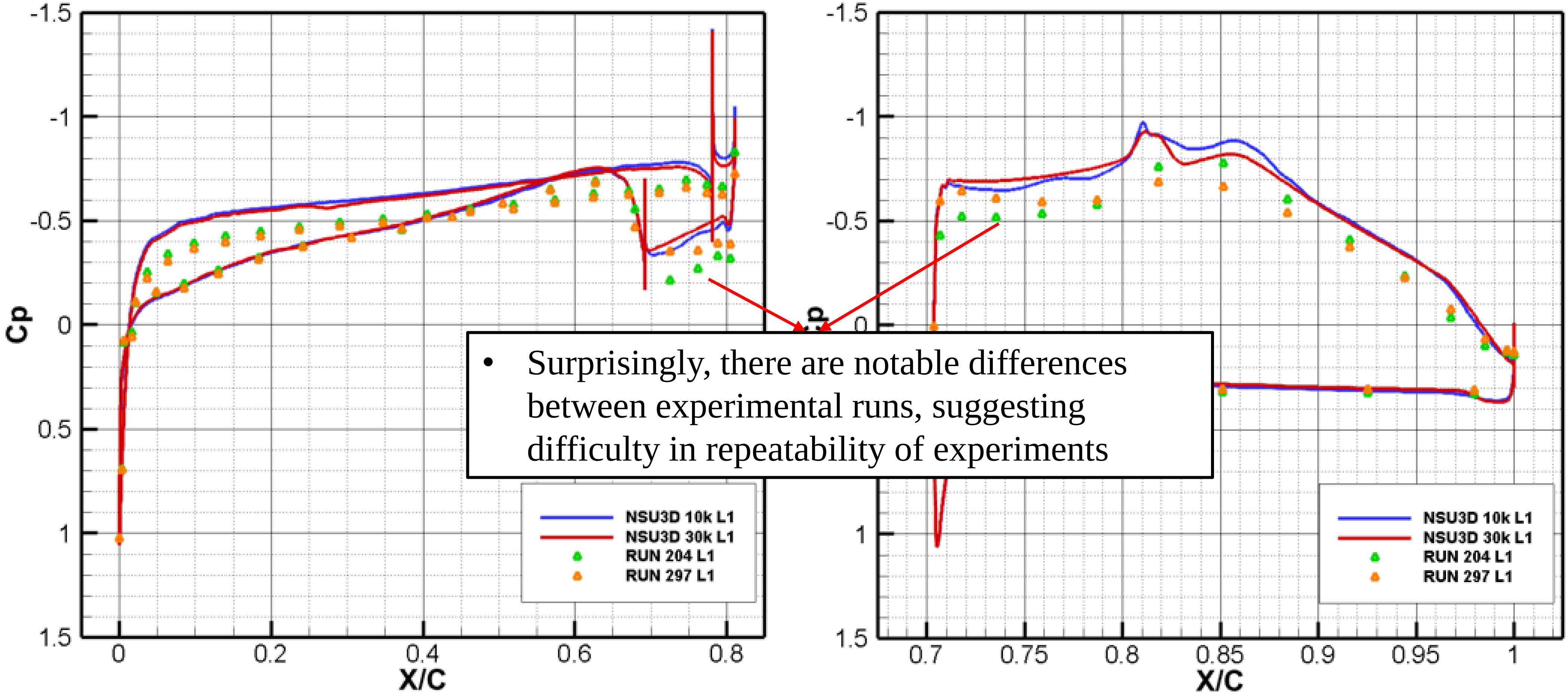

- Surprisingly, there are notable differences between experimental runs, suggesting difficulty in repeatability of experiments

5.3 Computational Results for the Wind Tunnel Model

- To investigate differences further, surface pressure profile comparisons were made pressure port data
- Two wind tunnel runs were conducted at flow conditions close to Mach=0.7, AOA=0
  - The run data was post-processed and provided by ULI associates at Texas A&M

Pressure Profile Comparisons Between Wind Tunnel Tests L1 Pressure Port Data and
2 Free Transition N_{crit}=6 Simulation

- CFD pressure profiles are lower than experimental runs on upper surface of flap and through the slot for L1 station

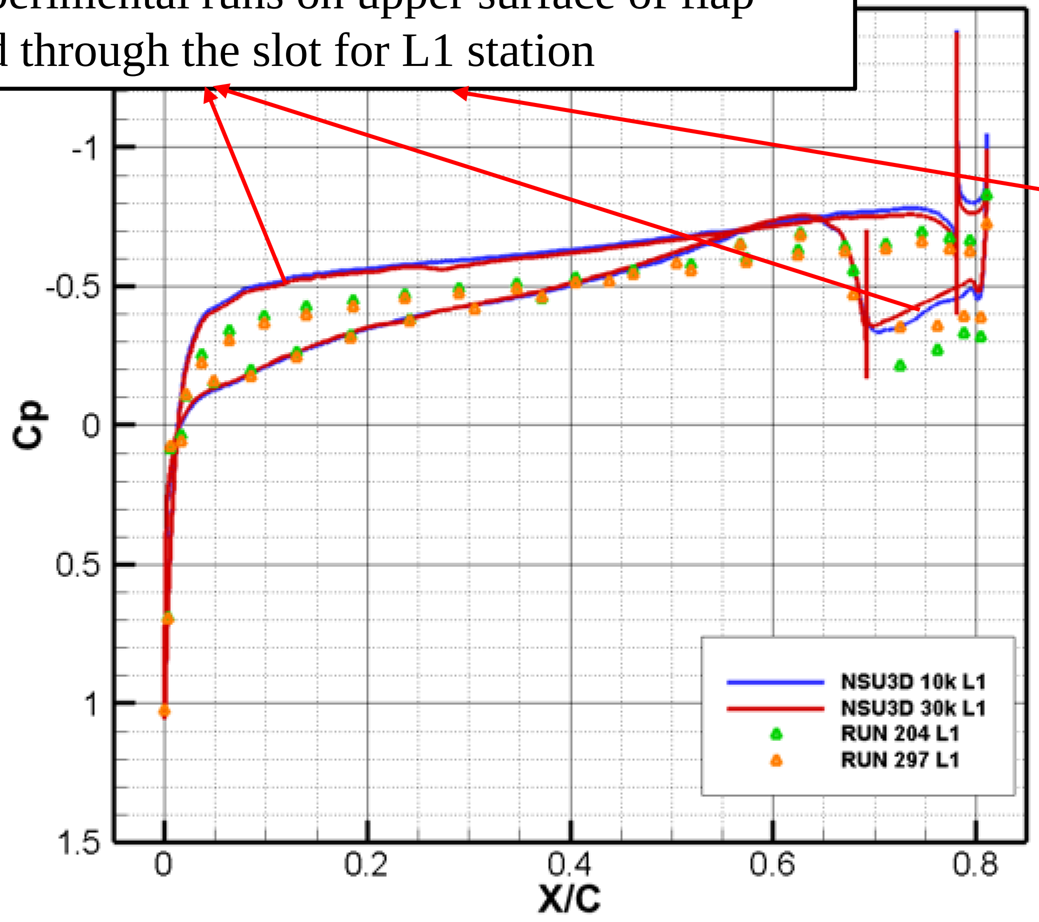

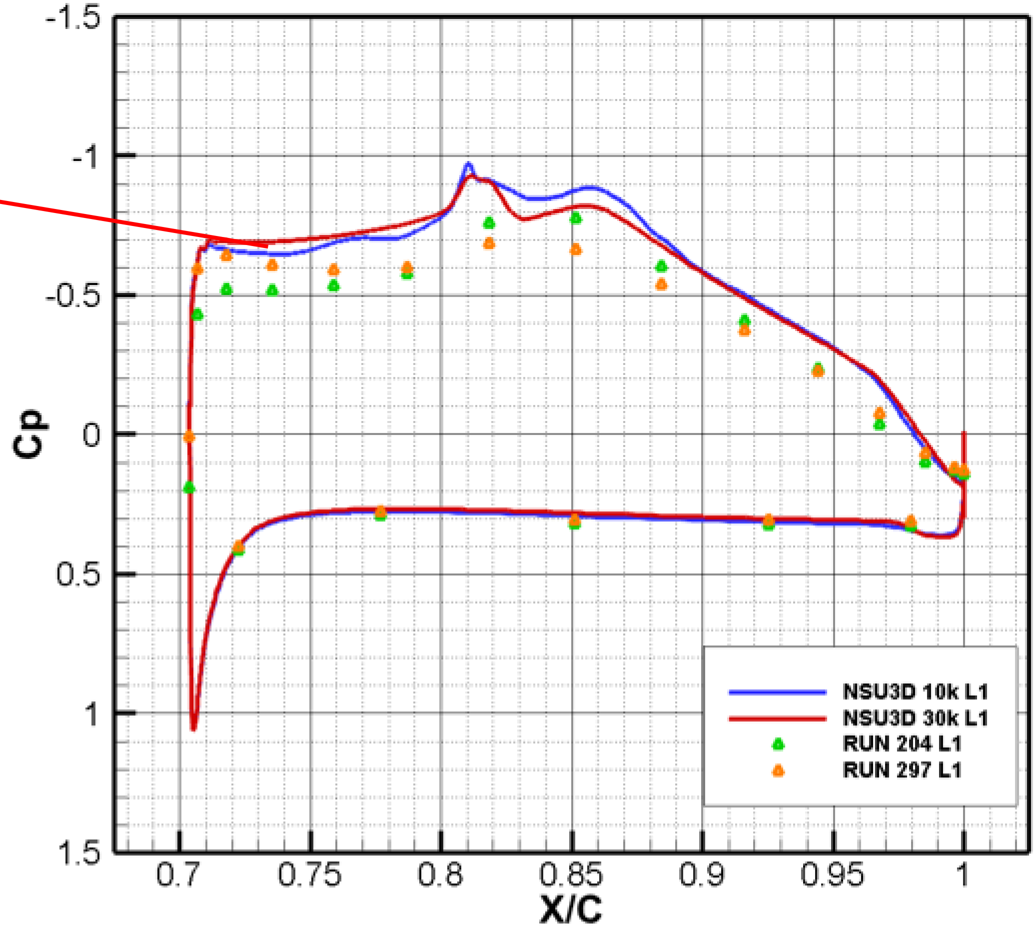

5.3 Computational Results for the Wind Tunnel Model

- To investigate differences further, surface pressure profile comparisons were made pressure port data
- Two wind tunnel runs were conducted at flow conditions close to Mach=0.7, AOA=0
  - The run data was post-processed and provided by ULI associates at Texas A&M

Pressure Profile Comparisons Between Wind Tunnel Tests L2 Pressure Port Data and NSU2D-SA-AFT2 Free Transition N_{crit}=6 Simulation

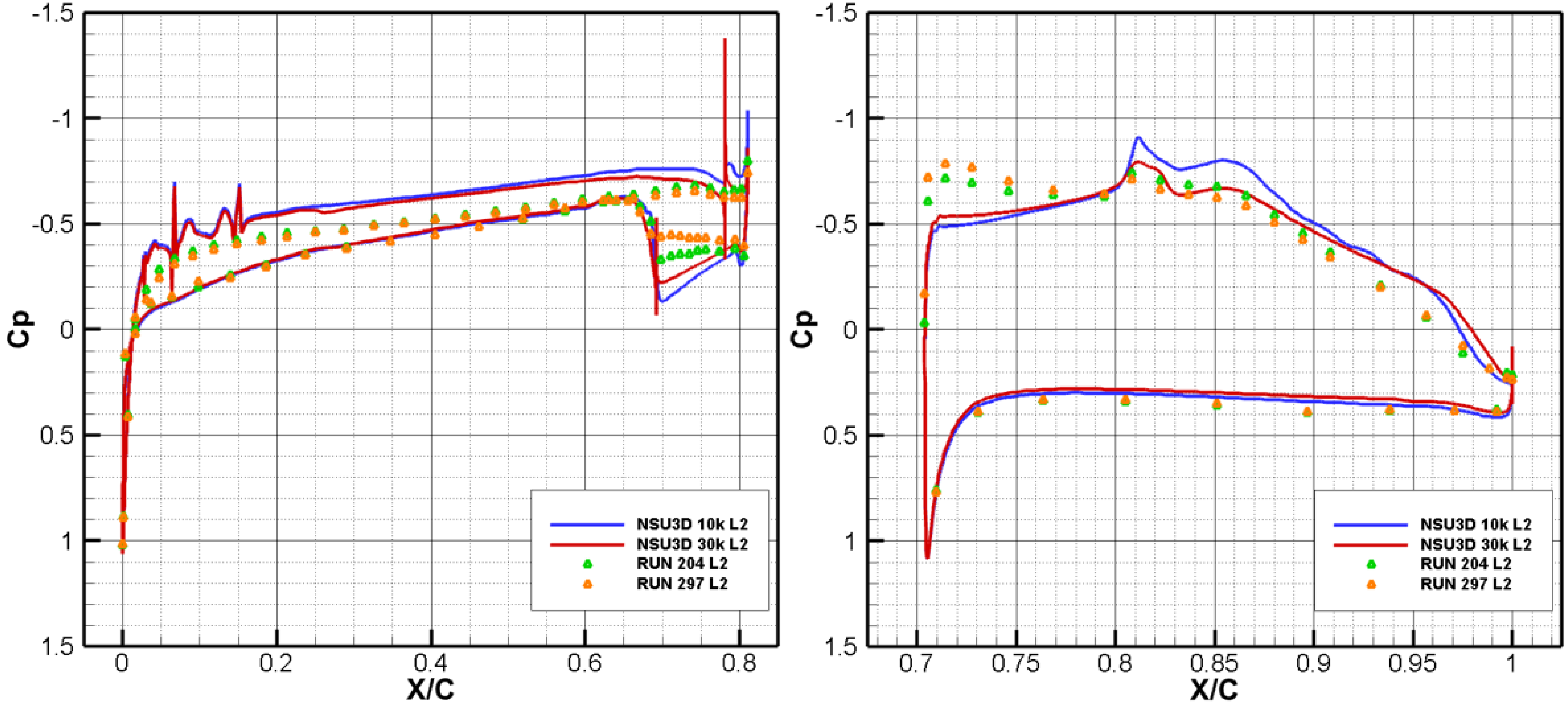

5.3 Computational Results for the Wind Tunnel Model

- To investigate differences further, surface pressure profile comparisons were made pressure port data
- Two wind tunnel runs were conducted at flow conditions close to Mach=0.7, AOA=0
  - The run data was post-processed and provided by ULI associates at Texas A&M

Pressure Profile Comparisons Between Wind Tunnel Tests L2 Pressure Port Data and NSU2D-SA-AFT2 Free Transition N_{crit}=6 Simulation

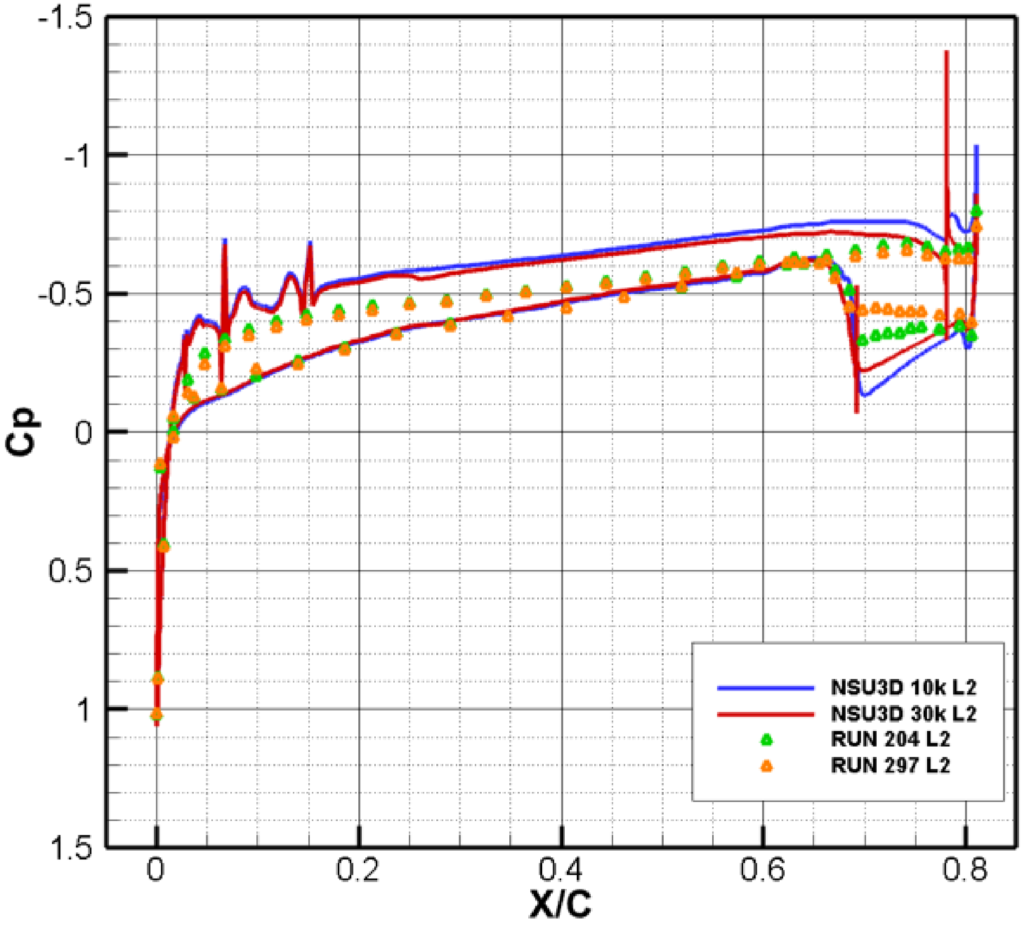

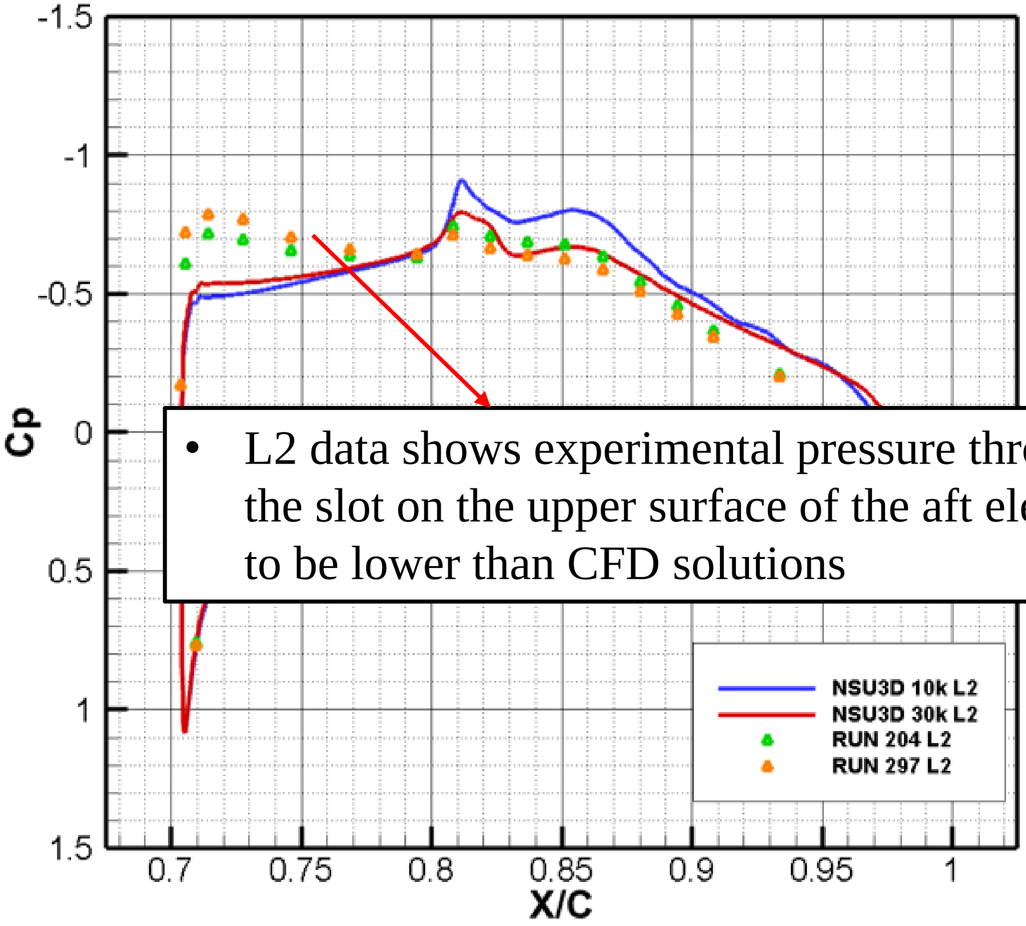

- L2 data shows experimental pressure through the slot on the upper surface of the aft element to be lower than CFD solutions

5.3 Computational Results for the Wind Tunnel Model

- To investigate differences further, surface pressure profile comparisons were made pressure port data
- Two wind tunnel runs were conducted at flow conditions close to Mach=0.7, AOA=0
  - The run data was post-processed and provided by ULI associates at Texas A&M

Pressure Profile Comparisons Between Wind Tunnel Tests L2 Pressure Port Data and NSU2D-SA-AFT2 Free Transition N_{crit}=6 Simulation

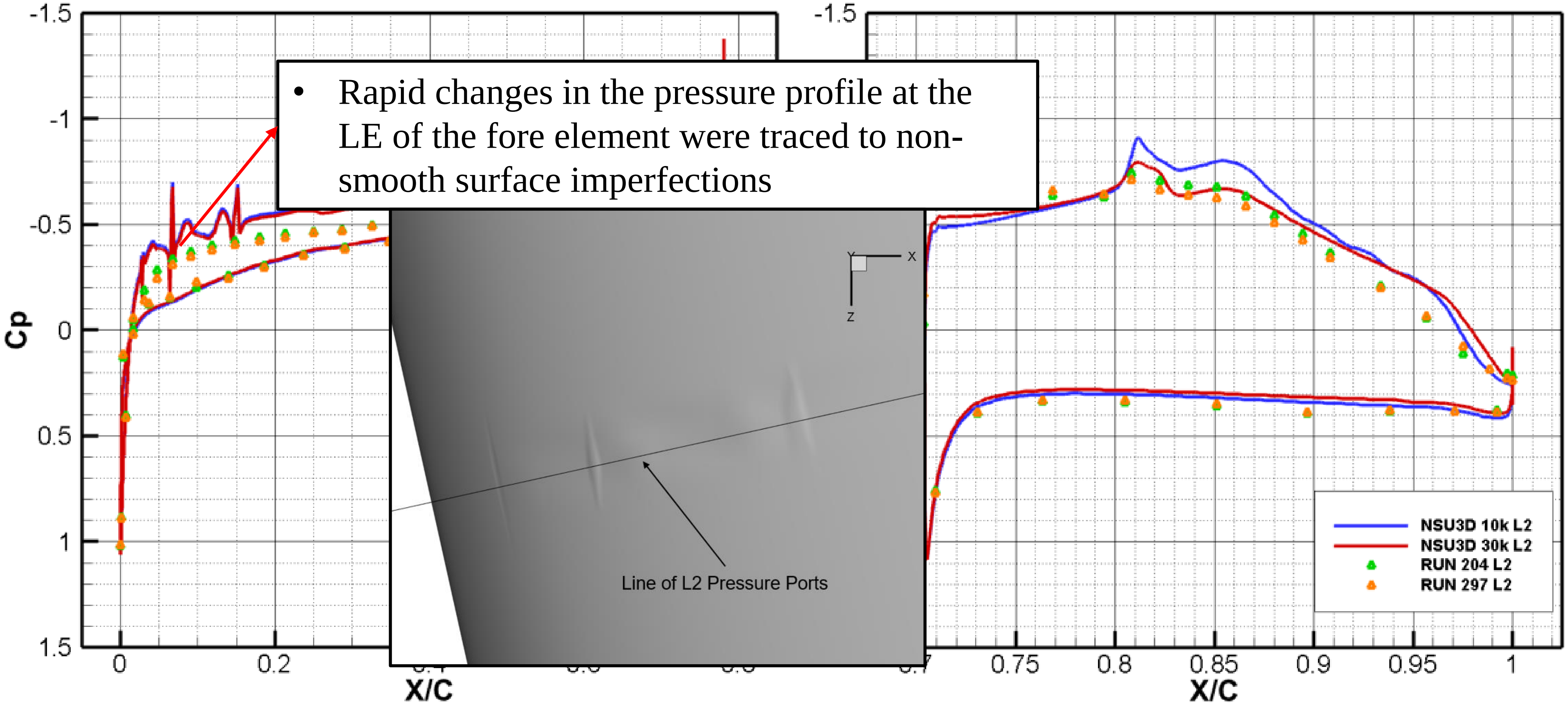

5.3 Computational Results for the Wind Tunnel Model

- To investigate differences further, surface pressure profile comparisons were made pressure port data
- Two wind tunnel runs were conducted at flow conditions close to Mach=0.7, AOA=0
  - The run data was post-processed and provided by ULI associates at Texas A&M

Pressure Profile Comparisons Between Wind Tunnel Tests L3 Pressure Port Data and NSU2D-SA-AFT2 Free Transition N_{crit}=6 Simulation

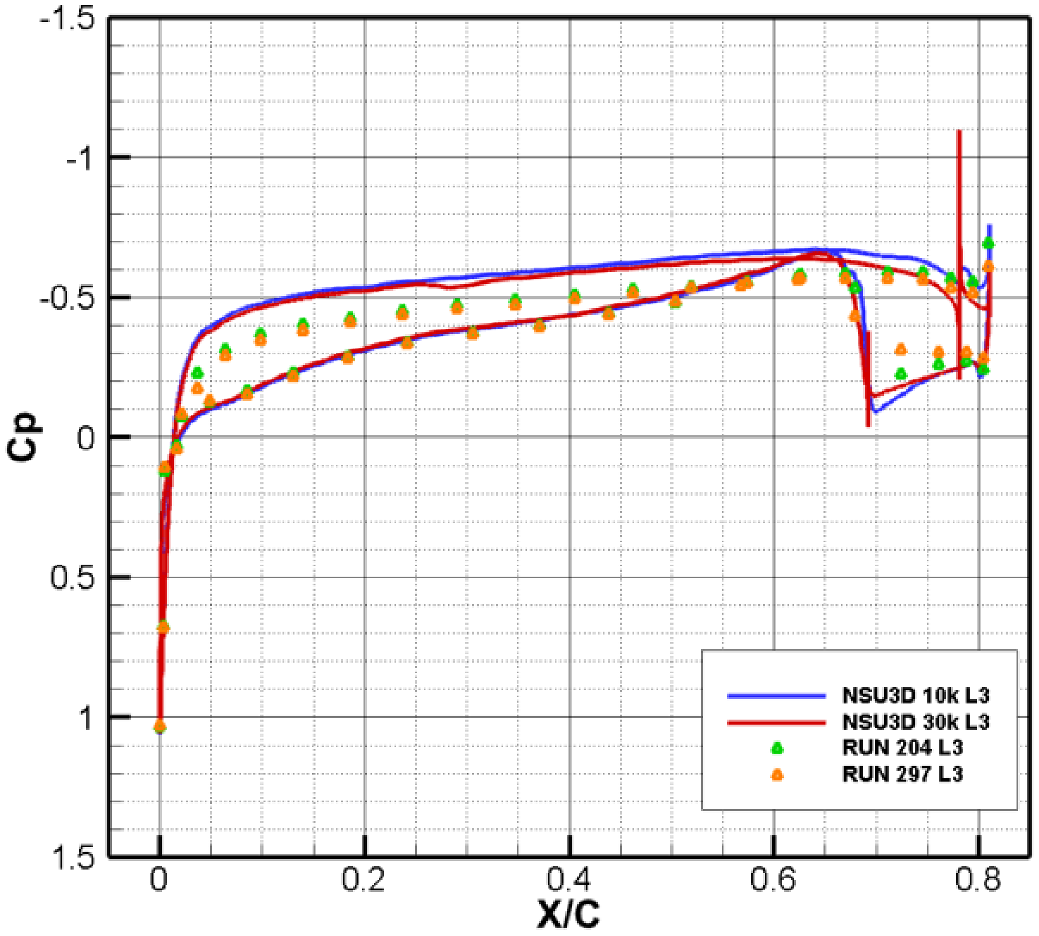

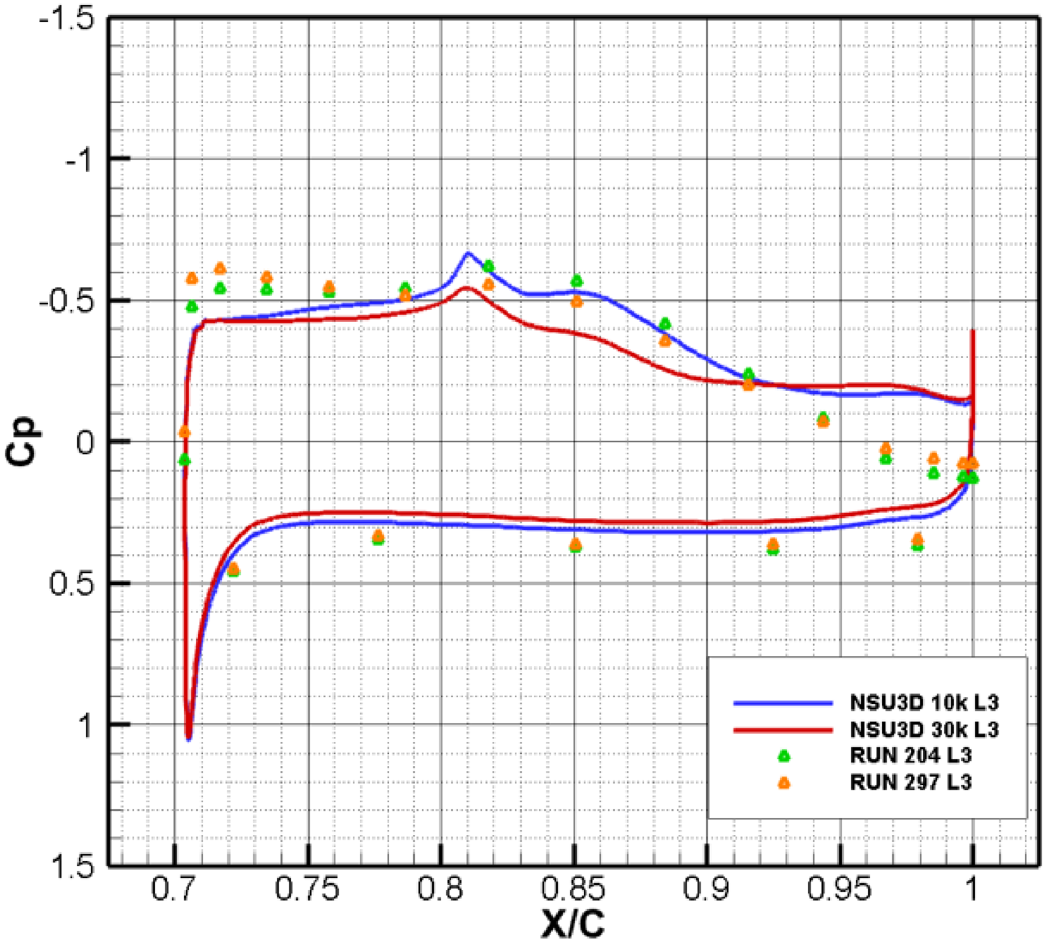

5.3 Computational Results for the Wind Tunnel Model

- To investigate differences further, surface pressure profile comparisons were made pressure port data
- Two wind tunnel runs were conducted at flow conditions close to Mach=0.7, AOA=0
  - The run data was post-processed and provided by ULI associates at Texas A&M

Pressure Profile Comparisons Between Wind Tunnel Tests L3 Pressure Port Data and NSU2D-SA-AFT2 Free Transition N_{crit}=6 Simulation

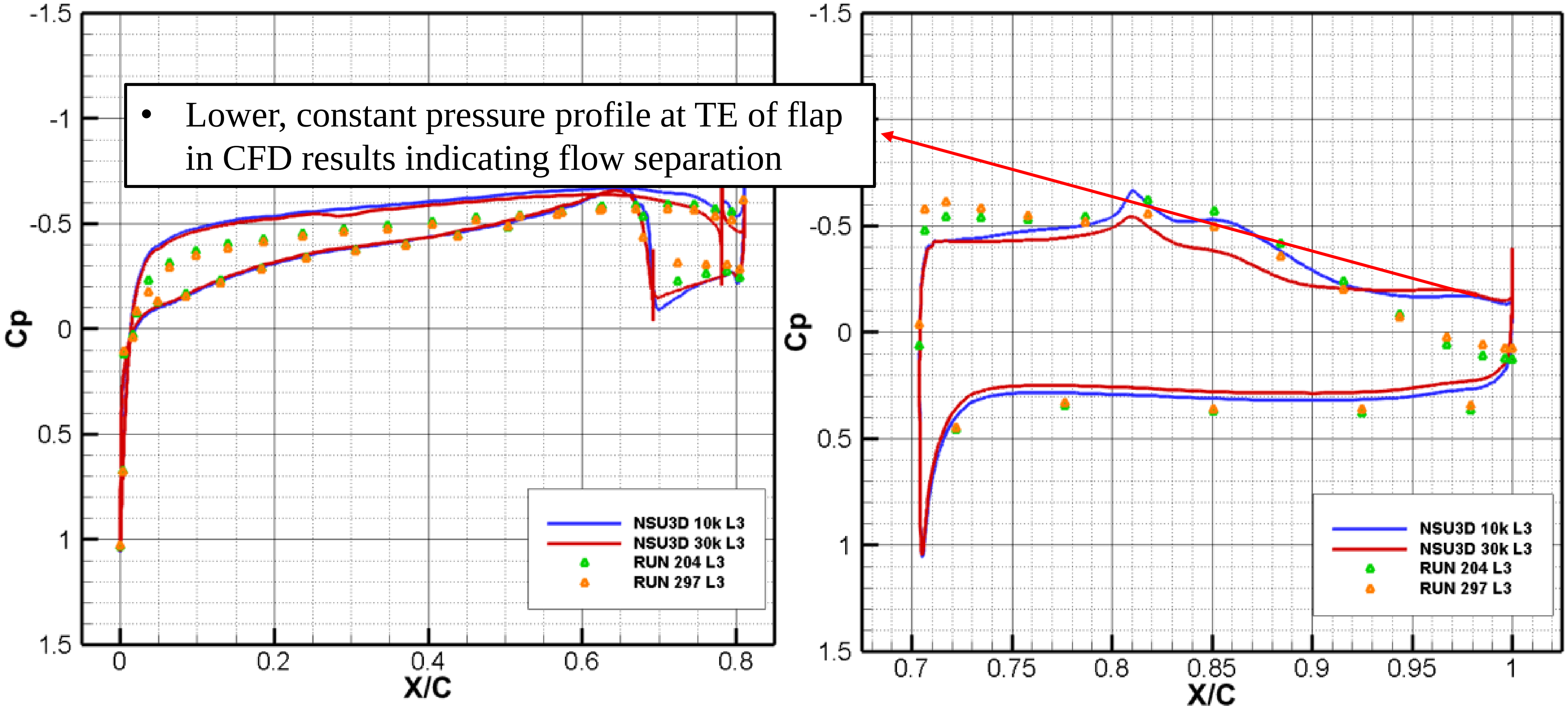

- Lower, constant pressure profile at TE of flap in CFD results indicating flow separation

5.3 Computational Results for the Wind Tunnel Model

- Additional runs were made for an N_{crit}=8.4 prior to the N_{crit}=6.0 simulation

Lift Coefficient Convergence History for N_{crit}=8.4 Wind Tunnel Model Simulations

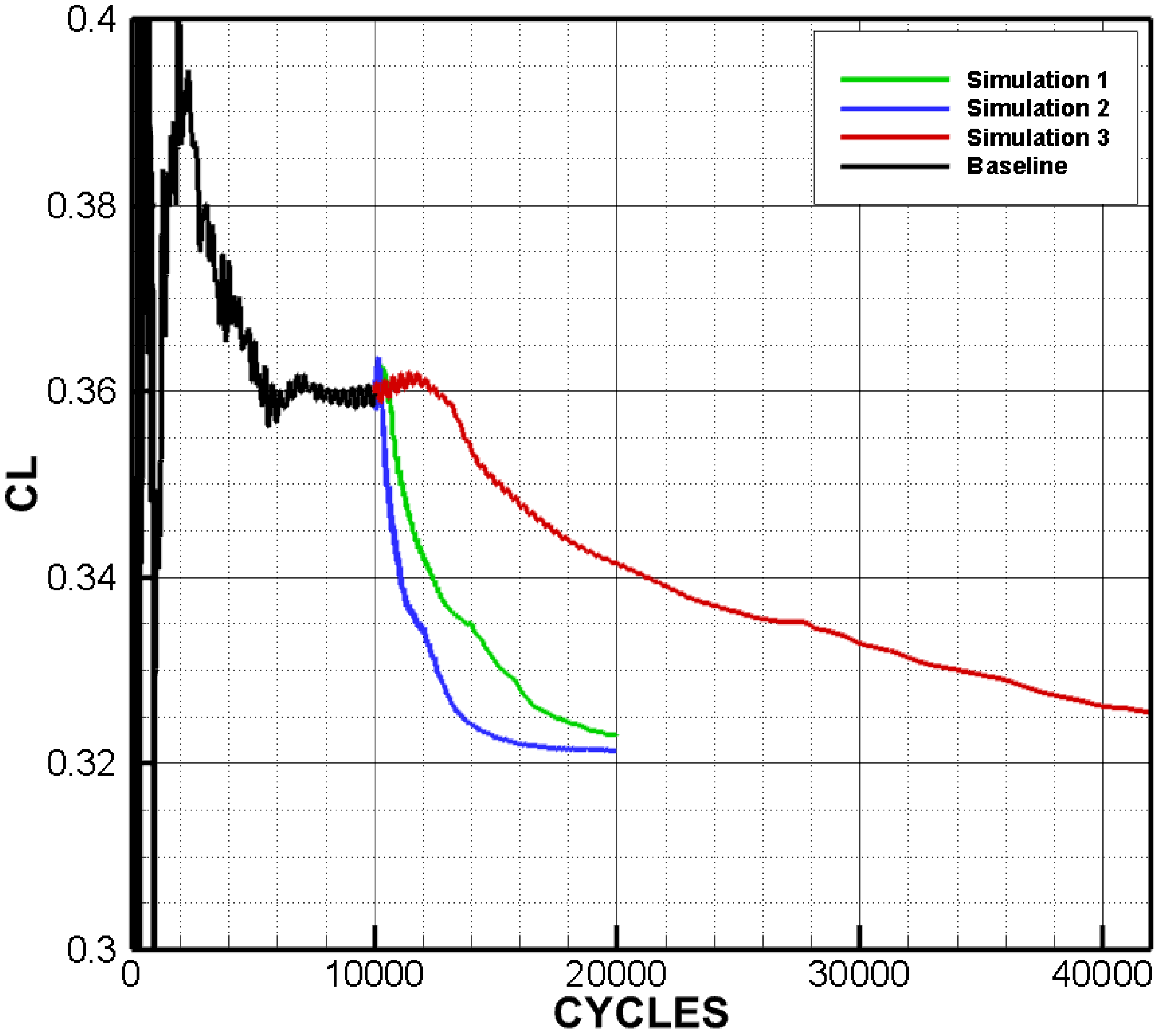

N_{crit}=8.4 Simulations Summary

Case	CFL	Initial Condition	Total Cycles	CL	CD
Baseline	2	Freestream	10000	0.4260	0.02947
Simulation 1	10	Baseline	10000	0.3230	0.02715
Simulation 2	25	Baseline	10000	0.3214	0.02731
Simulation 3	2	Baseline	32000	0.3254	0.02696

- Lift coefficients are roughly 0.32, in agreement with the N_{crit}=6.0
- Transition lines behave in a similar way to the N_{crit}=6.0 simulation

6. Conclusions

Conclusions

- Computational analysis of the S207 SNLF airfoil in two dimensions was successful in reproducing anticipated performance as set forth in the original S207 airfoil design report

Conclusions

- Computational analysis of the S207 SNLF airfoil in two dimensions was successful in reproducing anticipated performance as set forth in the original S207 airfoil design report

- Computed lift coefficient and drag coefficient values were in proximity of the low-drag bucket for the S207 airfoil, and slightly lower than its upper limit

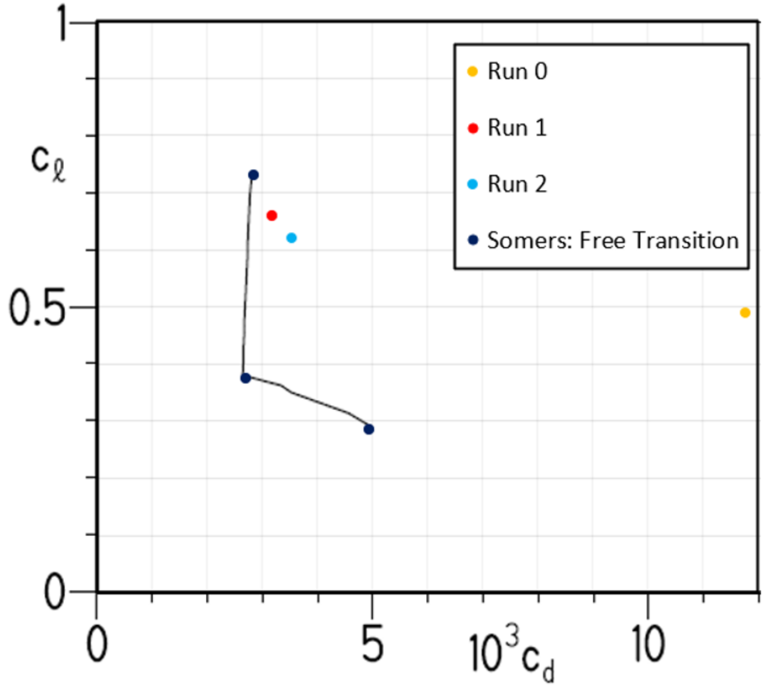

Conclusions

- Computational analysis of the S207 SNLF airfoil in two dimensions was successful in reproducing anticipated performance as set forth in the original S207 airfoil design report

- Computed lift coefficient and drag coefficient values were in proximity of the low-drag bucket for the S207 airfoil, and slightly lower than its upper limit

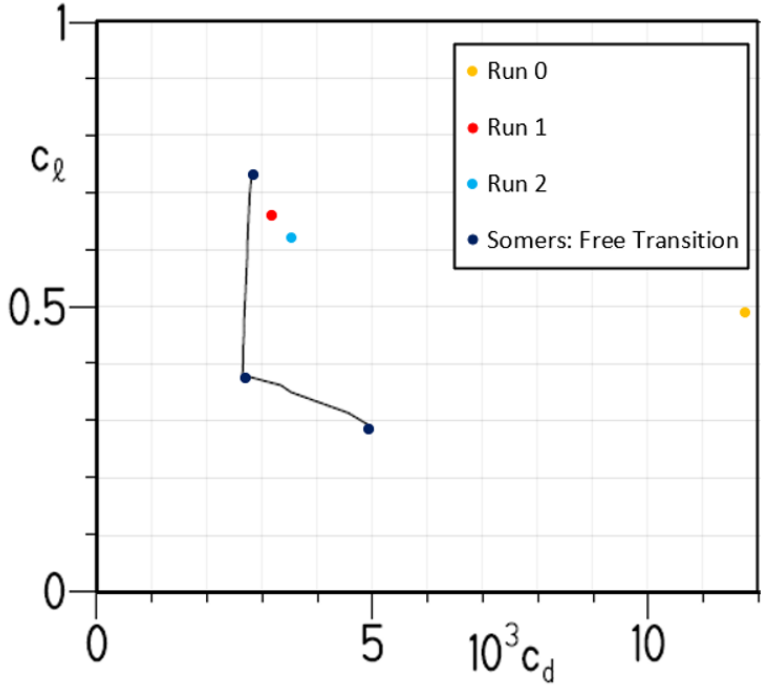

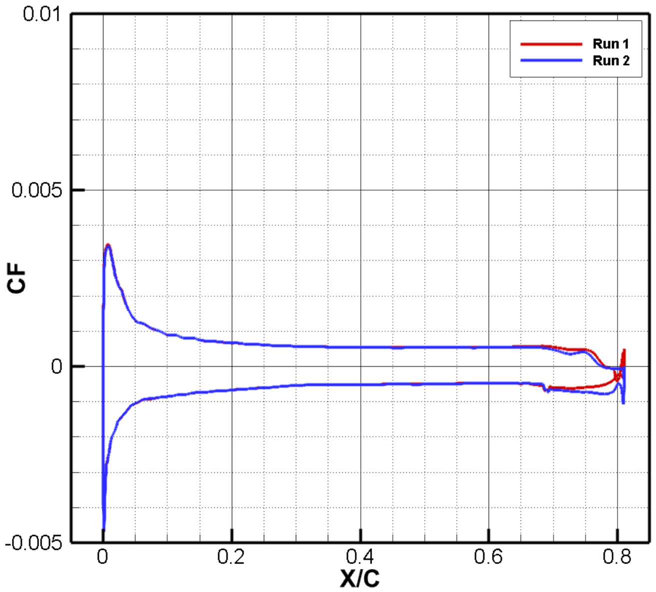

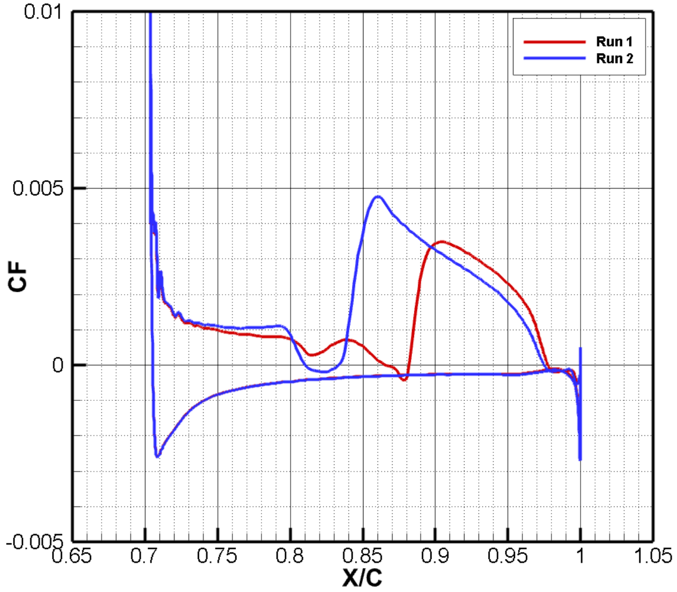

- Extent of laminar flow was identified to be up to 84% to 88% the chord length
    - Turbulence isolated to upper surface of aft element

Conclusions

- A sensitivity study computed using the fully turbulent flow assumption showed flap displacements should be less than 0.1% chord length to prevent sever impact to airfoil performance
  - Performance trend can be assumed to apply with the use of free transition as well

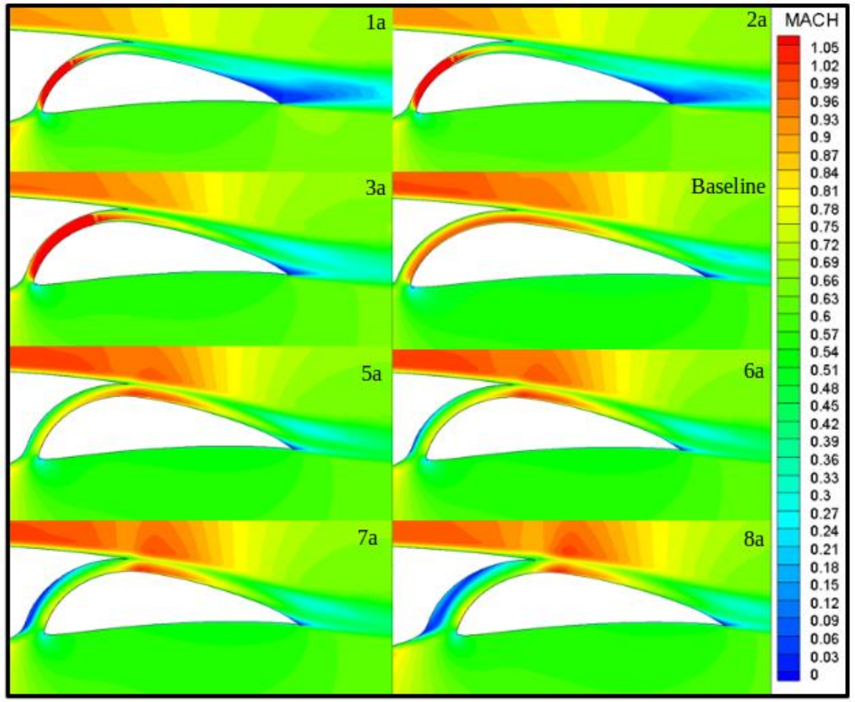

Conclusions

- A sensitivity study computed using the fully turbulent flow assumption showed flap displacements should be less than 0.1% chord length to prevent sever impact to airfoil performance
  - Performance trend can be assumed to apply with the use of free transition as well

- Results helped inform why the shockwave observed in 3D configuration 1 was forming
- Differences in Configuration 1 and 2 were within the range of 0.1% chord displacements

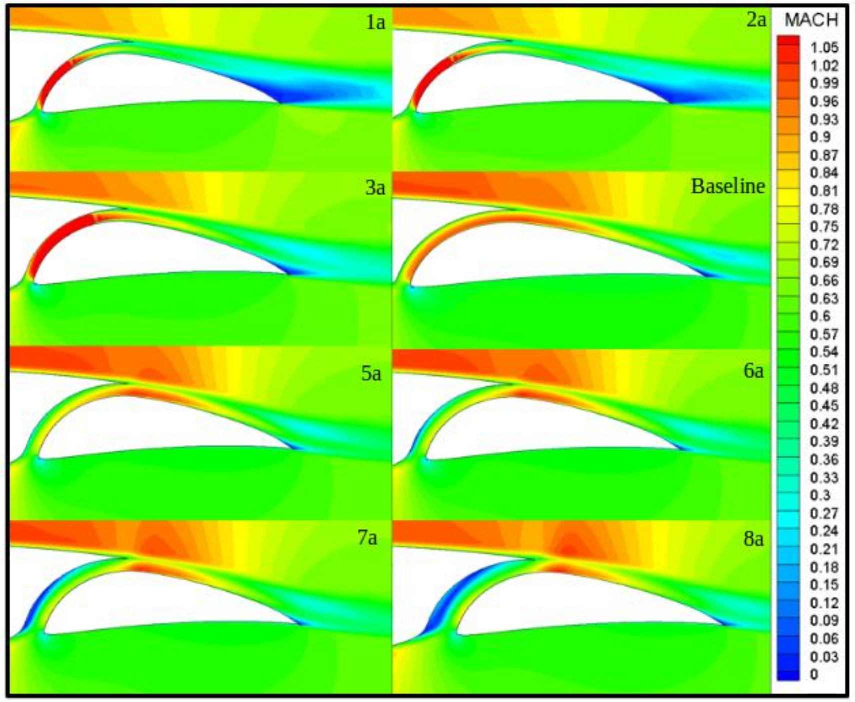

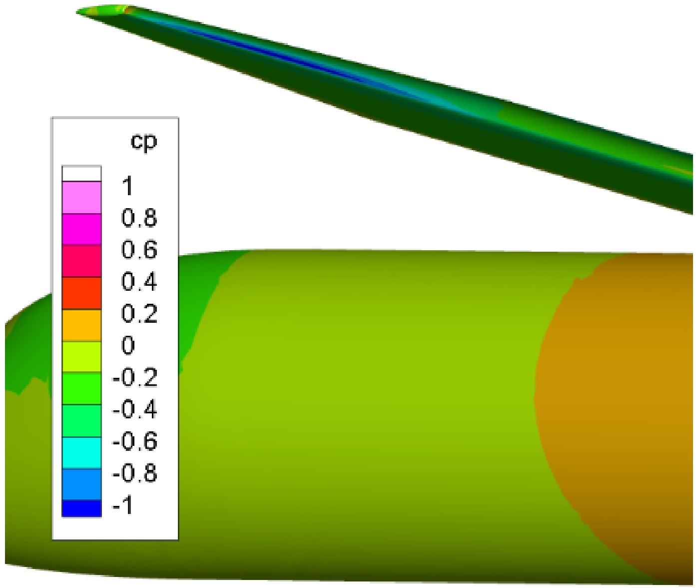

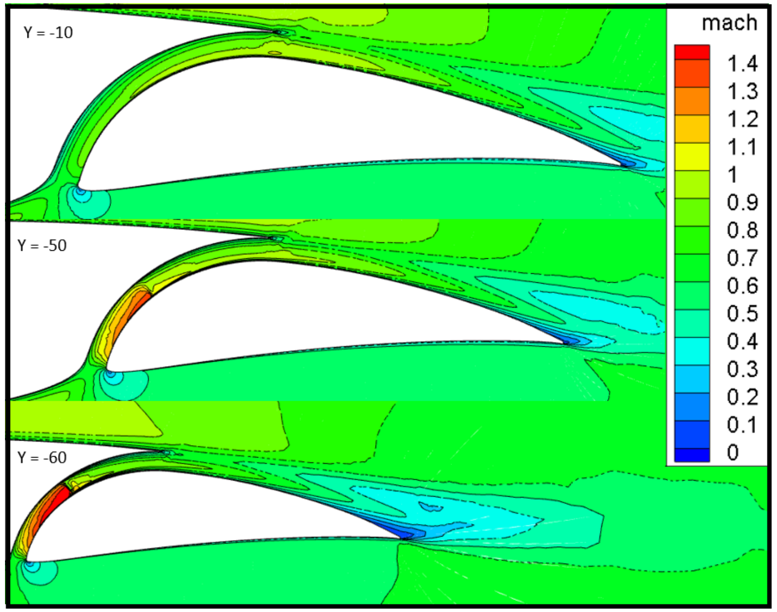

Conclusions

- Results for the final configuration using the AFT2 model showed that some design metrics were met in 3D

Conclusions

- Results for the final configuration using the AFT2 model showed that some design metrics were met in 3D

- Laminar flow observed for angles of attack between -2 and 1 degrees
- Spanwise lift coefficients fall within low-drag bucket limits of the S207 airfoil

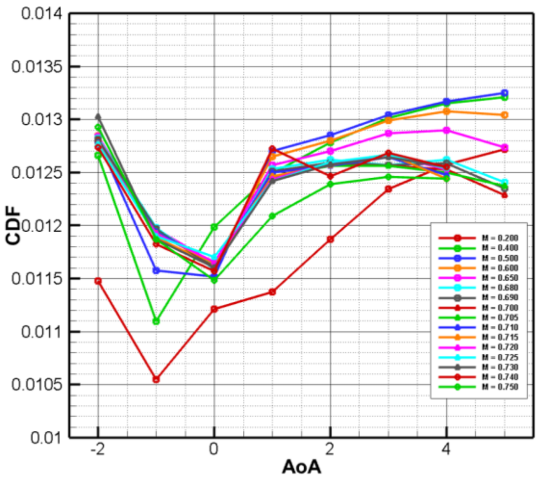

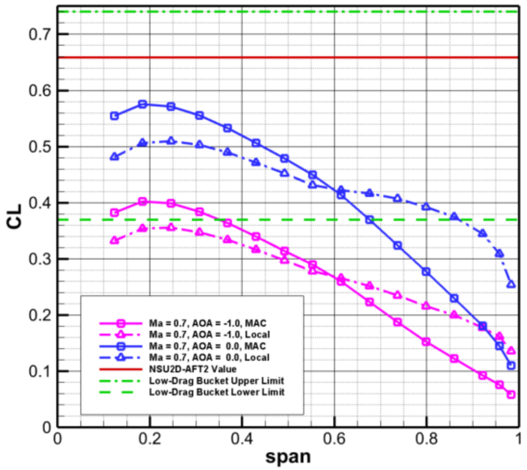

Conclusions

- Results for the final configuration using the AFT2 model showed that some design metrics were met in 3D

- Laminar flow observed for angles of attack between -2 and 1 degrees
- Spanwise lift coefficients fall within low-drag bucket limits of the S207 airfoil

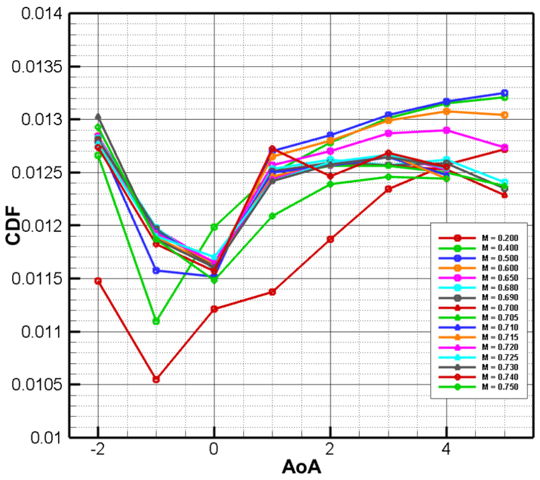

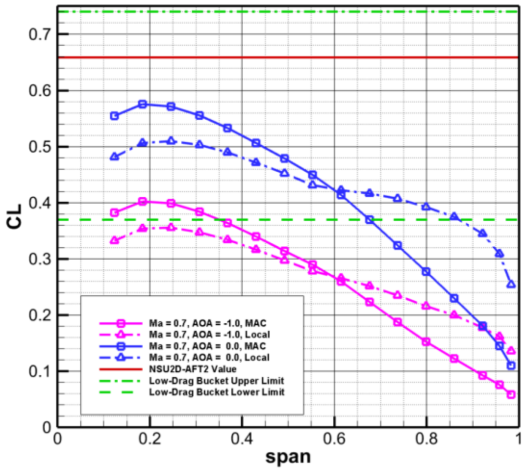

- Fully turbulent sectional surface pressure profiles compared to the 2D surface pressure profiles revealed some lack of agreement between 2D and 3D results

- Understanding of where these discrepancies originate is still being developed
  - Three-dimensional effects likely play a role
  - Geometric changes or optimization process are still viable for increasing performance of swept SNLF wings

Conclusions

- Results for the final configuration using the AFT2 model showed that some design metrics were met in 3D

- Laminar flow observed for angles of attack between -2 and 1 degrees
- Spanwise lift coefficients fall within low-drag bucket limits of the S207 airfoil

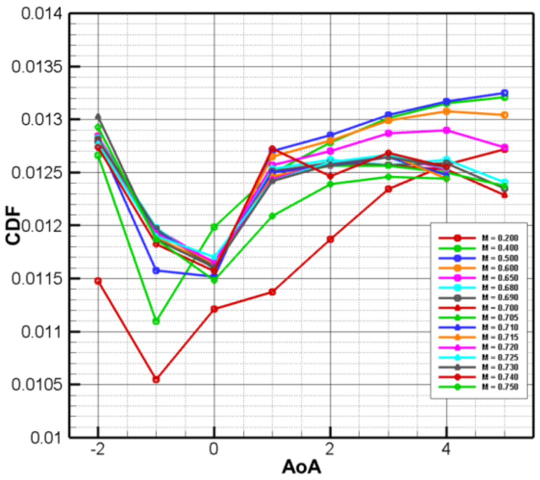

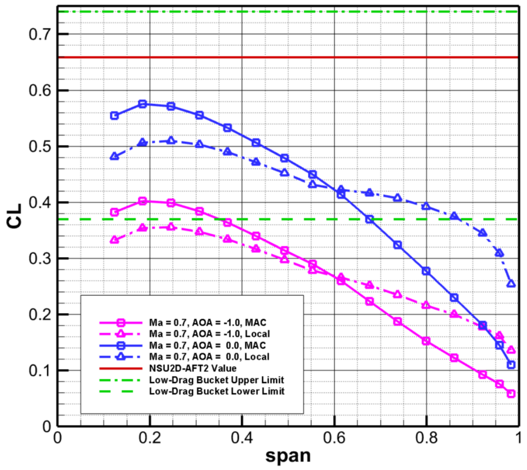

- Fully turbulent sectional surface pressure profiles compared to the 2D surface pressure profiles revealed some lack of agreement between 2D and 3D results

- Understanding of where these discrepancies originate is still being developed
  - Three-dimensional effects likely play a role
  - Geometric changes or optimization process are still viable for increasing performance of swept SNLF wings

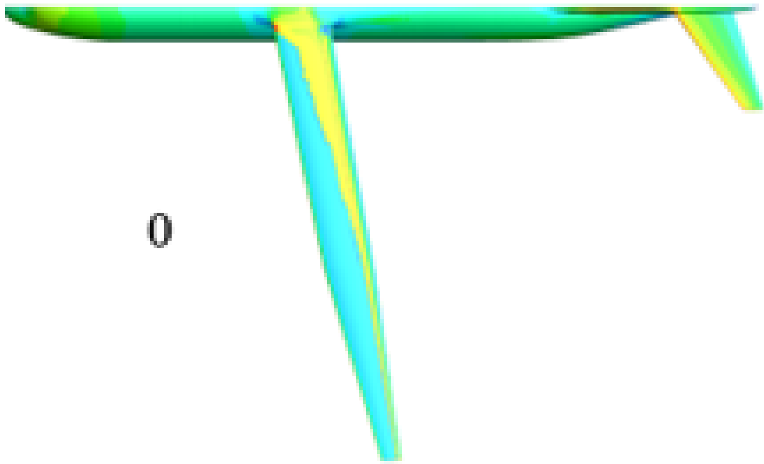

- Configuration suffers from a poorly designed fairing, producing regions of separation that may be bleeding onto the wing

Section 5

- Simulations conducted in support of wind tunnel tests conducted at NASA Ames resulted in notable differences between computational and experimental results

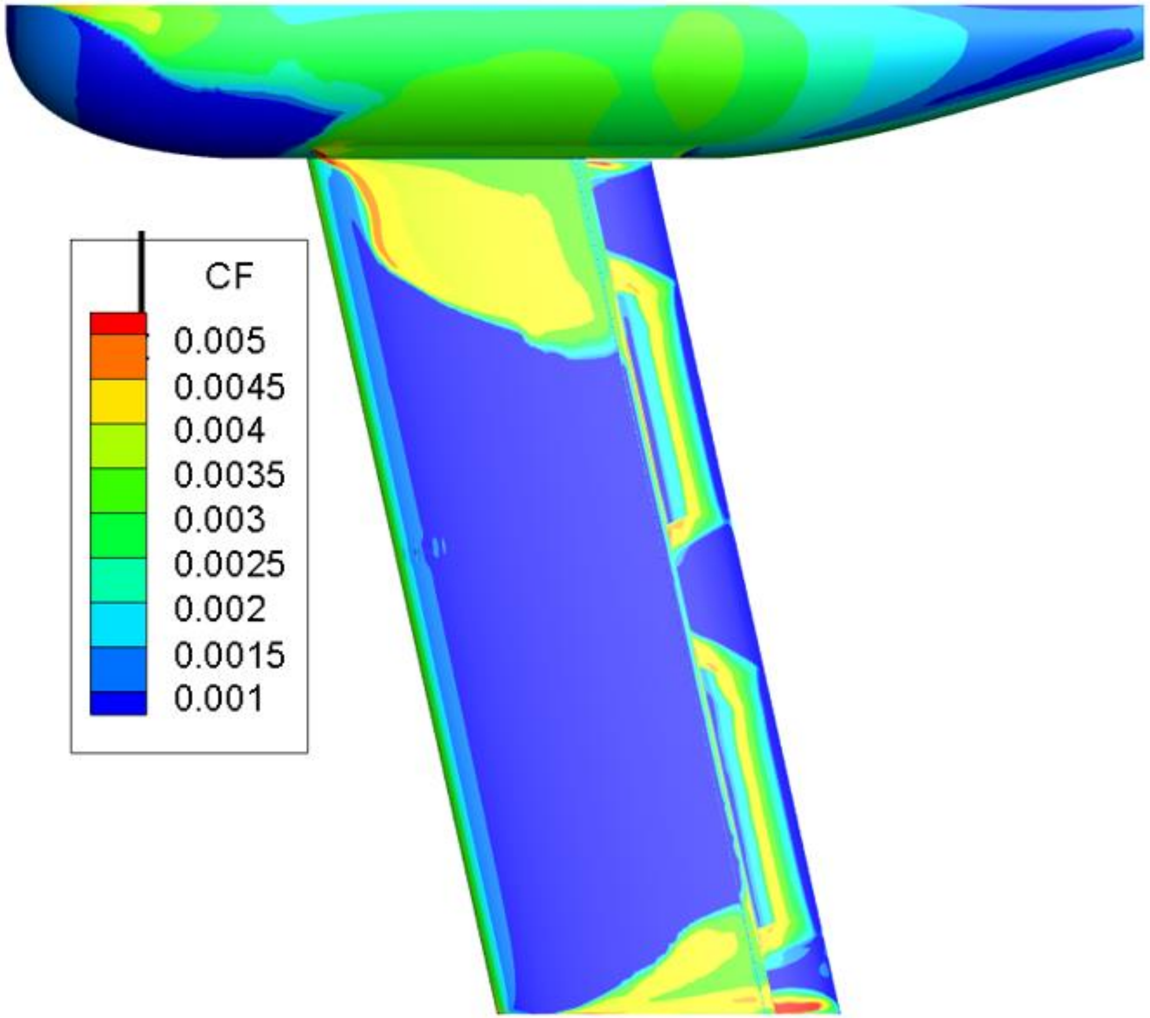

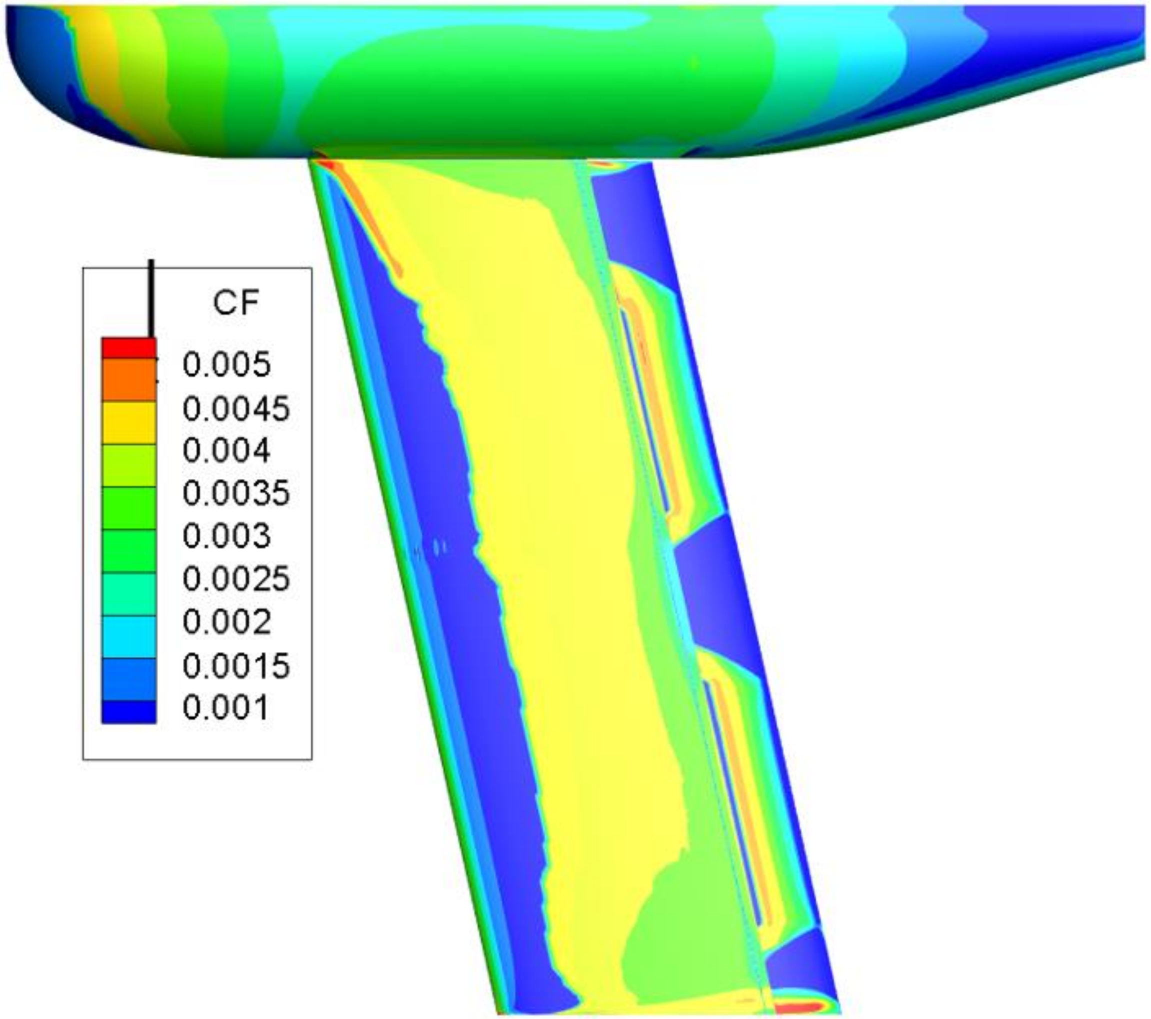

Section 5

- Simulations conducted in support of wind tunnel tests conducted at NASA Ames resulted in notable differences between computational and experimental results

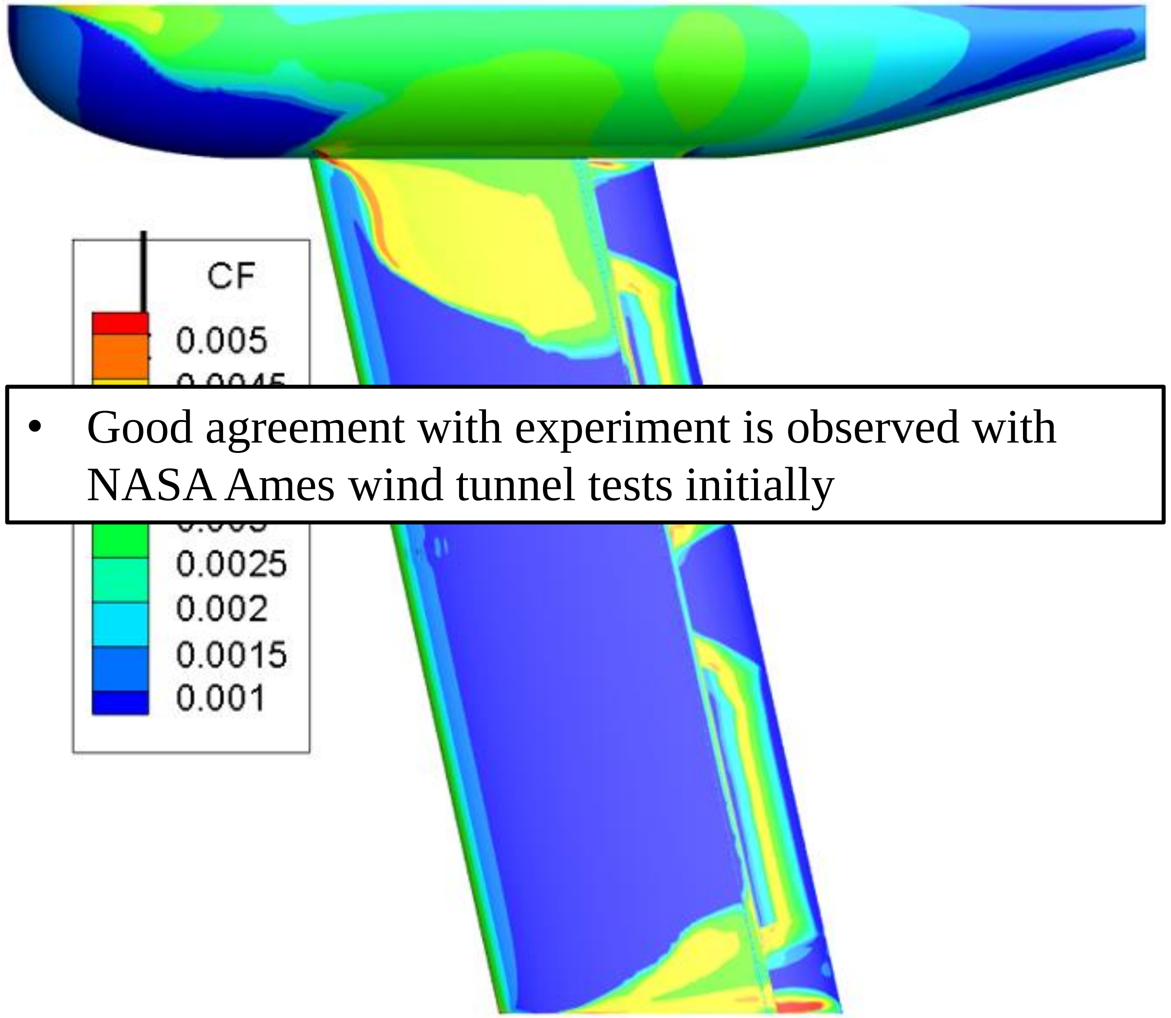

- Good agreement with experiment is observed with NASA Ames wind tunnel tests initially

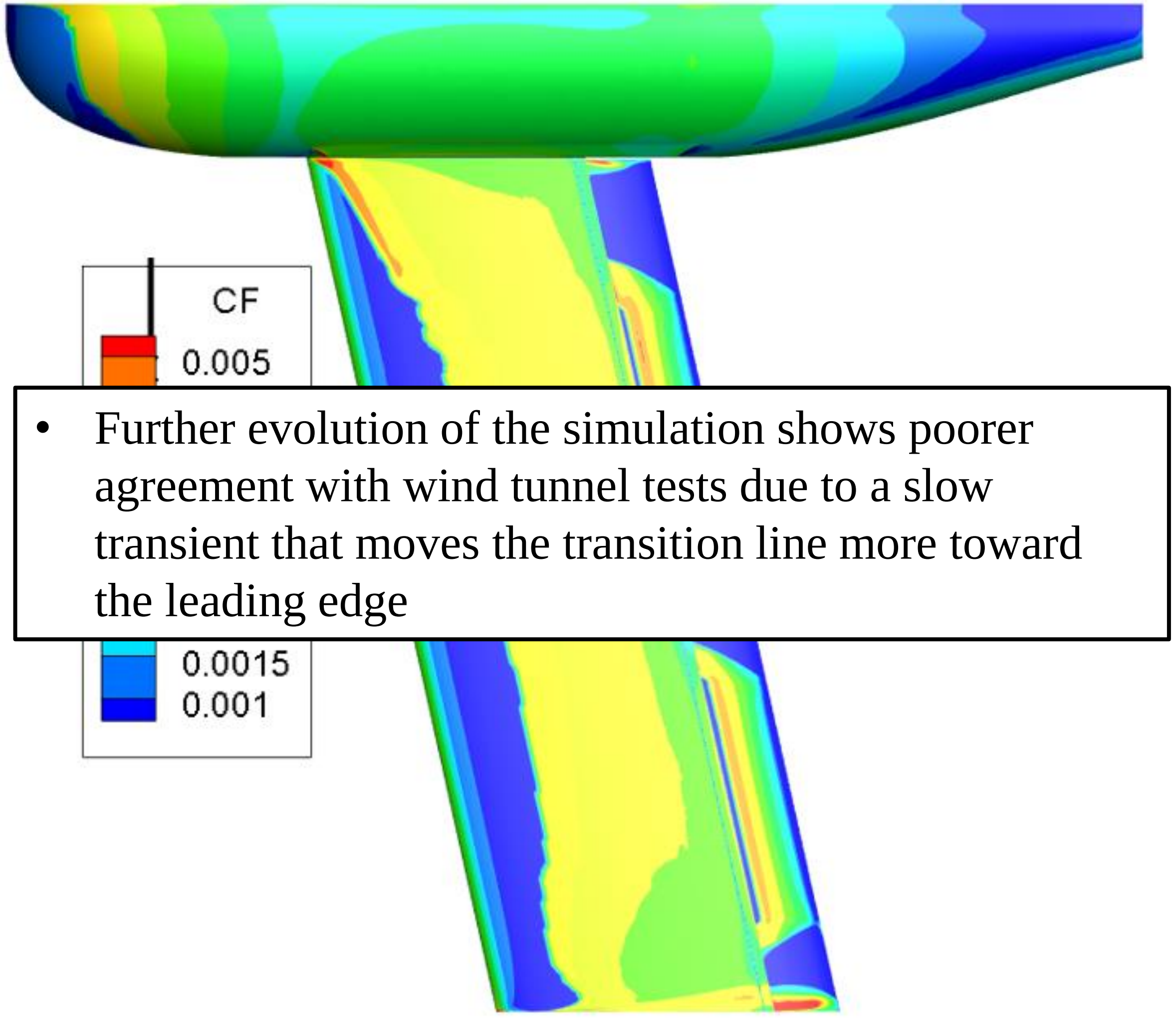

- Further evolution of the simulation shows poorer agreement with wind tunnel tests due to a slow transient that moves the transition line more toward the leading edge

Additional Conclusions: Value of CFD

- Benefits of using a CFD approach for the analysis of SNLF technology has been demonstrated both in 2D and 3D. Solutions can be generated using a fully turbulent flow modeling and free transition flow modeling and then compared to precisely quantify the benefits of laminar flow

Additional Conclusions: Value of CFD

- Benefits of using a CFD approach for the analysis of SNLF technology has been demonstrated both in 2D and 3D. Solutions can be generated using a fully turbulent flow modeling and free transition flow modeling and then compared to precisely quantify the benefits of laminar flow

- This was shown for the S207 airfoil geometry in 2D through plotting of the fully turbulent and free transitional results to original design data, and through comparison of fully turbulent and free transitional results generated for each iteration of the SNLF TTBW configuration

Additional Conclusions: Value of CFD

- Benefits of using a CFD approach for the analysis of SNLF technology has been demonstrated both in 2D and 3D. Solutions can be generated using a fully turbulent flow modeling and free transition flow modeling and then compared to precisely quantify the benefits of laminar flow

- This was shown for the S207 airfoil geometry in 2D through plotting of the fully turbulent and free transitional results to original design data, and through comparison of fully turbulent and free transitional results generated for each iteration of the SNLF TTBW configuration

- Impact of laminar flow can be further explored through application of free transition modeling to specific surfaces as shown with initial results for configuration 3

Additional Conclusions: Value of CFD

- Benefits of using a CFD approach for the analysis of SNLF technology has been demonstrated both in 2D and 3D. Solutions can be generated using a fully turbulent flow modeling and free transition flow modeling and then compared to precisely quantify the benefits of laminar flow

- This was shown for the S207 airfoil geometry in 2D through plotting of the fully turbulent and free transitional results to original design data, and through comparison of fully turbulent and free transitional results generated for each iteration of the SNLF TTBW configuration

- Impact of laminar flow can be further explored through application of free transition modeling to specific surfaces as shown with initial results for configuration 3

- Demonstrated with the initial polars developed at Mach = 0.7273 for the final SNLF TTBW configuration

Additional Conclusions: Value of CFD

- Benefits of using a CFD approach for the analysis of SNLF technology has been demonstrated both in 2D and 3D. Solutions can be generated using a fully turbulent flow modeling and free transition flow modeling and then compared to precisely quantify the benefits of laminar flow

- This was shown for the S207 airfoil geometry in 2D through plotting of the fully turbulent and free transitional results to original design data, and through comparison of fully turbulent and free transitional results generated for each iteration of the SNLF TTBW configuration

- Impact of laminar flow can be further explored through application of free transition modeling to specific surfaces as shown with initial results for configuration 3

- Demonstrated with the initial polars developed at Mach = 0.7273 for the final SNLF TTBW configuration

- Fully turbulent modeling has shown value in gaining insight to performance trends without having to consider convergence difficulties and computational time associated with transition prediction modeling

Work Moving Forward

- Redesign of the wing-junction fairing on the SNLF TTBW configuration and subsequent reevaluation

Work Moving Forward

- Redesign of the wing-junction fairing on the SNLF TTBW configuration and subsequent reevaluation

- Further investigation of disagreement between 2d and 3D results is necessary
  - Further geometric changes
  - Optimization processes

Work Moving Forward

- Redesign of the wing-junction fairing on the SNLF TTBW configuration and subsequent reevaluation

- Further investigation of disagreement between 2d and 3D results is necessary
  - Further geometric changes
  - Optimization processes

- Improvement on the computational solvers
  - Consideration of crossflow instabilities
  - Methodology for more rapid convergence of transition prediction model
    - Slow transients and incomplete convergence make it difficult to assess if observed differences in data are geometry or convergence based

Work Moving Forward

- Redesign of the wing-junction fairing on the SNLF TTBW configuration and subsequent reevaluation

- Further investigation of disagreement between 2d and 3D results is necessary
  - Further geometric changes
  - Optimization processes

- Improvement on the computational solvers
  - Consideration of crossflow instabilities
  - Methodology for more rapid convergence of transition prediction model
    - Slow transients and incomplete convergence make it difficult to assess if observed differences in data are geometry or convergence based

- Further grid study is needed, such as streamwise, spanwise, and boundary layer resolutions
  - Boundary layer resolution needs to be revaluated because laminar boundary layers are thinner so typical gridding practices may not suffice

Previous Publications

C. Perkins, Z. Yang, I. Topcuoglu, D. Mavriplis, J. Coder, E. Hereth, and C. Axten, "Aerodynamic Analysis of a Slotted, Natural-Laminar-Flow Transonic Trussed-Braced Wing Aircraft Configuration," AIAA Paper 2022-2536, 2021 AIAA SciTech Forum, Jan 3rd-7th, San Diego, CA.

References

1) International Energy Agency, "CO2 Emmissions From Fuel Combustion: Highlights," 2017.
2) S. Gossling and A. Humpe, "The Global Scale, Distribution and Growth of Aviation: Implications for Climate Change," Global Environmental Change, vol. 65, 2021.
3) O. Boucher, A. Borella, T. Gasser, and D. Hauglustaine, "On the Contribution of Global Aviation to the CO2 Radiative Forcing of Climate," Atmospheric Environment, vol. 267, 2018.
4) NASA Aeronautics, "Strategic Implementation Plan: 2019 Update," 2019.
5) D. Somers, "Laminar Flow Airfoil," US Patent 6905092 B2, June 14, 2005.
6) S. Gudmundsson, "Aircraft Drag Analysis," in General Aviation Aircraft Design, pp. 661–760, Butterworth-Heinemann, 2014.
7) D. Somers, "An Exploratory Investigation of a Slotted, Natural-Laminar-Flow Airfoil," NASA/CR-2012-217560, July, 2012.
8) J. Coder and D. Somers, "Design of a Slotted, Natural-Laminar-Flow Airfoil for Commercial Transport Applications," Aerospace Science and Technology, vol. 106, Nov. 2020.
9) A.M.O. Smith, "High-Lift Aerodynamics," Journal of Aircraft, vol. 12, no. 6.
10) D. Somers, "Design of a Slotted, Natural-Laminar-Flow Airfoil for Transport Aircraft," NASA/CR-2019-220403, June, 2019.

References

11) M. Bradley and C. Droney, “Subsonic Ultra Green Aircraft Research Phase 2: N+4 Advanced Concept Development,” NASA/CR-20120217556, May, 2012.
12) J. Coder, “Advanced Aerodynamic Design Center for ultra-Efficient Commercial Vehicles: ARMD Strategic Thrust: Ultra-Efficient Commercial Vehicles (Thrust 3A),” Presented at the University Leadership Initiative Annual Review, Sep., 2021.
13) P. Camacho, K. Pham, L. Chou, N Harrison and A. Khodadoust, “Progress on Aero-dynamic Performance Analysis of SNLF Transonic Truss-Braced Wing,” AIAA Paper 2020-1025, 2020 AIAA SciTech Forum, Jan. 6-10, Orlando, FL.
14) F.R. Menter, P.E. Smirnov, and T. Liu, “A One-Equation Local Correlation-Based Transition Model,” Flow, Turbulence and Combustion, vol. 95, pp. 583–619, July 2015.
15) F. Menter, R. Langtry and S. Volker, “Transition Modelling for General Purpose CFD,” Flow, Turbulence and Combustion, vol. 77, no. 1, pp. 202–277, Nov. 2006.
16) R. Nichols, “Addition of a Local Correlation-Based Boundary Layer Transition model to the CREATETM-AV Kestrel Unstructured Flow Solver,” 2019. AIAA Paper 2019-1343, 2019 AIAA SciTech Forum, Jan. 7-11, San Diego, CA.
17) J. Coder, “Further Development of the Amplification Factor Transport Transition Model for Aerodynamic Flows,” AIAA Paper 2019-0039, 2019 AIAA SciTech Forum, Jan. 7-11, San Diego, CA.
18) L. Mack, “Transition and Laminar Instability,” 1977. NASA CR-153203.
19) Z. Yang and D. Mavriplis, “Implementation of Transition Modeling for Analysis and Optimization of Two-Dimensional Airfoil Problems,” AIAA Paper 2019-0293, 2019 AIAA SciTech Forum, Jan. 7-11, San Diego, CA.

References

20) W. Valarezo and D. Mavriplis, “Navier-Stokes Applications to High-Lift Airfoil Analysis,” Journal of aircraft, vol. 32, no. 3, pp. 618–624, 1995.

21) P. Spalart and S. Allmaras, “A One-Equation Turbulence Model for Aerodynamic Flow,” Recherche Aerospatiale, pp. 5–21, 1994.

22) D. Mavriplis, “An Advancing Front Delaunay Triangulation Algorithm Designed for Robustness,” Journal of Computational Physics, vol. 117, no. 1, pp. 90–101, 1995.

23) K. Mani and D. Mavriplis, “Unstructured Mesh Solution Techniques Using the NSU3D Solver,” 2014. AIAA Paper 2014-0081, 52nd Aerospace Sciences Meeting, January 2014.

24) M. Park, K. Laflin, M. Chaffin, N. Powell and D. Levy, “CFL3D, FUN3D, and NSU3D Contributions to the Fifth Drag Prediction Workshop,” Journal of Aircraft, vol. 51, no. 4, pp. 1268–1283, July 2014.

25) D. Mavriplis, M. Long, T. Lake and M. Langlois, “NSU3D Results for the Second AIAA High lift Prediction Workshop,” Journal of Aircraft, vol. 52, no. 4, pp. 1063–1081, Aug. 2015.

26) D. Mavriplis, Z. Yang and M. Long, “Results Using NSU3D for the First Aeroelastic Prediction Workshop,” AIAA Paper 2013-0786, 51st AIAA Aerospace Sciences Meeting, Jan. 7-10, 2013, Dallas/FT. Worth, TX.

27) D. Mavriplis, Z. Yang, and E. Anderson, “Development of an Analysis and Optimization Tool for Slotted Wing Natural-Laminar-Flow Aircraft,” AIAA Paper 2020-1292, 2020 AIAA SciTech Forum, Jan 6-10, Orlando, FL.

28) D. Somers, “Design of a Slotted, Natural-Laminar-Flow Airfoil for Business Jet Applications,” NASA/CR20120217559, April, 2012.

References

29) R. Petzold and R. Radespiel, “Transition on a Wing with Spanwise Varying Crossflow and Linear Stability Analysis,” AIAA Journal, vol. 53, no. 2, pp. 321–255, Feb. 2015.

30) M. Drela, A User’s Guide to MSES 3.05. MIT Department of Aeronautics and Astronautics.

31) A. Bottai, R. Campbell and M. Jonson, “Vibrations of a High-Aspect Ratio, Two Element Wing,” 2022. AIAA Paper 2022-2537, AIAA SciTech Forum, San Diego, CA., Jan 3-7, 2022.

32) M. Bradley and C. Droney, “Subsonic Ultra Green Aircraft Research: Phase 2. Volume 2; Hybrid Electric Design Exploration,” NASA/CR-2015-218704/Volume II, NASA Langley Research Center, Hampton, VA, April 2015.

33) L. Metkowski and M. Maughmer, “Winglet and Strut Configuration Study for a Slotted, Natural-Laminar-Flow Strut-Braced Transport Aircraft,” AIAA Paper 2021-0843, AIAA Scitech Forum 2021, Virtual event, January 2021

34) K. Risse, F. Schueltke and E. Stumpf, “Conceptual Wing Design Methodology for Aircraft with Hybrid Laminar Flow Control,” AIAA Paper 2014-0023, AIAA SciTech 2014 Forum, Jan. 1014.

35) R. Cummings, W. Mason, S. Morton and D. McDaniel, “Applied Computational Aerodynamics: A Modern Engineering Approach,” 2015. Cambridge Aerospace Series, NewYork NY.

Acknowledgments

- Committee Members: Dimitri Mavriplis, Michael Stoellinger, Bart Geerts
- Dr. Coder and the NASA ULI Vision-Vehicle Integration Subgroup
- Mavriplis CFD Lab Members and Alum: Zhi Yang, Emmett Padway, Ilker Topcuoglu, Andrew Kirby, Soudeh Kamali, Enrico Fabiano, Sung Yoon
- Friends & Family
- University of Wyoming ARCC and the NCAR Wyoming Supercomputer Alliance

- This work is supported by the National Aeronautics and Space Administration (NASA) University Leadership Initiative (ULI) "Advanced Aerodynamics Design Center for Ultra-Efficient Commercial Vehicles" (Award NNX17AJ95A) led by the University of Tennessee at Knoxville

Questions?

3.2 Simulations at Cruise

NSU2S-SA-AFT2 Free Transition Density Residual Convergence Histories for Mach = 0.7, Re = 13.2 Million, AOA= -1.3

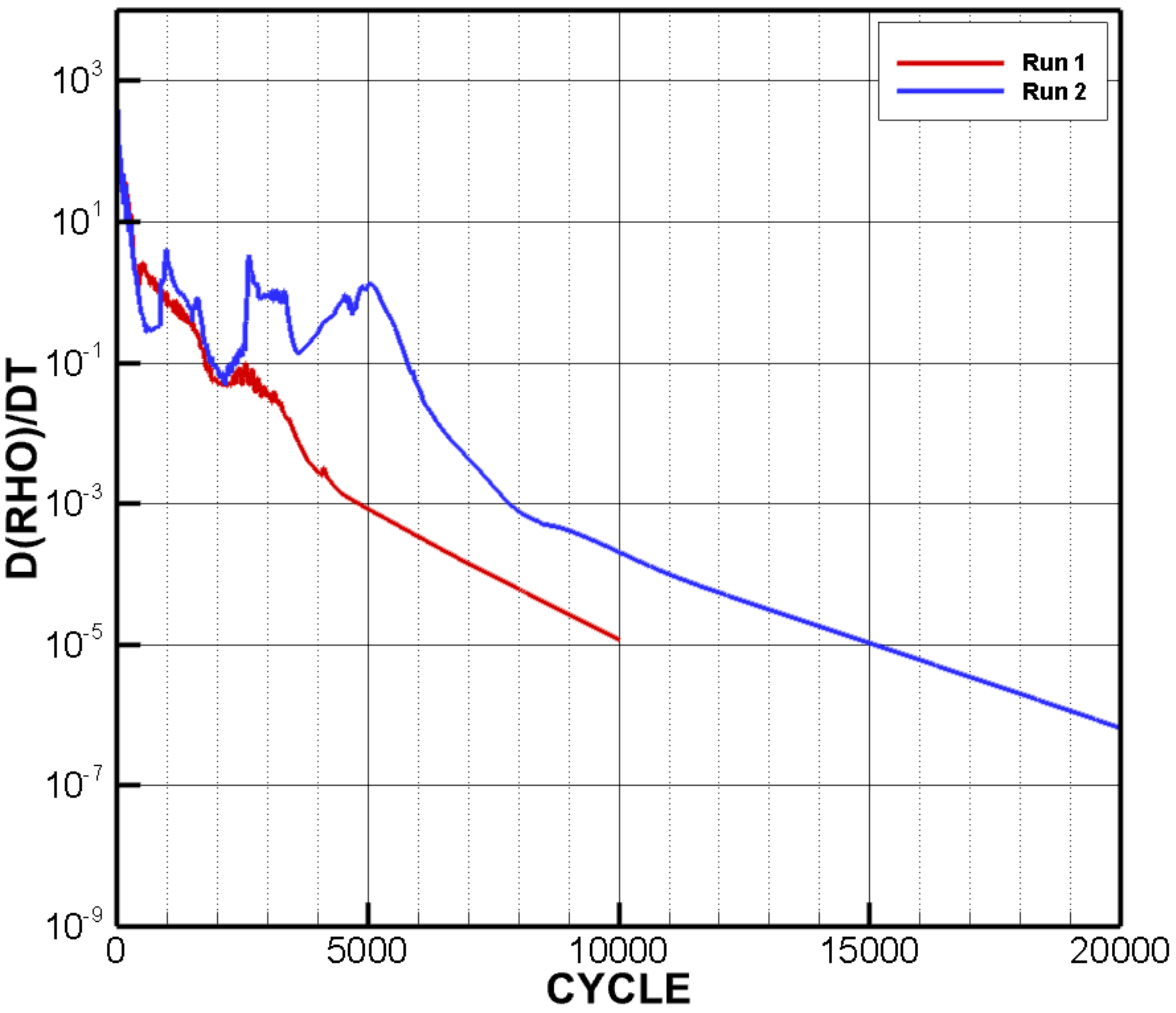

NSU2S-SA-AFT2 Free Transition C_L Convergence Histories for Mach = 0.7, Re = 13.2 Million, AOA= -1.3

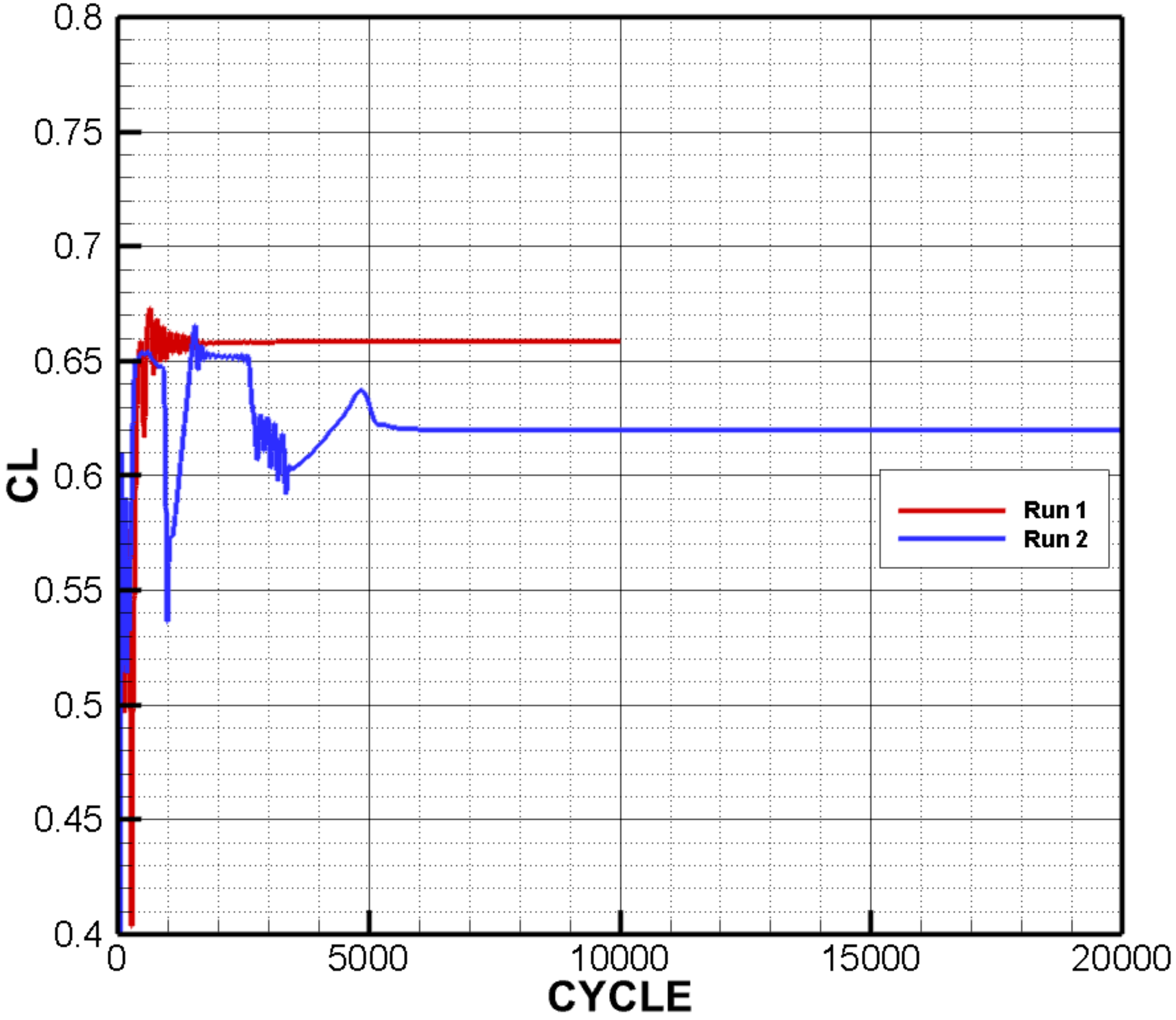

3.2 Simulations at Cruise

- Examination of flow field eddy viscosity provides insight to flow behavior

Run 1 Eddy Visc

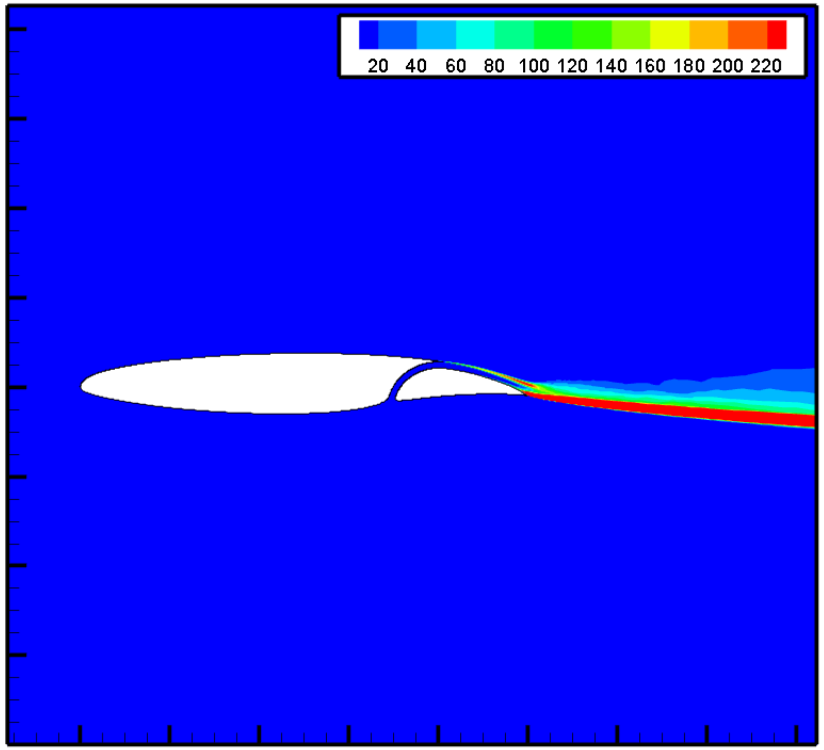

Run 2 Eddy Visc

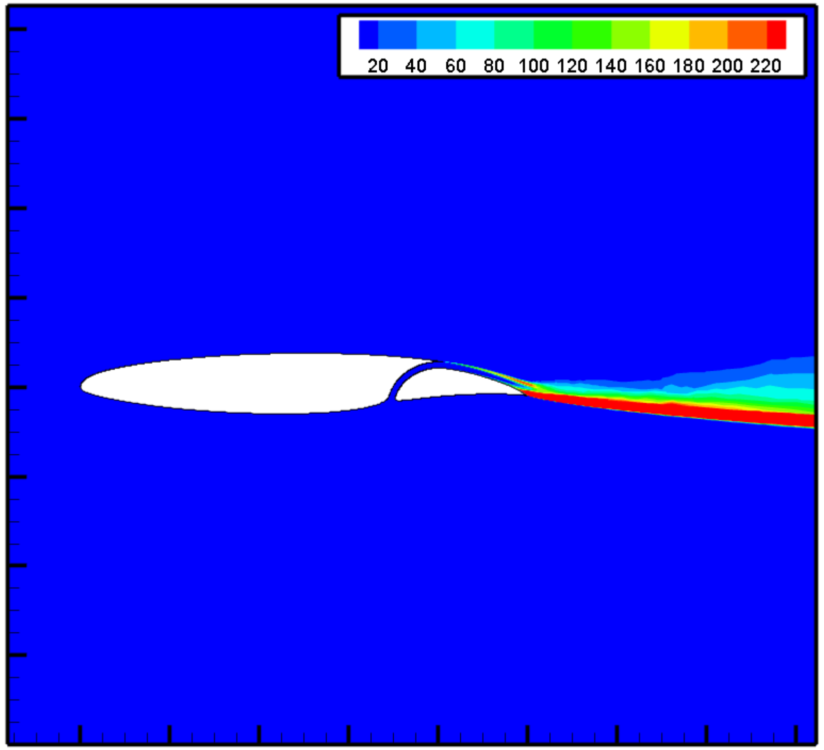

3.2 Simulations at Cruise

- Examination of flow field eddy viscosity provides insight to flow behavior

Run 1 Eddy Visc

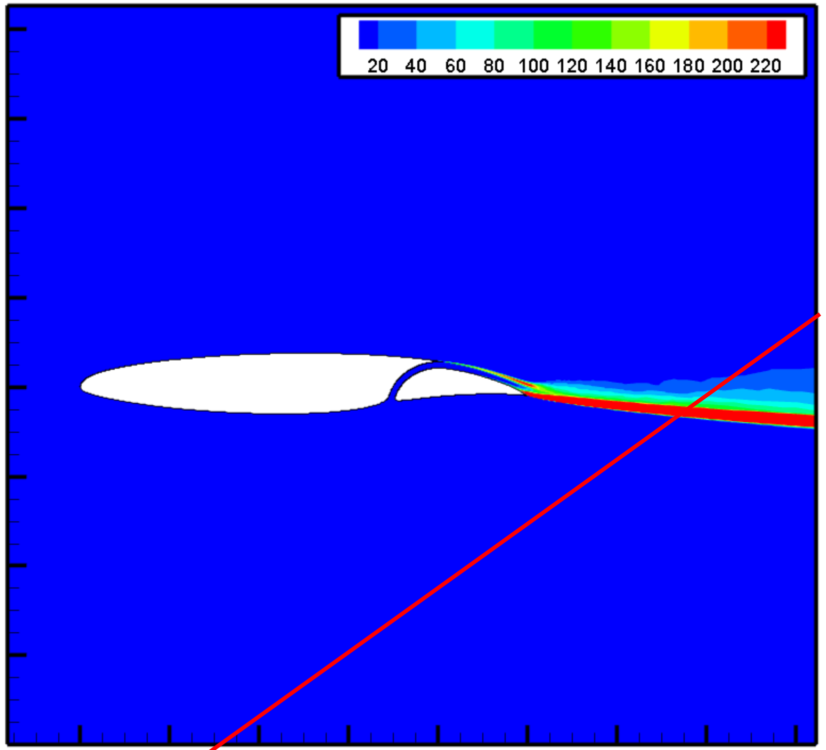

Run 2 Eddy Visc

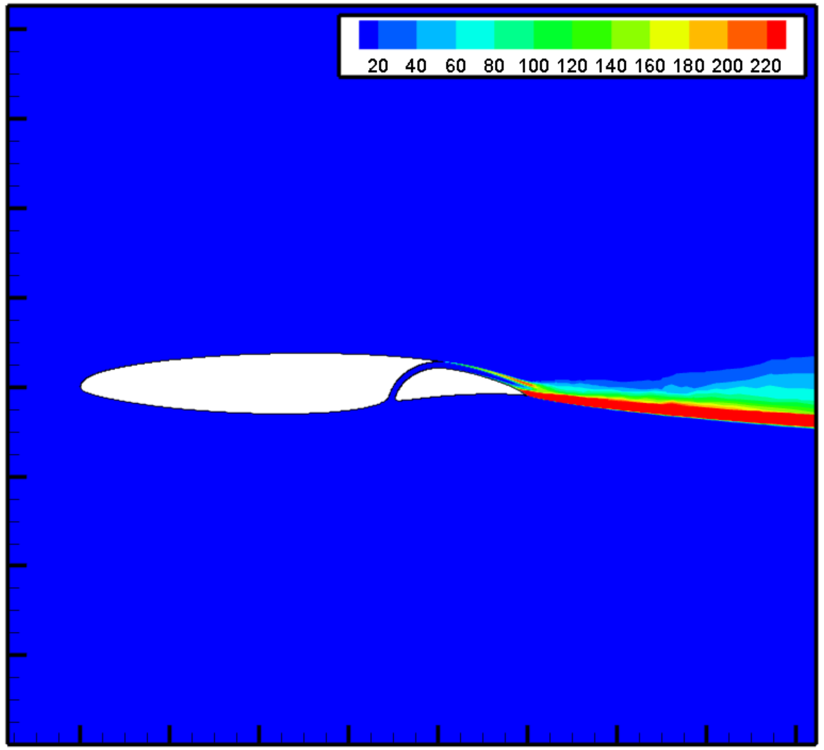

- Eddy viscosity indicates smooth, laminar flow up until the upper surface of the aft element

3.2 Simulations at Cruise

- Examination of flow field Mach numbers provides insight to the presence of discontinuities (shock waves)

Run 1 Mach Contour for Aft Element

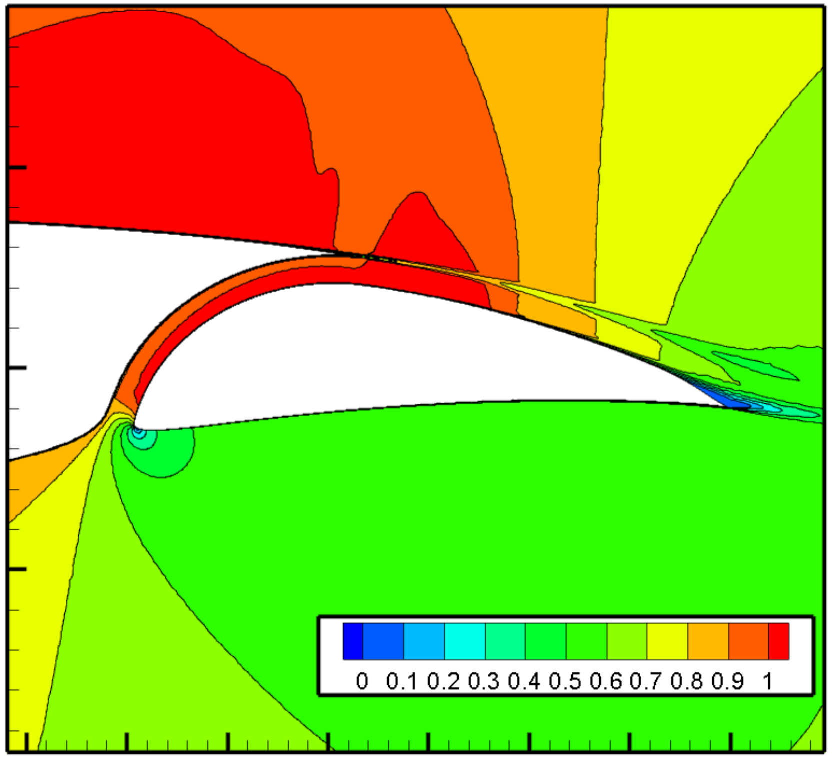

Run 2 Mach Contour for Aft Element

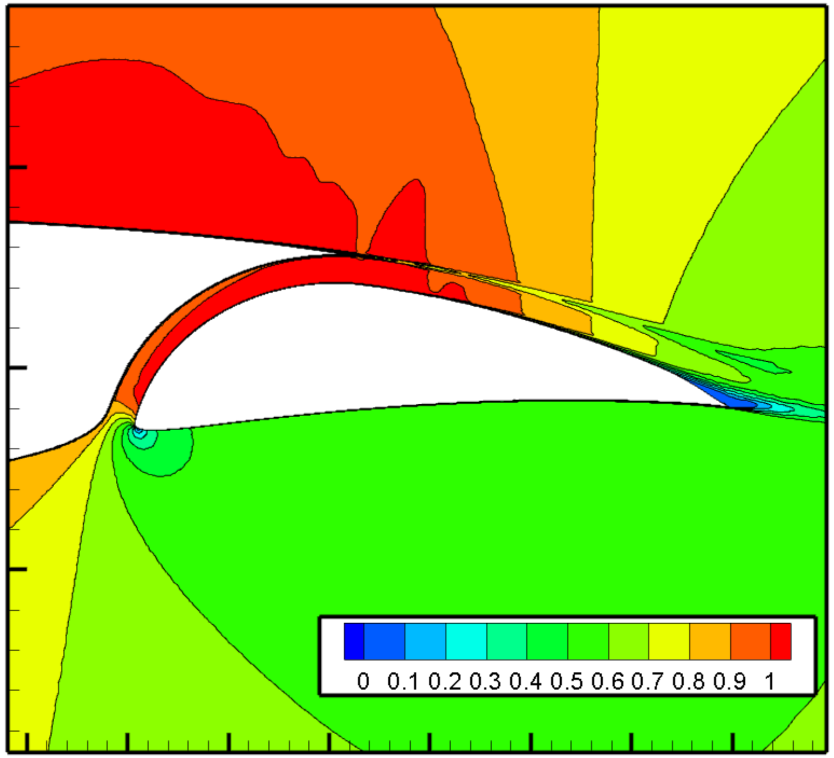

- Eddy viscosity indicates smooth, laminar flow up until the upper surface of the aft element

3.2 Simulations at Cruise

- Examination of flow field Mach numbers provides insight to the presence of discontinuities (shock waves)

Run 1 Mach Contour for Aft Element

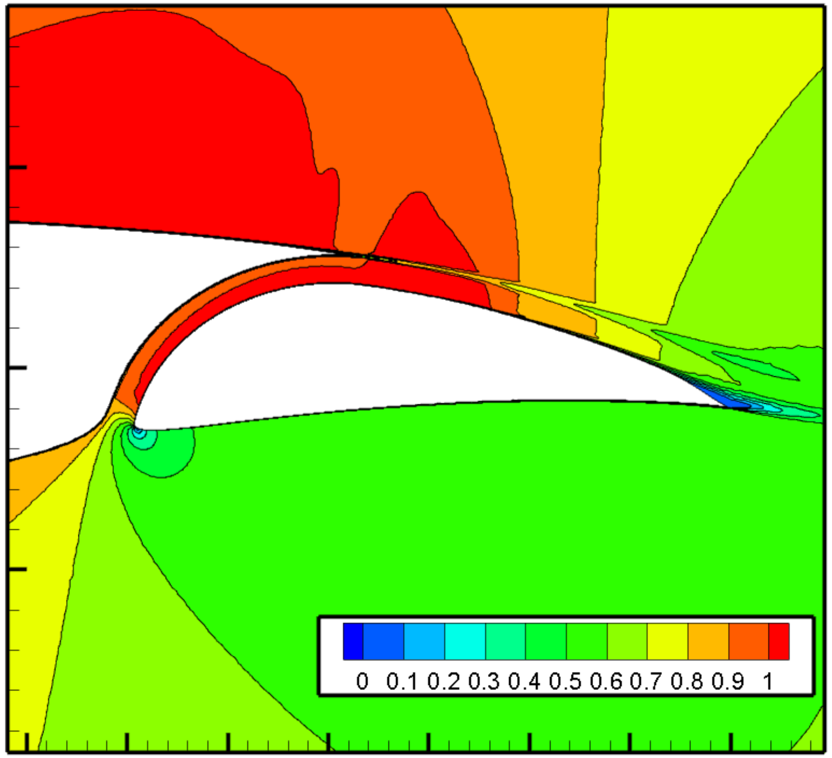

Run 2 Mach Contour for Aft Element

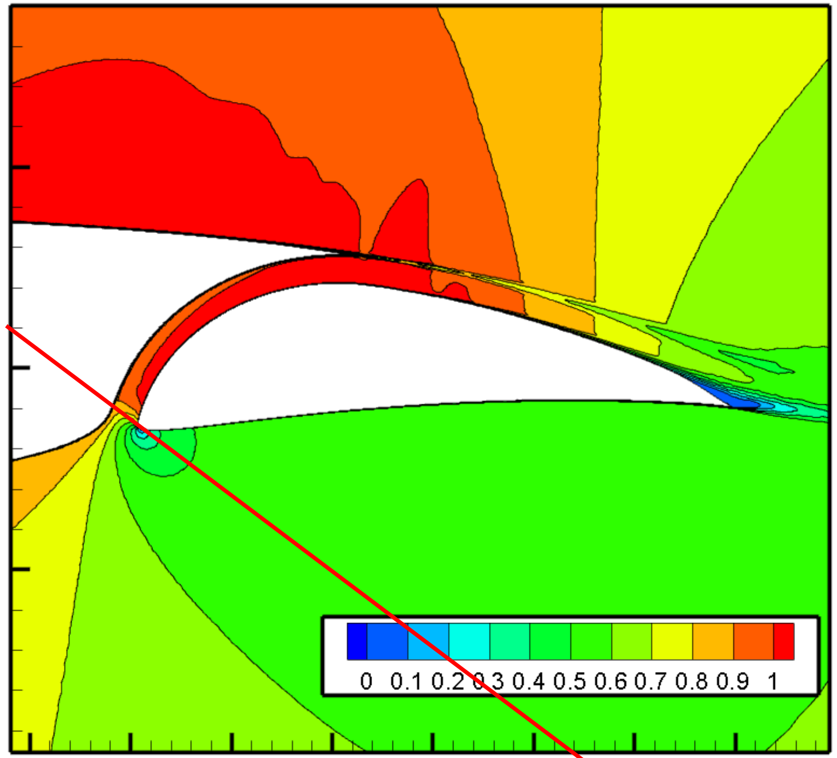

- Eddy viscosity indicates smooth, laminar flow up until the upper surface of the aft element

- Mach number contour distributions indicate that no discontinuities are present to destabilize the BL

3.4 Results for Morphed Leading-Edge Variants

- ULI project members at University of Illinois and UTK explored the application of morphed leading-edges
  - Increase lift and delay stall under circumstances where AOA of attack is high (take off and landing)
  - Compatible with laminar flow, no steps are introduced to the geometry [31]

Derived Morphed LE Variants of the S207

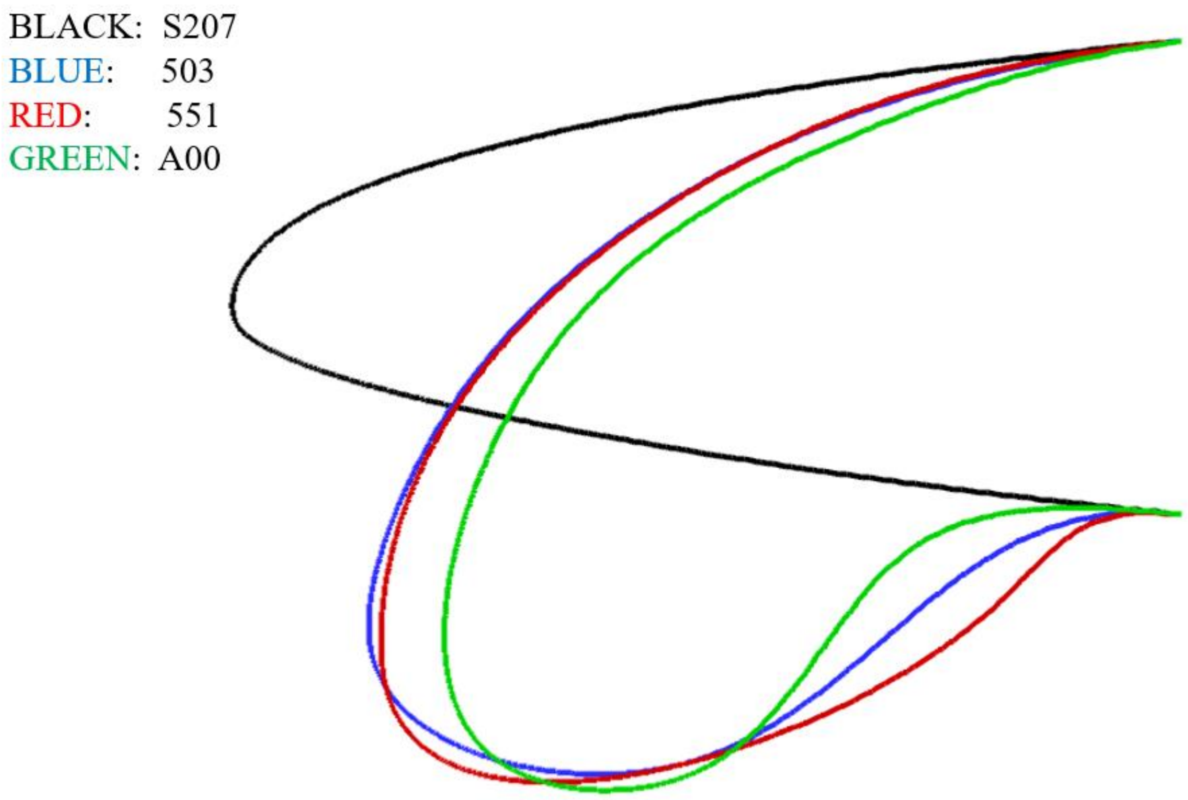

3.4 Results for Morphed Leading-Edge Variants

- ULI project members at University of Illinois and UTK explored the application of morphed leading-edges
  - Increase lift and delay stall under circumstances where AOA of attack is high (take off and landing)
  - Compatible with laminar flow, no steps are introduced to the geometry [31]

Derived Morphed LE Variants of the S207

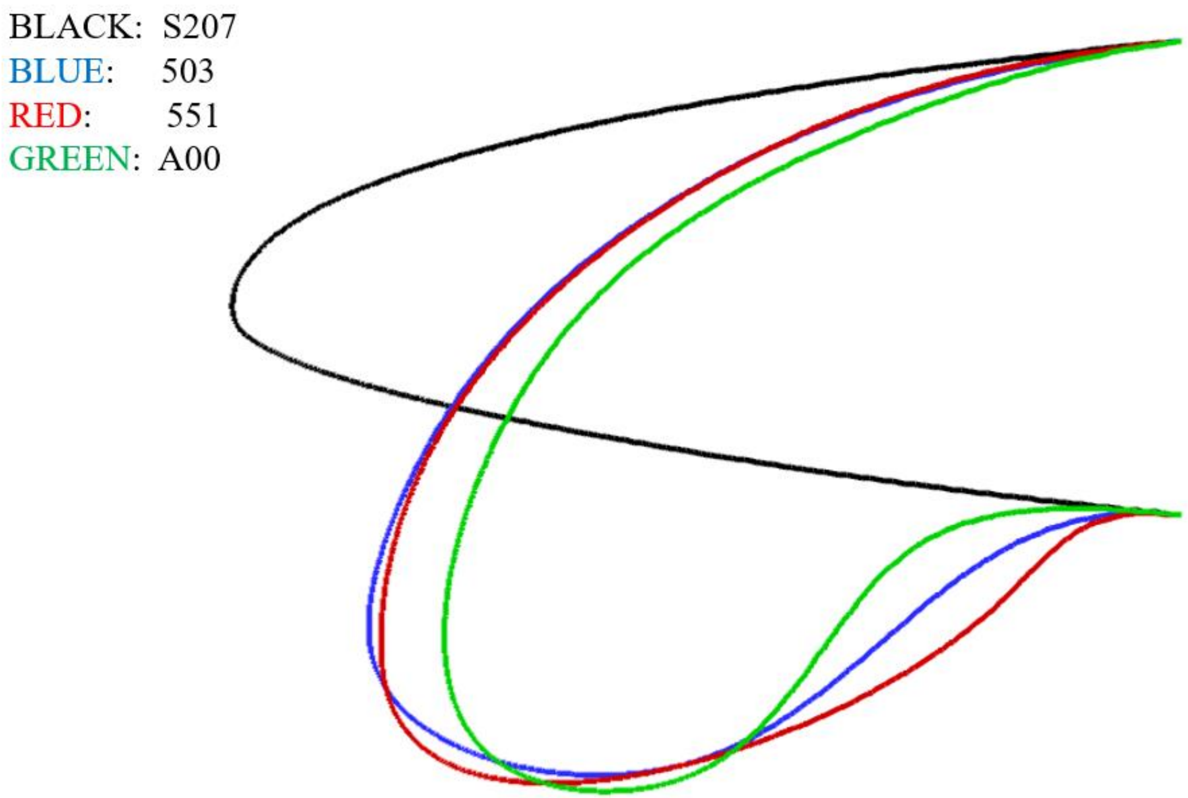

- Derived from a UI-developed genetic algorithm [32]
- Analyzed at UI with MSES [33]
- Performance trends predicted by MSES and observed in the UI wind tunnel are in agreement [34]

- UTK computationally analyzed the variants using OVERFLOW

3.4 Results for Morphed Leading-Edge Variants

- Computational support was provided to both UI and UTK with simulations of the variants using NSU2D

NSU2D-SA Fully Turbulent Lift Curves for Morphed LE S207 Variants at Mach = 0.225, Re = 16 Million

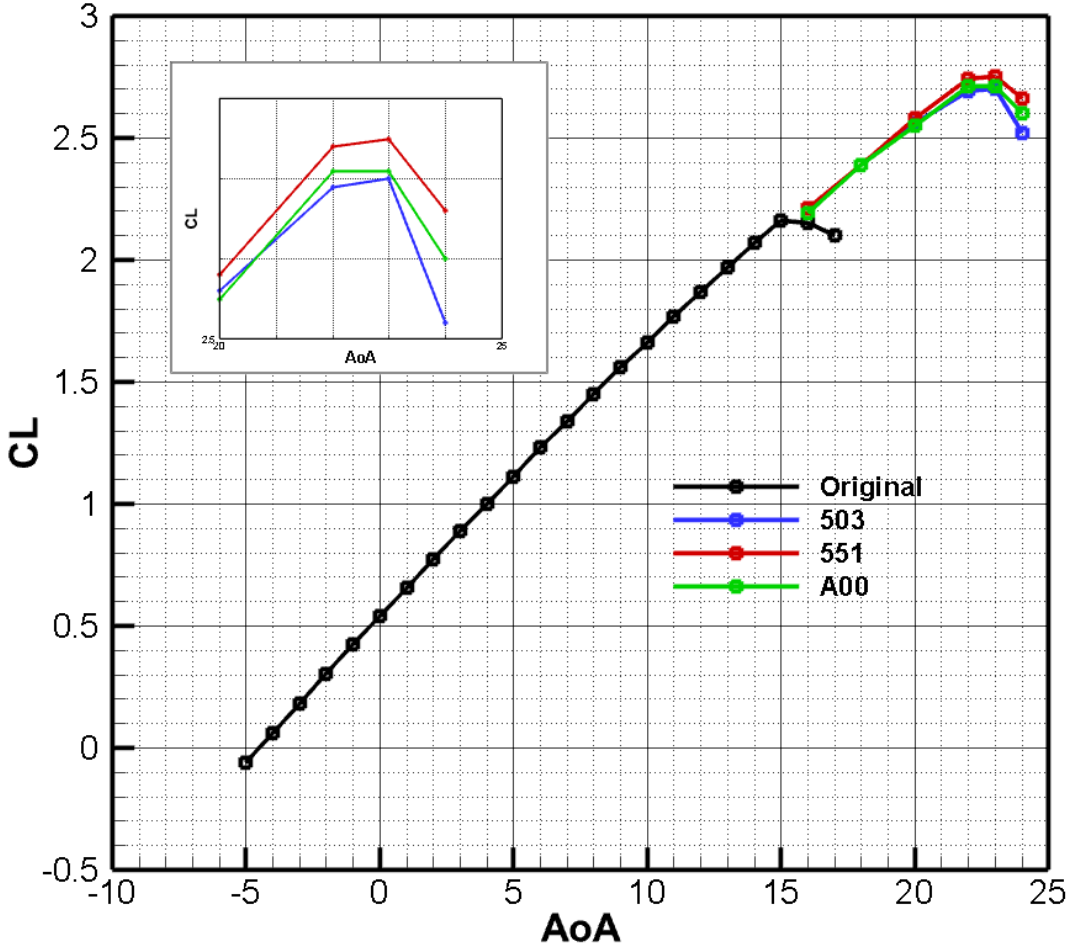

3.4 Results for Morphed Leading-Edge Variants

- Computational support was provided to both UI and UTK with simulations of the variants using NSU2D

NSU2D-SA Fully Turbulent Lift Curves for Morphed LE S207 Variants at Mach = 0.225, Re = 16 Million

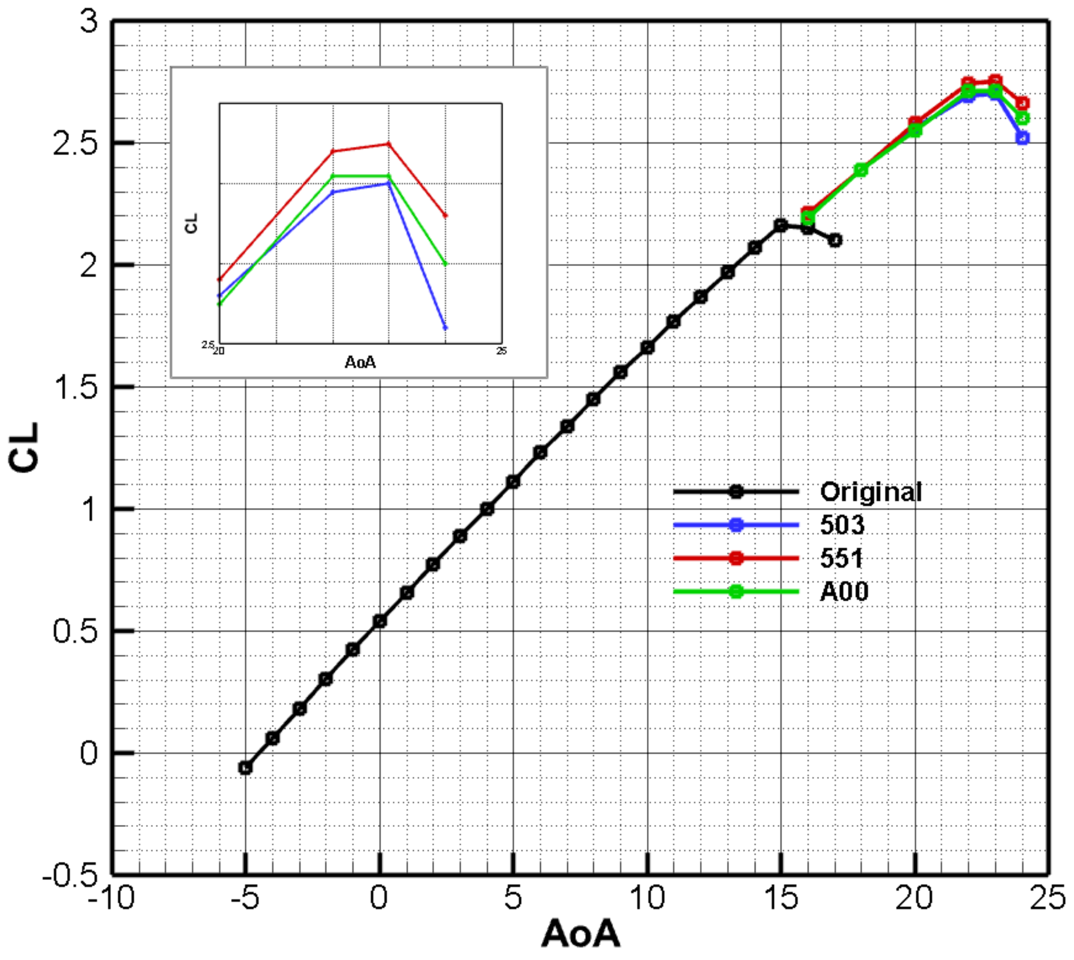

Morphed LE S207 Variants Fully Turbulent Results Comparison between MSES and NSU2D for Mach=0.225, Re=16 Million

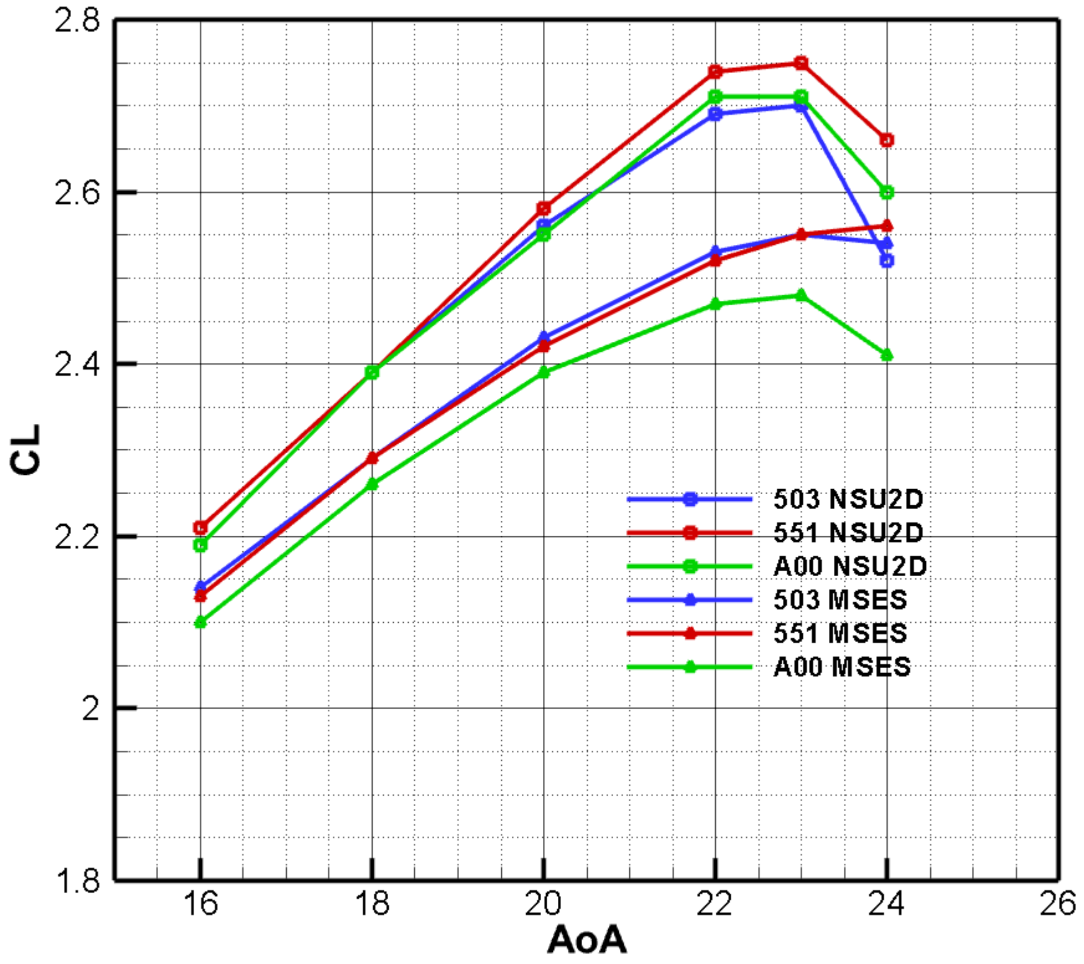

3.4 Results for Morphed Leading-Edge Variants

- Computational support was provided to both UI and UTK with simulations of the variants using NSU2D

NSU2D-SA Fully Turbulent Lift Curves for Morphed LE S207 Variants at Mach = 0.180, Re = 1.4 Million

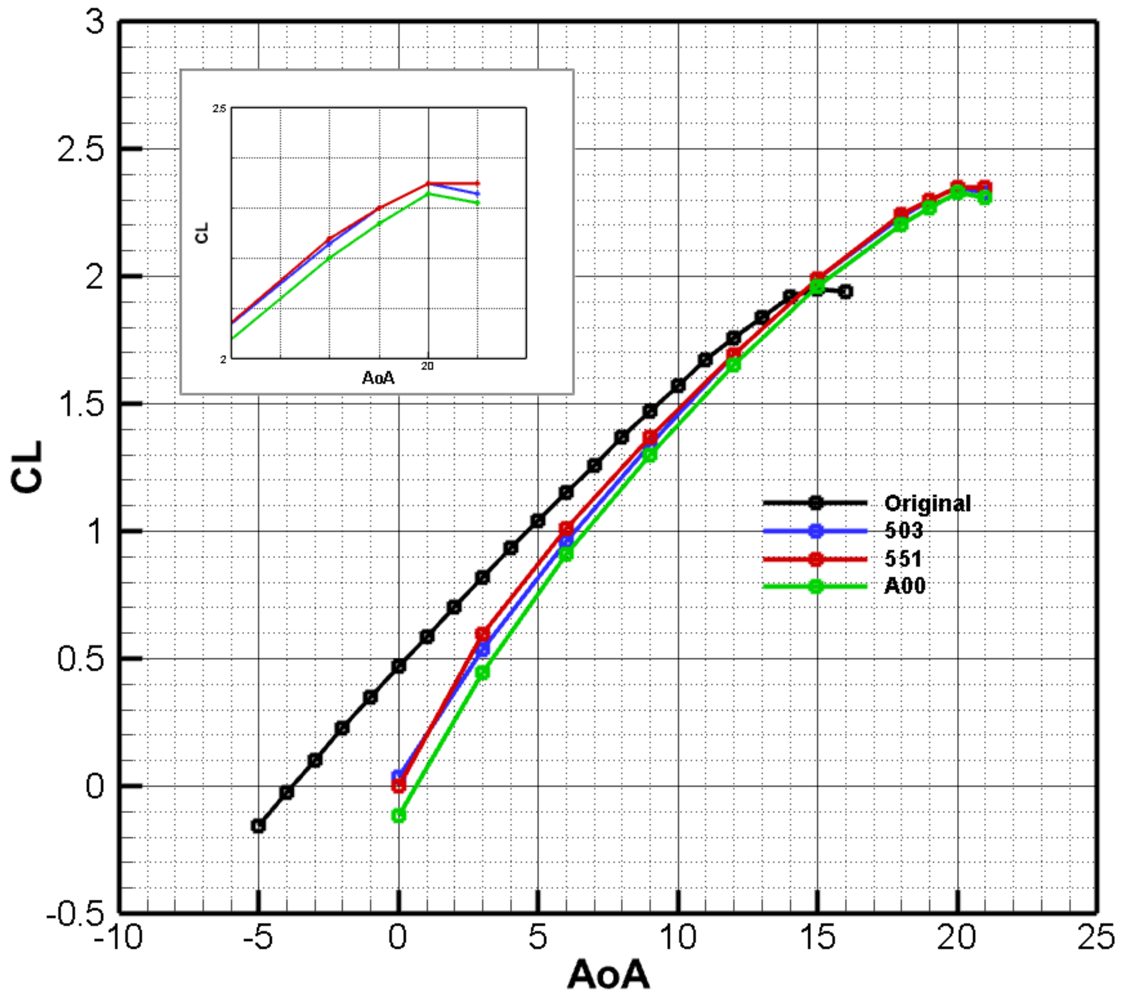

3.4 Results for Morphed Leading-Edge Variants

- Computational support was provided to both UI and UTK with simulations of the variants using NSU2D

NSU2D-SA Fully Turbulent Lift Curves for Morphed LE S207 Variants at Mach = 0.180, Re = 1.4 Million

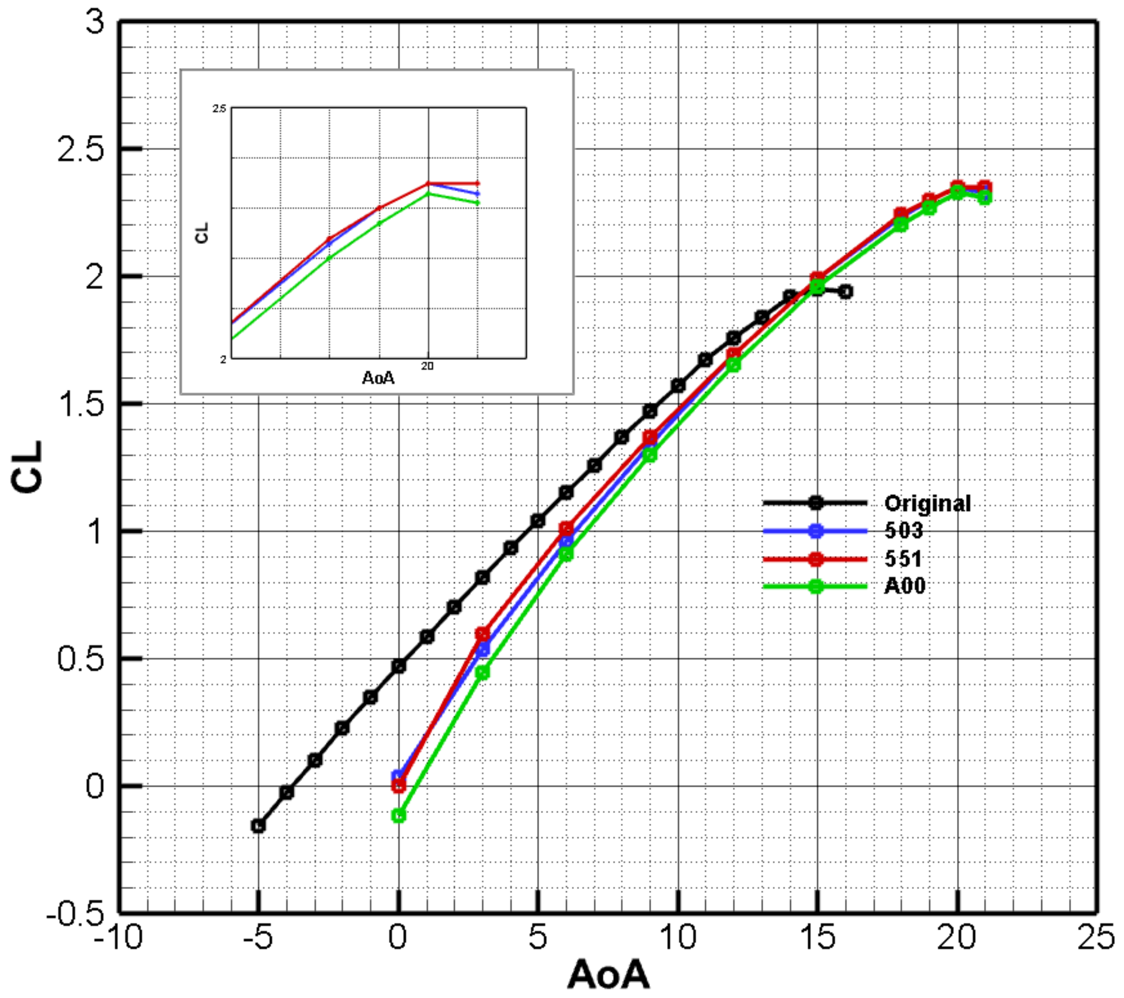

Morphed LE S207 Variants Fully Turbulent Results Comparison between OVERFLOW and NSU2D for Mach=0.180, Re=1.4 Million

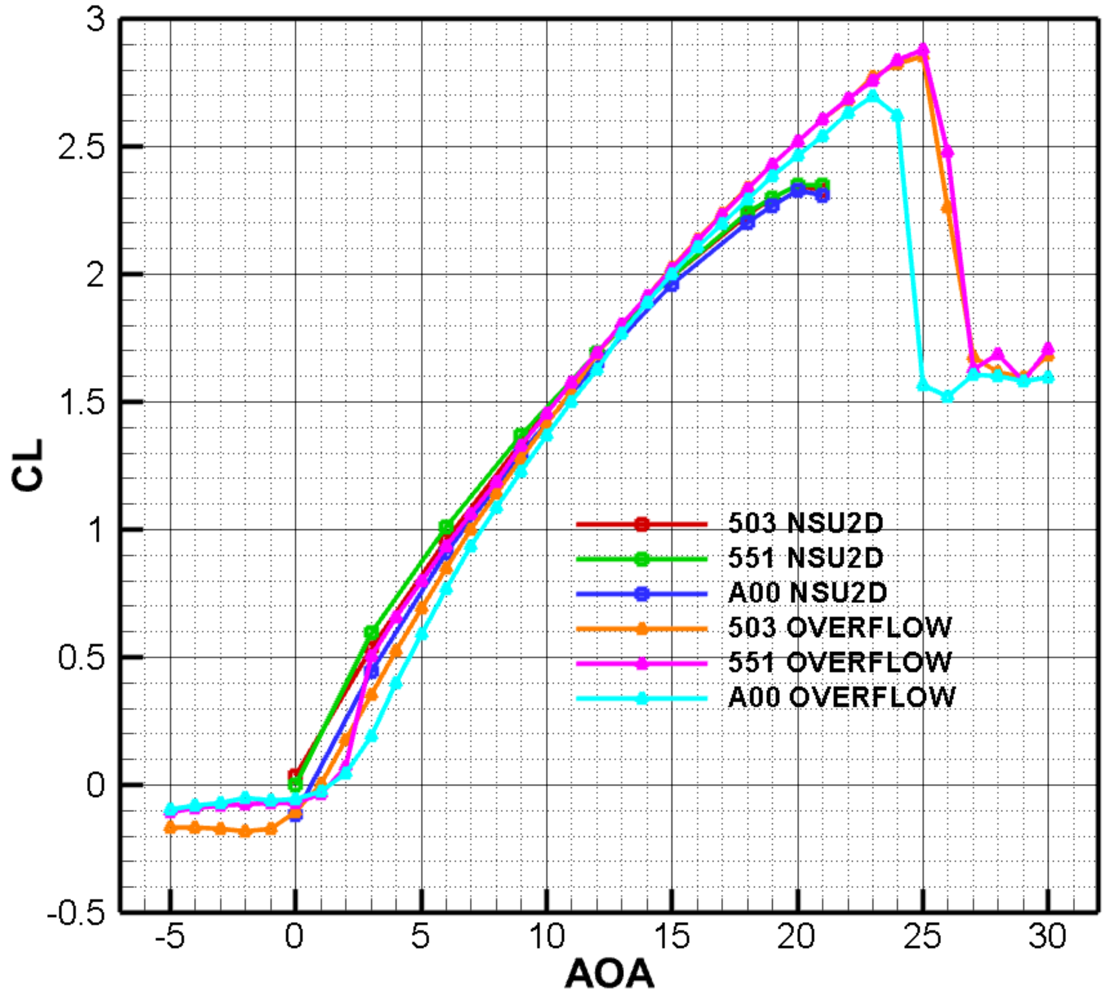

3.4 Results for Morphed Leading-Edge Variants

- Computational support was provided to both UI and UTK with simulations of the variants using NSU2D

NSU2D-SA Fully Turbulent Lift Curves for Morphed LE S207 Variants at Mach = 0.180, Re = 1.4 Million

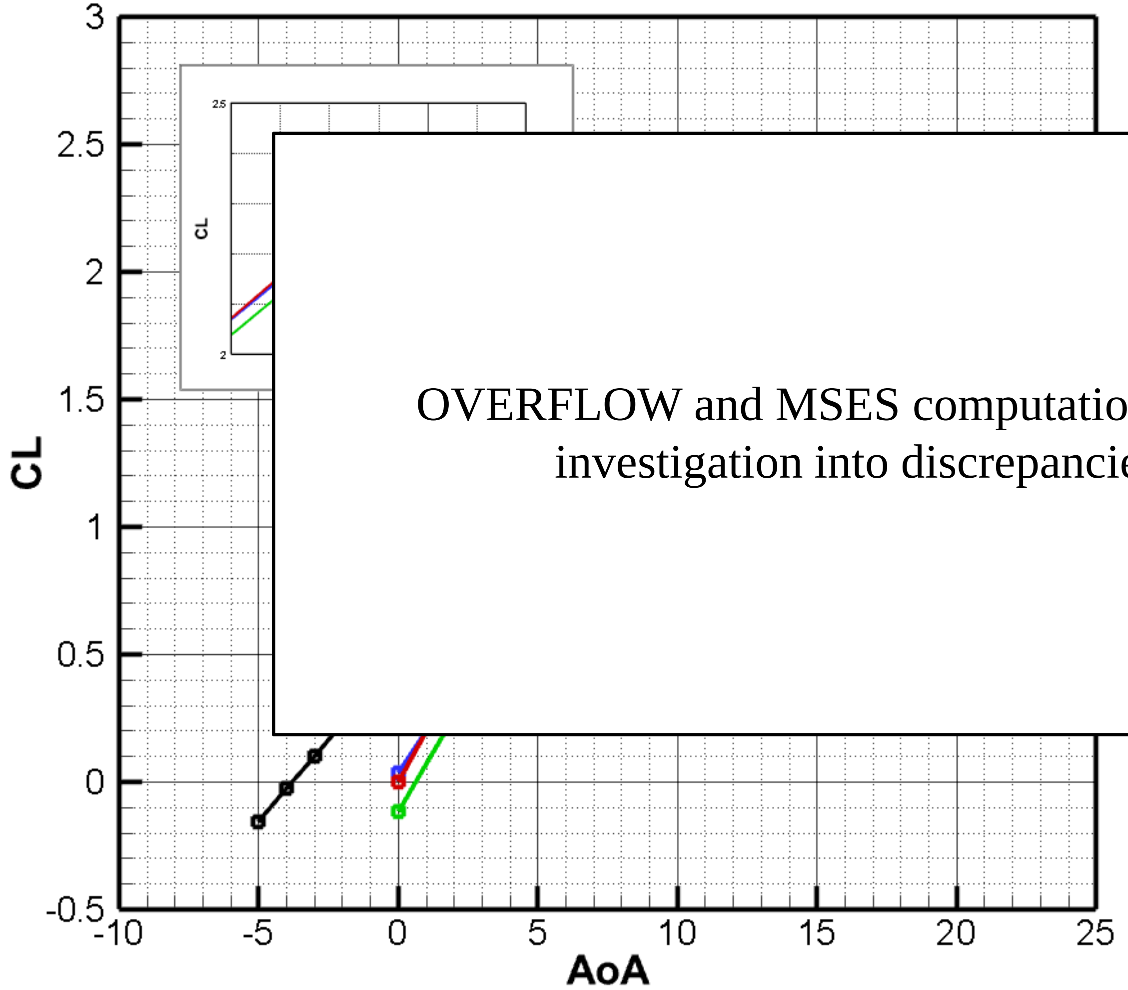

Morphed LE S207 Variants Fully Turbulent Results Comparison between OVERFLOW and NSU2D for Mach=0.180, Re=1.4 Million

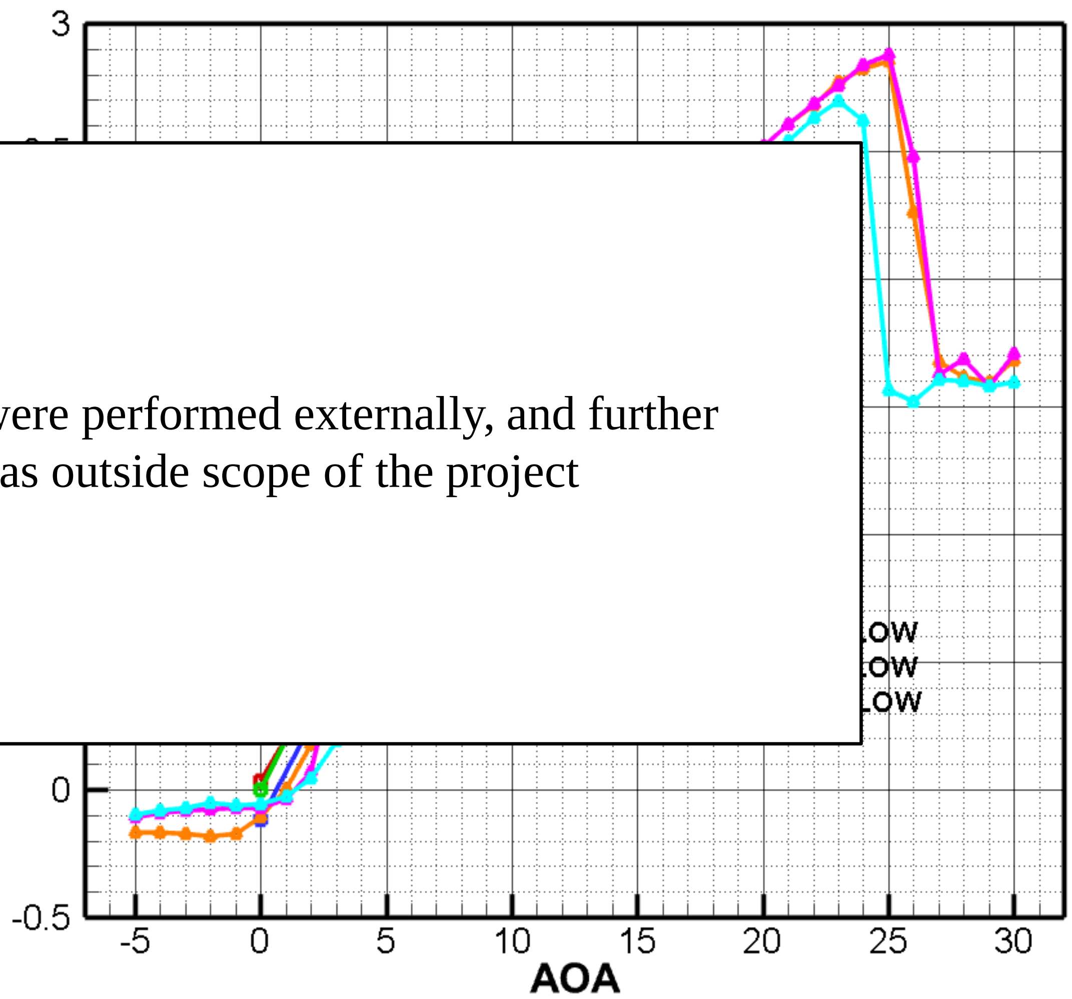

OVERFLOW and MSES computations were performed externally, and further investigation into discrepancies was outside scope of the project

4.3 Results for Configuration 2

- In the design of the aircraft wing, a sweep transformation was used on the S207 airfoil to define profiles parallel to the freestream [37,38]
  - A miscalculation was discovered, and its correction led to the generation of Configuration 2

Flap Differences Between Configuration and Configuration 2 at an Outboard Section

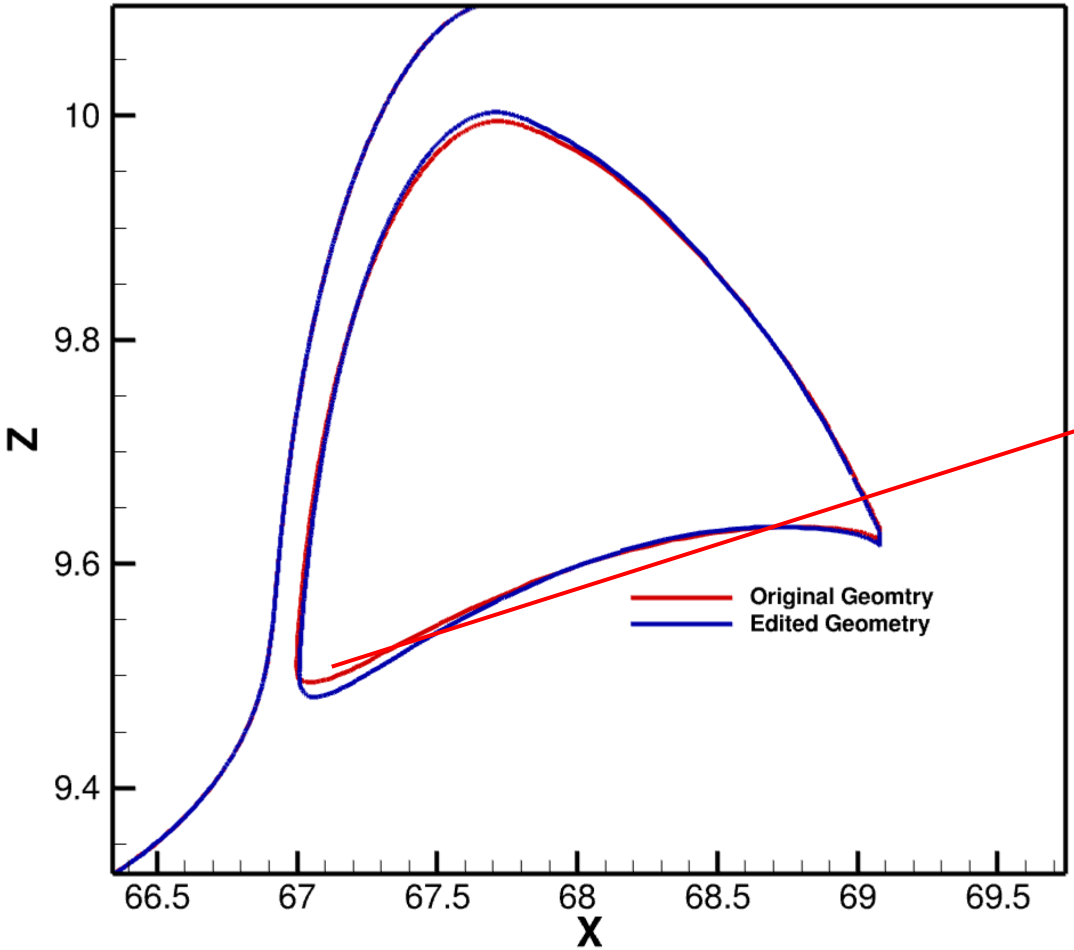

- Difference in coordinates at the entrance of the slot was 0.13 inches in the horizontal direction, and 0.16 in the vertical direction
  - This is in the range of the 0.1% chord variations found to be detrimental to performance in Section 3.3
  - Larger than manufacturing tolerances

4.3 Results for Configuration 2

- Fully turbulent simulation at Mach = 0.7, AOA = 0 degrees, Re = 12.3 million was examined for this configuration
  - No shock formation or accompanying region of low pressure

Fully Turbulent Mach Contour Distributions at Mach = 0.7, AOA = 0.0° for Configuration 2

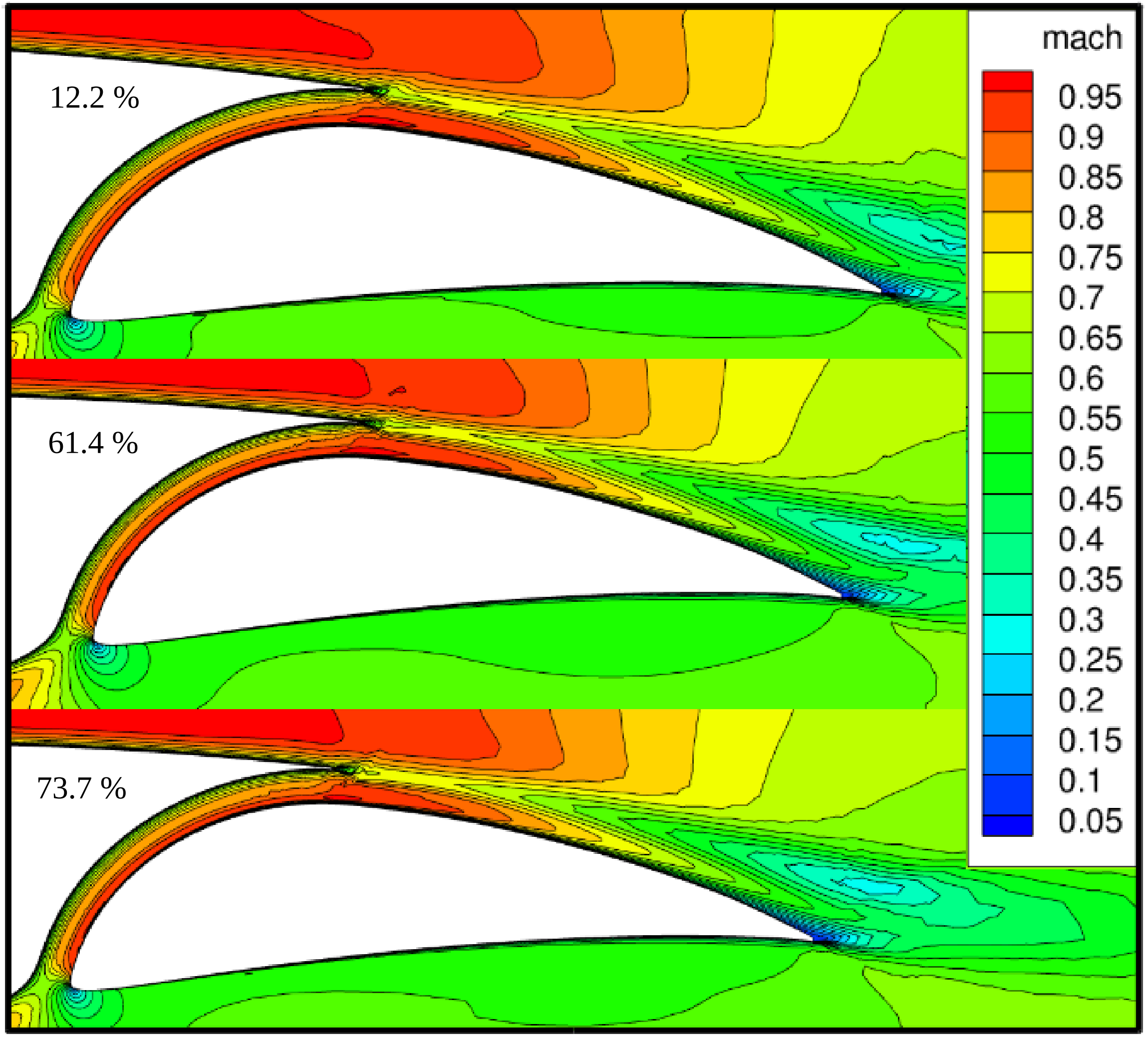

Pressure Coefficient Profile at Mach = 0.7, AOA =0.0 for Configuration 2 (Aft Element Removed)

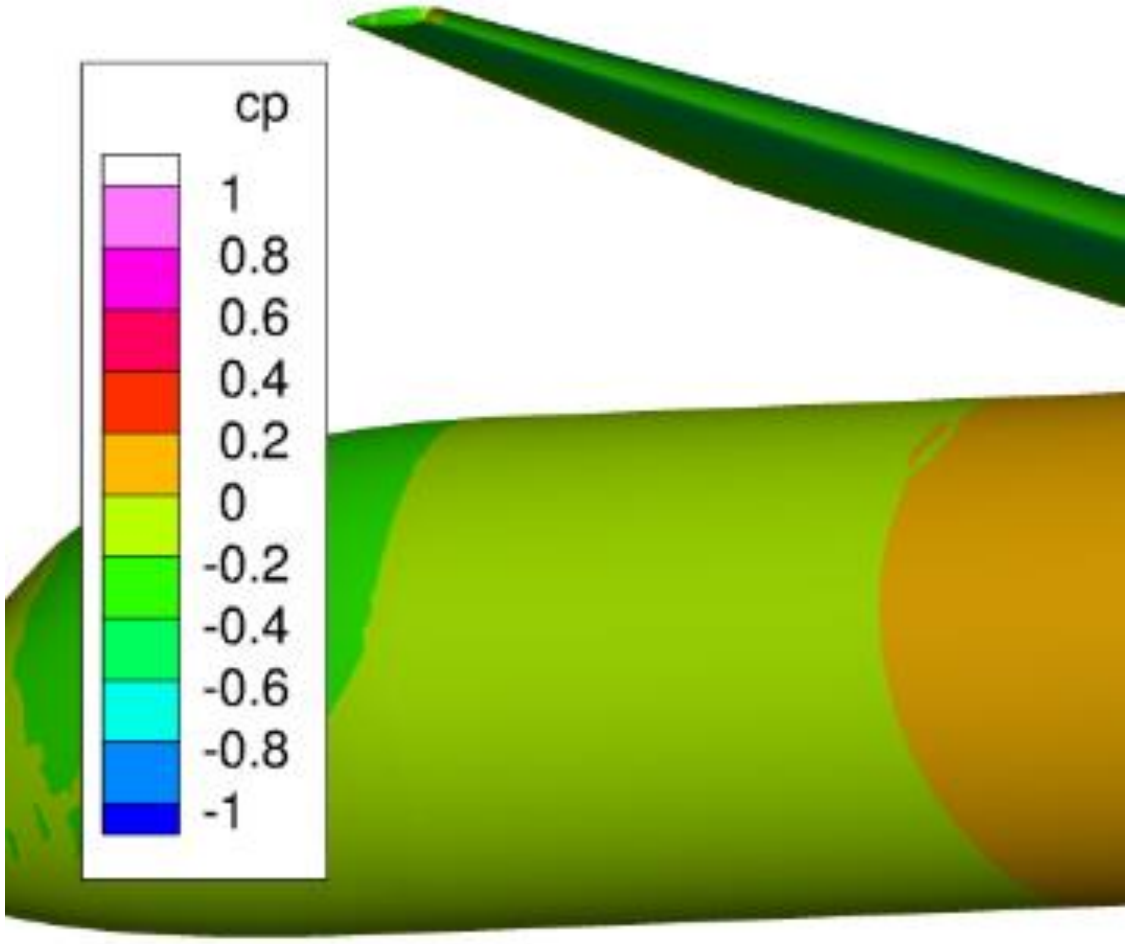

4.3 Results for Configuration 2

- Configuration 2 was again used to develop a full set of drag polars to serve as input to Boeing's performance analysis
  - Mach number ranged from 0.200 to 0.750, angles of attack ranged from -2.0 degrees to 5.0 degrees (128 cases)
  - Every case was run using SA fully turbulent approach and SA-Menter free transition approach
  - Re = 1.4 million/ft with MAC=8.786ft, MAC-based Re=12.3 million

4.3 Results for Configuration 2

- Configuration 2 was again used to develop a full set of drag polars to serve as input to Boeing's performance analysis
  - Mach number ranged from 0.200 to 0.750, angles of attack ranged from -2.0 degrees to 5.0 degrees (128 cases)
  - Every case was run using SA fully turbulent approach and SA-Menter free transition approach
  - Re = 1.4 million/ft with MAC=8.786ft, MAC-based Re=12.3 million

Configuration 2 NSU3D-SA-Menter Free Transition Drag Polars

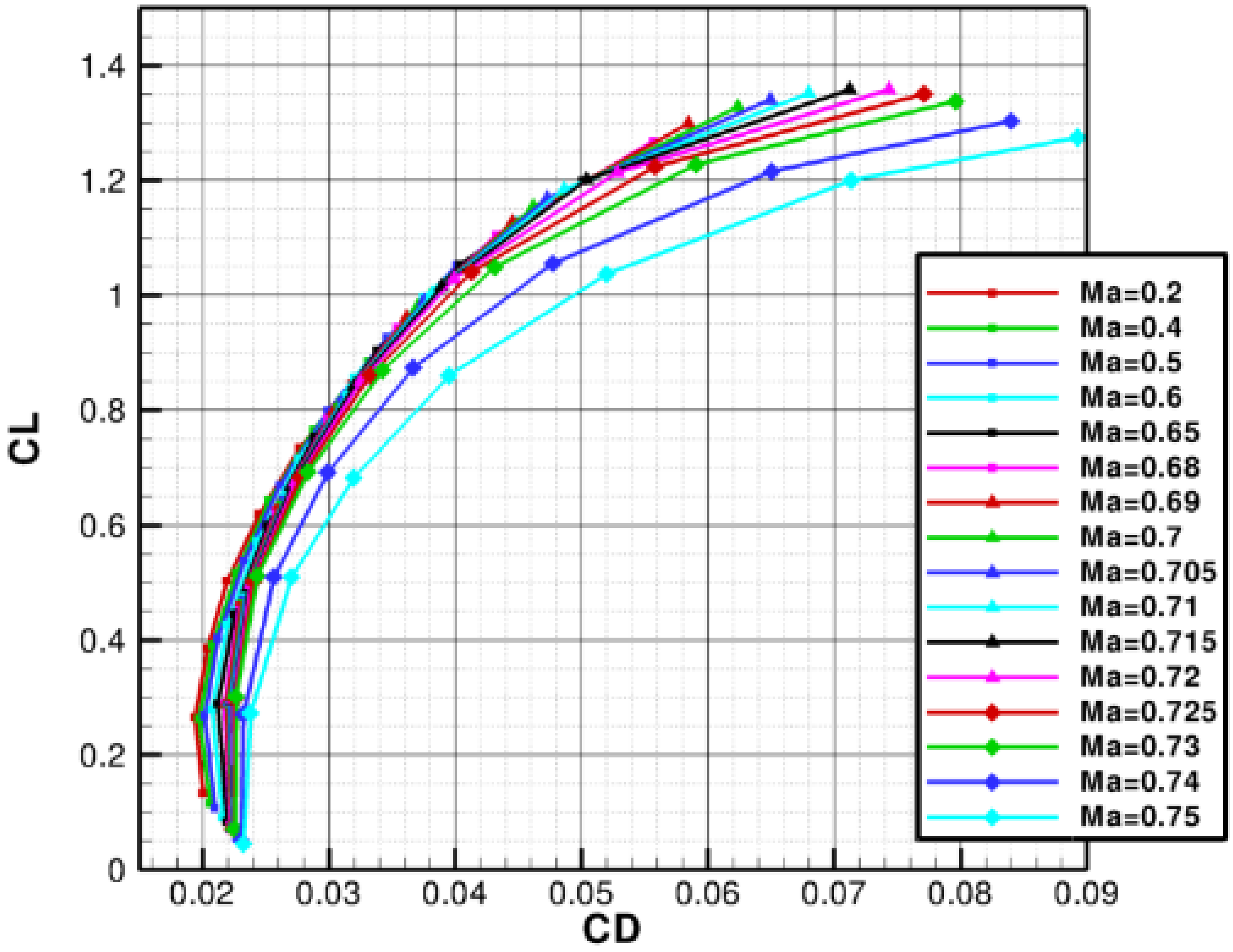

Configuration 2 NSU3D-SA Fully Turbulent Drag Polars

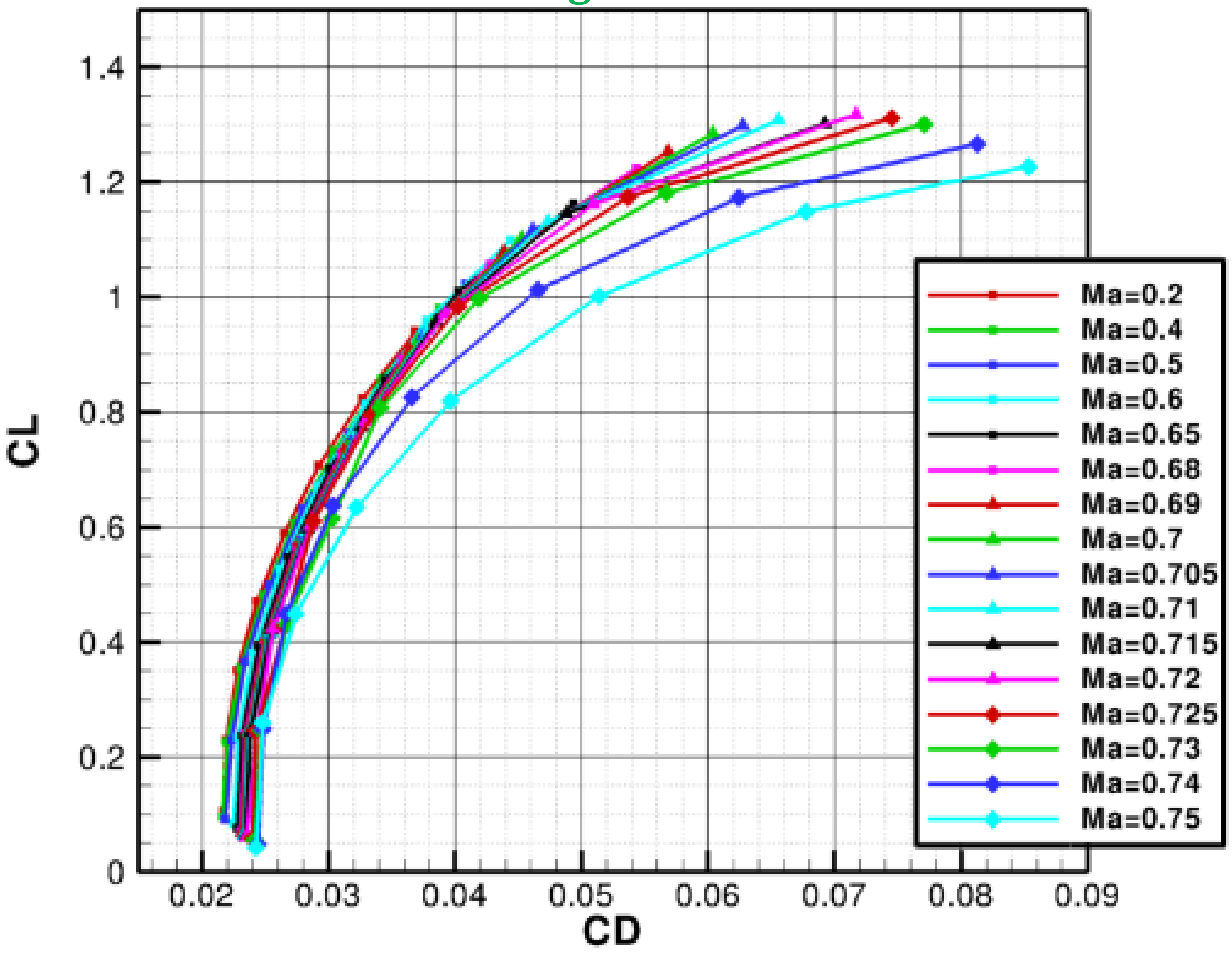

4.3 Results for Configuration 2

- Effect of free transition more precisely quantified through drag polars and lift curves for Mach = 0.5 and Mach = 0.7

Configuration 2 Polars for Mach = 0.5 and Mach = 0.7

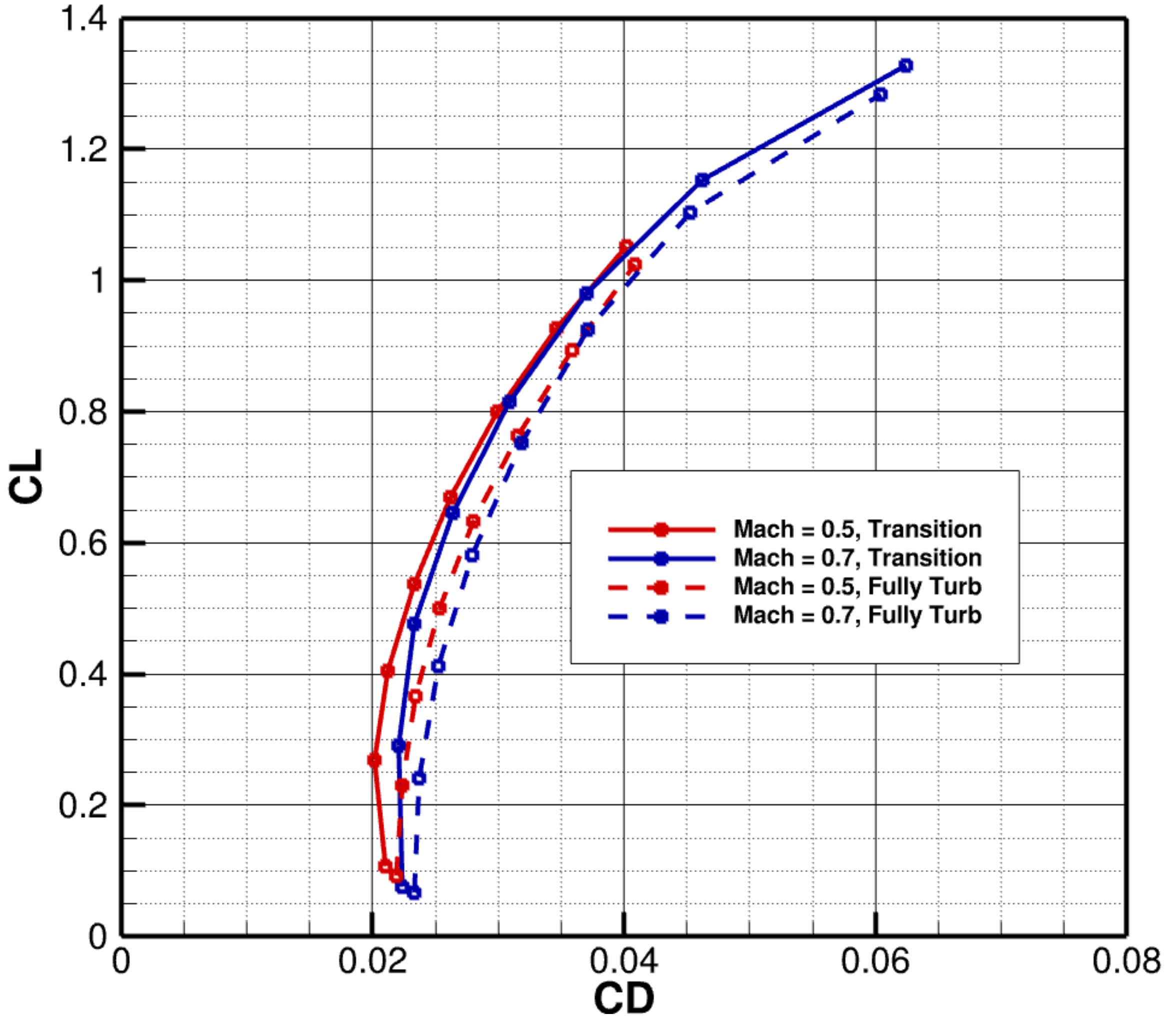

Configuration 2 Lift Curves for Mach = 0.5 and Mach = 0.7

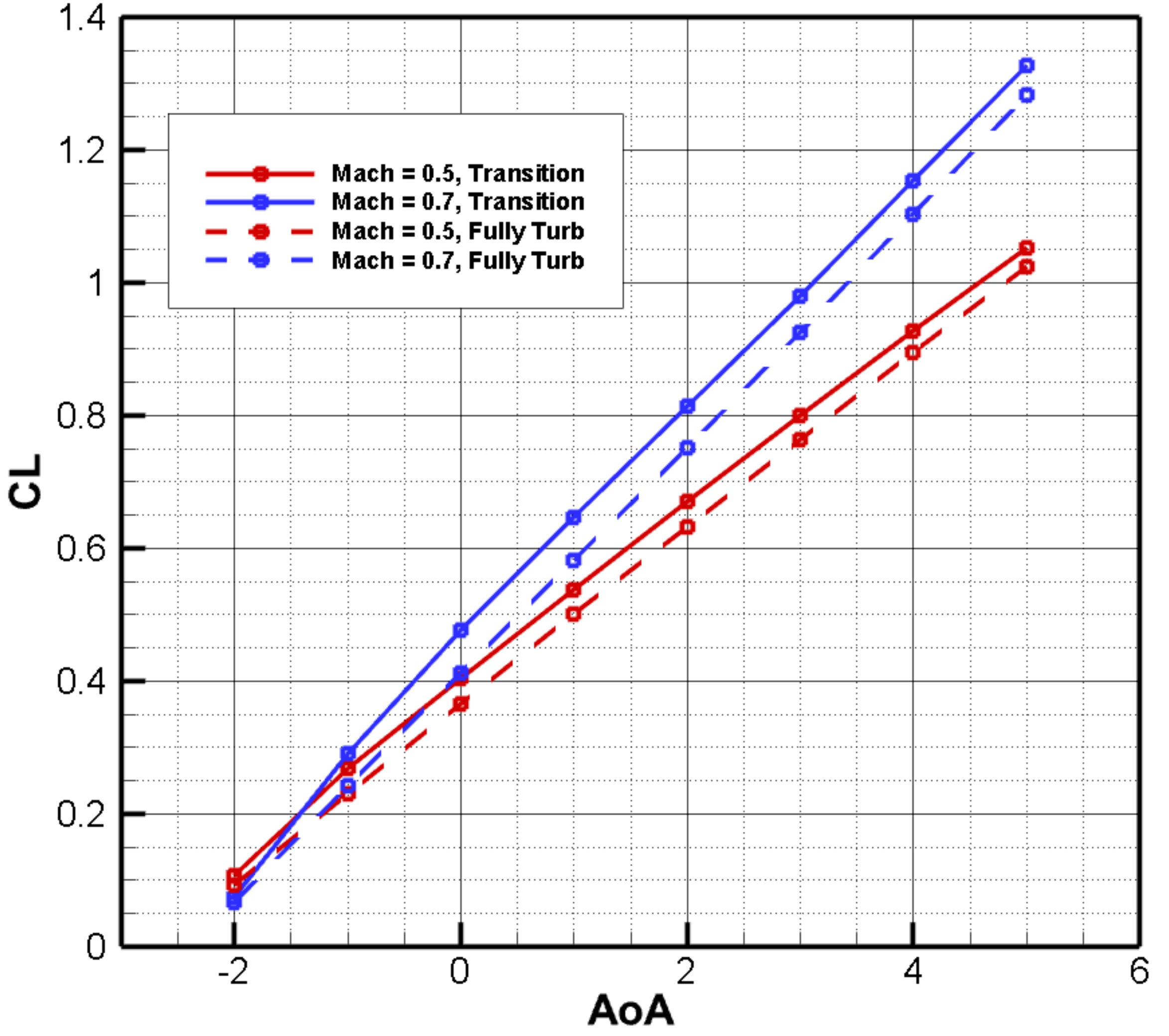

4.3 Results for Configuration 2

- Effect of free transition more precisely quantified through drag polars and lift curves for Mach = 0.5 and Mach = 0.7

Configuration 2 Polars for Mach = 0.5 and Mach = 0.7

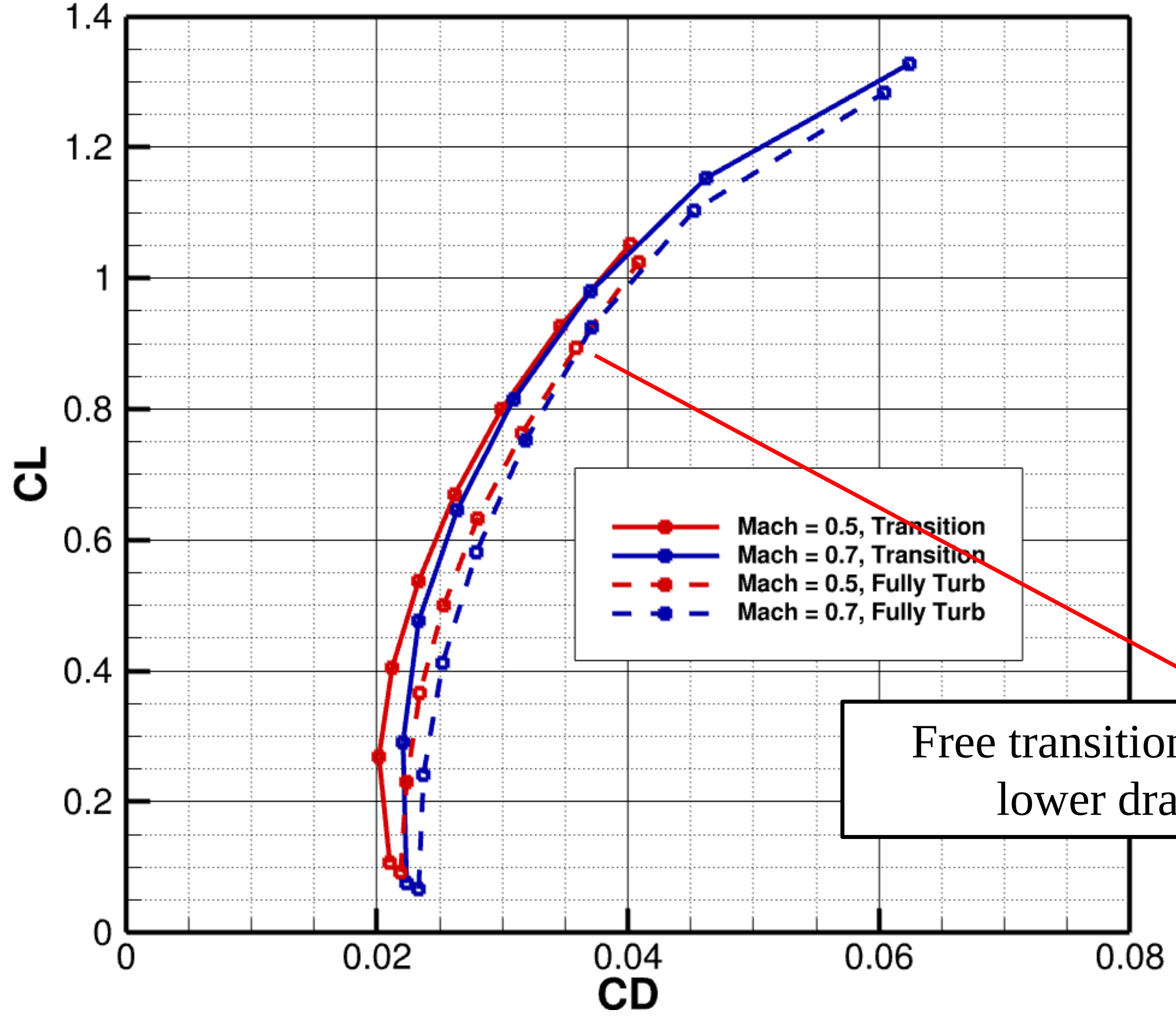

Configuration 2 Lift Curves for Mach = 0.5 and Mach = 0.7

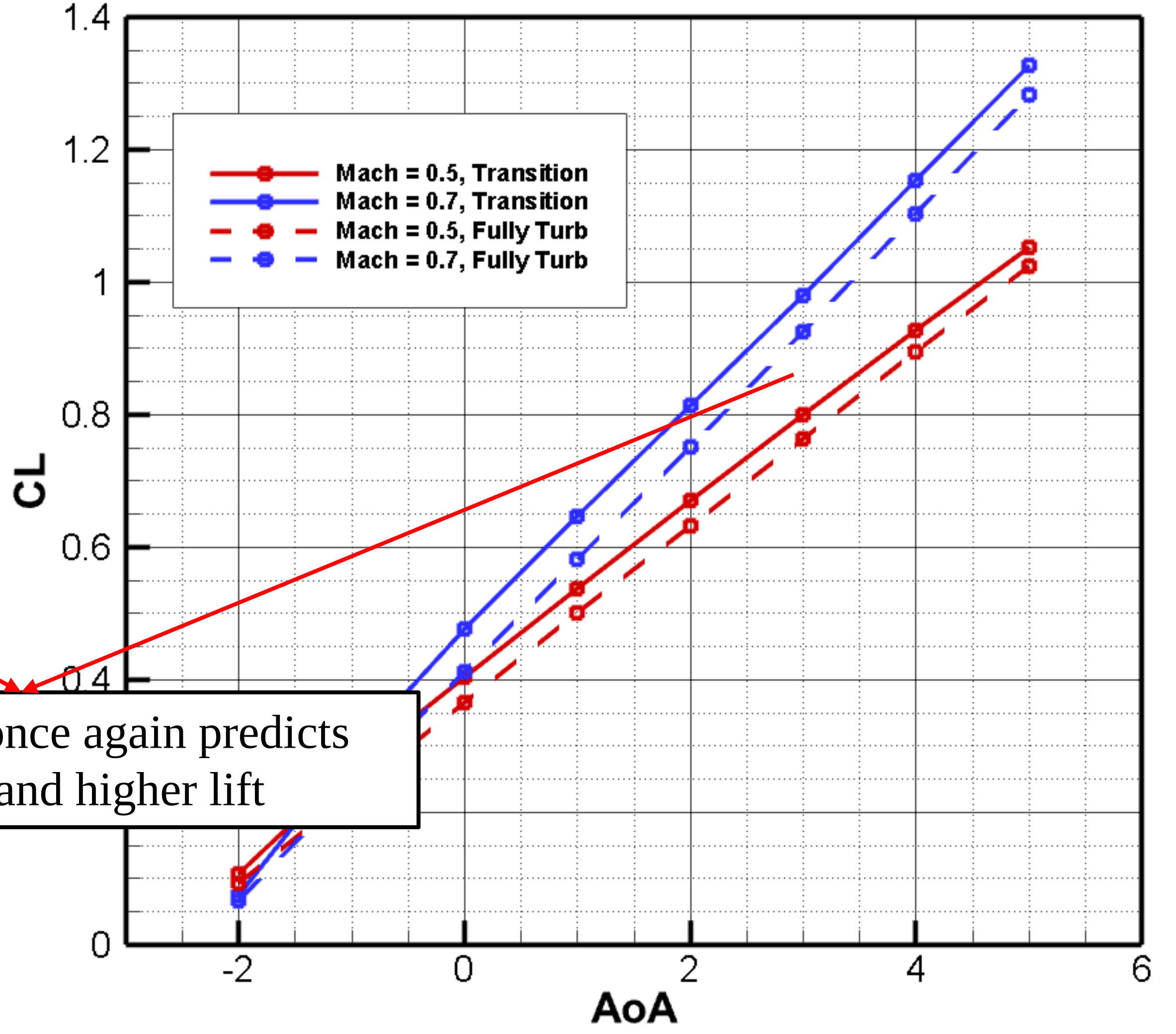

Free transition once again predicts lower drag and higher lift

4.3 Results for Configuration 2

- Quantification of skin friction drag can be used to further highlight the differences in free transition and fully turbulent modeling approaches

Configuration 2 NSU2D-SA-Menter Free Transition C_{DF} Profiles

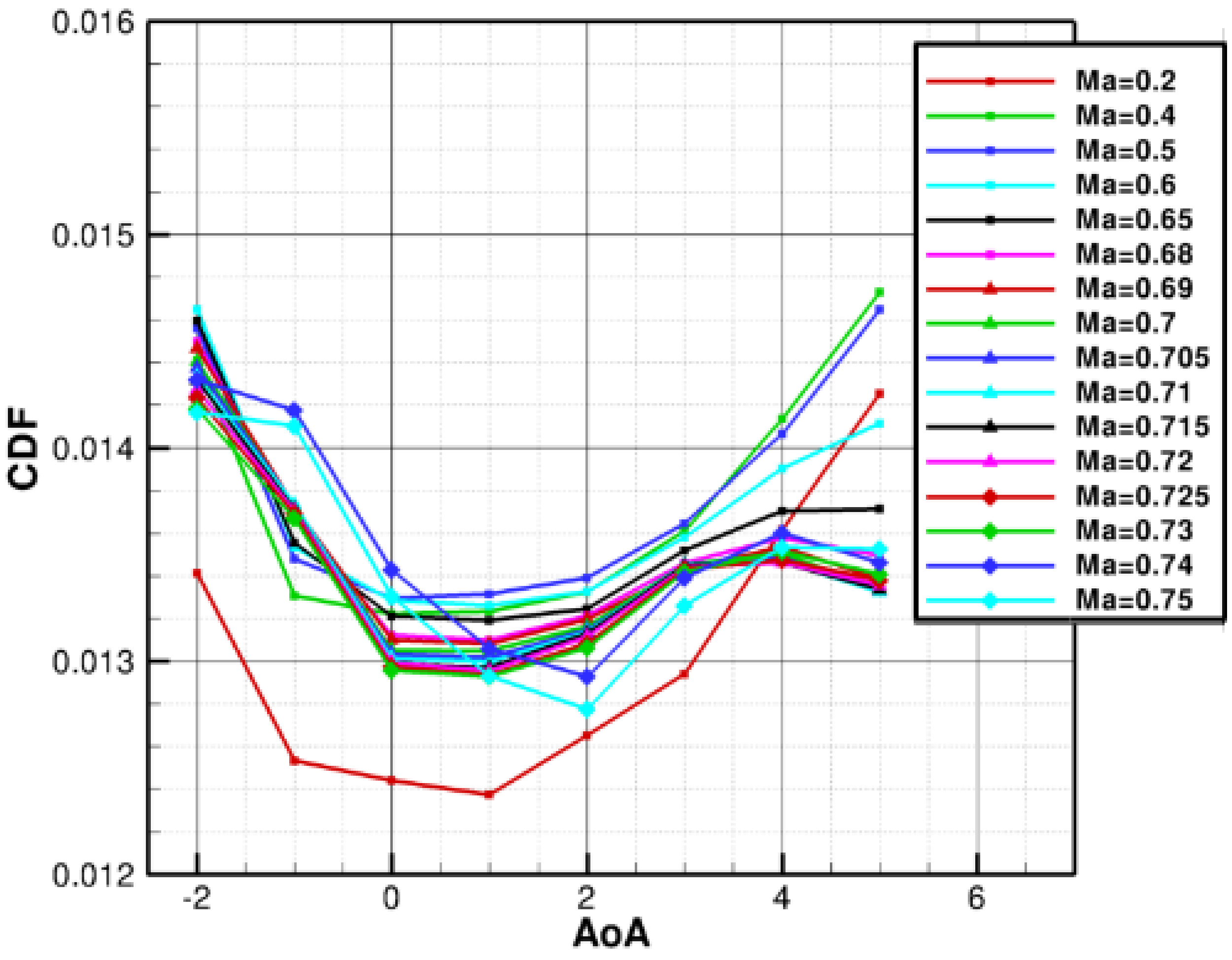

Configuration 2 NSU2D-SA Fully Turbulent C_{DF} Profiles

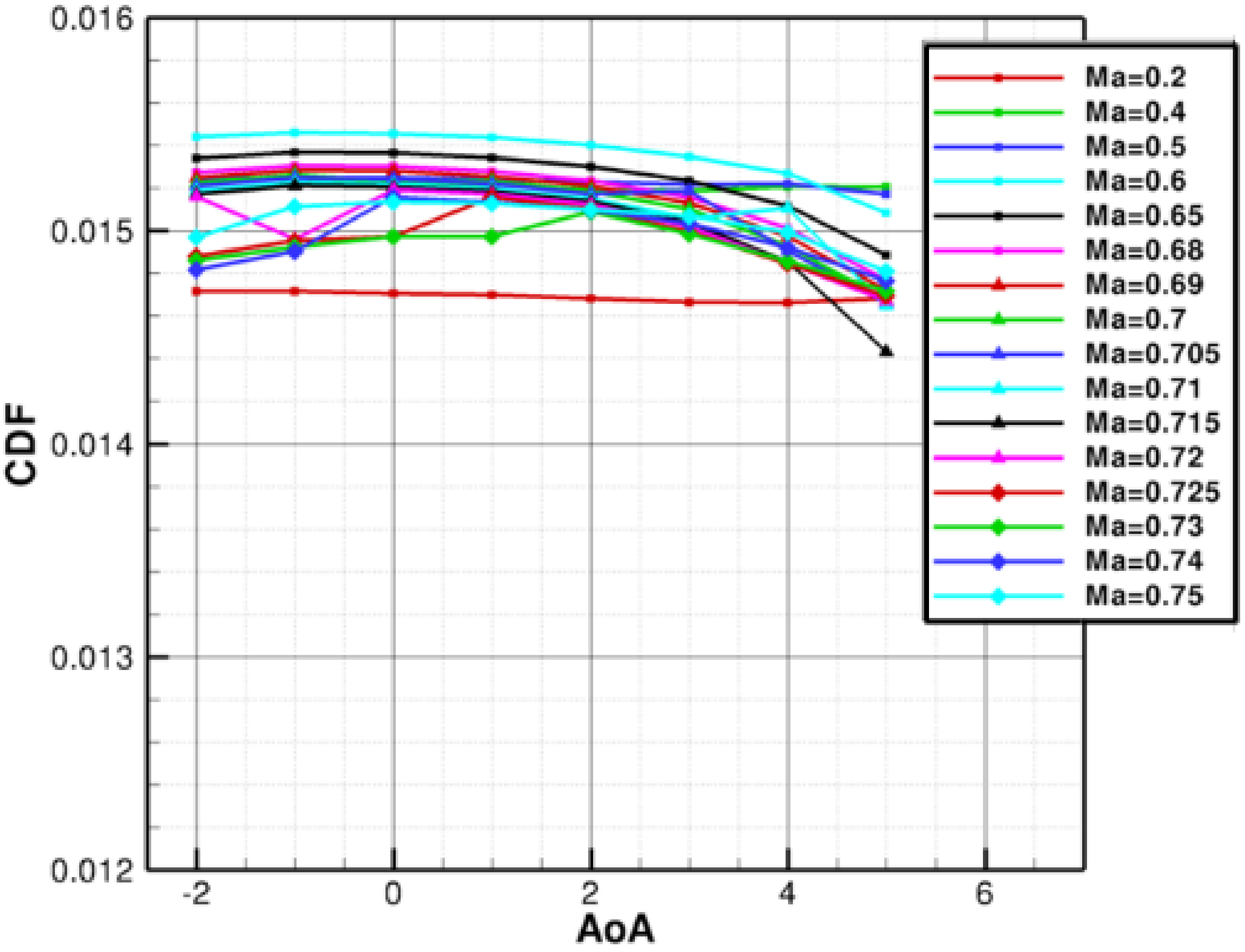

4.3 Results for Configuration 2

- Quantification of skin friction drag can be used to further highlight the differences in free transition and fully turbulent modeling approaches

Configuration 2 NSU2D-SA-Menter Free Transition C_{DF} Profiles

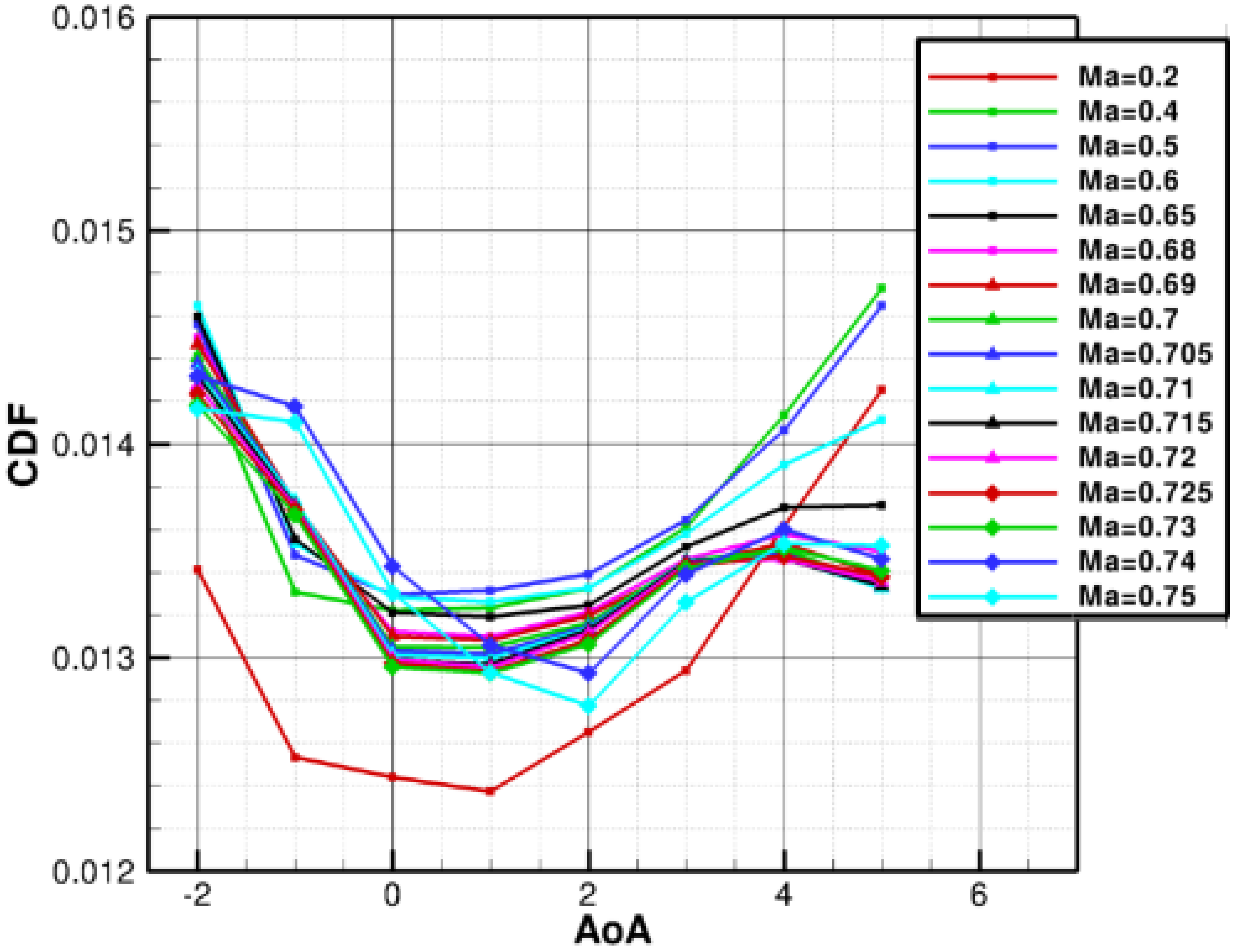

Configuration 2 NSU2D-SA Fully Turbulent C_{DF} Profiles

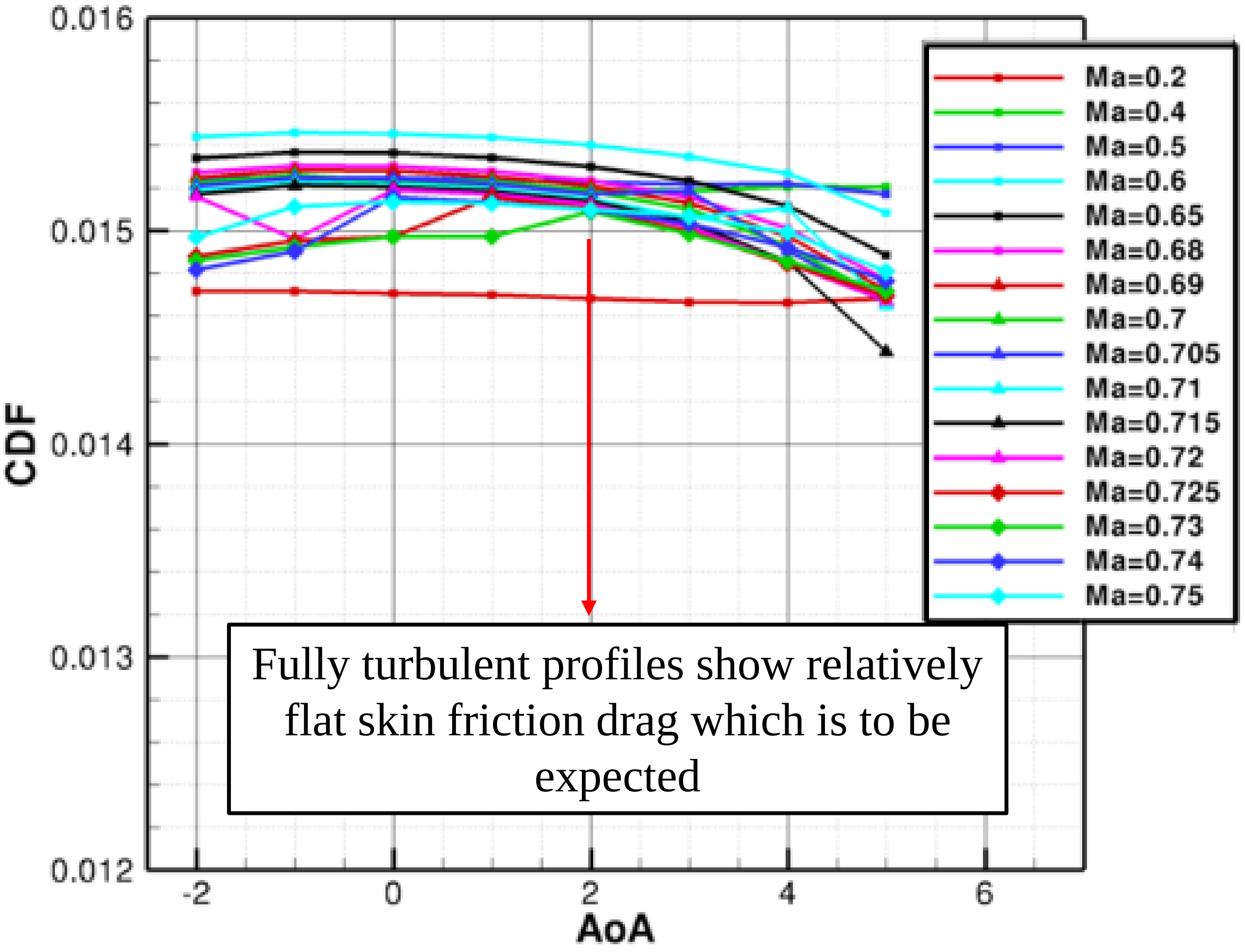

4.3 Results for Configuration 2

- Quantification of skin friction drag can be used to further highlight the differences in free transition and fully turbulent modeling approaches

Configuration 2 NSU2D-SA-Menter Free Transition C_{DF} Profiles

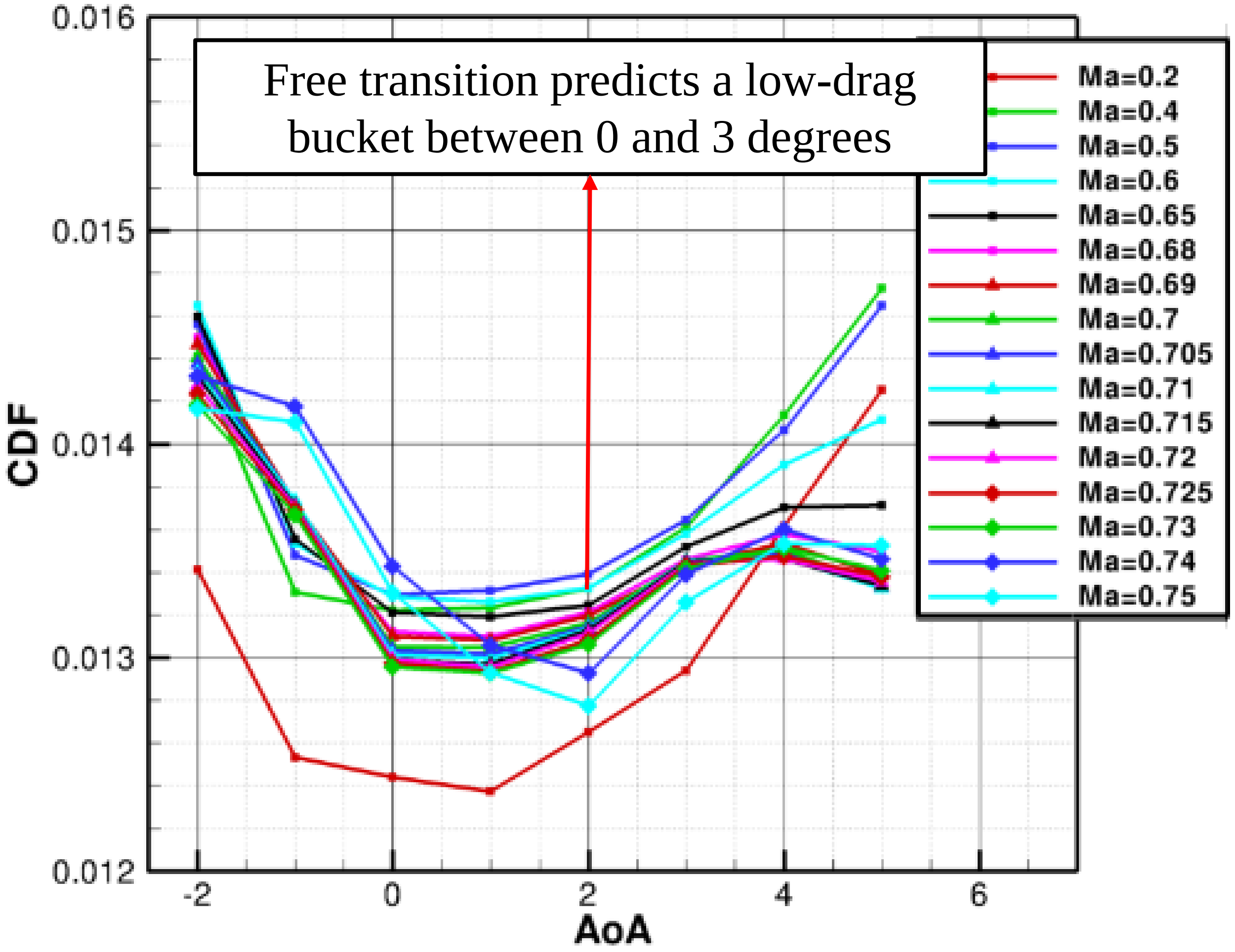

Configuration 2 NSU2D-SA Fully Turbulent C_{DF} Profiles

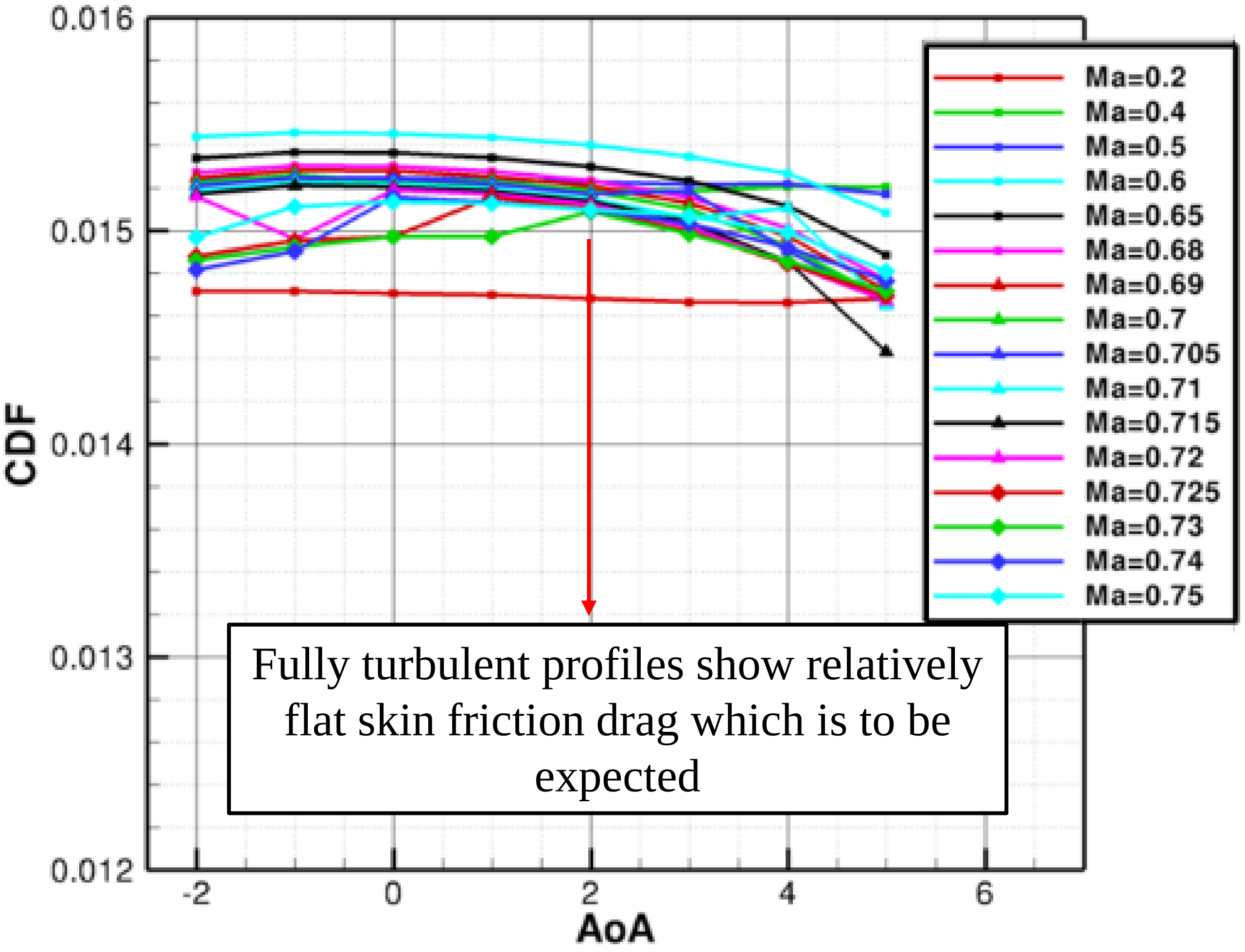

4.3 Results for Configuration 2

- Like in 2D, the location of the transition line can be determined from examination of the surface skin friction drag

Configuration 2 Surface Skin Friction Drag for Mach = 0.7, AOA =0 degrees

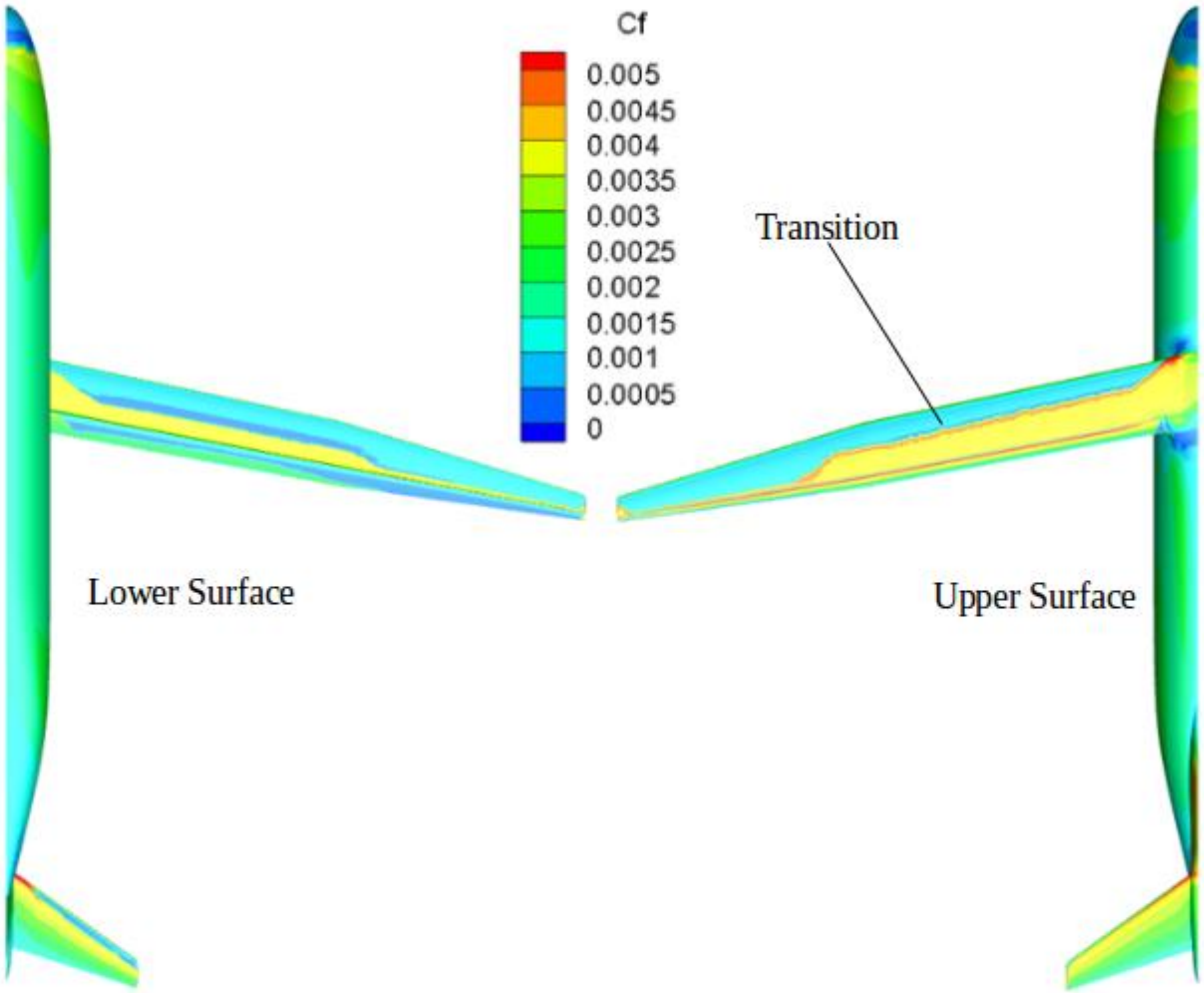

4.3 Results for Configuration 2

- Like in 2D, the location of the transition line can be determined from examination of the surface skin friction drag

Configuration 2 Surface Skin Friction Drag for Mach = 0.7, AOA =0 degrees

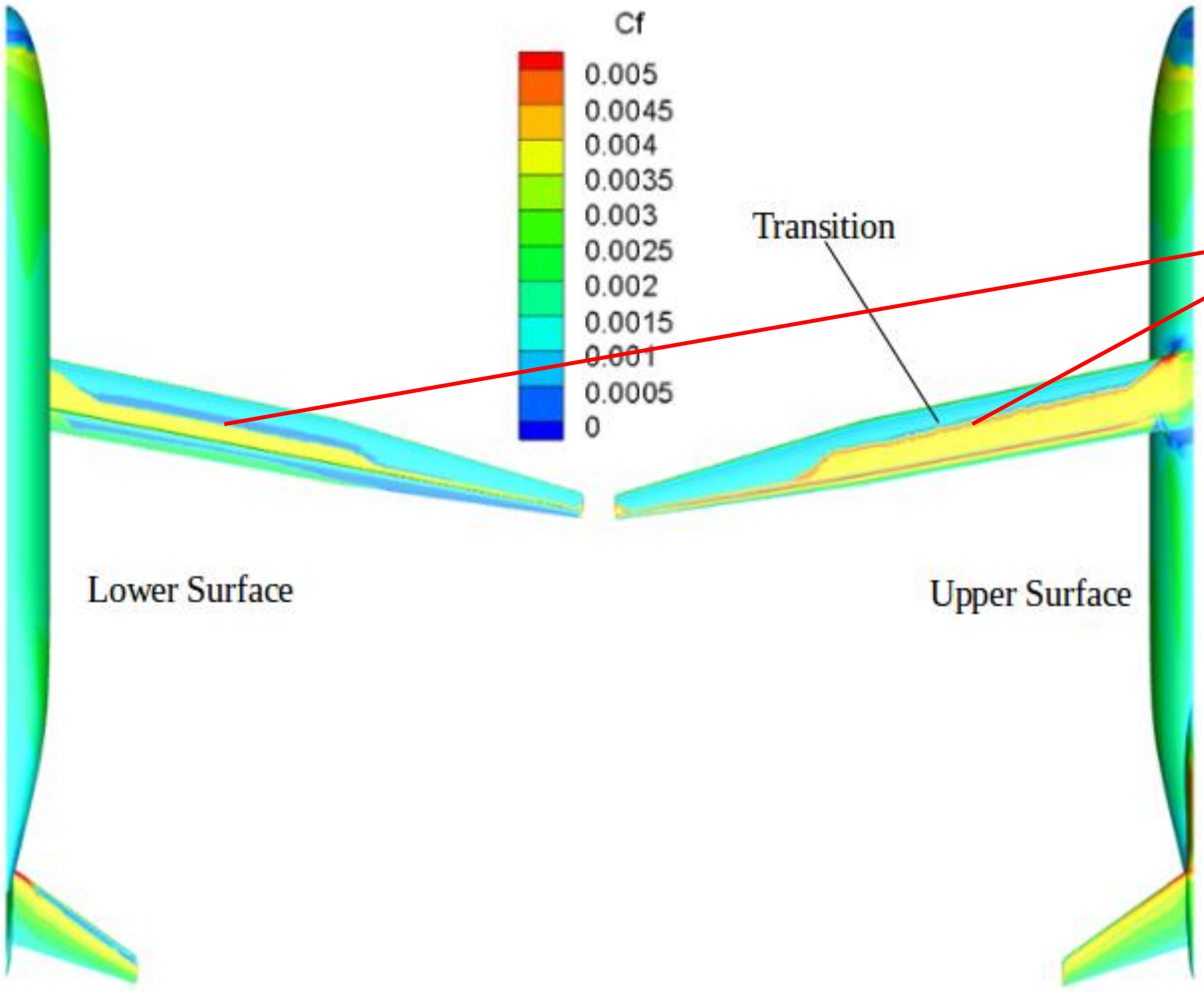

- Transition occurred much further upstream on both the upper and lower surfaces of the wing than expected on Configuration 1
  - This is not in line with design intent as the fore element should be all laminar

4.5 Polars for Configuration 3

NSU3D-SA-AFT2 (Full Wing) Pitching Moment Curves for Re = 12.3 Million

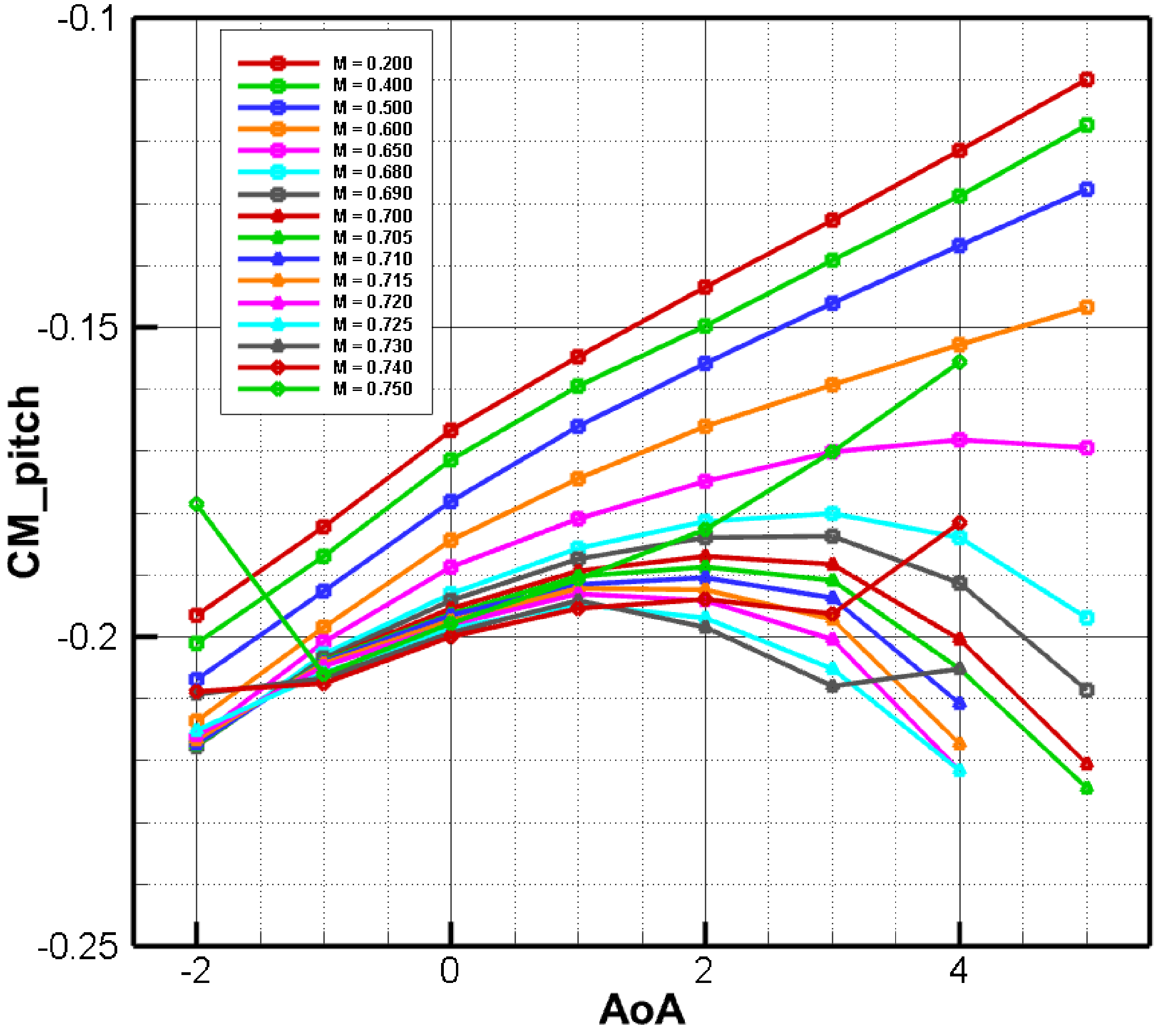

NSU3D-SA-AFT2 (Full Wing) Pressure Drag Curves for Re = 12.3 Millions

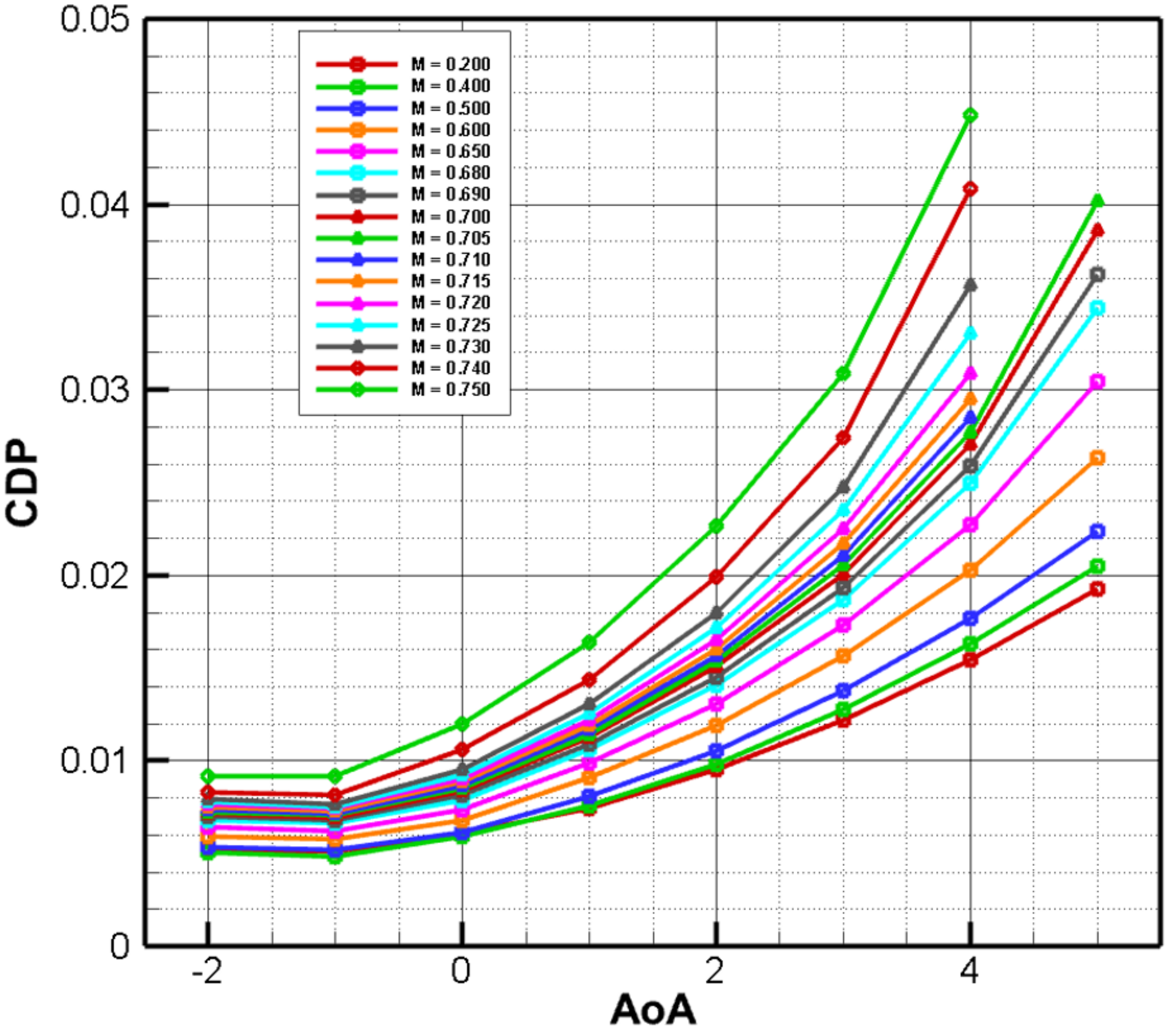

4.2 Results for the Initial Configuration

- Configuration 1 was used to develop a full set of drag polars requested by ULI associates at Boeing
  - Serves as input to their analysis
  - Mach number ranged from 0.200 to 0.750, angles of attack ranged from -2.0 degrees to 5.0 degrees (128 cases)
  - Every case was run using SA fully turbulent approach and SA-Menter free transition approach
  - Re = 1.4 million/ft with MAC=8.786ft, MAC-based Re=12.3 million

Configuration 1 Performance Polars

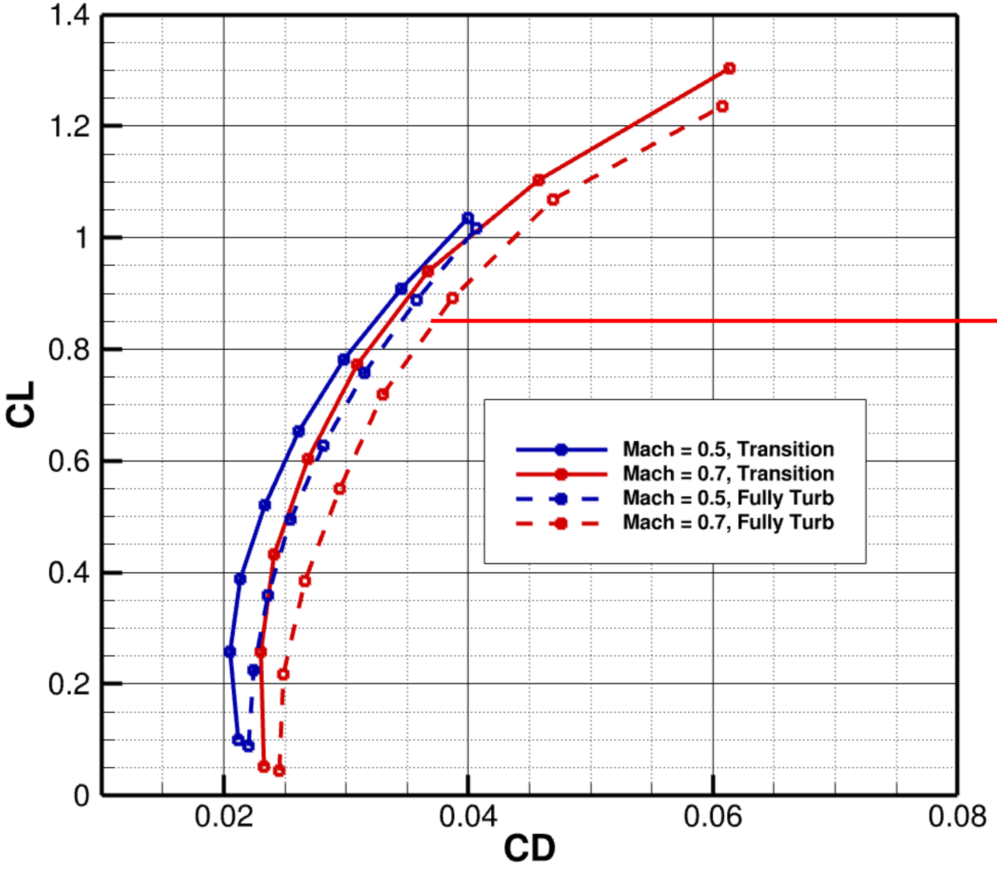

Configuration 1 Free Transition Spanwise Lift Distributions based on MAC

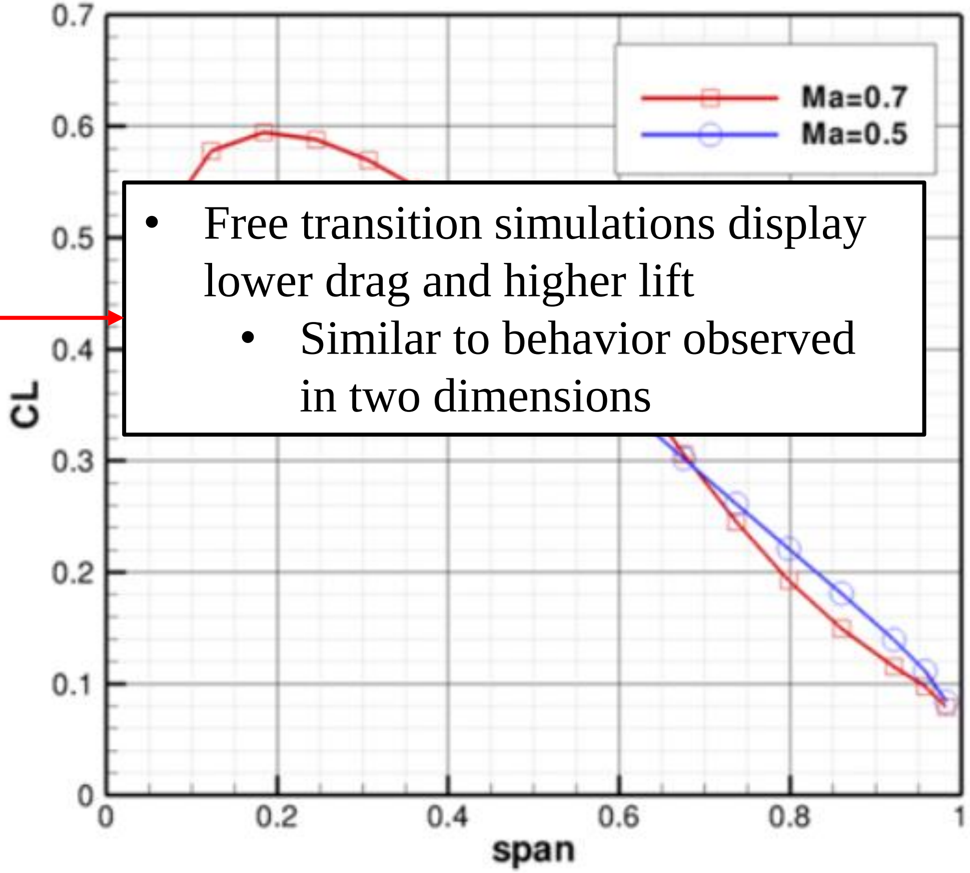

- Free transition simulations display lower drag and higher lift
  - Similar to behavior observed in two dimensions

4.3 Results for Configuration 2

- Further investigation into 3D performance can be made through examination of the spanwise lift coefficient based on both MAC and local chord

NSU3D-SA-Menter Free Transition Spanwise C_L Values Compared to NSU2D-SA-AFT2 Free Transition Results at Mach = 0.7, AOA = 0.0

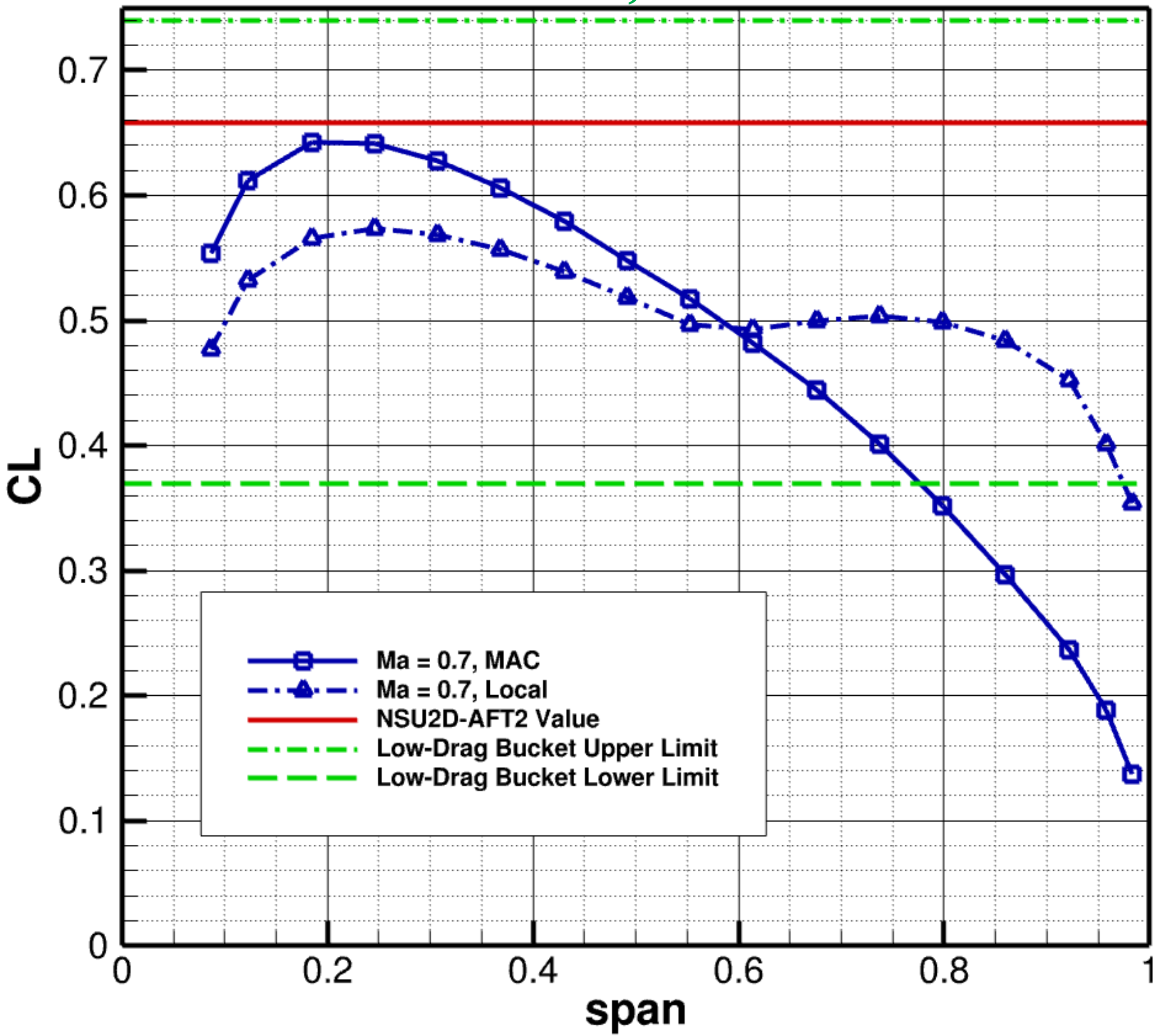

4.3 Results for Configuration 2

- Further investigation into 3D performance can be made through examination of the spanwise lift coefficient based on both MAC and local chord

NSU3D-SA-Menter Free Transition Spanwise C_L Values Compared to NSU2D-SA-AFT2 Free Transition Results at Mach = 0.7, AOA = 0.0

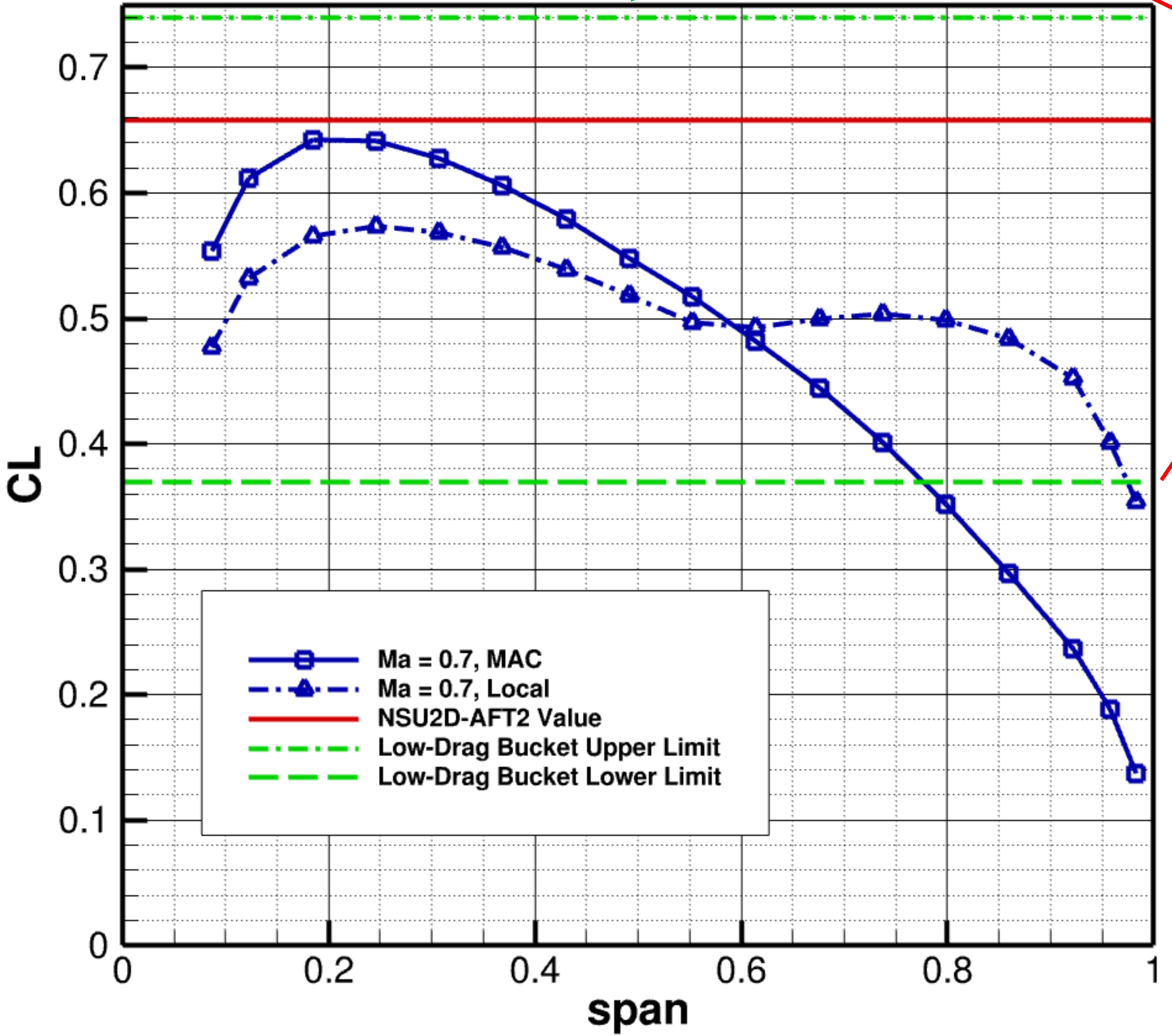

- Lift coefficient values, particularly local chord-based, fall between the upper and lower limits of the low-drag bucket for the S207 airfoil [10]

4.3 Results for Configuration 2

- Further investigation into 3D performance can be made through examination of the spanwise lift coefficient based on both MAC and local chord

NSU3D-SA-Menter Free Transition Spanwise C_L Values Compared to NSU2D-SA-AFT2 Free Transition Results at Mach = 0.7, AOA = 0.0

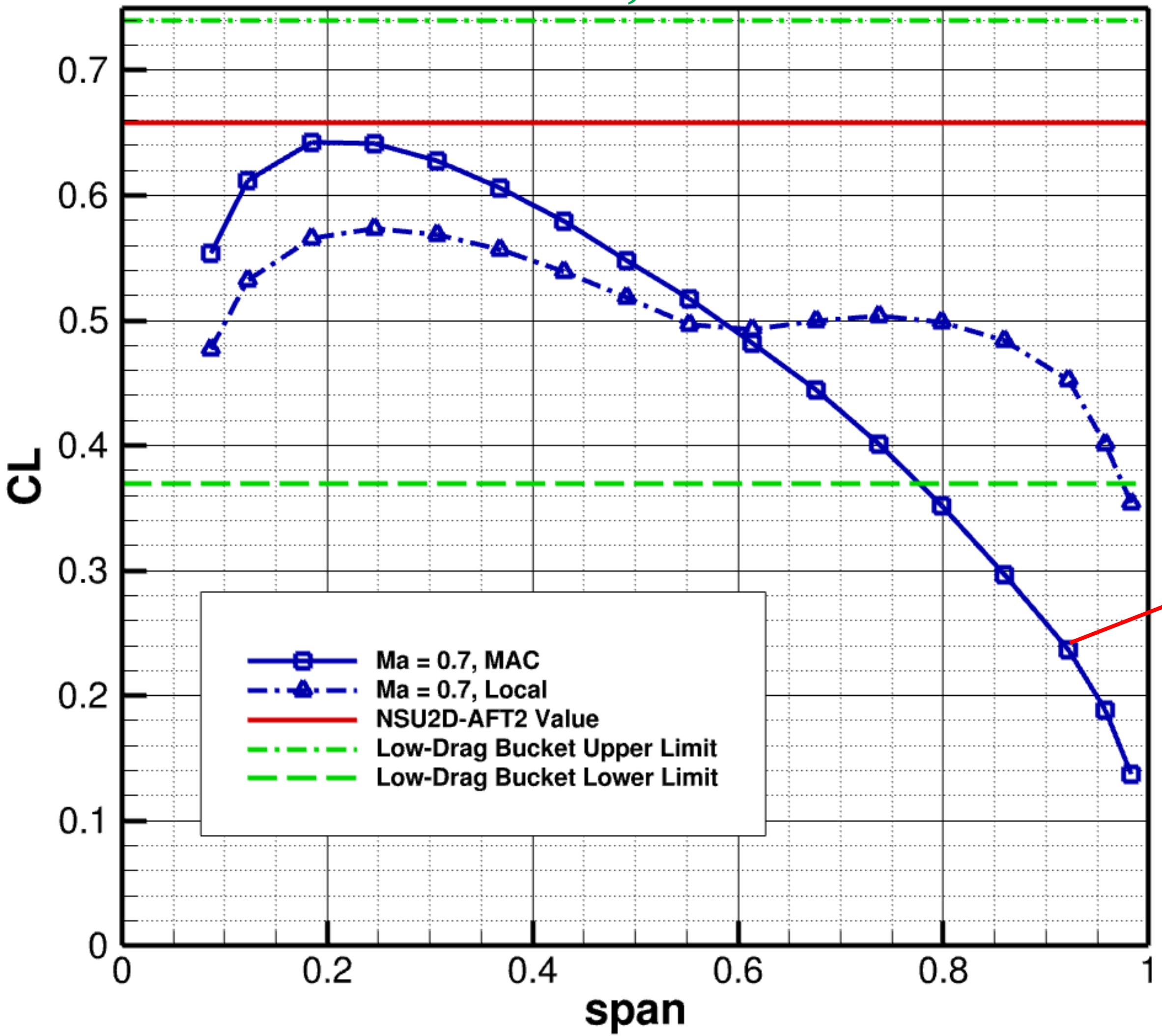

- Lift coefficient values, particularly local chord-based, fall between the upper and lower limits of the low-drag bucket for the S207 airfoil [10]

- MAC-based spanwise lift coefficient values show a nearly elliptic distribution for the Configuration 2 wing design
  - Further evidence of no shock wave in the slot at the outboard region

4.3 Results for Configuration 2

- To further investigate the observed early transition on Configuration 2, compute surface pressure profiles at select spanwise location were selected for comparison to 2D surface pressure profiles
  - Analysis performed with fully turbulent results to eliminate need to consider discrepancies between transition prediction models

NSU3D-SA Fully Turbulent Cp Profile at 8.6% Span on Configuration 2 Compared to NSU2D-SA Fully Turbulent Cp Profile

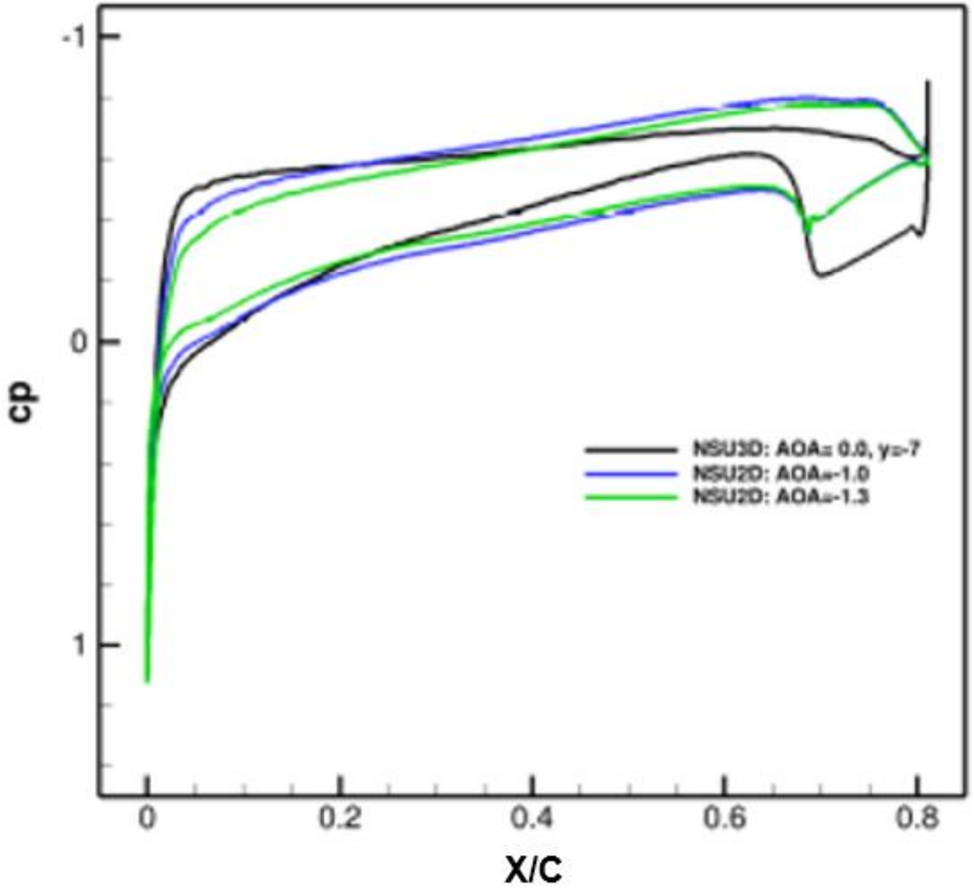

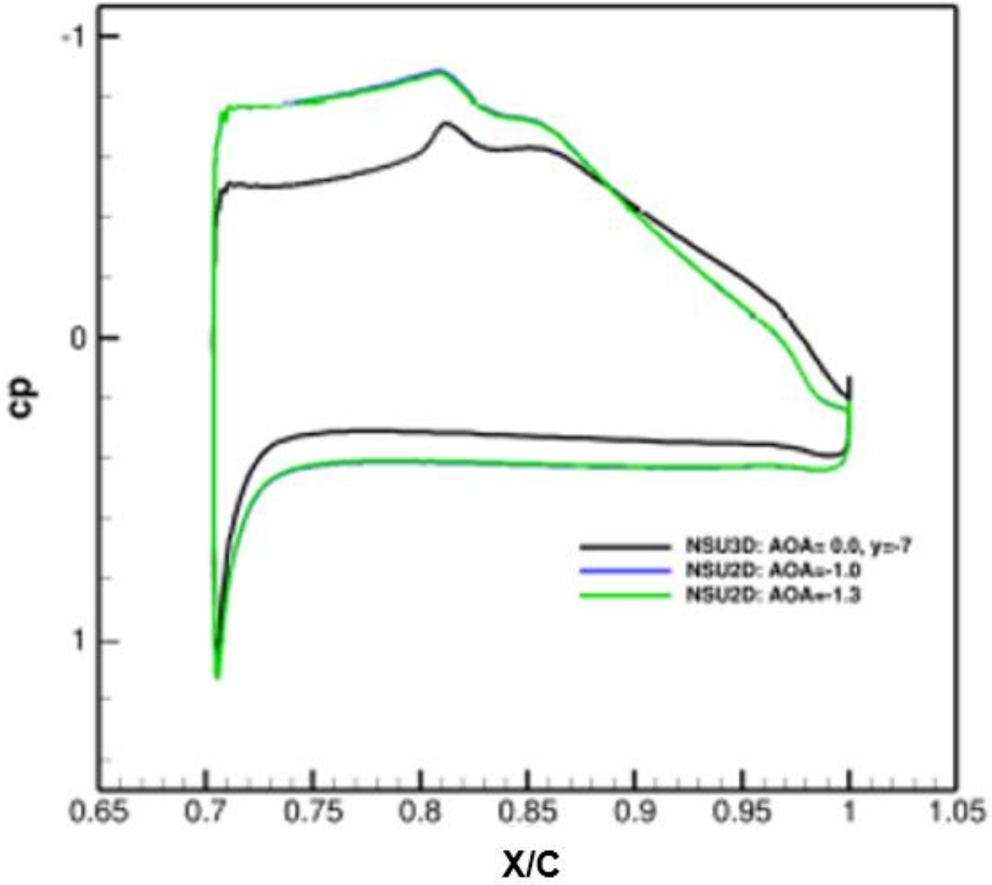

4.3 Results for Configuration 2

- To further investigate the observed early transition on Configuration 2, compute surface pressure profiles at select spanwise location were selected for comparison to 2D surface pressure profiles
  - Analysis performed with fully turbulent results to eliminate need to consider discrepancies between transition prediction models

NSU3D-SA Fully Turbulent Cp Profile at 8.6% Span on Configuration 2 Compared to NSU2D-SA Fully Turbulent Cp Profile

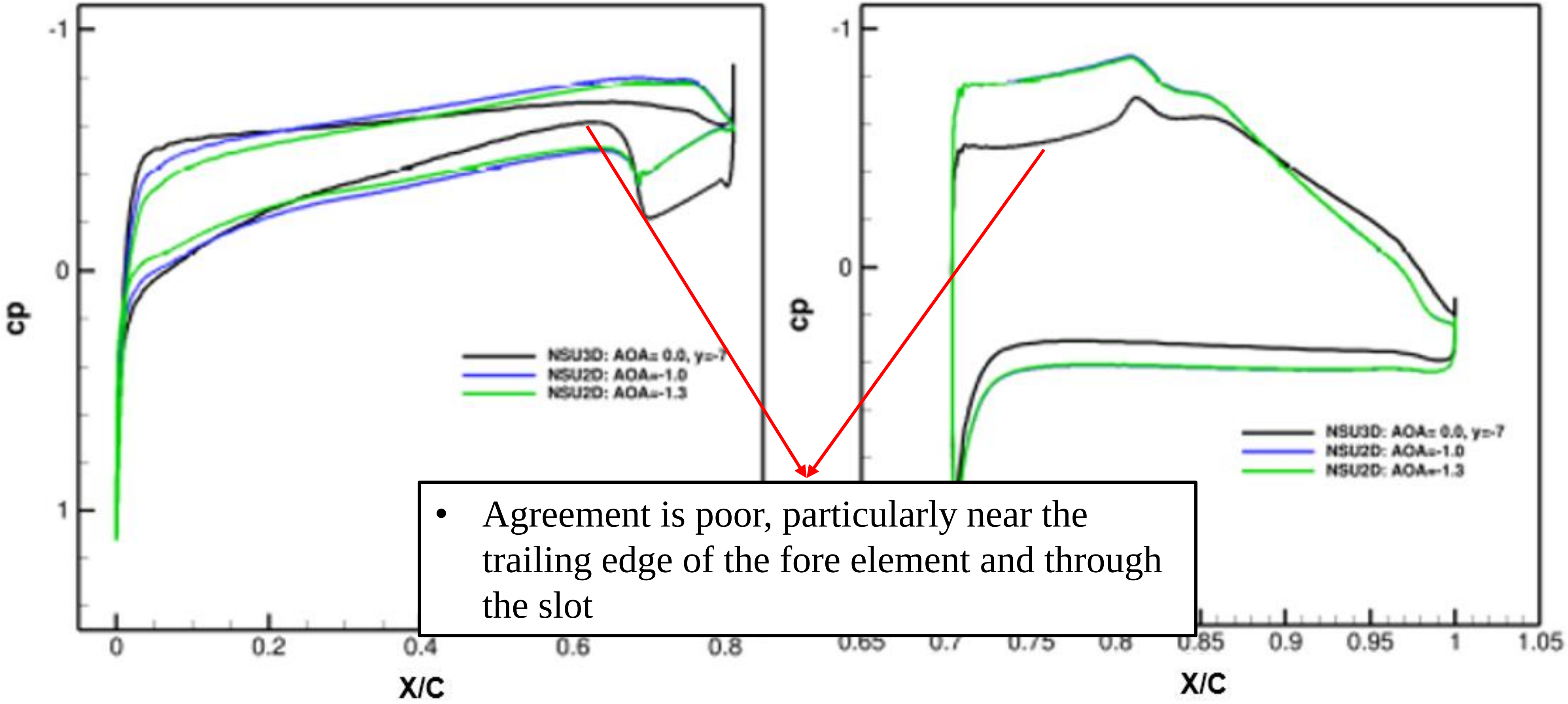

- Agreement is poor, particularly near the trailing edge of the fore element and through the slot

4.3 Results for Configuration 2

- To further investigate the observed early transition on Configuration 2, compute surface pressure profiles at select spanwise location were selected for comparison to 2D surface pressure profiles
  - Analysis performed with fully turbulent results to eliminate need to consider discrepancies between transition prediction models

NSU3D-SA Fully Turbulent Cp Profile at 18.4% Span on Configuration 2 Compared to NSU2D-SA Fully Turbulent Cp Profile

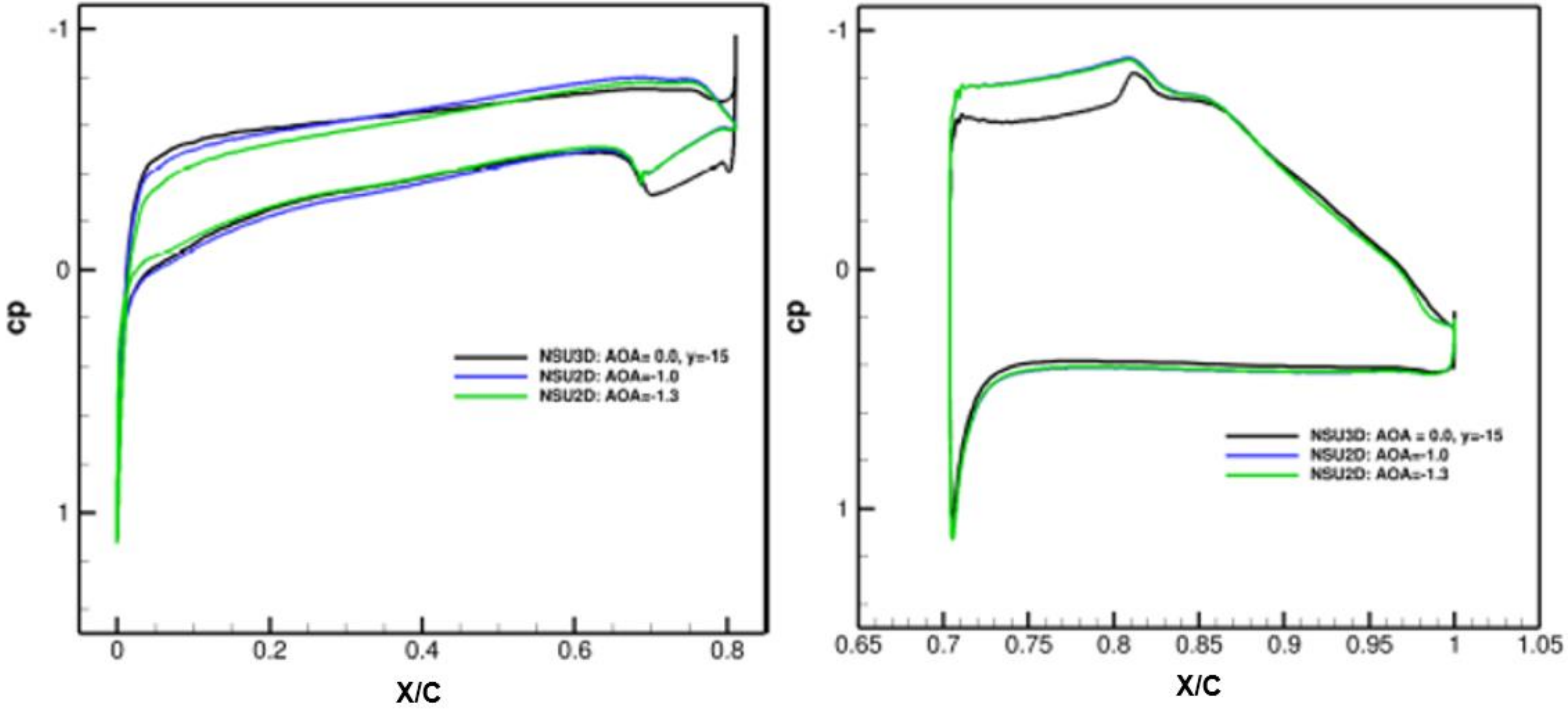

4.3 Results for Configuration 2

- To further investigate the observed early transition on Configuration 2, compute surface pressure profiles at select spanwise location were selected for comparison to 2D surface pressure profiles
  - Analysis performed with fully turbulent results to eliminate need to consider discrepancies between transition prediction models

NSU3D-SA Fully Turbulent Cp Profile at 18.4% Span on Configuration 2 Compared to NSU2D-SA Fully Turbulent Cp Profile

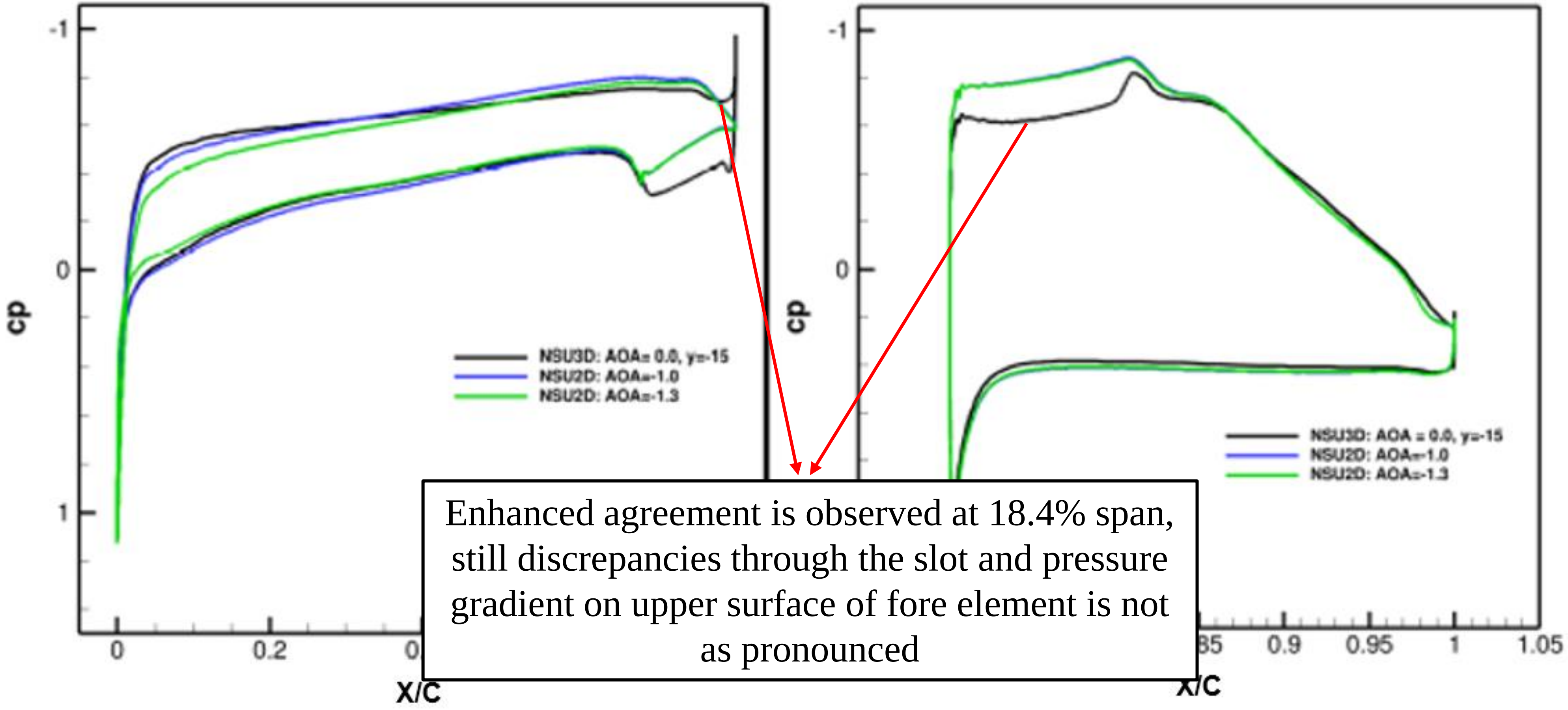

Enhanced agreement is observed at 18.4% span, still discrepancies through the slot and pressure gradient on upper surface of fore element is not as pronounced

4.3 Results for Configuration 2

- To further investigate the observed early transition on Configuration 2, compute surface pressure profiles at select spanwise location were selected for comparison to 2D surface pressure profiles
  - Analysis performed with fully turbulent results to eliminate need to consider discrepancies between transition prediction models

NSU3D-SA Fully Turbulent Cp Profile at 36.9% Span on Configuration 2 Compared to NSU2D-SA Fully Turbulent Cp Profile

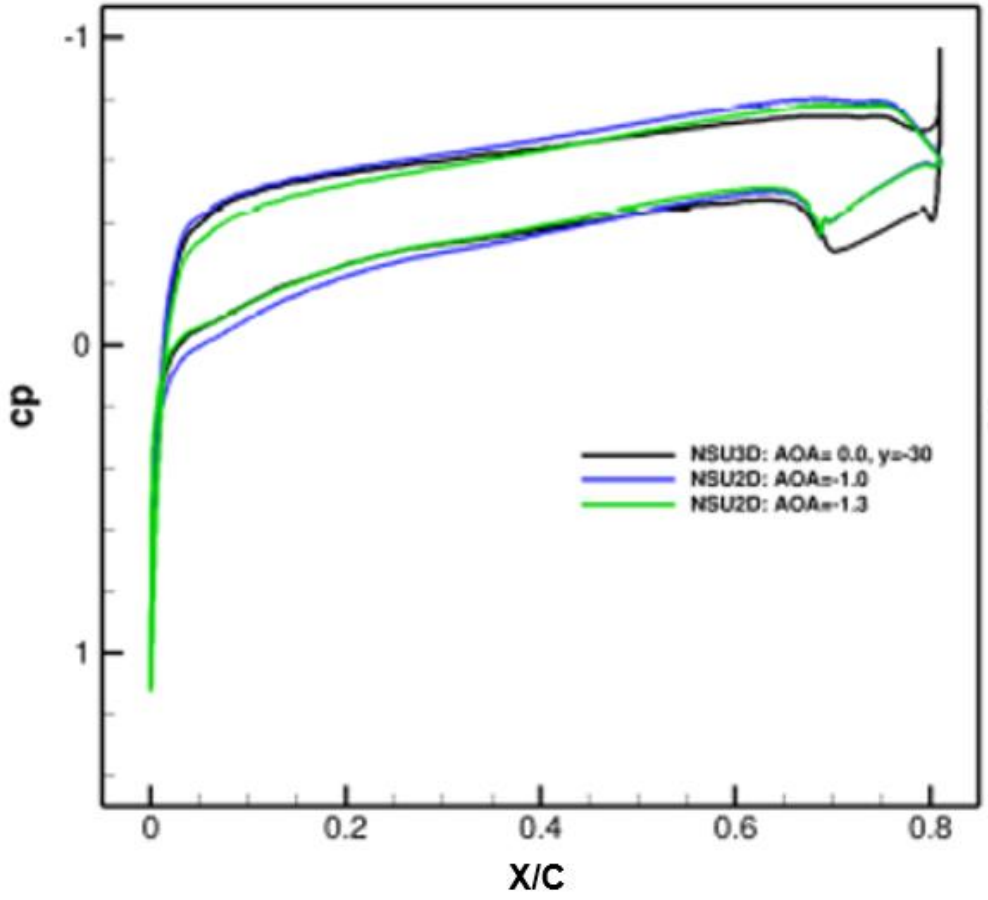

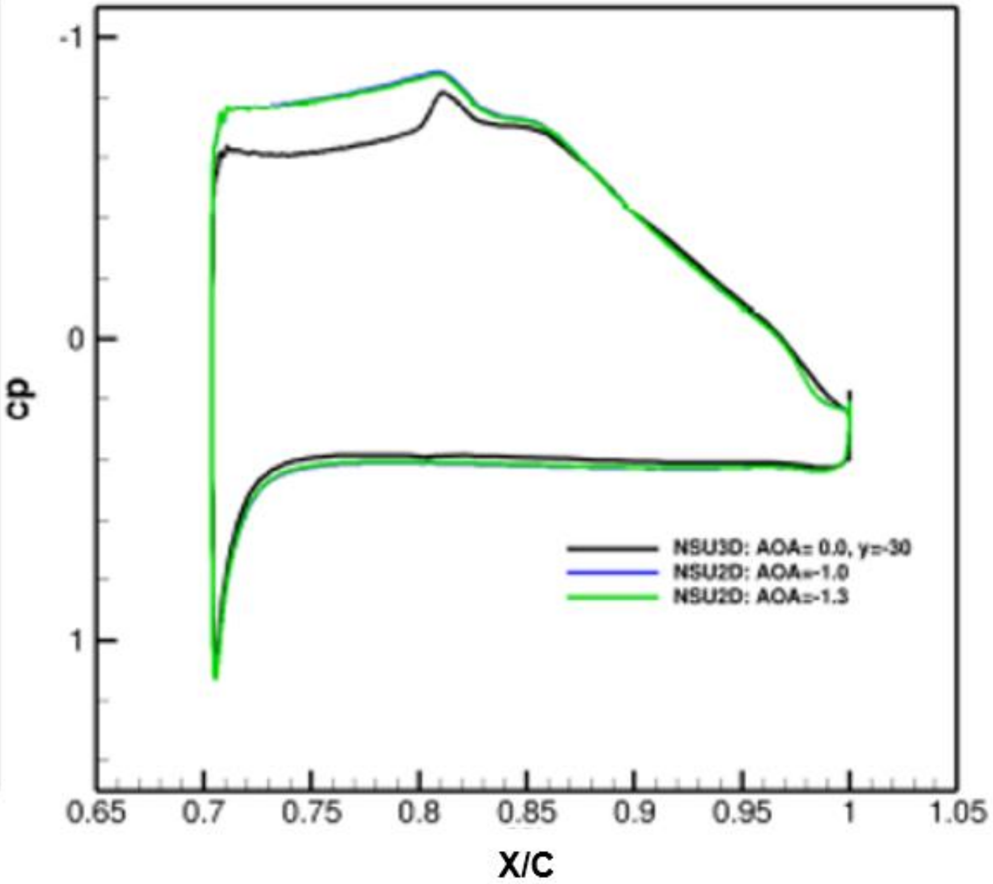

4.3 Results for Configuration 2

- To further investigate the observed early transition on Configuration 2, compute surface pressure profiles at select spanwise location were selected for comparison to 2D surface pressure profiles
  - Analysis performed with fully turbulent results to eliminate need to consider discrepancies between transition prediction models

NSU3D-SA Fully Turbulent Cp Profile at 36.9% Span on Configuration 2 Compared to NSU2D-SA Fully Turbulent Cp Profile

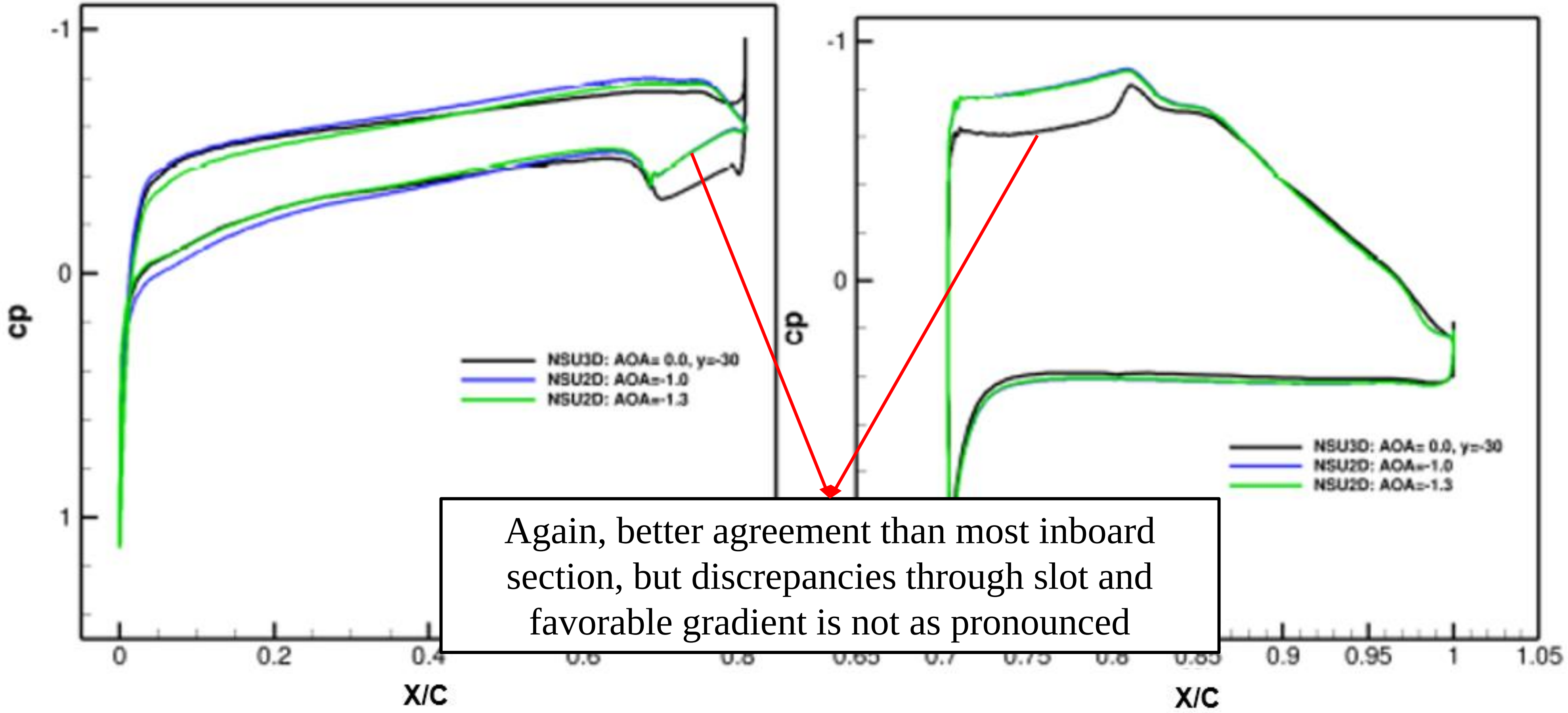

Again, better agreement than most inboard section, but discrepancies through slot and favorable gradient is not as pronounced

5.3 Results for Initial Simulations

- First simulation competed used a fully turbulent approach
  - Establish success in avoiding numerical divergence
  - Gain insight to computation time given the size of the grid

Convergence History for Wind Tunnel Model at Mach = 0.700, AOA=0.0, Re=12 Million

5.3 Results for Initial Simulations

- First simulation competed used a fully turbulent approach
  - Establish success in avoiding numerical divergence
  - Gain insight to computation time given the size of the grid

Convergence History for Wind Tunnel Model at Mach = 0.700, AOA=0.0, Re=12 Million

- Plot takes a significantly long time to converge, as it is still in the process at 10000 cycles

5.3 Results for Initial Simulations

- First simulation competed used a fully turbulent approach
  - Establish success in avoiding numerical divergence
  - Gain insight to computation time given the size of the grid

Convergence History for Wind Tunnel Model at Mach = 0.700, AOA=0.0, Re=12 Million

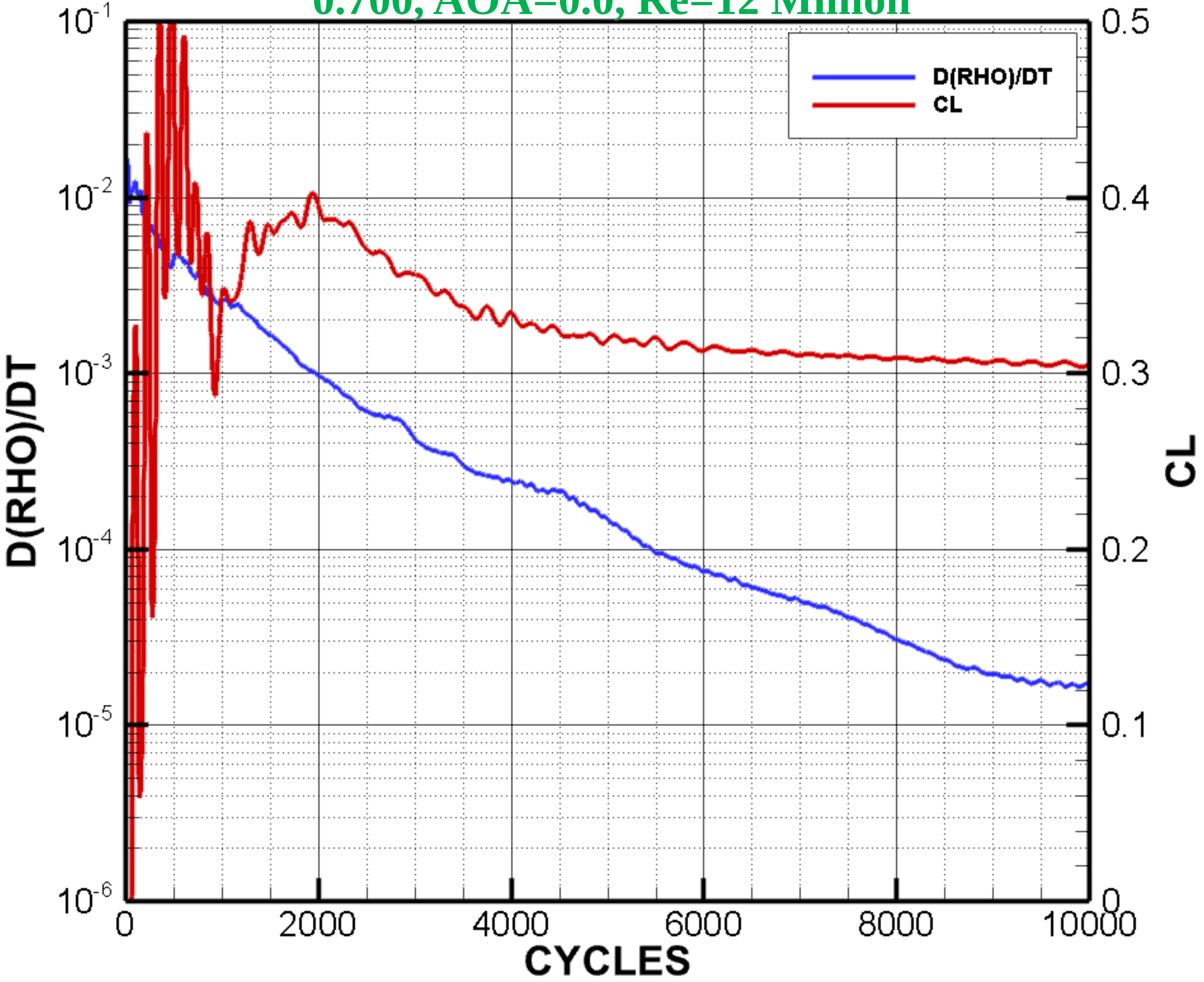

- Plot takes a significantly long time to converge, as it is still in the process at 10000 cycles

- Behavior can be expected to be more severe when the transition prediction model is used

5.3 Results for Initial Simulations

- In anticipation of the increased computational time and to ensure changes in CFL did not impact the transition line, a numerical effort was undertaken in which three transition simulations were completed
  - N_{crit} value of 8.4 (Tu_{inf} roughly of 0.07%)
  - Denoted Simulations 1, 2, 3
  - Mach = 0.7, AOA = 0.0, Re = 12 Million

Wind Tunnel Cruise Simulations Summary

Case	CFL	Initial Condition	Total Cycles	CL	CD
Baseline	2	Freestream	10000	0.4260	0.02947
Simulation 1	10	Baseline	10000	0.3230	0.02715
Simulation 2	25	Baseline	10000	0.3214	0.02731
Simulation 3	2	Baseline	32000	0.3254	0.02696

5.3 Results for Initial Simulations

- In anticipation of the increased computational time and to ensure changes in CFL did not impact the transition line, a numerical effort was undertaken in which three transition simulations were completed
  - N_{crit} value of 8.4 (Tu_{inf} roughly of 0.07%)
  - Denoted Simulations 1, 2, 3
  - Mach = 0.7, AOA = 0.0, Re = 12 Million

Wind Tunnel Cruise Simulations Summary

Case	CFL	Initial Condition	Total Cycles	CL	CD
Baseline	2	Freestream	10000	0.4260	0.02947
Simulation 1	10	Baseline	10000	0.3230	0.02715
Simulation 2	25	Baseline	10000	0.3214	0.02731
Simulation 3	2	Baseline	32000	0.3254	0.02696

- Numerical divergence was observed for CFL number greater than 2 if initial condition was freestream values
- Baseline served as an initial condition for cases with higher CFL to avoid this

5.3 Results for Initial Simulations

Density Residual Convergence History for N_{crit}=8.4 Wind Tunnel Model Simulations

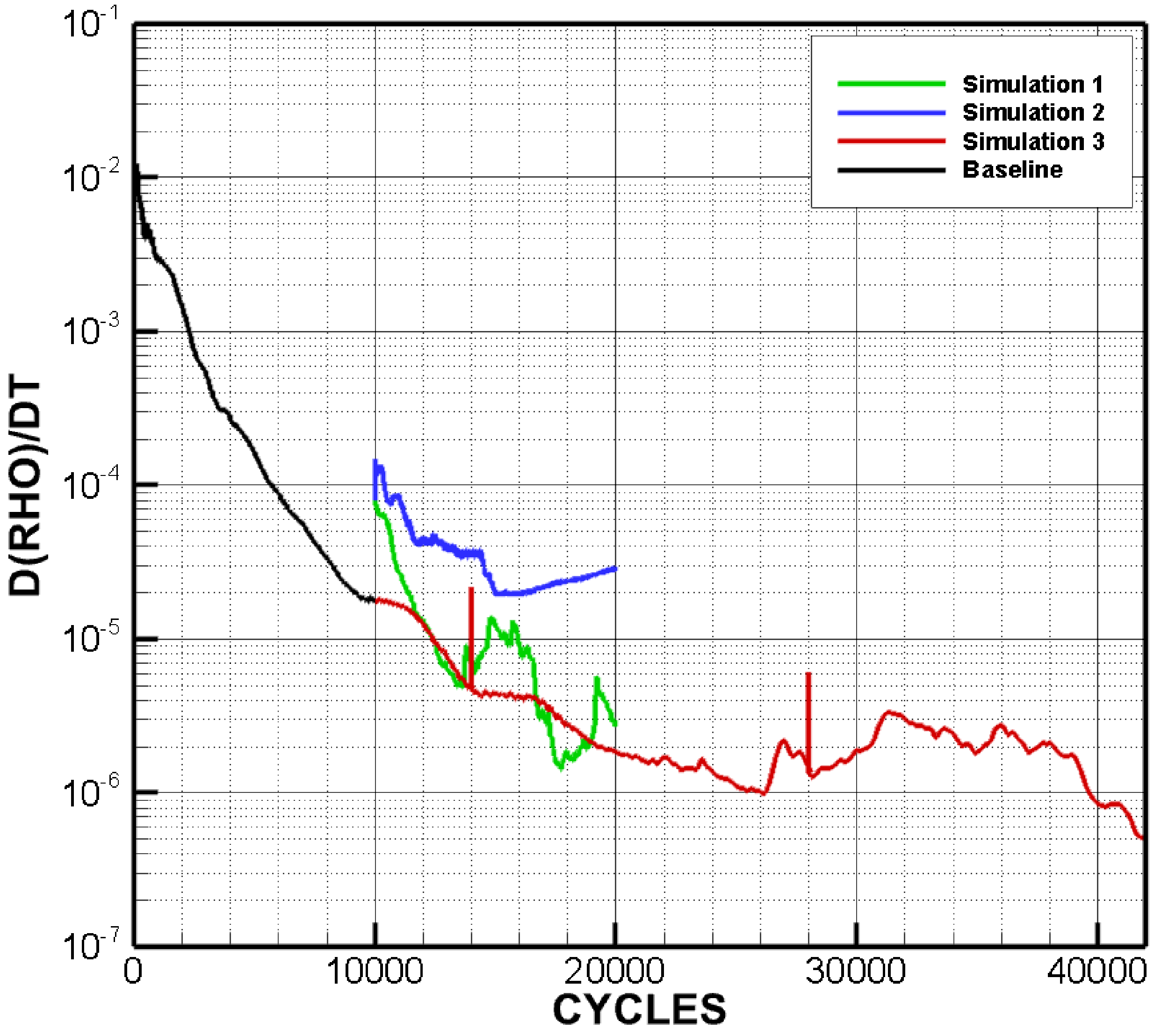

Lift Coefficient Convergence History for N_{crit}=8.4 Wind Tunnel Model Simulations

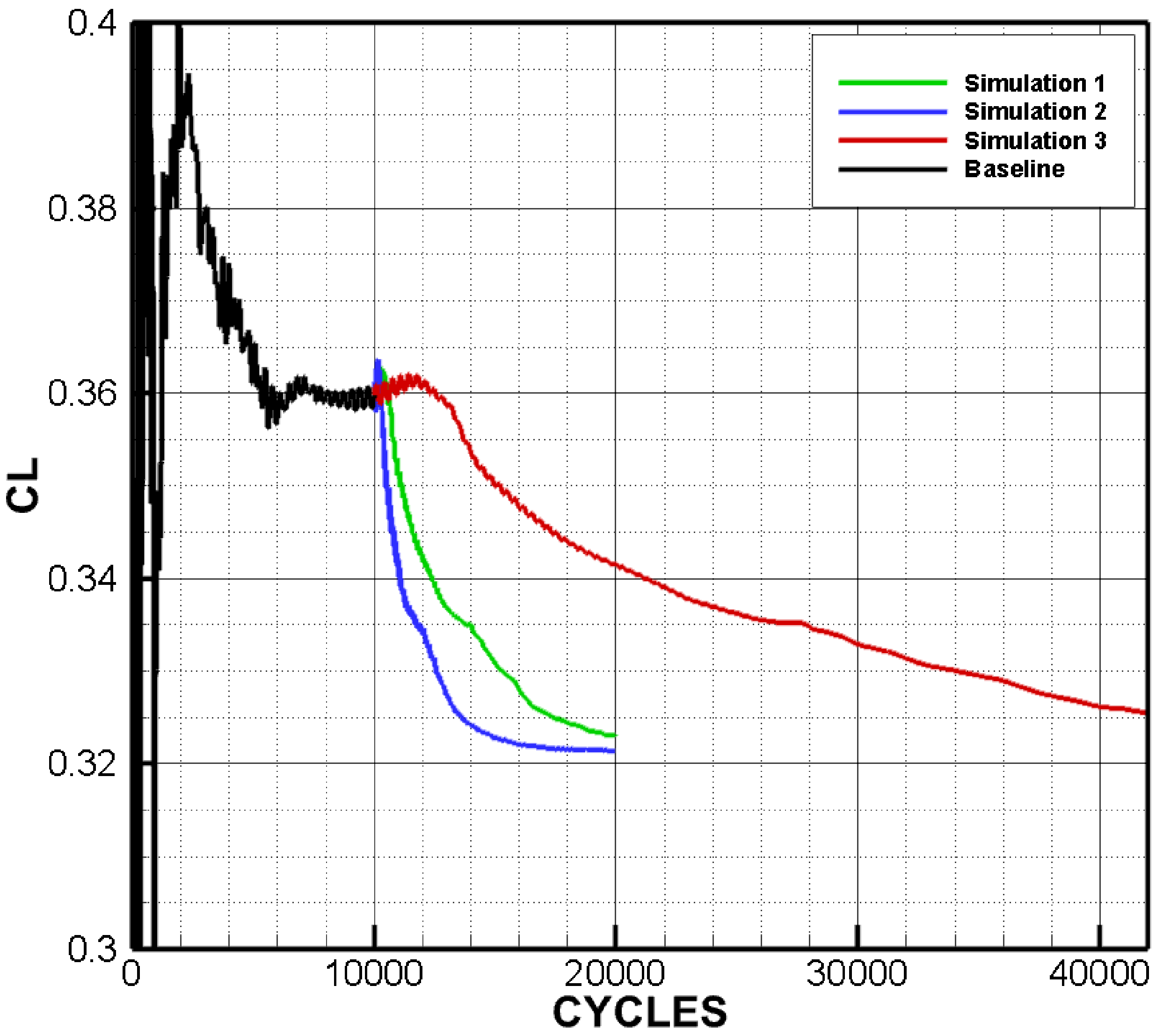

5.3 Results for Initial Simulations

Density Residual Convergence History for N_{crit}=8.4 Wind Tunnel Model Simulations

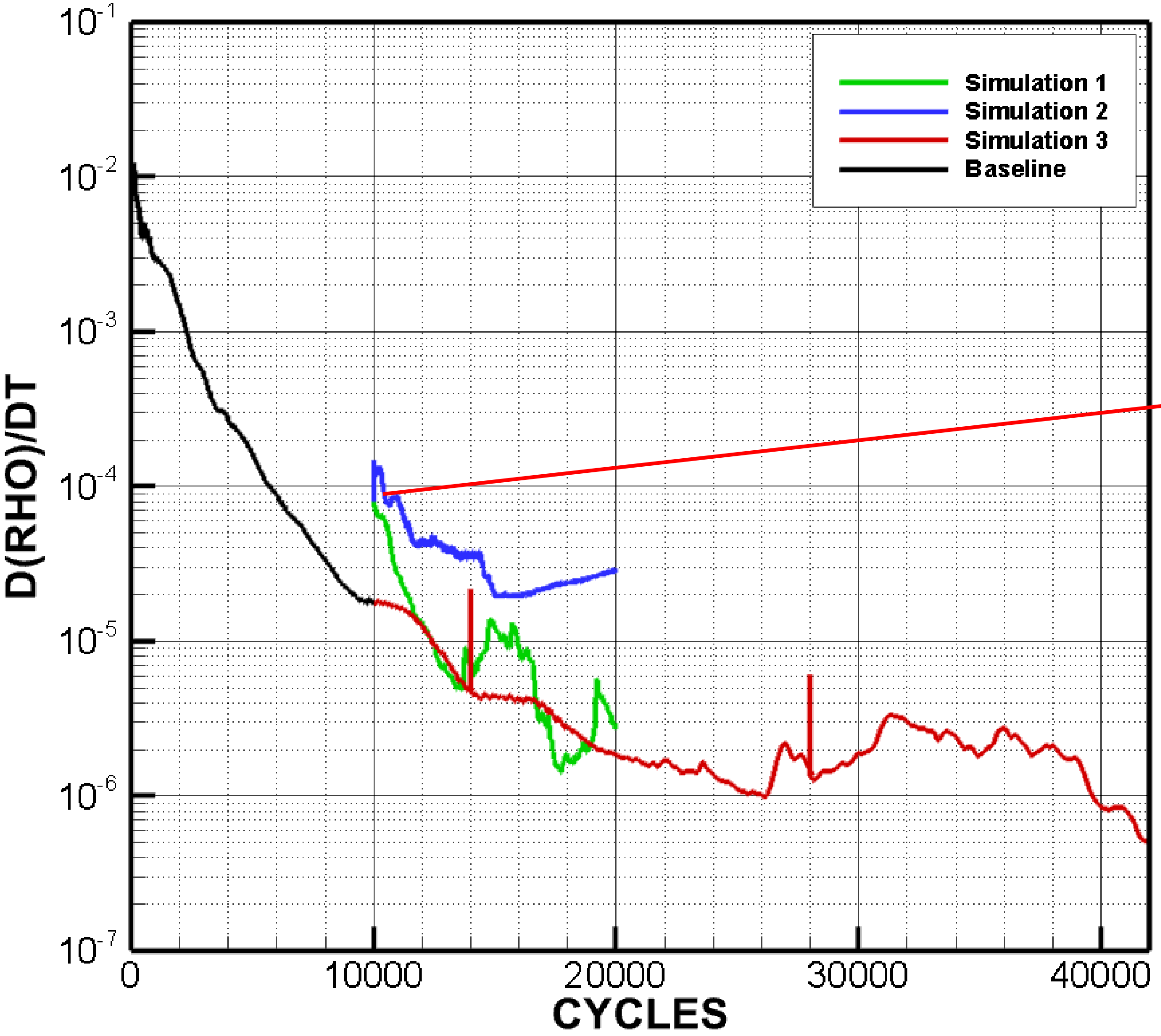

Lift Coefficient Convergence History for N_{crit}=8.4 Wind Tunnel Model Simulations

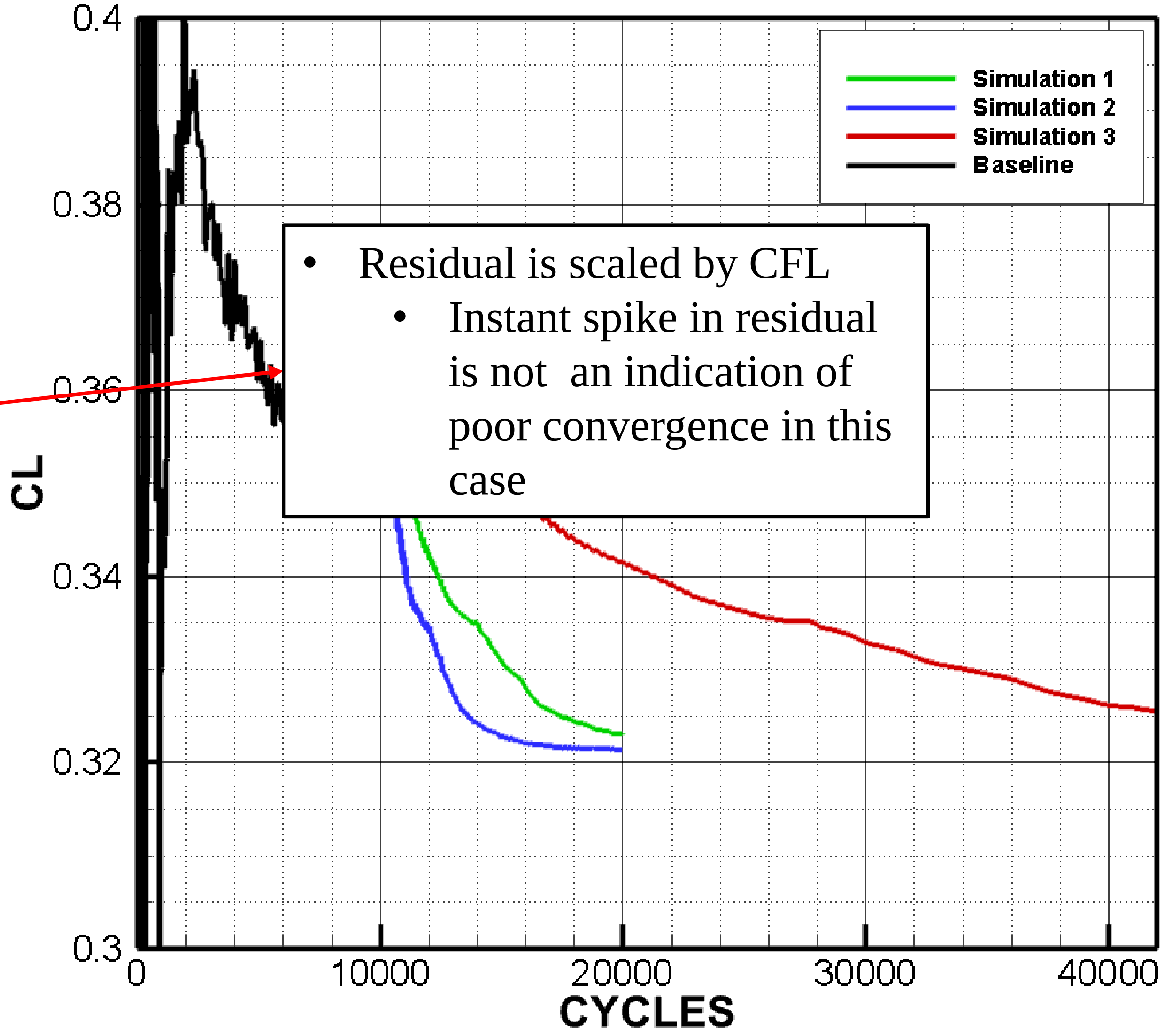

5.3 Results for Initial Simulations

Density Residual Convergence History for N_{crit}=8.4 Wind Tunnel Model Simulations

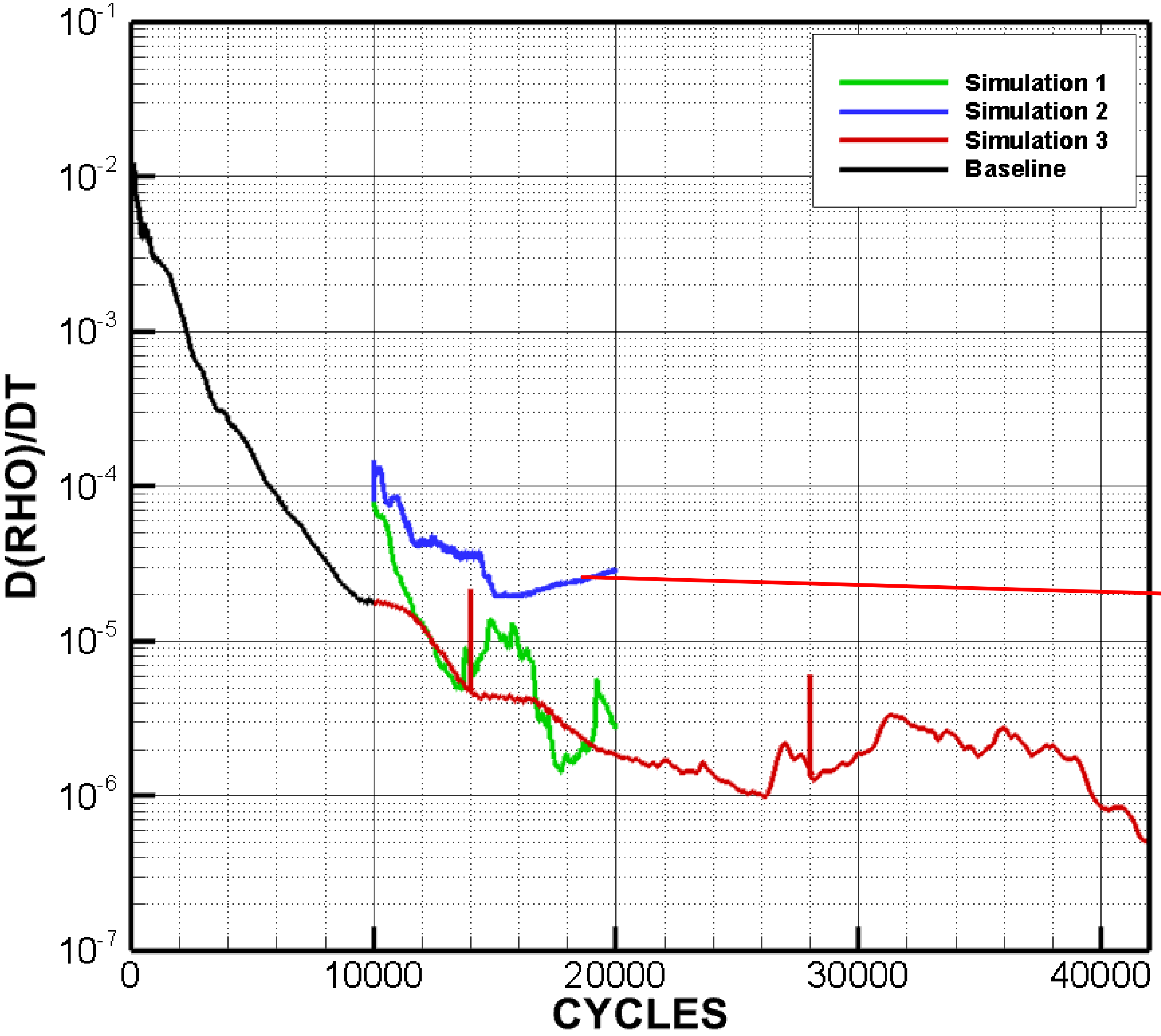

Lift Coefficient Convergence History for N_{crit}=8.4 Wind Tunnel Model Simulations

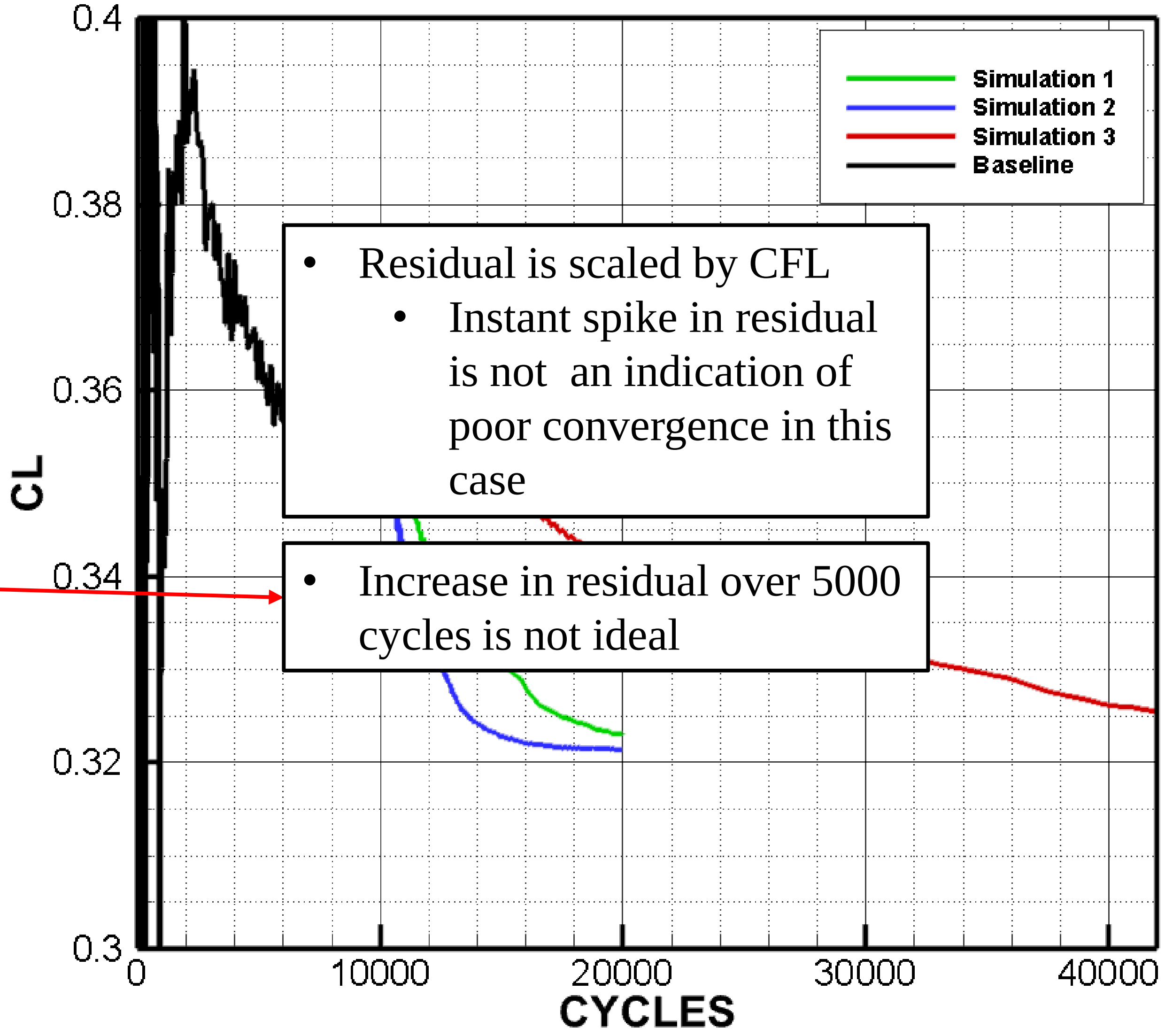

- Residual is scaled by CFL
  - Instant spike in residual is not an indication of poor convergence in this case

- Increase in residual over 5000 cycles is not ideal

5.3 Results for Initial Simulations

Case	CFL	Initial Condition	Total Cycles	CL	CD
Baseline	2	Freestream	10000	0.4260	0.02947
Simulation 1	10	Baseline	10000	0.3230	0.02715
Simulation 2	25	Baseline	10000	0.3214	0.02731
Simulation 3	2	Baseline	32000	0.3254	0.02696

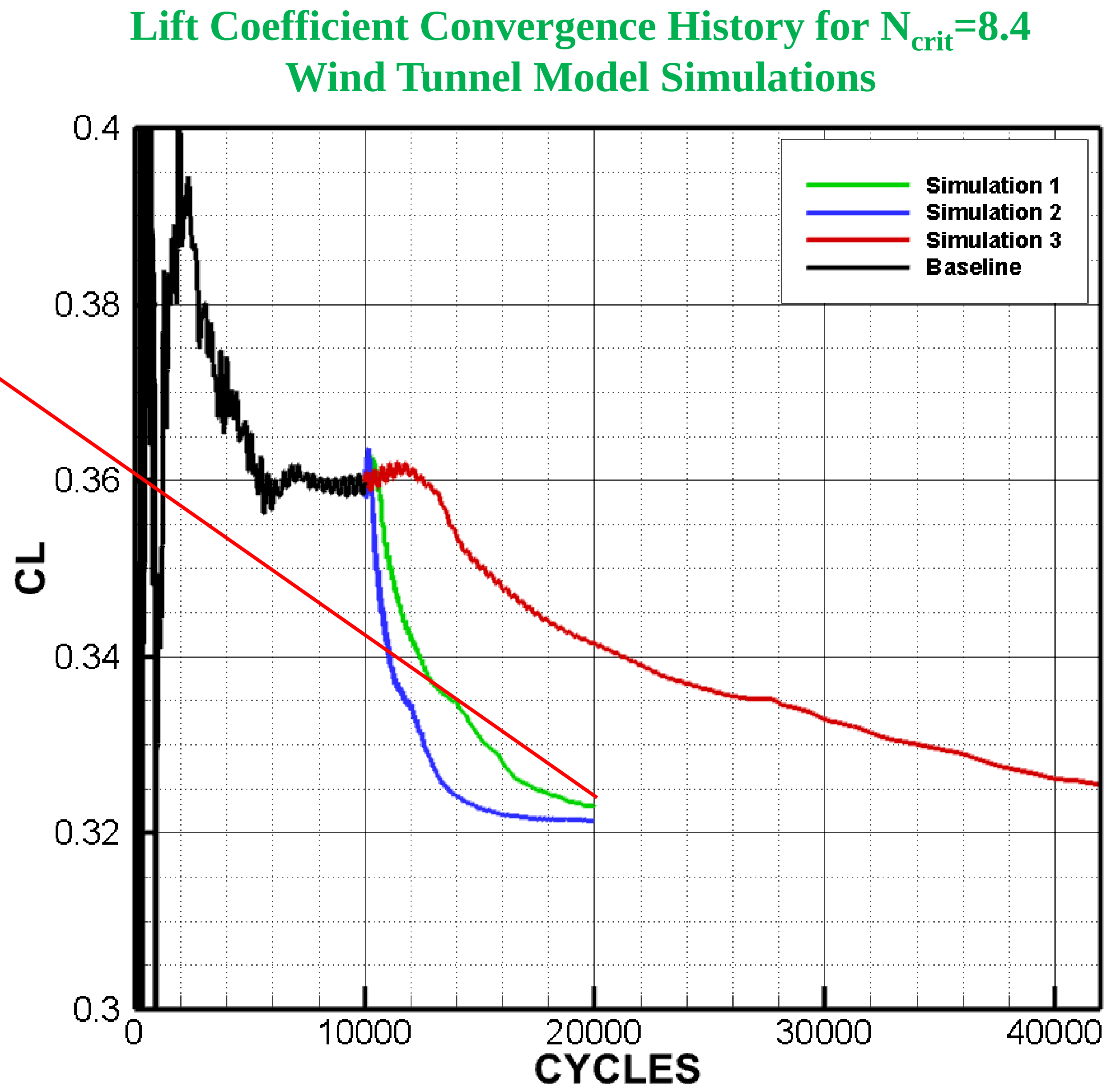

5.3 Results for Initial Simulations

Case	CFL	Initial Condition	Total Cycles	CL	CD
Baseline	2	Freestream	10000	0.4260	0.02947
Simulation 1	10	Baseline	10000	0.3230	0.02715
Simulation 2	25	Baseline	10000	0.3214	0.02731
Simulation 3	2	Baseline	32000	0.3254	0.02696

- All solutions converge to roughly the same lift and drag values indicating that the change in CFL does not significantly impact the solution

Lift Coefficient Convergence History for N_{crit}=8.4
Wind Tunnel Model Simulations

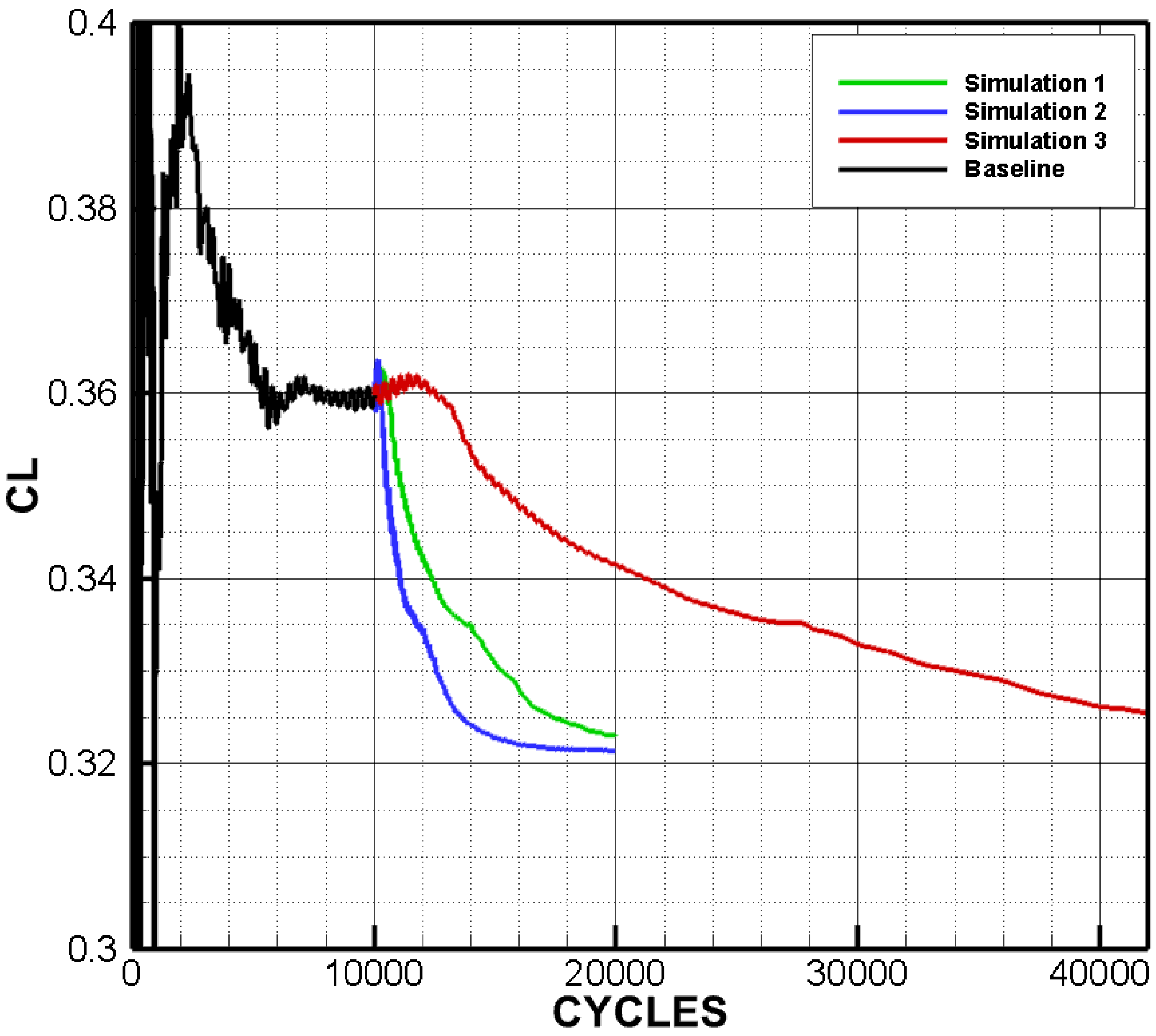

5.3 Results for Initial Simulations

- Skin friction drag results indicate that the transition line moves upstream very slowly as the simulation evolves

NSU3D-SA-AFT2 Free Trans
Friction Drag Prof

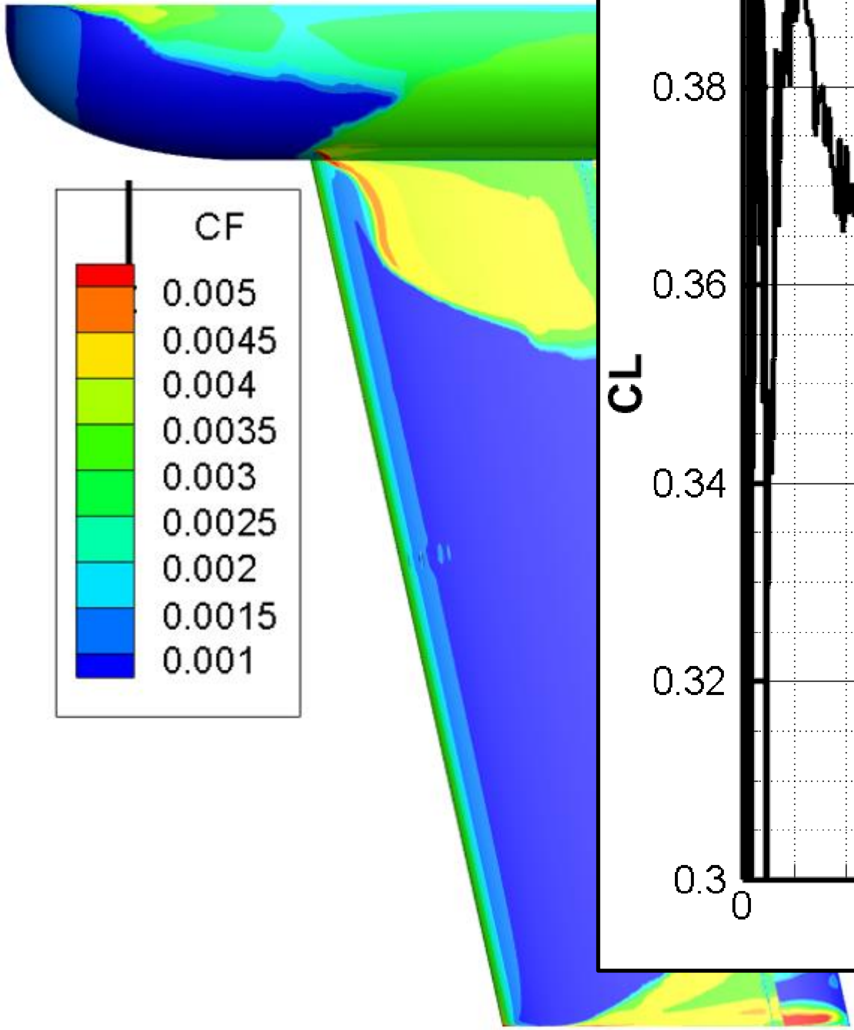

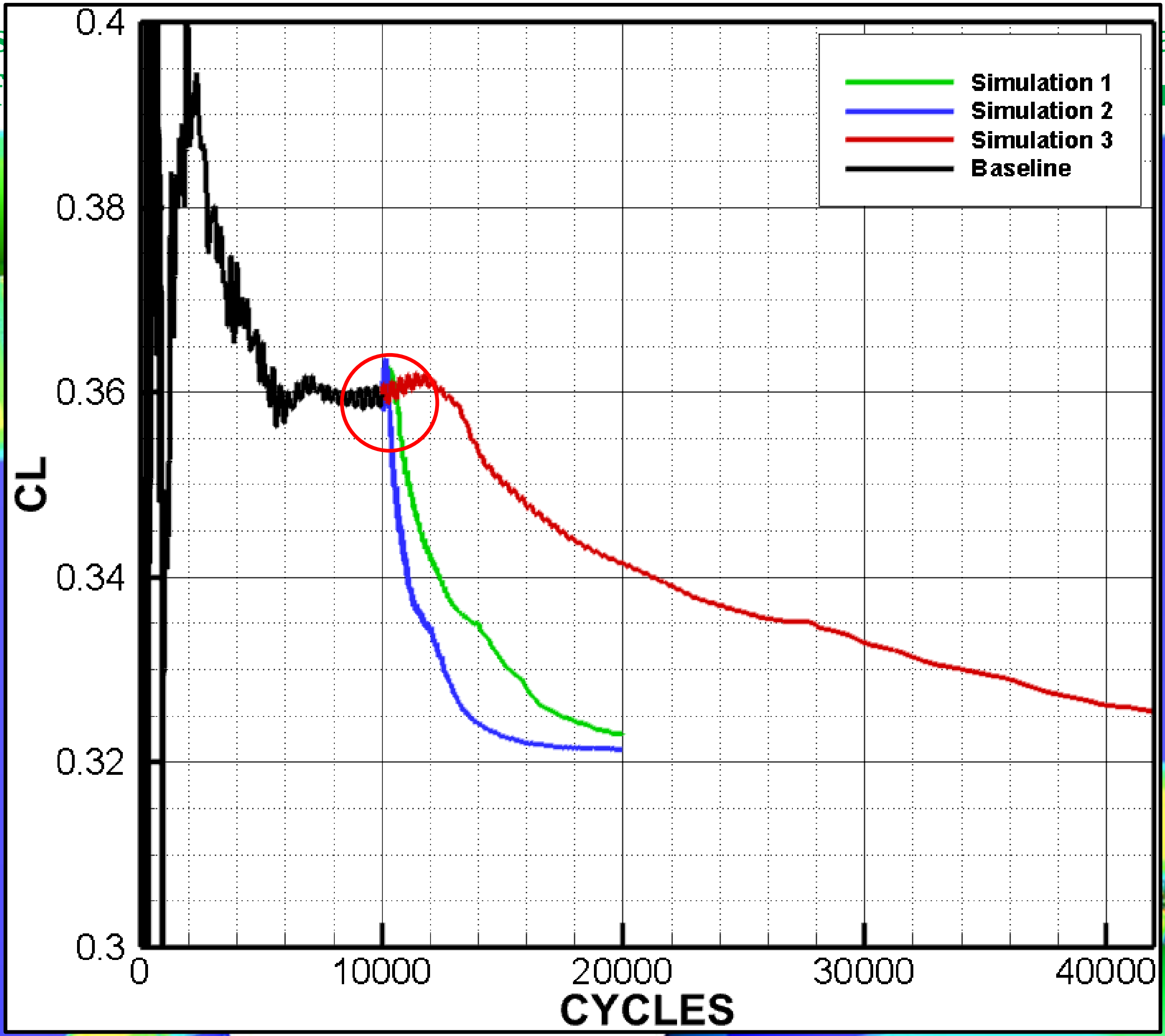

ansition Lower Surface Skin
rofile for Baseline

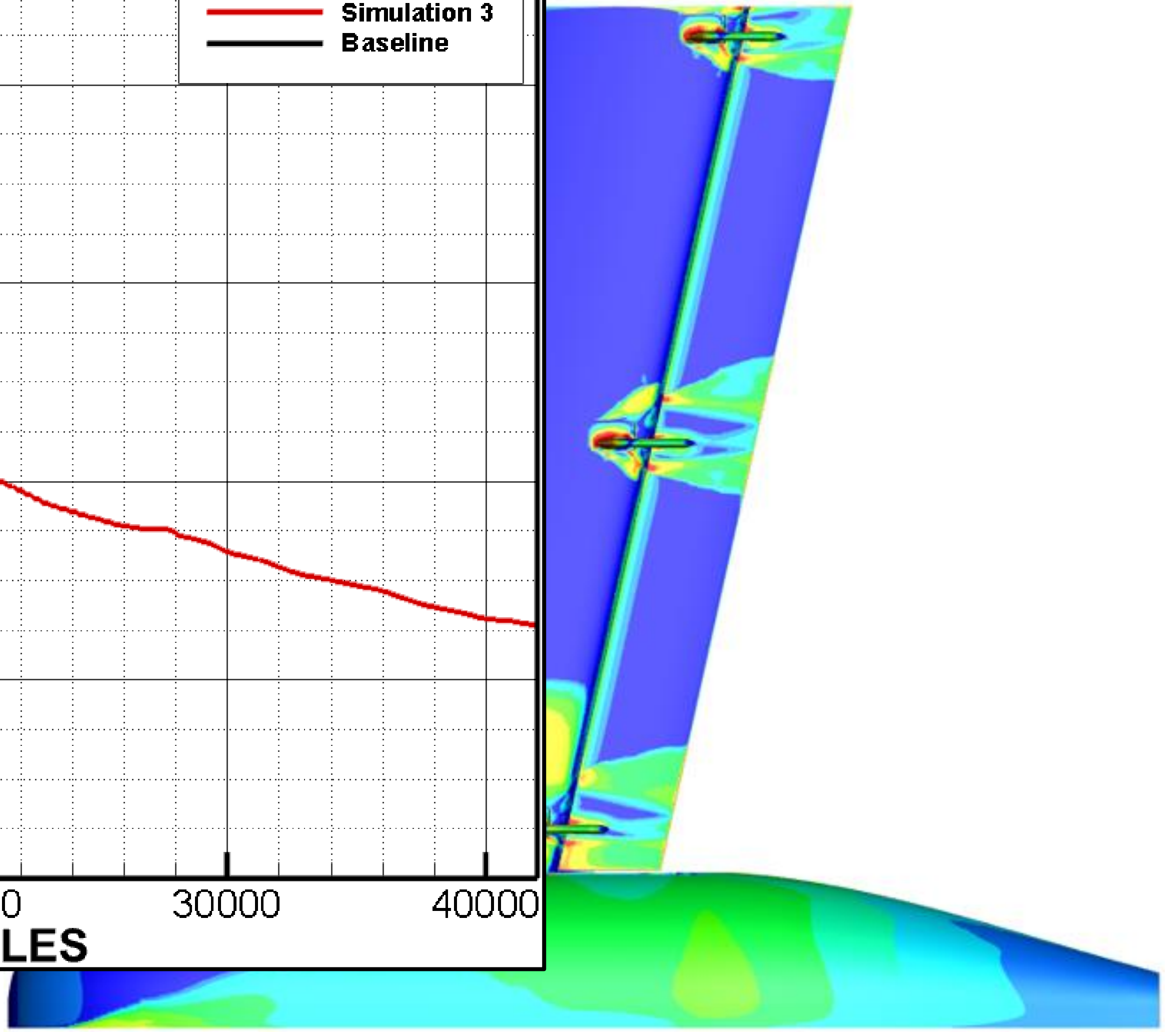

5.3 Results for Initial Simulations

- Skin friction drag results indicate that the transition line moves upstream very slowly as the simulation evolves

NSU3D-SA-AFT2 Free Transition Upper Surface Skin Friction Drag Profile for Baseline

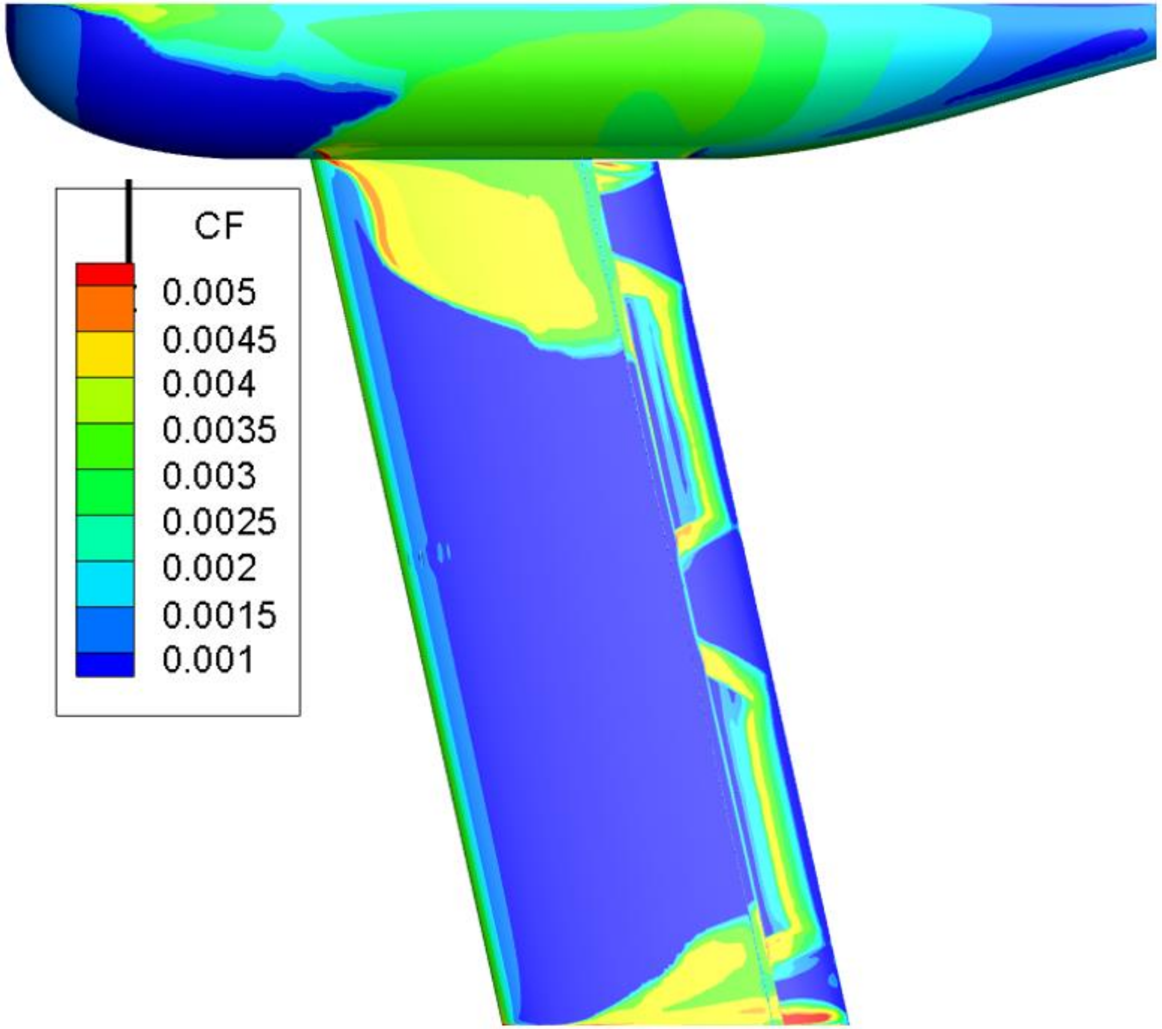

NSU3D-SA-AFT2 Free Transition Lower Surface Skin Friction Drag Profile for Baseline

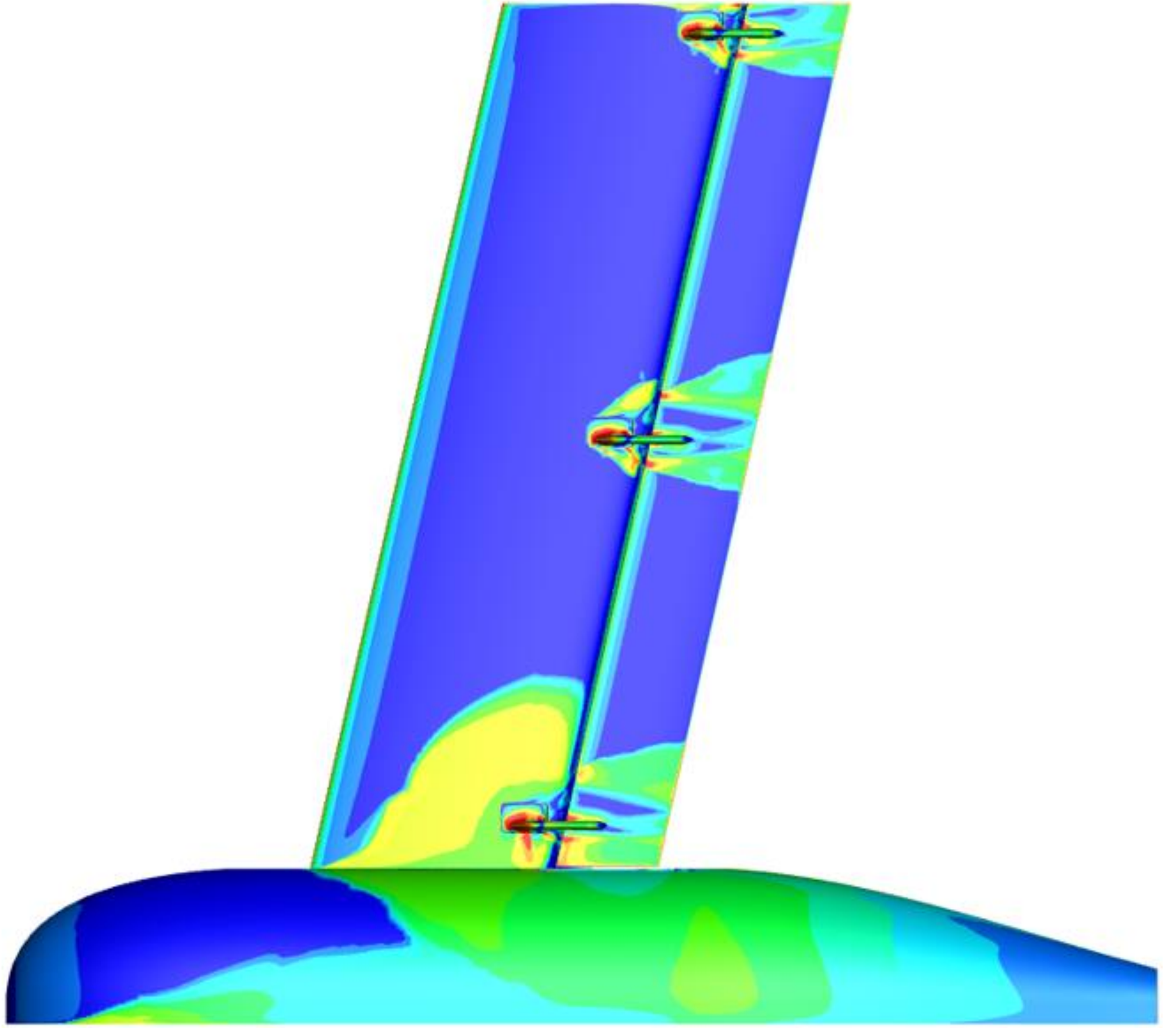

5.3 Results for Initial Simulations

- Skin friction drag results indicate that the transition line moves upstream very slowly as the simulation evolves

NSU3D-SA-AFT2 Free Transiti
Friction Drag Profile fo

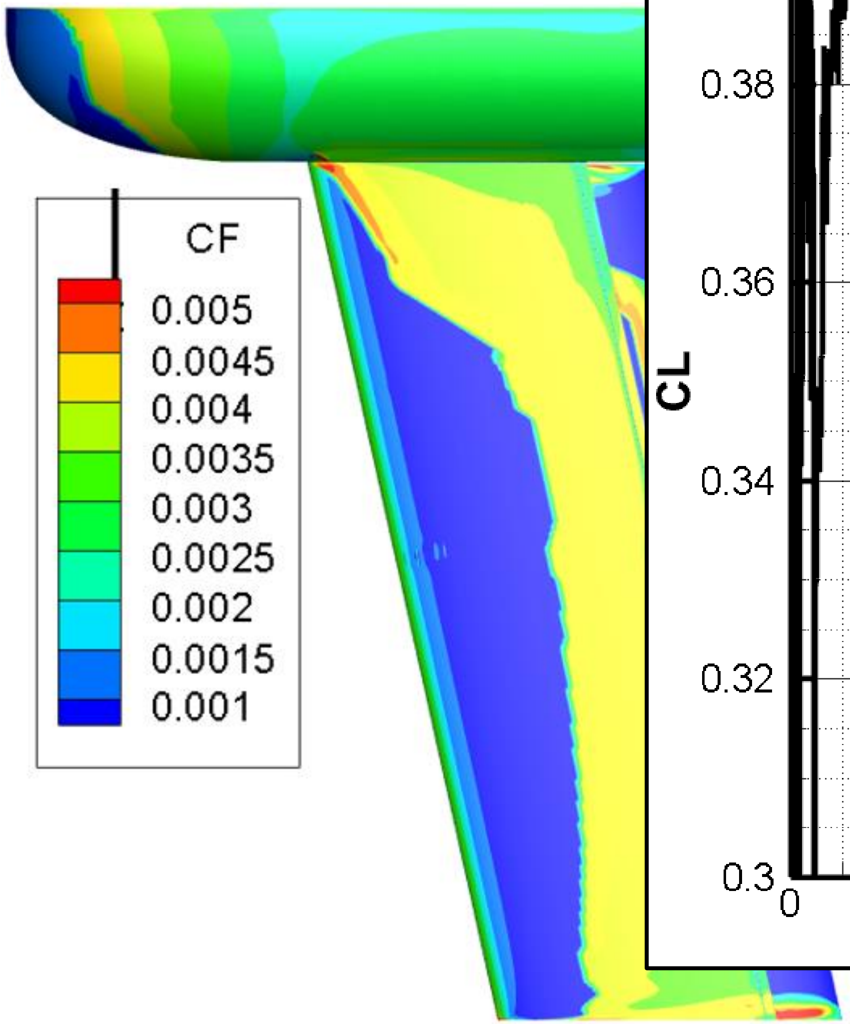

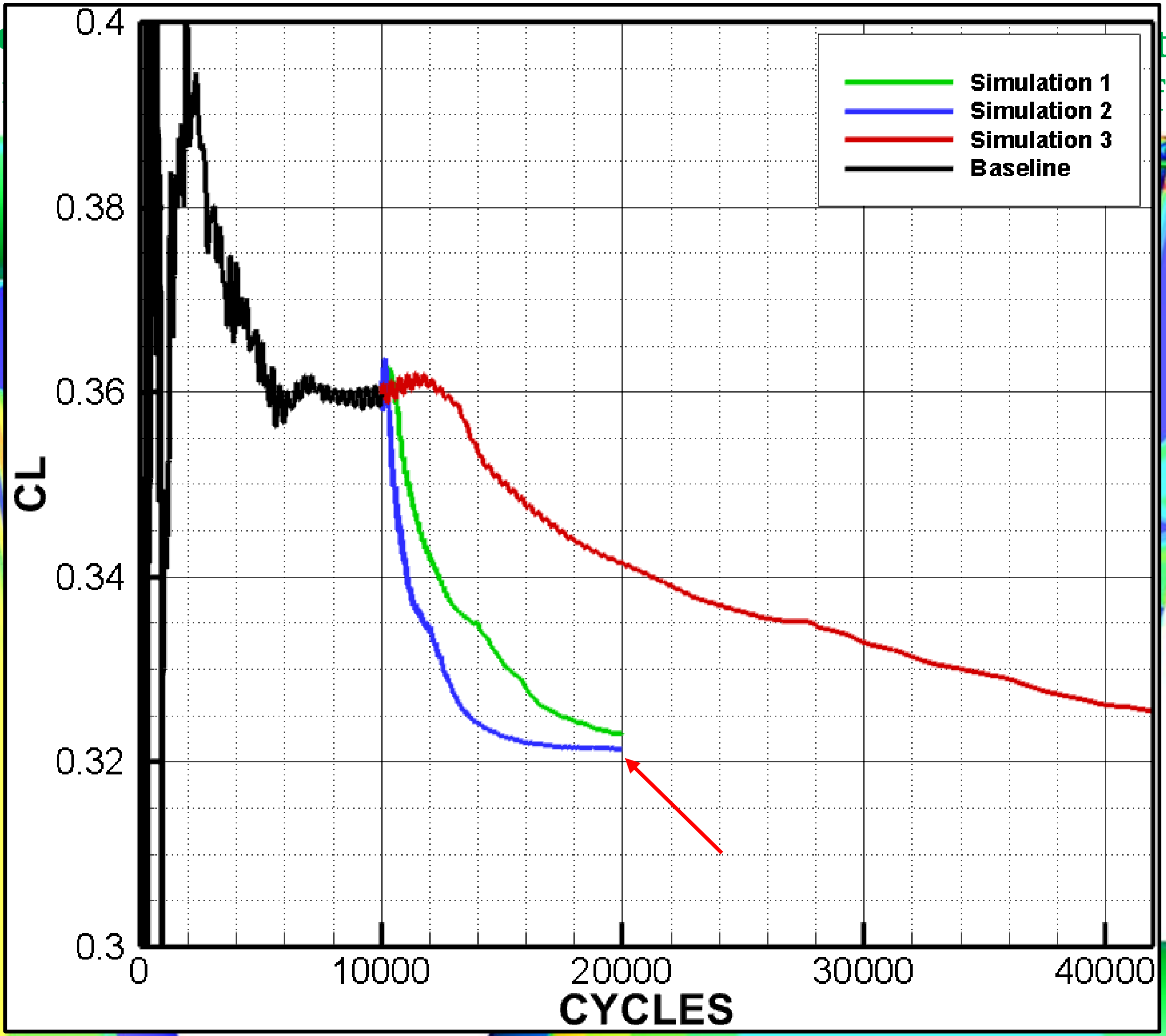

tion Lower Surface Skin
for Simulation 1

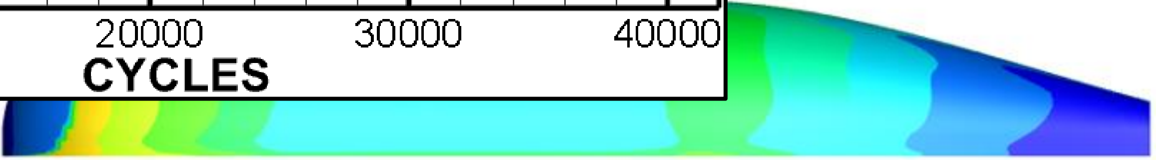

5.3 Results for Initial Simulations

- Skin friction drag results indicate that the transition line moves upstream very slowly as the simulation evolves

NSU3D-SA-AFT2 Free Transition Upper Surface Skin Friction Drag Profile for Simulation 1

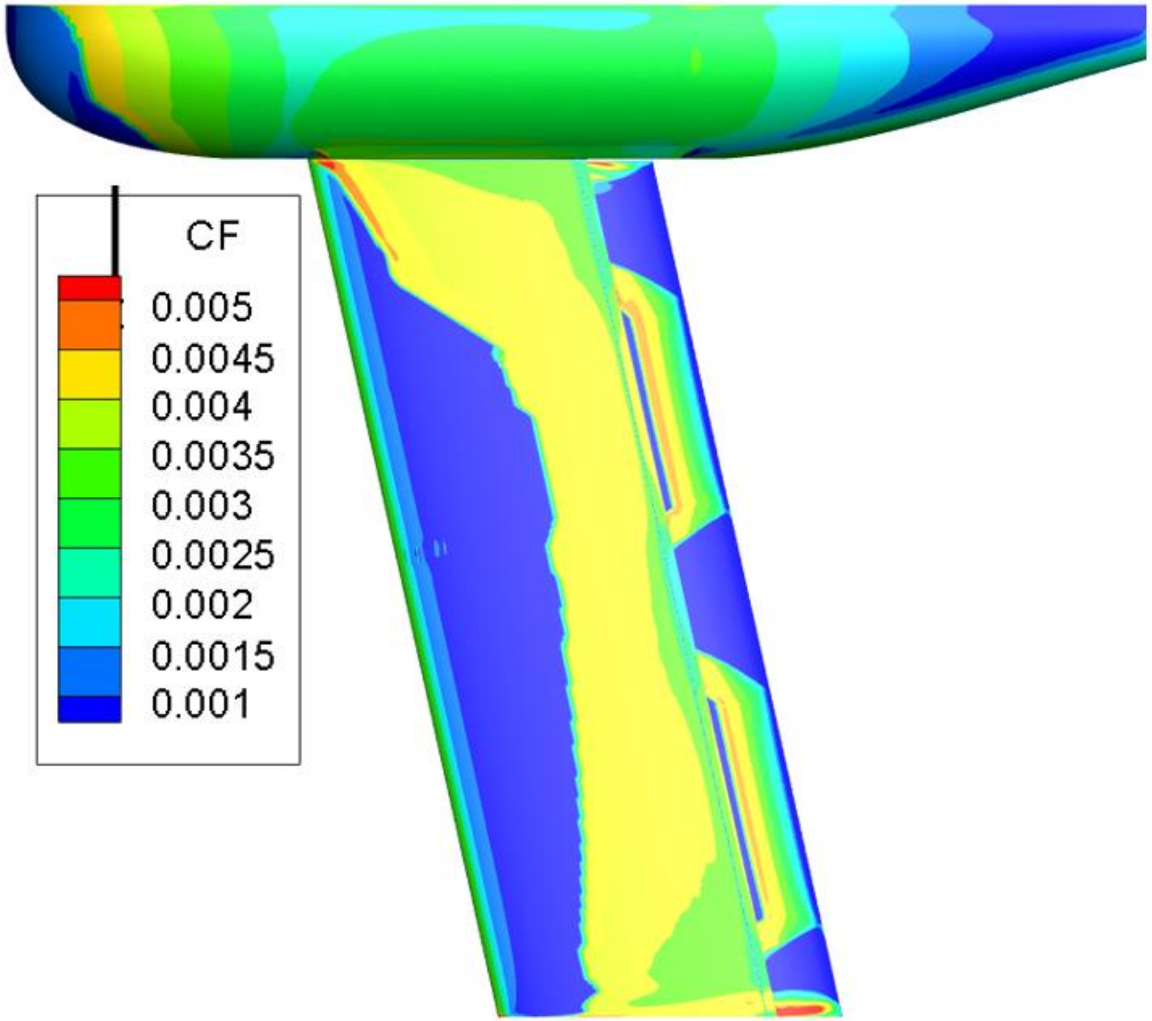

NSU3D-SA-AFT2 Free Transition Lower Surface Skin Friction Drag Profile for Simulation 1

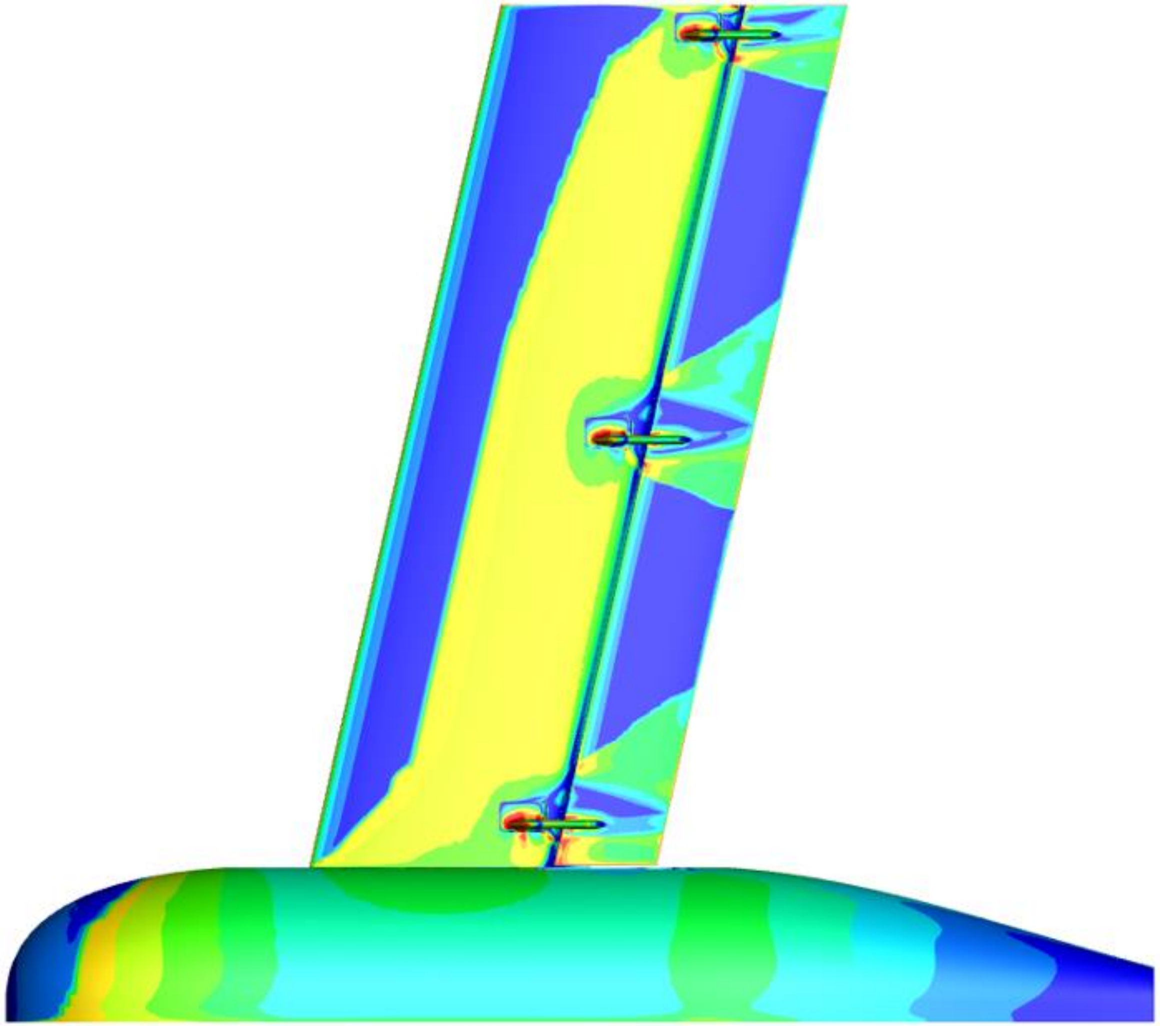

5.3 Results for Initial Simulations

- Skin friction drag results indicate that the transition line moves upstream very slowly as the simulation evolves

NSU3D-SA-AFT2 Free Tran
Friction Drag Profil

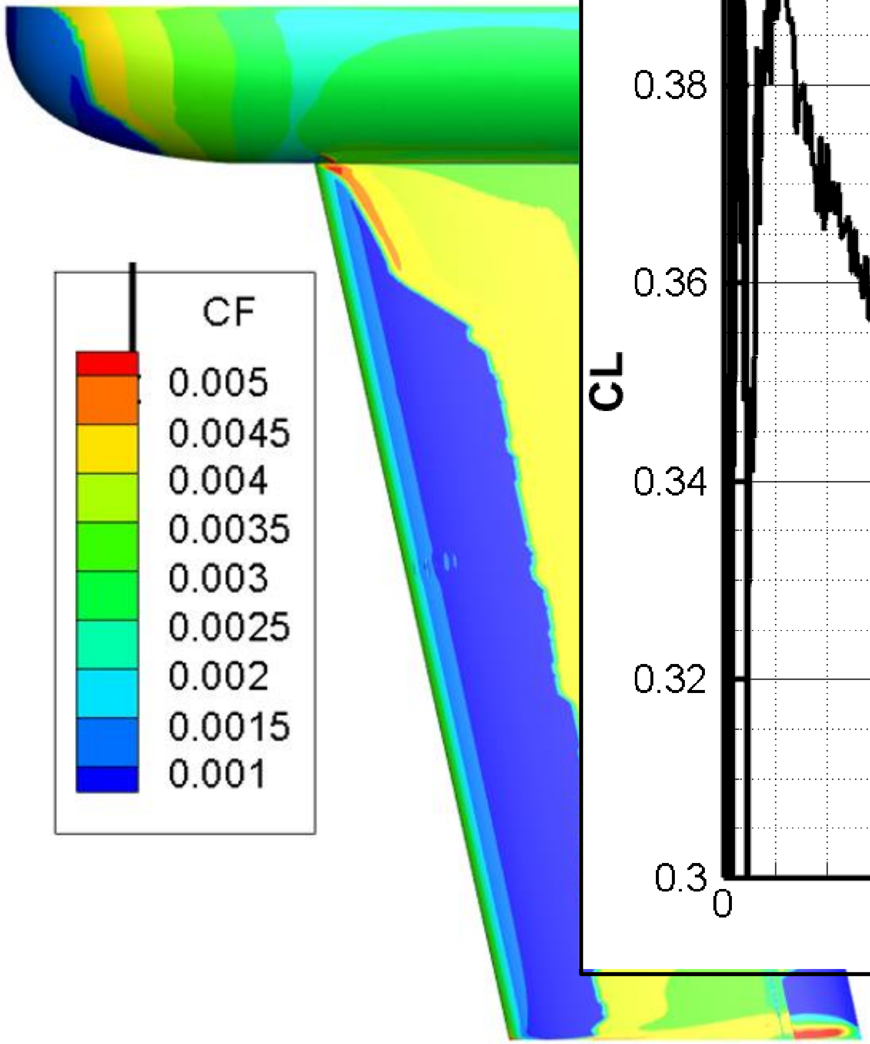

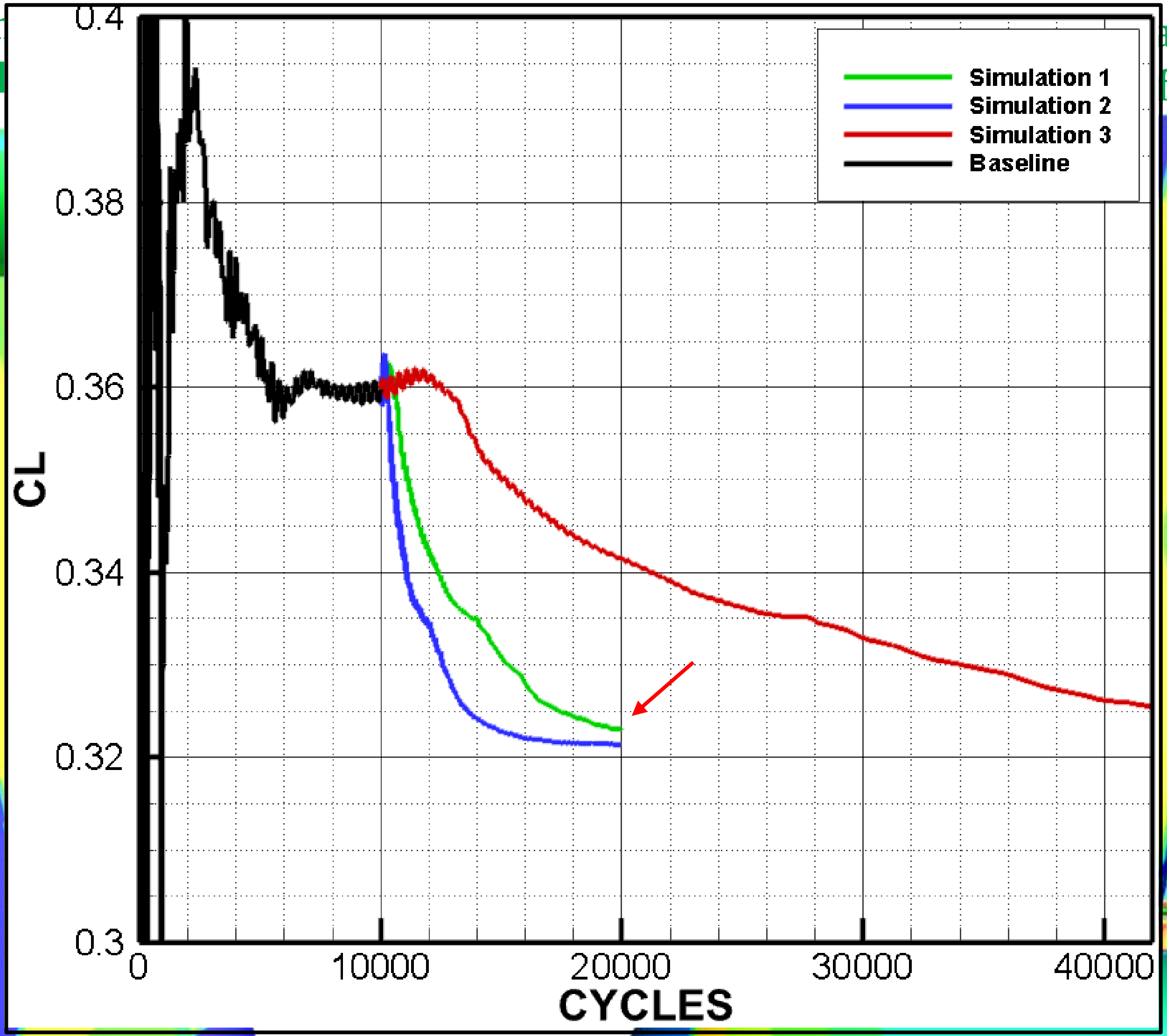

ansition Lower Surface Skin
file for Simulation 2

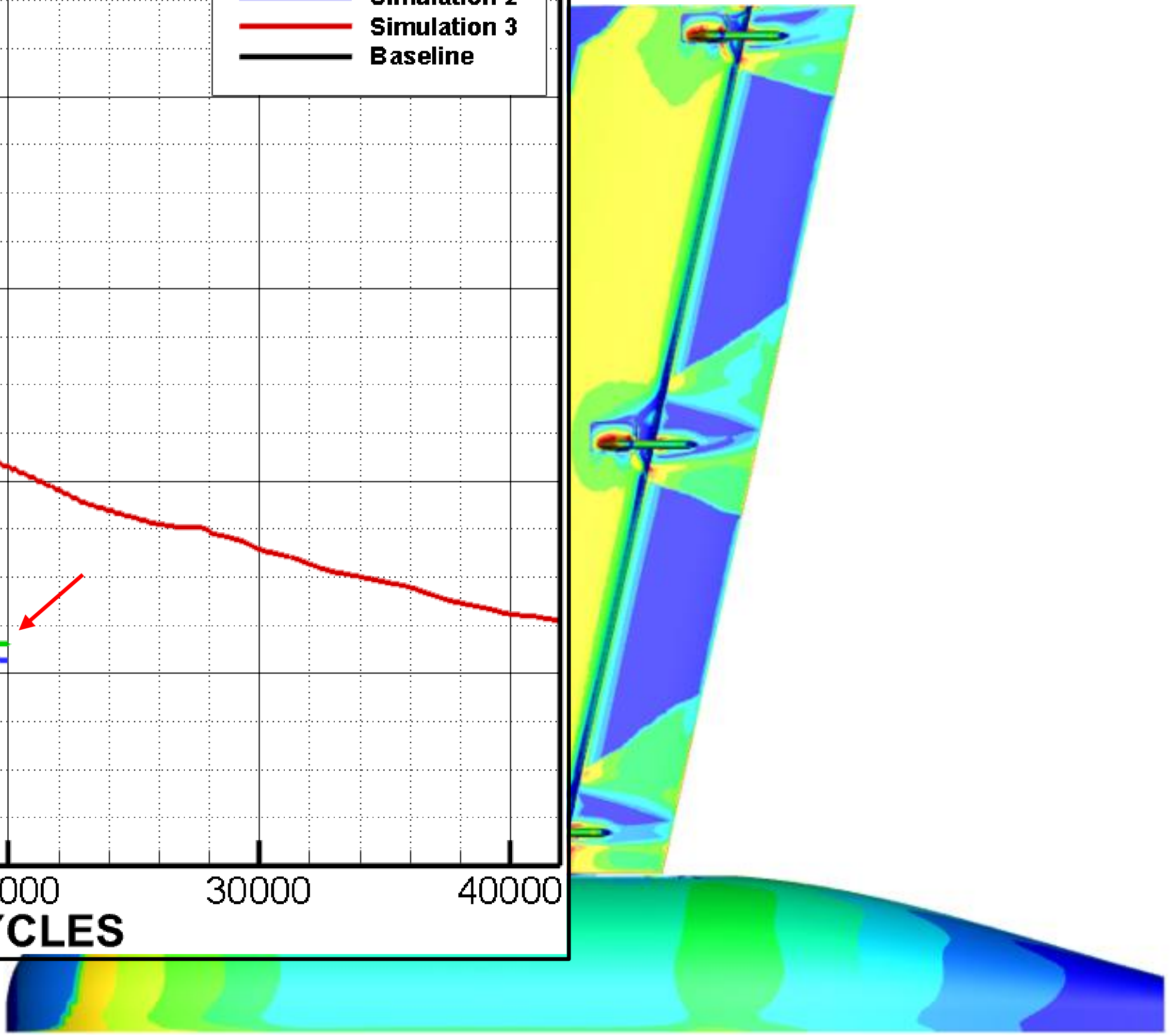

5.3 Results for Initial Simulations

- Skin friction drag results indicate that the transition line moves upstream very slowly as the simulation evolves

NSU3D-SA-AFT2 Free Transition Upper Surface Skin Friction Drag Profile for Simulation 2

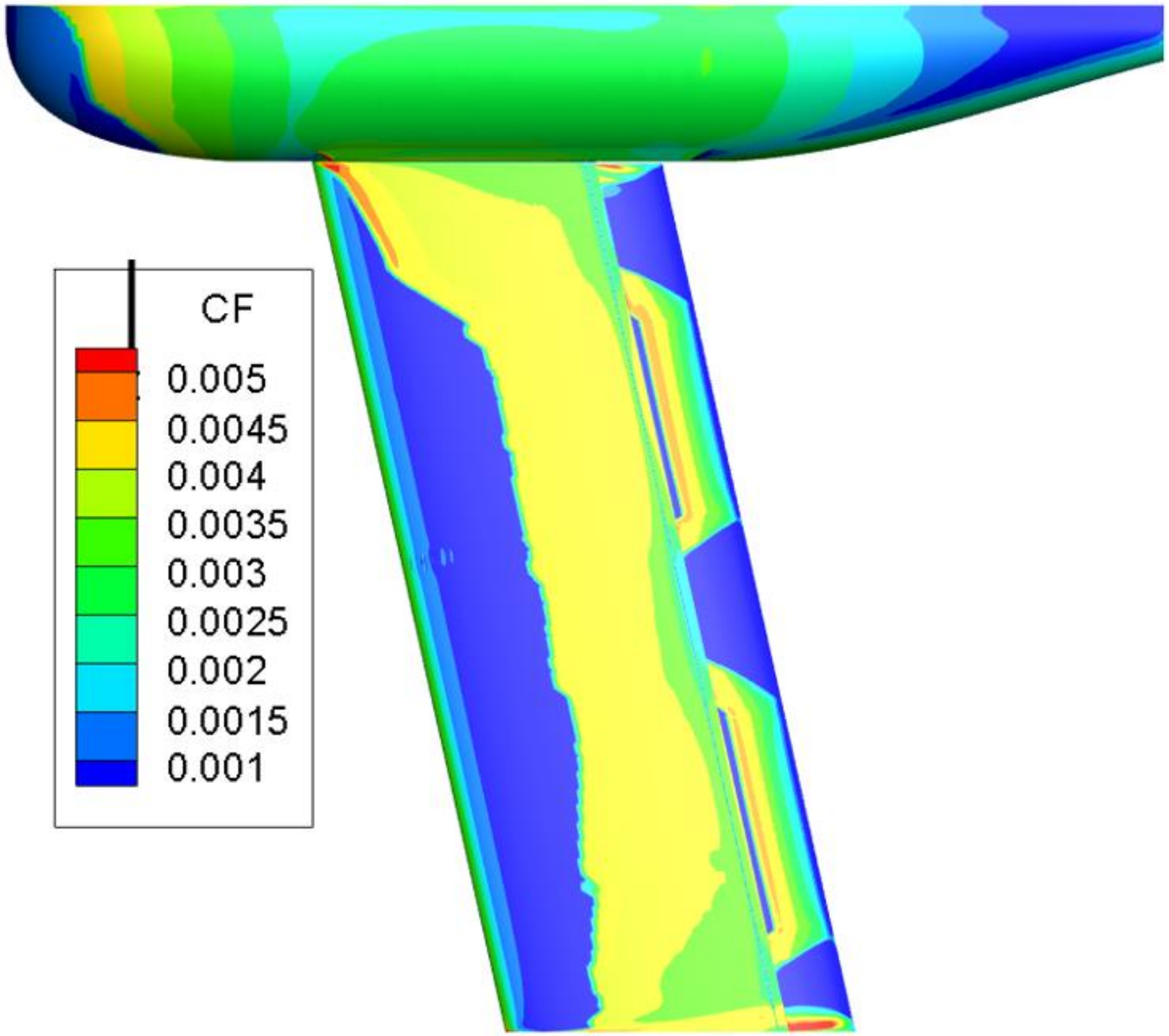

NSU3D-SA-AFT2 Free Transition Lower Surface Skin Friction Drag Profile for Simulation 2

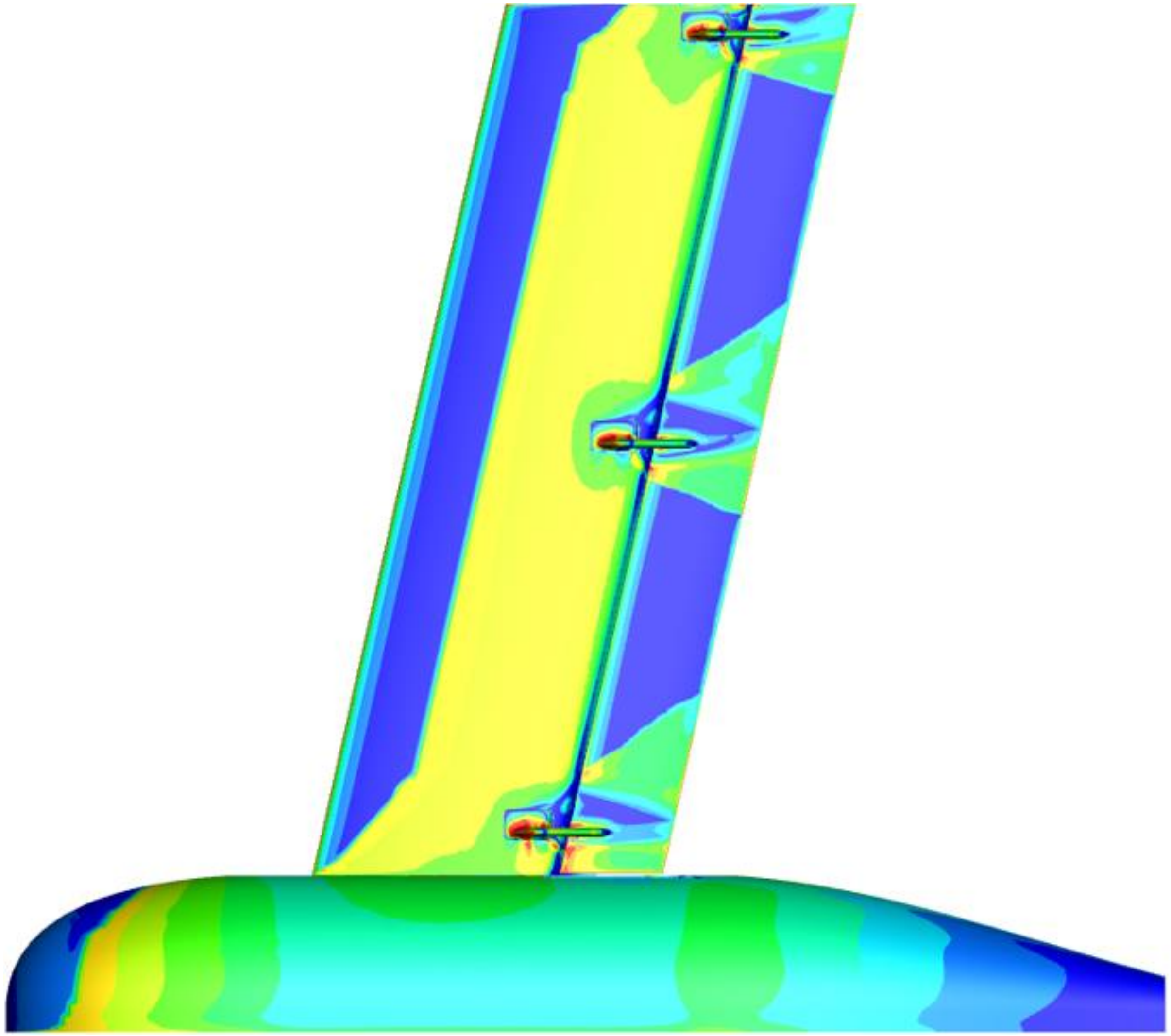

5.3 Results for Initial Simulations

- Skin friction drag results indicate that the transition line moves upstream very slowly as the simulation evolves

NSU3D-SA-AFT2 Free Tran
Friction Drag Profile f

ansition Lower Surface Skin
e for Simulation 3 18k

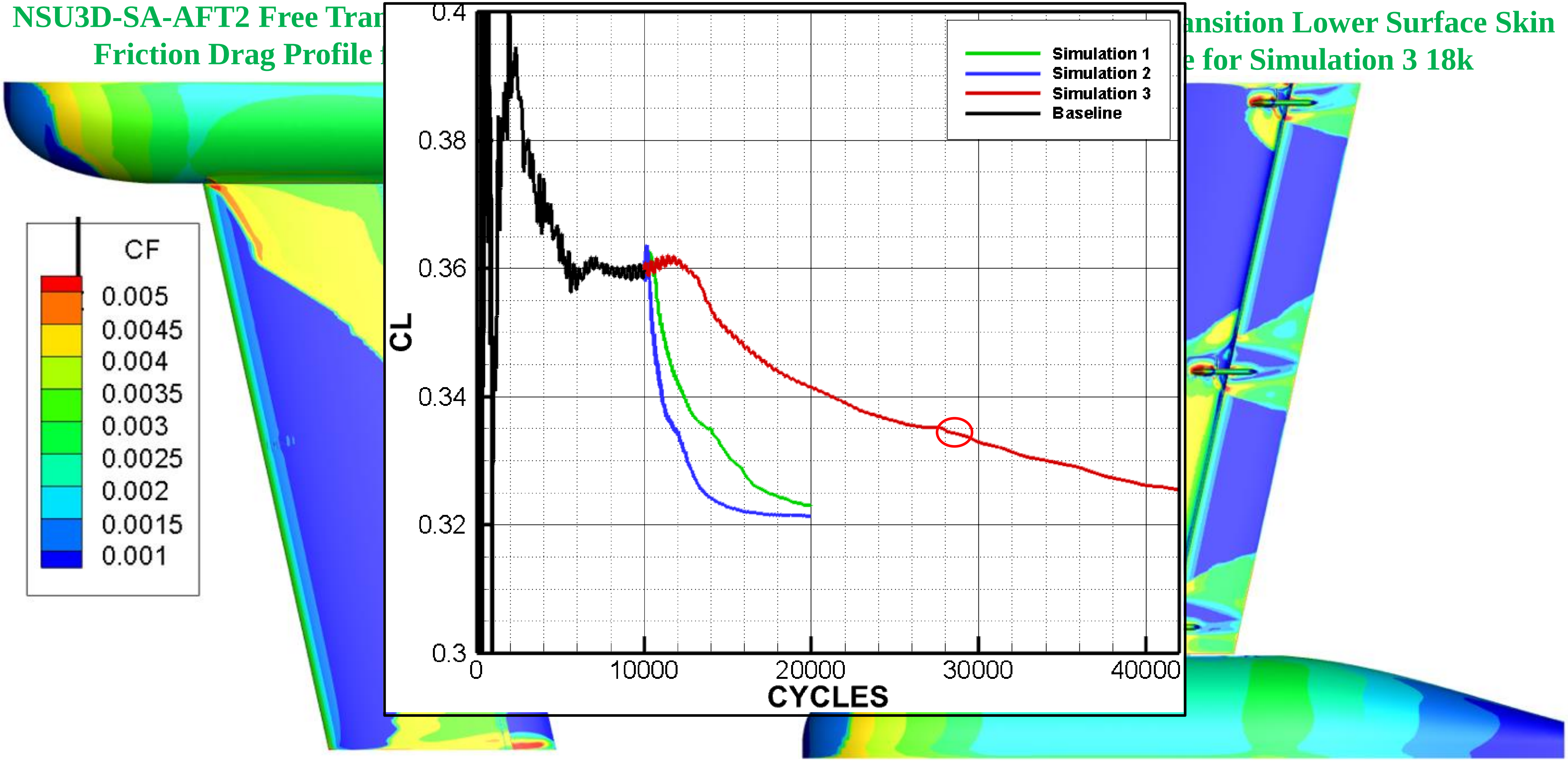

5.3 Results for Initial Simulations

- Skin friction drag results indicate that the transition line moves upstream very slowly as the simulation evolves

NSU3D-SA-AFT2 Free Transition Upper Surface Skin Friction Drag Profile for Simulation 3 18k

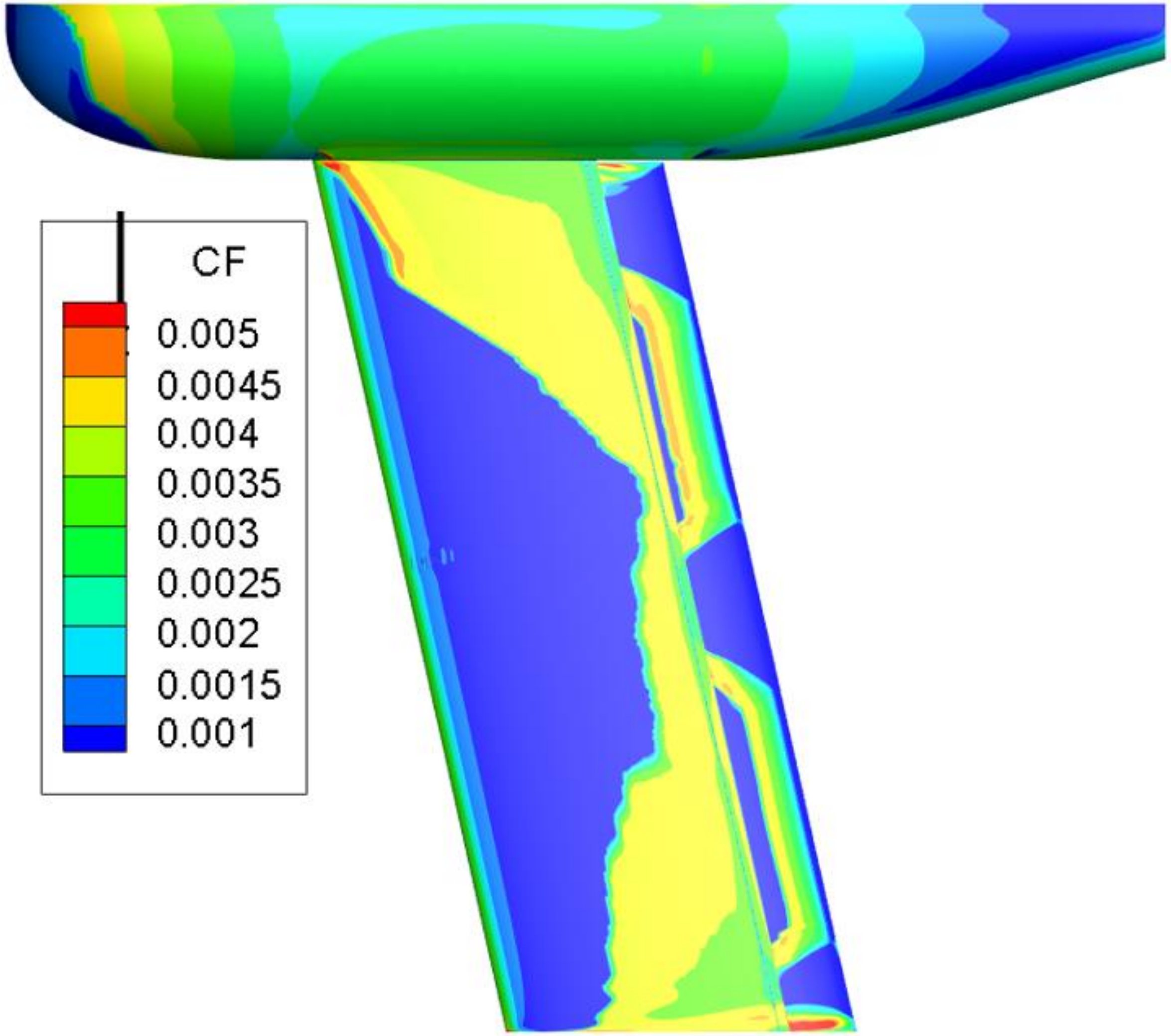

NSU3D-SA-AFT2 Free Transition Lower Surface Skin Friction Drag Profile for Simulation 3 18k

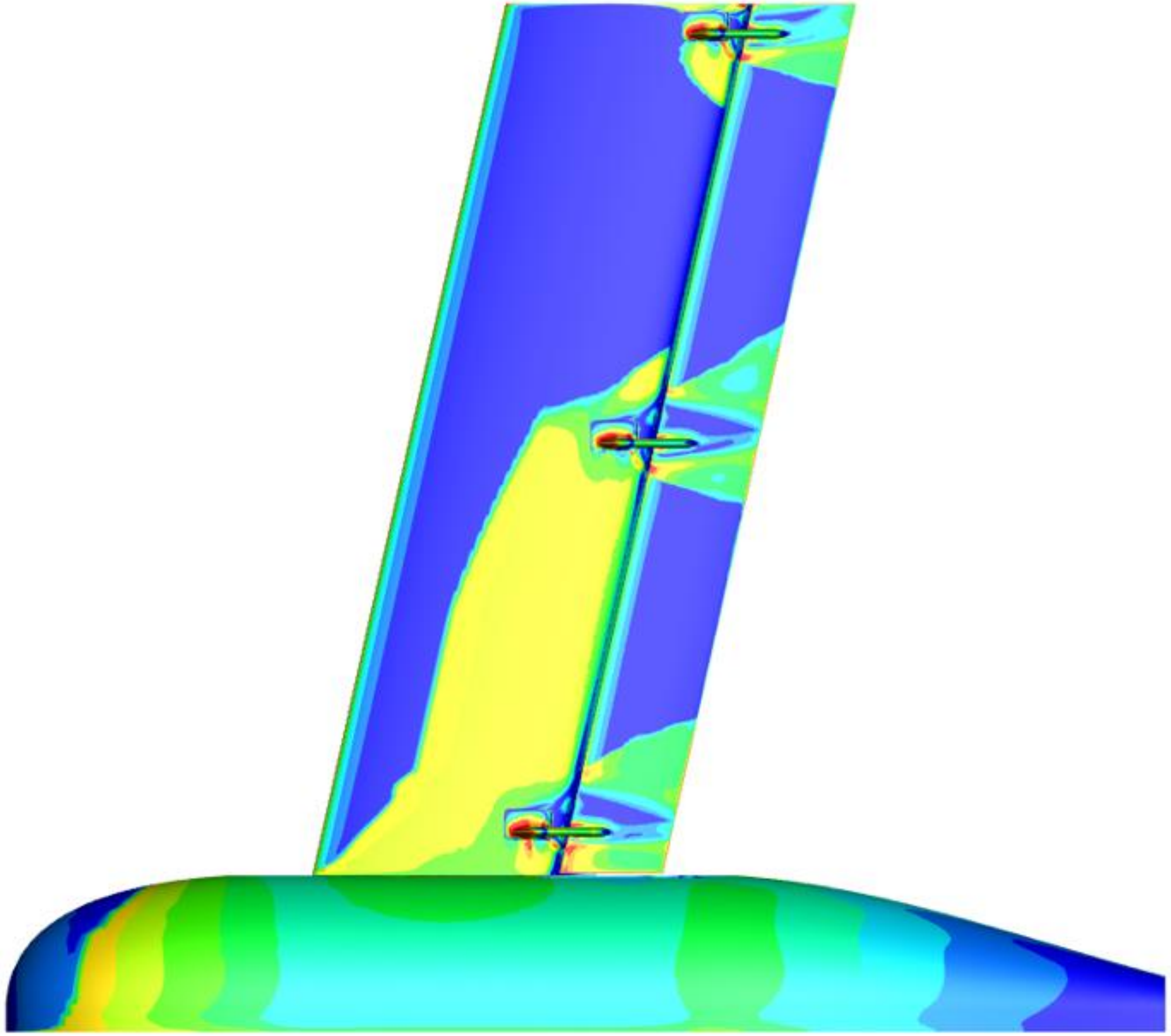

5.3 Results for Initial Simulations

- Skin friction drag results indicate that the transition line moves upstream very slowly as the simulation evolves

NSU3D-SA-AFT2 Free Tran
Friction Drag Profile f

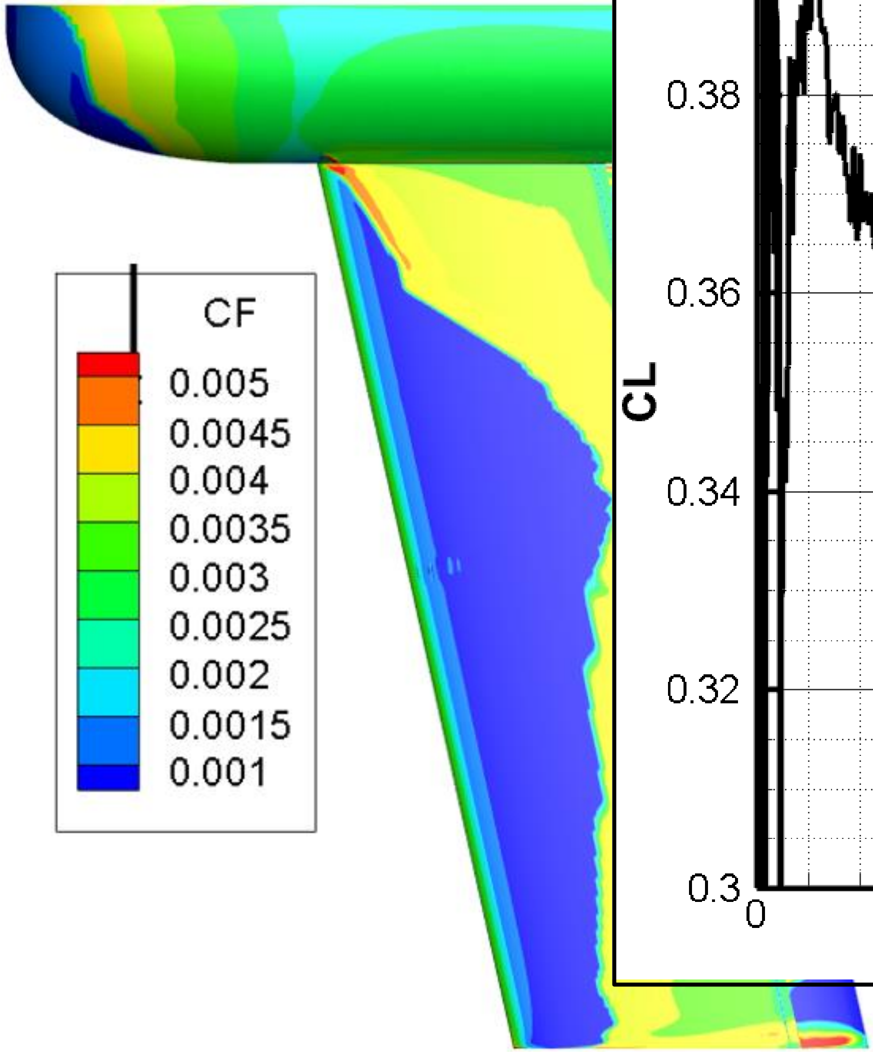

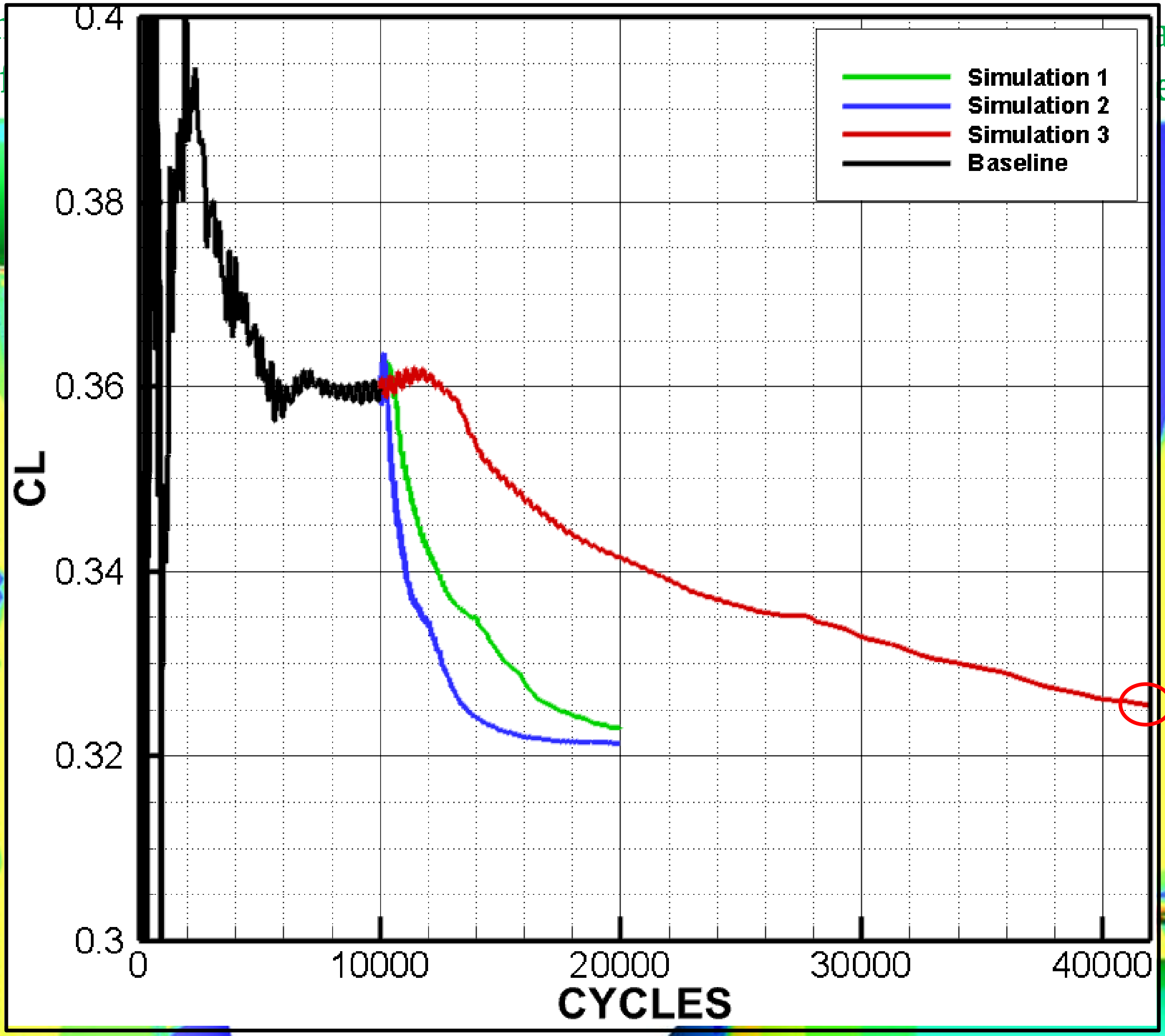

ansition Lower Surface Skin
e for Simulation 3 18k

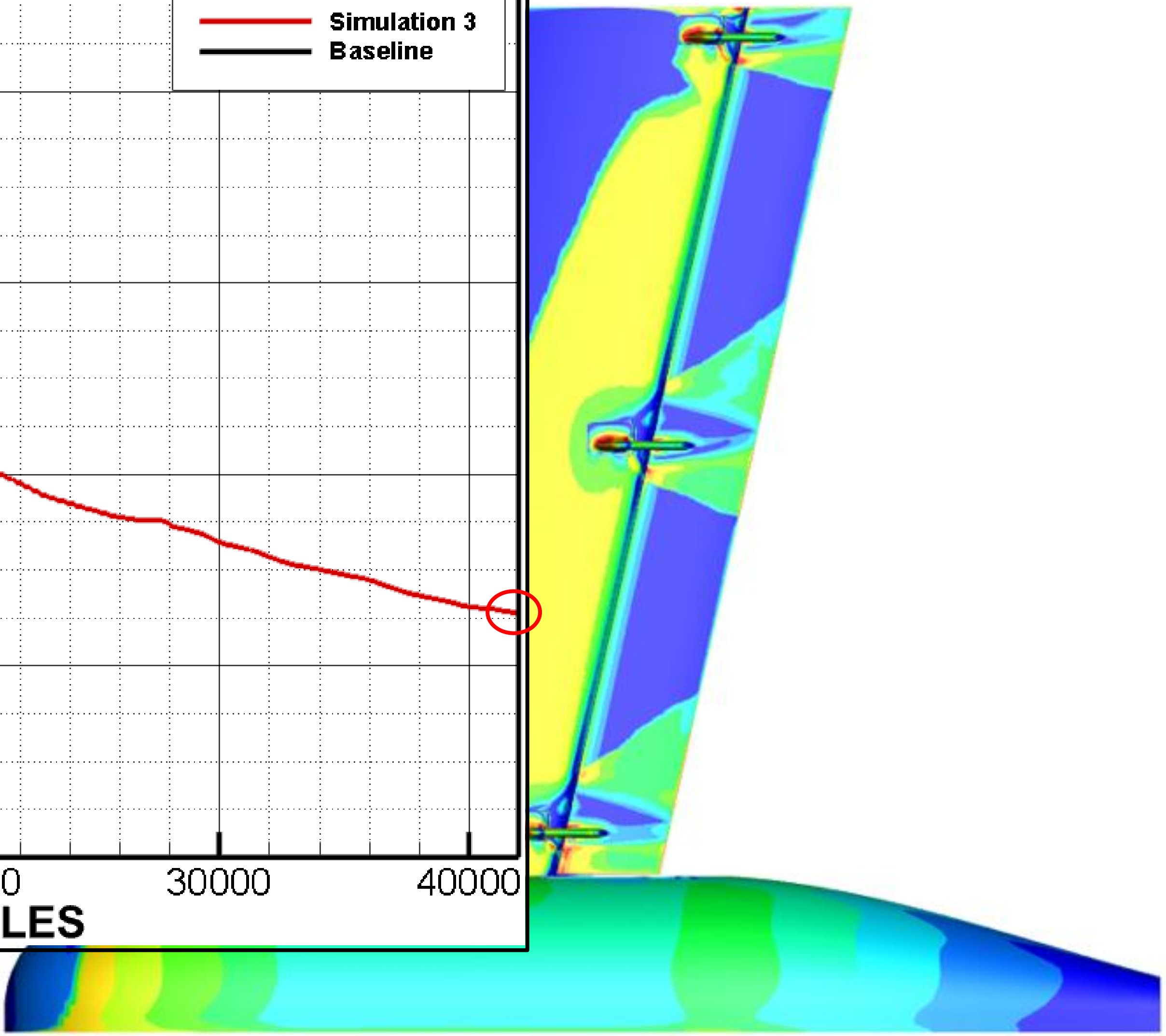

5.3 Results for Initial Simulations

- Skin friction drag results indicate that the transition line moves upstream very slowly as the simulation evolves

NSU3D-SA-AFT2 Free Transition Upper Surface Skin Friction Drag Profile for Simulation 3 18k

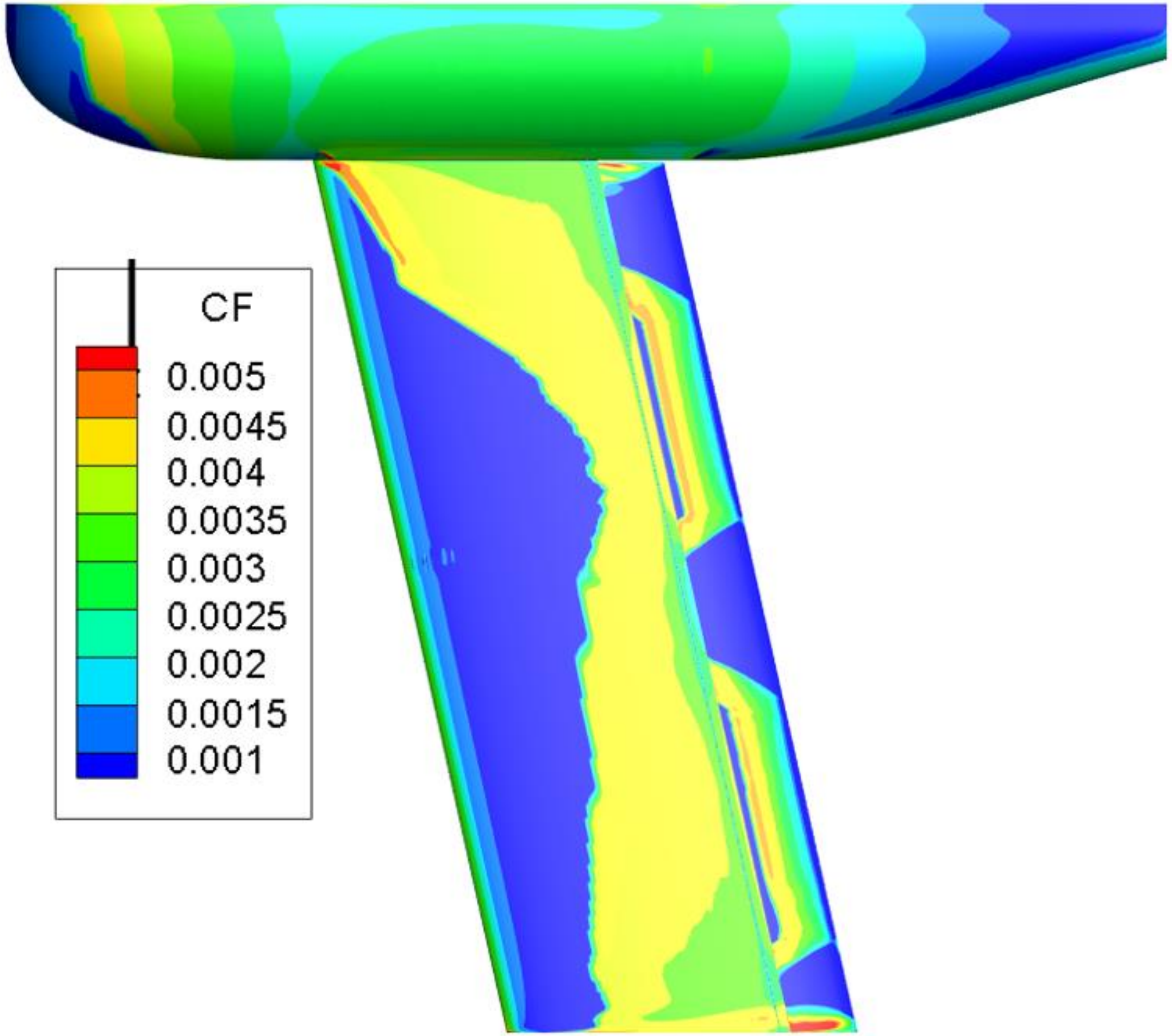

NSU3D-SA-AFT2 Free Transition Lower Surface Skin Friction Drag Profile for Simulation 3 18k

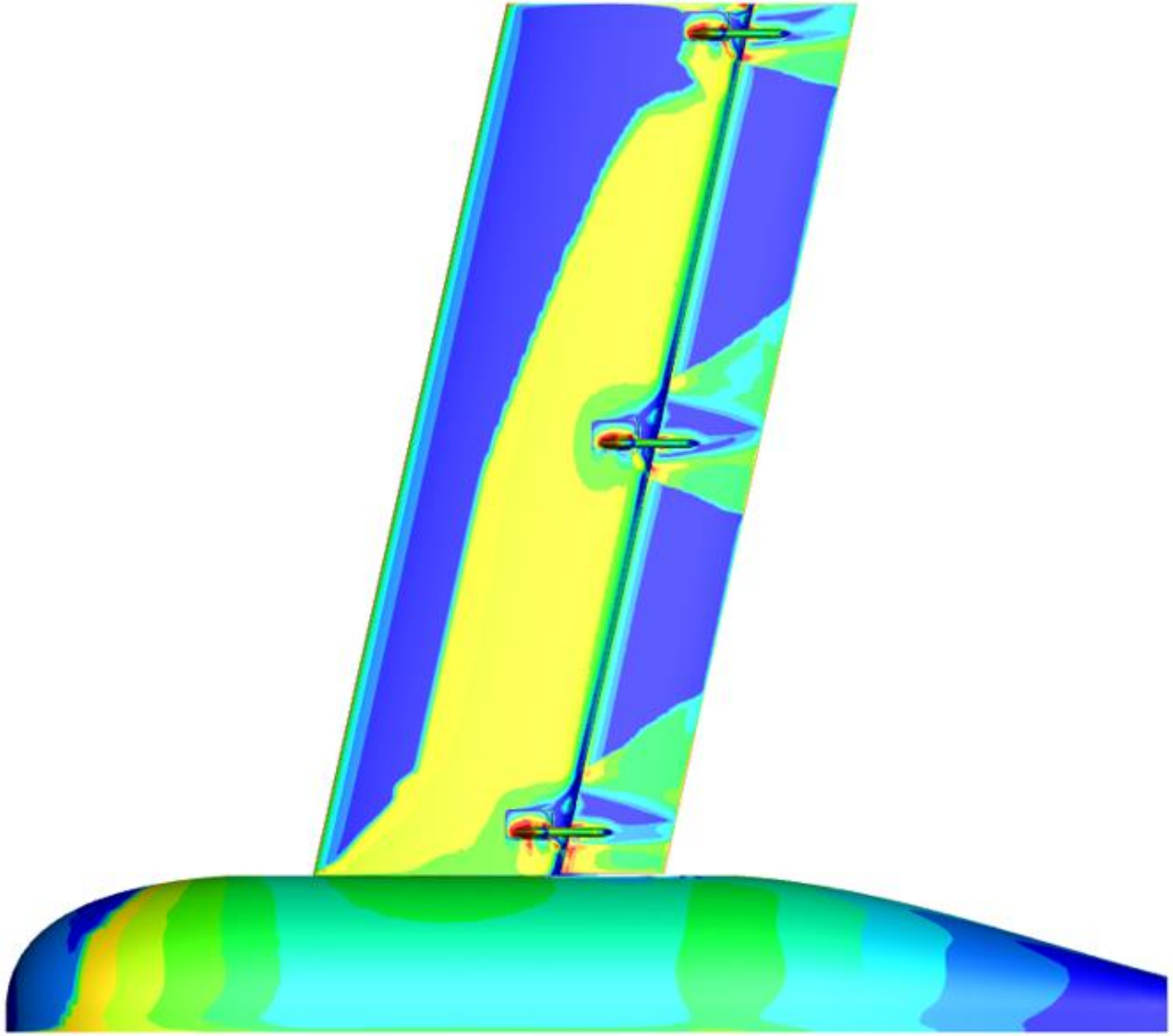

5.3 Results for Initial Simulations

- Summary remarks on initial wind tunnel tests…

- Simulations 1, 2, and 3 show that the transition line moves, albeit very slowly, toward the leading-edge of the fore element as the solution converges
- Transition line becomes stationary at roughly 40% the chord length by all runs if given sufficient number of cycles
- Results depict much less laminar flow than what was observed in the wind tunnel experiment